AD-A108 615 CALIFORNIA UNIV BERKELEY DEPT OF GEOLOGY AND GEOPHYSICS F/G 8/11
STATE-OF-THE-ART FOR ASSESSING EARTHQUAKE HAZARDS IN THE UNITED--ETC(U)
OCT 81 B A BOLT DACW39-78-C-0061

UNCLASSIFIED WES-MP-S-73-1-17 NL

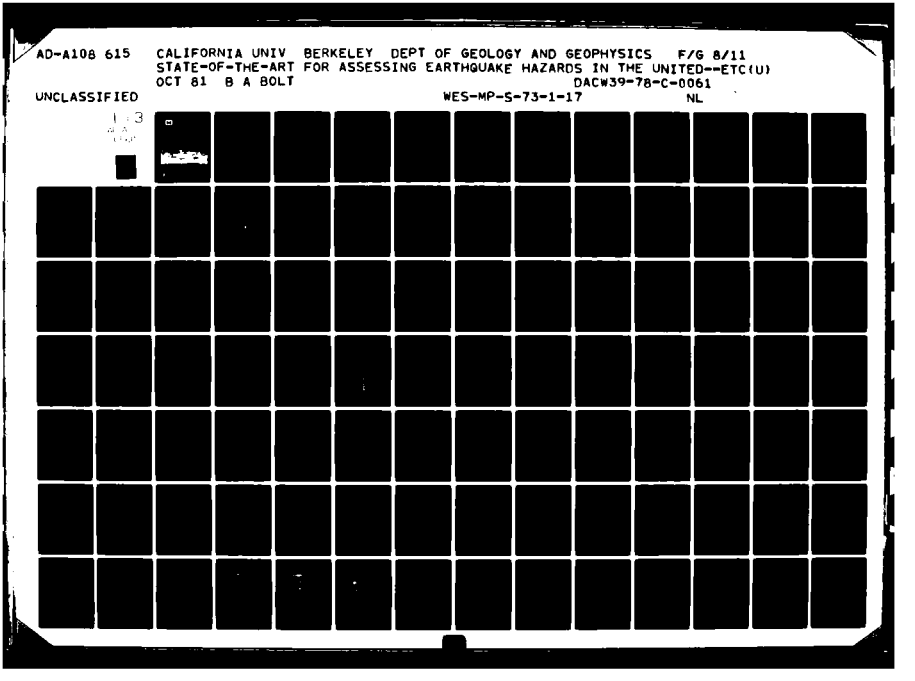

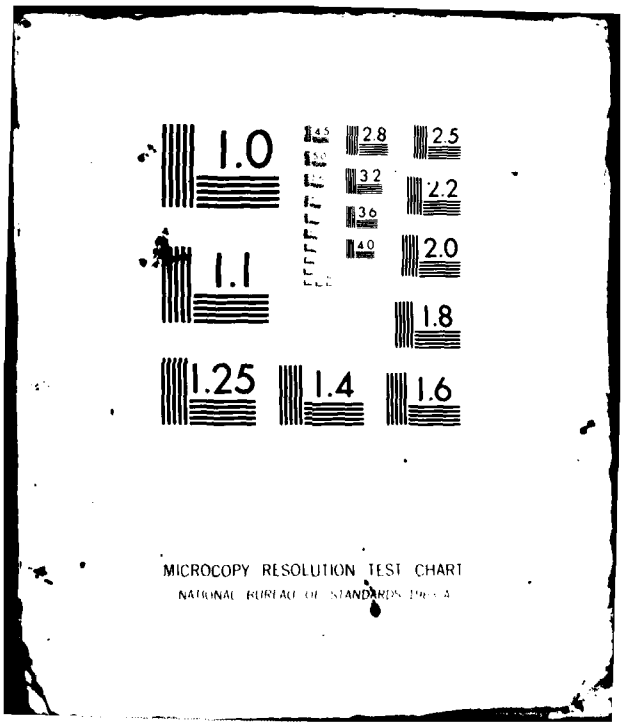
1.0
1.1
1.25
1.4
1.6
2.8
3.2
3.6
4.0
2.5
2.2
2.0
1.8
MICROCOPY RESOLUTION TEST CHART
NATIONAL BUREAU OF STANDARDS 1963-A

MISCELLANEOUS PAPER S-73-1

STATE-OF-THE-ART FOR ASSESSING EARTHQUAKE HAZARDS IN THE UNITED STATES

Report 17

INTERPRETATION OF STRONG GROUND MOTION RECORDS

by

Bruce A. Bolt

Department of Geology and Geophysics
University of California
Berkeley, Calif. 94720

October 1981

Report 17 of a Series

Prepared for Office, Chief of Engineers, U. S. Army
Washington, D. C. 20314

Under Contract No. DACW39-78-C-0061

Monitored by Geotechnical Laboratory
U. S. Army Engineer Waterways Experiment Station
P. O. Box 631, Vicksburg, Miss. 39180

Destroy this report when no longer needed. Do not return it to the originator.

The findings in this report are not to be construed as an official Department of the Army position unless so designated by other authorized documents.

The contents of this report are not to be used for advertising, publication, or promotional purposes. Citation of trade names does not constitute an official endorsement or approval of the use of such commercial products.

Unclassified

SECURITY CLASSIFICATION OF THIS PAGE (When Data Entered)

REPORT DOCUMENTATION PAGE	READ INSTRUCTIONS BEFORE COMPLETING FORM
1. REPORT NUMBER: Miscellaneous Paper S-73-1 · 1	2. GOVT ACCESSION NO.: AD-A108 615
	3. RECIPIENT'S CATALOG NUMBER:
4. TITLE (and Subtitle): STATE OF THE ART FOR ASSESSING EARTHQUAKE HAZARDS IN THE UNITED STATES; Report 17, INTERPRETATION OF STRONG GROUND MOTION RECORDS	5. TYPE OF REPORT & PERIOD COVERED: Report 17 of a series
	6. PERFORMING ORG. REPORT NUMBER:
7. AUTHOR(s): Bruce A. Bolt	8. CONTRACT OR GRANT NUMBER(s): Contract No. DACW39-78-C-0061
9. PERFORMING ORGANIZATION NAME AND ADDRESS: Department of Geology and Geophysics, University of California, Berkeley, Calif. 94720	10. PROGRAM ELEMENT, PROJECT, TASK AREA & WORK UNIT NUMBERS:
11. CONTROLLING OFFICE NAME AND ADDRESS: Office, Chief of Engineers, U. S. Army, Washington, D. C. 20314	12. REPORT DATE: October 1981
	13. NUMBER OF PAGES: 215
14. MONITORING AGENCY NAME & ADDRESS(if different from Controlling Office): U. S. Army Engineer Waterways Experiment Station, Geotechnical Laboratory, P. O. Box 631, Vicksburg, Miss. 39180	15. SECURITY CLASS. (of this report): Unclassified
	15a. DECLASSIFICATION/DOWNGRADING SCHEDULE:

16. DISTRIBUTION STATEMENT (of this Report)

Approved for public release; distribution unlimited.

17. DISTRIBUTION STATEMENT (of the abstract entered in Block 20, if different from Report)

18. SUPPLEMENTARY NOTES

Available from National Technical Information Service, 5285 Port Royal Road, Springfield, Va. 22151.

19. KEY WORDS (Continue on reverse side if necessary and identify by block number)

Earthquake engineering	Earthquakes
Earthquake hazards	Ground motion
Earthquake resistant design	Seismology

20. ABSTRACT (Continue on reverse side if necessary and identify by block number)

In this report, an attempt is made to extend the usual seismological analyses of seismograms to strong-motion records. A description is given of the main patterns of motions recorded on accelerograms near to the causative fault in terms of P and S waves and Love and Rayleigh waves. In order to achieve this, the effects of source dimensions and the physical and kinematical properties of the fault zone are included in the analysis. The two main aims of the work were, first, to make an initial step toward the routine

(Continued)

DD FORM 1 JAN 73 1473 EDITION OF 1 NOV 65 IS OBSOLETE

Unclassified

SECURITY CLASSIFICATION OF THIS PAGE (When Data Entered)

071 15

20. ABSTRACT (Continued).

interpretation of the recorded strong ground motions and, as a consequence, to provide a basis which would allow ground motions in future large earthquakes to be predicted. Both aspects of strong-motion seismology are of interest to the engineering profession for the design of critical structures in earthquake country, such as large dams and bridges.

The research has been based on the detailed study of near-field records obtained in moderate to large earthquakes in the last few decades. In particular, analysis is made of strong-motion records of 10 important earthquakes that includes: the 1952 Kern County, California, earthquake; the 1971 San Fernando, California, earthquake; the 1972 Managua, Nicaragua, earthquake; the 1977 Romania earthquake; the 1979 Imperial Valley, California, earthquake; and the 1980 Livermore Valley, California, earthquake. The analysis works from first physical principles and, so far as possible, uses elementary ray theory and kinematic arguments. Nevertheless, elements of the more sophisticated theory of earthquake mechanisms and seismic wave propagation in the near field were taken into account in the interpretive work.

As a special part of the present analysis, field studies were made of the 1979 Coyote Lake, the 1979 Imperial Valley, and the 1980 Livermore Valley earthquakes in California. A program was written to convert strong-motion accelerometer records into standard Wood-Anderson records, and it is demonstrated how this transformation assists in wave interpretations. Other special parts of the work involved finite element analyses to investigate the effect of trenches and scarps on the propagation of seismic waves and the computation of seismic moment from near-field records. Finally, some empirical rules are developed for the construction of representative seismograms for strong ground motions, given information on the seismic source and distance to the site.

PREFACE

This report was prepared by Dr. Bruce A. Bolt, Department of Geology and Geophysics, University of California, Berkeley, under Contract No. DACW39-78-C-0061. It is part of ongoing work at the U. S. Army Engineer Waterways Experiment Station (WES) in the Civil Works Investigation Study, "Methodologies for Selecting Design Earthquakes," sponsored by the Office, Chief of Engineers, U. S. Army.

Preparation of this report was under the direction of Dr. E. L. Krinitzsky, Engineering Geology and Rock Mechanics Division (EGRMD), Geotechnical Laboratory (GL). General direction was by Dr. D. C. Banks, Chief, EGRMD; Dr. P. F. Hadala, Assistant Chief, GL; and Dr. W. F. Marcuson, III, Chief, GL.

Special acknowledgement is made to Dr. R. Uhrhammer, Mr. N. Mouyiaris, Dr. J. P. Singh, Dr. T. May, and Mr. J. Marrone for considerable contributions to the content of the report and to Mr. R. Miller and Mr. R. McKenzie for their assistance with the tables and figures.

COL Nelson P. Conover, CE, and COL Tilford C. Creel, CE, were Commanders and Directors of WES during the period of this study. Mr. Fred R. Brown was Technical Director.

CONTENTS

			Page
PREFACE			1
PART I	INTRODUCTION		4
	1.1 Problems of Seismological Interpretation		4
	1.2 Interpretation of Conventional Seismograms		10
	1.3 Role of Theory		13
	1.4 Aims of This Study		24
PART II	MAJOR NEAR-FIELD PROBLEMS OF ENGINEERING INTEREST		26
	2.1 Maximum (Peak) Amplitudes		26
	2.2 Duration		31
	2.3 Patterns of Arrivals - Deterministic and Stochastic		34
	2.4 Spectral Content		40
	2.5 Effect of Fault Properties		45
	2.6 Directivity and Focussing		48
	2.7 Effect of Complex Propagation Paths in Ground Structure		51
PART III	CASE STUDIES		58
	3.1 Kern County, CA	July 21, 1952	58
	3.2 Parkfield, CA	June 28, 1966	67
	3.3 Borrego Mt., CA	April 9, 1968	86
	3.4 San Fernando, CA	February 9, 1971	94
	3.5 Managua, Nicaragua	December 23, 1972	108
	3.6 Gazli, Uzbek, USSR	May 17, 1976	117
	3.7 Bucharest, Romania	March 4, 1977	123
	3.8 Coyote Lake, CA	August 6, 1979	130
	3.9 Imperial Valley, CA	October 15, 1979	140
	3.10 Livermore Valley, CA	January 24, 1980	156
PART IV	DISCUSSION		163
	4.1 Broad Principles of Interpretation		163
	4.2 Robust Estimation of Parameters		171
	4.3 Some Remarks on High-Acceleration Values		180
	4.4 The Focussing Controversy		183

4.5	Need for Strong-Motion Instrument Arrays	187
4.6	Use of Mathematical Response Transformations	193
REFERENCES		197
BIBLIOGRAPHY		204
APPENDIX A	COMPUTATION OF RICHTER LOCAL MAGNITUDE FROM STRONG-MOTION RECORDS	207
APPENDIX B	COMPUTATION OF SEISMIC MOMENT FROM BROAD-BAND RECORDS	212

PART I

INTRODUCTION

1.1 Problems of Seismological Interpretation

To a large extent, because of tradition and direct interest in strong earthquakes and structural response, the responsibility for strong-motion recording of seismic waves has been carried by the engineering community. Seismologists have largely concerned themselves with the interpretation of seismograms with very small amplitude waves, usually at considerable distances from the seismic source. For such work, infinitesimal strain, linear elasticity, and isotropic theory are sufficient and the asymptotic forms of the waves can, to a good approximation, be treated by ray theory.

There have been two recent developments which change the situation. First, the engineering profession is now involved in the design of critical structures in earthquake country, such as large dams, nuclear reactors, hospitals, bridges, and highrise buildings. Such design requires realistic inputs of ground motion at close distances from seismic sources of specified size. Secondly, there has been a great increase in the number of strong-motion seismographs that (a) have the dynamic range, both in frequency and amplitude, to remain on scale in even the most severe shaking, and (b) have absolute (UT) time marks on them. These instruments are now producing informative seismograms of very energetic seismic waves quite near to the source of the wave energy.

The new challenges, therefore, for seismologists are, first, to explain the characteristics of the recorded ground motions and, as a consequent step, to predict ground motions in future specified earthquakes. Until recently, because the theory was not developed and the observational base was primitive,

seismological ability to undertake these two tasks was restricted. The recent availability of more representative seismograms of strong ground motions has stimulated development of the theory, aided by high-speed computers needed to perform wave analysis and synthesis for near-source motions.

The physics of the problem indicates that elastic waves recorded within a few wave lengths of an extended source (the "near field") are likely to be complicated and difficult to interpret uniquely. There are at least four components involved in the understanding of such complex motions. The first component arises from the generation of the waves by the rupturing fault. The accepted model for the source of a large tectonic earthquake is a moving dislocation which sweeps out an area of slip along a fault plane in a given time. The signature of the faulting mechanism is a function of a finite number of dislocation parameters such as stress drop, fault dimension, and rupture velocity (see Section 1.3). Elastic waves of various types radiate from the moving dislocation in all directions. The geometry of the fault will affect critically the pattern of radiation from it. Also, it is suspected that the linear elastic constitutive relations usually assumed in elastic wave theory may be defective along the fault zone itself (see Section 2.5).

The second component of the problem concerns the passage of the waves through the intervening medium to the site. Although in the near field some wave properties such as dispersion are not as significant as for distant (teleseismic) recording, nevertheless attenuation and scattering properties may affect the appearance of a wave train in the near field at a point on the surface. Questions also arise concerning the effect of the surficial

layers of low rigidity materials such as soils and the diffraction and focussing of the waves due to structural anomalies in the medium.

The third component treats the conditions at the recording site such as topography and the effect of low velocity and highly attenuating soils. It is helpful, from a seismological point of view, that the latter aspect of the problem be eliminated so far as possible by choosing strong-motion records that are obtained on rock or "firm" sites. The additional interpretational complications can then be treated separately.

The final component of the interpretation of strong ground motion records is the effect of the recording instruments which must be removed from the records if the actual ground motion is to be analyzed. Fortunately, this can now be done readily, when necessary, using instrument response equations programmed for a highspeed computer. In the work that follows, we consider mainly the first and second components of the problem of interpretation.

It is not possible in the present report to review all published papers which contain interpretations of strong-motion records. A reasonably comprehensive list is, however, given in the References for convenience. Recent interpretations have been based on various assumptions and approaches ranging from simple ray theory to numerical modeling of dynamical aspects of the earthquake source (Johnson, 1979). Mainly, interpretations have been restricted to small to moderate earthquakes and, for these, theory and observation are close. This success suggests that when the source is limited in extent, at least for periods above one or two seconds, enough physical and mathematical understanding is available to explain the various onsets in terms of a reasonable source model. There is, however, always a problem of uniqueness. There are in the literature a number of different explanations and interpretations

of the main onsets on several specific strong-motion records (e.g., Pacoima, see Section 3.4). The main sources of the disagreements are the unknown structure of the Earth's crust, the unknown properties of the fault process, and also the (arbitrary) choice of parameters to define the source and medium (i.e., lack of completeness).

The interpretation of a seismogram is an example of what is termed in applied mathematics the "inverse" or "indirect" problem. If the source and Earth's structure were known, then calculations would yield directly wave motions ("synthetic seismograms") which could be compared with the observed ones and identification of seismic waves made. The inverse problem is to start with the strong-motion records themselves and infer from them the wave types, the structure of the media through which the waves propagated, and the definition of the source itself. Fortunately, in the inverse problem, some key parameters such as fault dimensions and rock structure can be obtained from geological maps, geophysical work, the distribution of aftershocks, and other independent means.

Perhaps the most widely analyzed strong-motion record in the near field was that obtained at Pacoima in the San Fernando earthquake of February 9, 1971 (M_L = 6.5). The three components of ground acceleration shown in Figure 1.1 indicate overall complexities and considerable differences between components of ground motion. (In fact, many strong-motion records are simpler than this example.)

One problem of interpretation for seismologists on older records of this type is the lack of absolute (UT) time. Normally, seismograms provided at seismographic stations have an absolute time scale so that correlations can be made between stations and seismic wave velocities from the earthquake

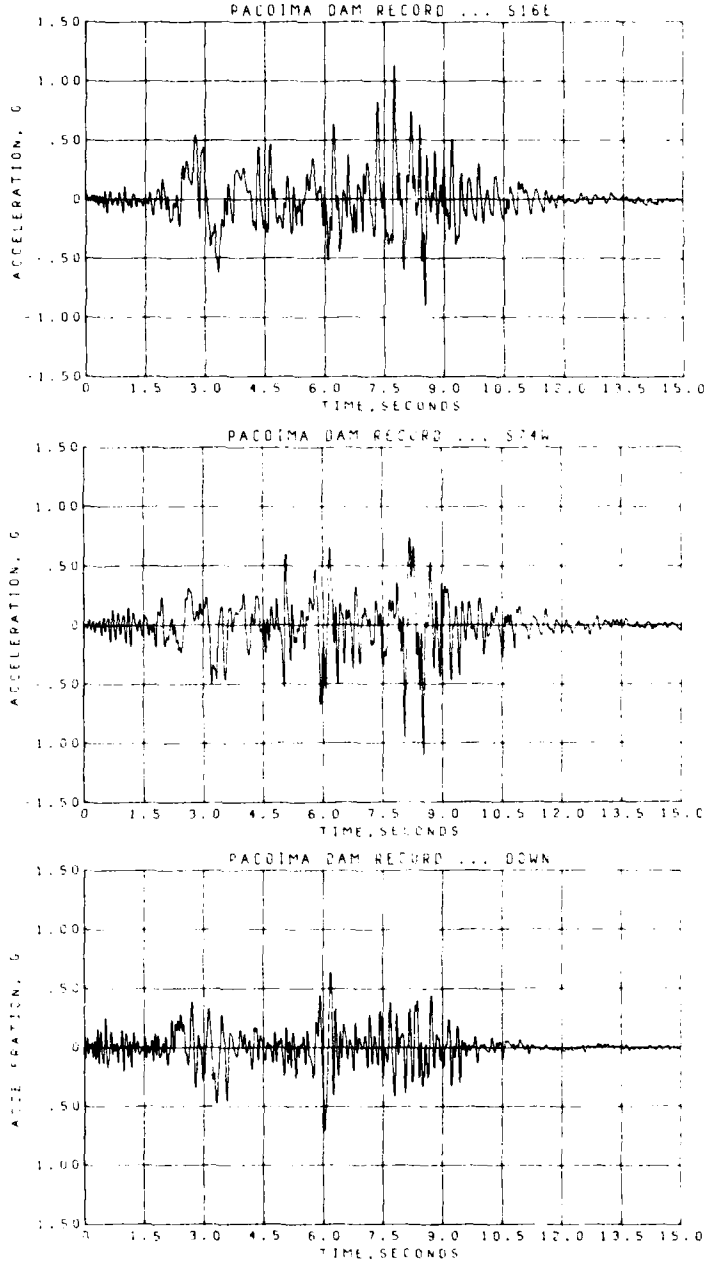

Figure 1.1. Three components of ground acceleration recorded at Pacoima in the February 9, 1971, San Fernando earthquake.

focus can be easily calculated. With the older type of strong-motion recording in Figure 1.1, there is also the difficulty that the first seismic wave may not have triggered the instrument. Presumably, in the sizable San Fernando earthquake, the first wave seen in Figure 1.1 is within 1 to 2 seconds of the first P wave which passed from the focus (the point of first rupture on the fault) to the Pacoima site. Fortunately, the new generation of strong-motion instruments now being deployed (see Section 4.5) eliminates these two problems and we will not refer to them again. Because of the design of analog accelerographs, there is also difficulty in ensuring that the longer period seismic waves are recorded with fidelity (Hudson, 1979). Usually, a base line correction is made by a specified, but arbitrary, procedure and this can make doubtful the measurement of waves with periods greater than about 10 seconds (Shoja-Taheri, 1977).

1.2 Interpretation of Conventional Seismograms

Nowadays, an experienced seismologist can go a long way in interpreting the wave pattern observed on a seismogram of a distant earthquake. This is because the assumptions of linear elasticity hold and ray theory can be used. The source can usually be approximated by a point or small sphere and at large distances the wavefronts are effectively planar, so that motions can be separated into longitudinal and transverse components.

There are, however, complications which are common. When an elastic wave encounters a boundary which separates rock of different elastic properties, it will, like sound and electromagnetic waves, undergo reflections, refraction, and diffraction. Within an homogeneous, isotropic, elastic medium, there are two body waves which propagate. The fastest is the dilatational wave, called the P or primary wave, and the slower is the shear wave, called the S or secondary wave. When such body waves encounter a boundary, a conversion between these types occurs, with either an incident P or S wave yielding a reflected P and S wave as well as a refracted P and S wave. In addition, the effects of rapid variations in the rock structure can be often observed in the form of scattering of the waves, producing seismic energy in regions which, on simple ray theory, there should be a shadow.

The free surface of the Earth permits the existence of additional seismic waves of surface wave type. Rayleigh waves have particle motions near the surface of the ground that are elliptical in a vertical plane. In addition, when layers are present near the surface or there is a gradient in elastic properties, horizontally polarized surface waves, called Love waves, also exist. At considerable distances from the source, the P, S, Rayleigh, and Love waves can be seen on seismograms clearly separated,

according to their respective velocities and, as well, there are often waves such as PP, SS, and so on which correspond to reflections of these waves at internal boundaries.

In addition to usual phases mentioned above on conventional seismograms of distant or small earthquakes, there are certain types of seismic waves (often pulselike) that are observed specially in the near field of the seismic source. These include "stopping phases" which are due to the intermittent stopping of the dislocation front and the final (sudden) cessation of the rupture. A special form of this stopping phase is called a "breakout" phase, which arises from the generation of a pulse when the rupture reaches the free surface of the Earth.

An example of a vertical component seismogram recorded by a conventional seismograph is shown in Figure 1.2. Time marks are shown, and the onsets of seismic body and surface waves are marked according to a seismological interpretation based on expected wave travel times from a focus 290 km away.

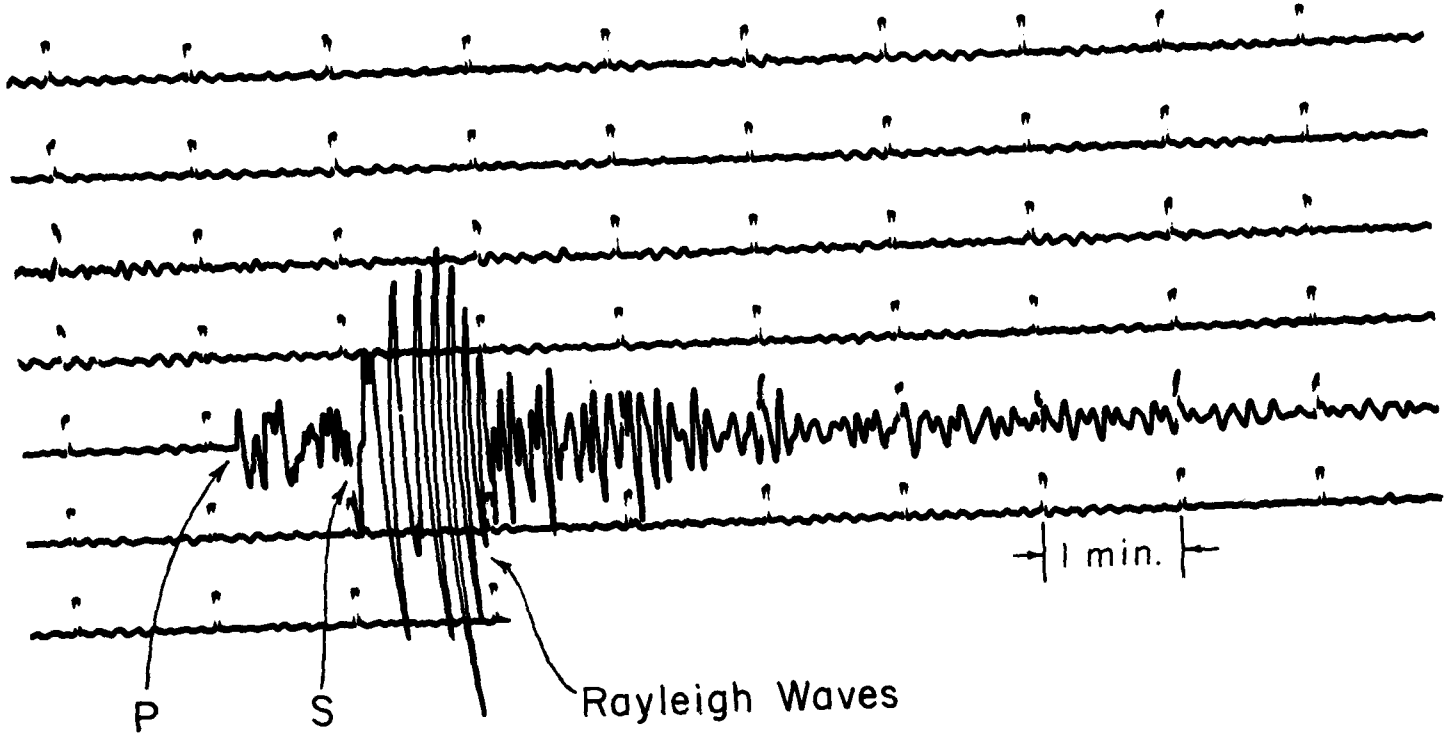

Figure 1.2. A vertical component seismogram recorded at Berkeley from the earthquake near Mammoth Lakes, May 26, 1980 (M_L = 5.1). Distance from Berkeley is 290 km.

1.3 Role of Theory

We cannot understand the complexity of seismic waves recorded by accelerometers unless the earthquake source is modeled in a realistic way. The first specification of the physics of generation of waves was made by H.F. Reid in his studies of the faulting that occurred along the San Andreas fault in the 1906 San Francisco earthquake. His model remains the basic physical model for the construction of synthetic seismograms today. It is, briefly, that strains build up in the faulted rocks and one of them finally reaches failure point. Rupture then takes place and the strained rock rebounds on each side of the fault under its own elastic stresses until the strain is largely or wholly relieved.

This elastic rebound theory of earthquake genesis means that near the fault there will be a "fling" or uni-directional heave of the ground. Reid, however, went on to give more detail. He stated, "It is probable that the whole movement at any point does not take place at once, but proceeds in irregular steps. The more-or-less sudden stopping of the movement, and the friction, gives rise to the vibrations which are propagated to a distance. The sudden starting of the motion would produce vibrations, just as would its sudden stopping, and vibrations are set up by the friction of the moving rock, just as the vibrations of a violin string are caused by the friction of the bow." Here we have recognition of irregular motions along the fault caused by intermittent locking, stress variations, or roughness. This property of fault rupture is now being used extensively in modeling earthquake sources. Alternatively, it is said that the fault surface contains "asperities" or "barriers." The slip over an area of the fault reduces the stress suddenly producing a local "stress drop," Δp, given by

$$\Delta p = \frac{1}{2}\frac{\mu D}{W} \qquad (1.1)$$

where μ is the rock rigidity, D is the offset, and W is the width of the rupture plane.

In 1964 and 1966, N. Haskell developed a model "in which the fault displacement is represented by a coherent wave only over segments of the fault and the radiations from adjacent sections are assumed to be statistically independent or incoherent." The physical situation in this model is that the rupture begins suddenly and then spreads with periods of acceleration and retardation along the weakly welded fault zone. In this model, the idea of statistical randomness of fault slip or "chattering" in irregular steps along the fault plane is introduced.

More recently, Das and Aki (1977a, b) have considered a fault plane having various barriers distributed over it. They conceive that rupture would start near one of the barriers and then propagate over the fault plane until it is brought to rest or slowed at the next barrier. Sometimes the barriers are broken by the dislocation; sometimes the barriers remain unbroken but the dislocation reinitiates on the far side and continues; sometimes the barrier is not broken initially but, due to local repartitioning of the stresses and possibly nonlinear effects, it eventually breaks, perhaps with the occurrence of aftershocks.

The elastic rebound model involving a moving dislocation along a fault plane over which roughnesses of various types are distributed stochastically is thus the starting point for the interpretation of near-field records. Based on this model, there have been recently quite a number of attempts to compute synthetic seismograms from points near to the source and comparisons have been made with observations.

From geological evidence, there are, of course, different kinds of fault ruptures. Some involve purely horizontal slip (strike-slip); some involve vertical slip (dip-slip). It must be expected that the wave patterns generated by fault mechanisms of different kinds will be different to a larger or lesser extent, due to the different radiation patterns produced.

The theory must also incorporate effects of the moving source. These Doppler-like consequences will depend on the speed of fault rupture and the direction of the faulting (Boore and Joyner, 1978). The physical problem is analogous (but more difficult) to the problem of sound emission from moving sources (Morse and Ingard, 1968). The problem can be approached both kinematically and dynamically. The acoustic problem shows that in the far field the pressure is the same as when the source is at rest. However, in the near field, the time dependence of both frequency and wave amplitude is a function of the azimuth of the site relative to the moving source. This aspect is taken up further in Section 2.6.

We now summarize the main lines of approach to modeling mathematically the earthquake source. The first model is the kinematic approach in which the time history of the slip on the generating fault is known a priori. Several defining parameters may be specified, such as the shape, duration, and amplitude of the source (or source time function and slip), the velocity of the slip over the fault surface, and the final area of the region over which the slip occurred. Theoretically, a Green's function representation is usually used to calculate the resulting displacements of the medium. Green's functions for the various classifications of faulting have been constructed, and numerous theoretical papers using this approach have been published (e.g., Israel and Kovach, 1977). The process is a kind of complicated curve fitting whereby the parameters of the source are varied in order

to estimate by inspection the closeness of fit with distant radiated seismic waves. Once the seismic source is defined by this process, using distant recordings, then the near-field parameters can be used to calculate the ground motions near to the source for engineering purposes.

A second approach is to use the differential equations involving the forces which produce the rupture. This dynamic procedure has received considerable emphasis lately. The basic model is a shear crack which is initiated in the pre-existing stress field and which causes stress concentrations around the tip of the crack. These concentrations, in turn, cause the crack to grow. Many of the articles on this subject have been built on the work of Kostrov (1966). For example, Burridge and Willis (1969) obtained analytic expressions for particle accelerations in given directions from a uniformly growing elliptical crack, although they did not include the effect of crack stoppage. (This unrealistic boundary condition is included in most work of this kind.) The key to the crack problem seems to be in modeling the physical processes of the typical crack where there is interaction between the rate of crack growth, the criterion of fracture, and the stress accumulation. Most of these studies on dynamic shear cracks are concerned primarily with the actual rupture process, and so the crack is assumed to be imbedded in an infinite homogeneous medium. Studies more concerned with the seismic waves that are recorded in the field need a numerical approach, such as finite elements or finite differences, to handle realistic structural conditions.

The studies mentioned under kinematic and dynamic models are built around the elastic rebound theory of slip on a fault. There are, however, more general studies that take a less specific view of the earthquake source. Recent work by Backus (1977a,b), for example, has taken up the important idea

of the uniqueness of the various source descriptions; the representation of an arbitrary source of seismic waves is given in terms of moment tensors. Any seismic source can, in principle, be expanded in terms of spatial moments, that of the long wave lengths compared to the fault dimensions; only the low degree terms of the expansion need to be included. Thus, for small earthquakes or far-field problems, it is sufficient to represent a seismic source in terms of a single first-degree moment of the equivalent force, which is a symmetric second-rank tensor. Then, the waves calculated can be interpreted in terms of any specific model. It turns out, however, that in practical attempts to represent the near field in this way, higher terms give very complicated tensor components and analytic evaluation may not be worthwhile. It should be mentioned here that the scalar seismic moment (direction of force couples along the fault ignored) is given by

$$M_0 = \mu AD \tag{1.2}$$

where A is the slipped area (see Appendix B).

Let us now summarize the physical model for the earthquake source now generally accepted (see Figure 3.10). The source extends over a fault plane in the Earth which is ruptured by a series of dislocations which initiate at some point (the focus) and spread out with various rupture velocities. The dislocation front changes speed as it passes through patches of roughness (barriers on the fault). At the dislocation itself, there is a finite time for a slip to take place and the form of the slip is an elastic rebound of each side of the fault leading to a decrease of overall strain. The slip can have vertical components, as well as horizontal components, and can vary along the fault itself. The waves are produced near the dislocation front due to the release of the strain energy in the slippage.

This model resembles in many ways radio waves being radiated from a finite antenna. In the far field, the theory of radio propagation gives complete solutions for the reception of radio signals through stratified media. However, when the receiver is very near to the extended antenna, the signal becomes jumbled due to the finiteness of the source and interference through end effects.

The main parameters in the model are:

Rupture length	L
Rupture width	W
Fault slippage (offset)	D
Rupture velocity	V
Rise time	T
Roughness (barrier) distribution density	$\Phi(\underset{\sim}{x})$

The main work in theoretical seismology on source properties today is to determine which of these parameters are essential, whether the set is an optimal one, and how best to estimate each parameter from both field observations and analysis of the seismograms made in both the near and the far field.

A number of papers have now been published that demonstrate that, in certain important cases, synthetic seismograms for seismic waves near their source can now be computed rather realistically. The synthetic motions can be compared with the three observed orthogonal components of either acceleration, velocity, or displacement at a site (see Figure 1.3a, 1.3b, and 1.3c). There remain difficulties, however, in modeling certain observed complexities and there is a lack of uniqueness in the physical formulations which lead to acceptable fits with observations. Three main procedures have been used. The first (Archambeau, 1968) is a deterministic method for predicting near field ground motion. He treats the seismic source as a generalized phase

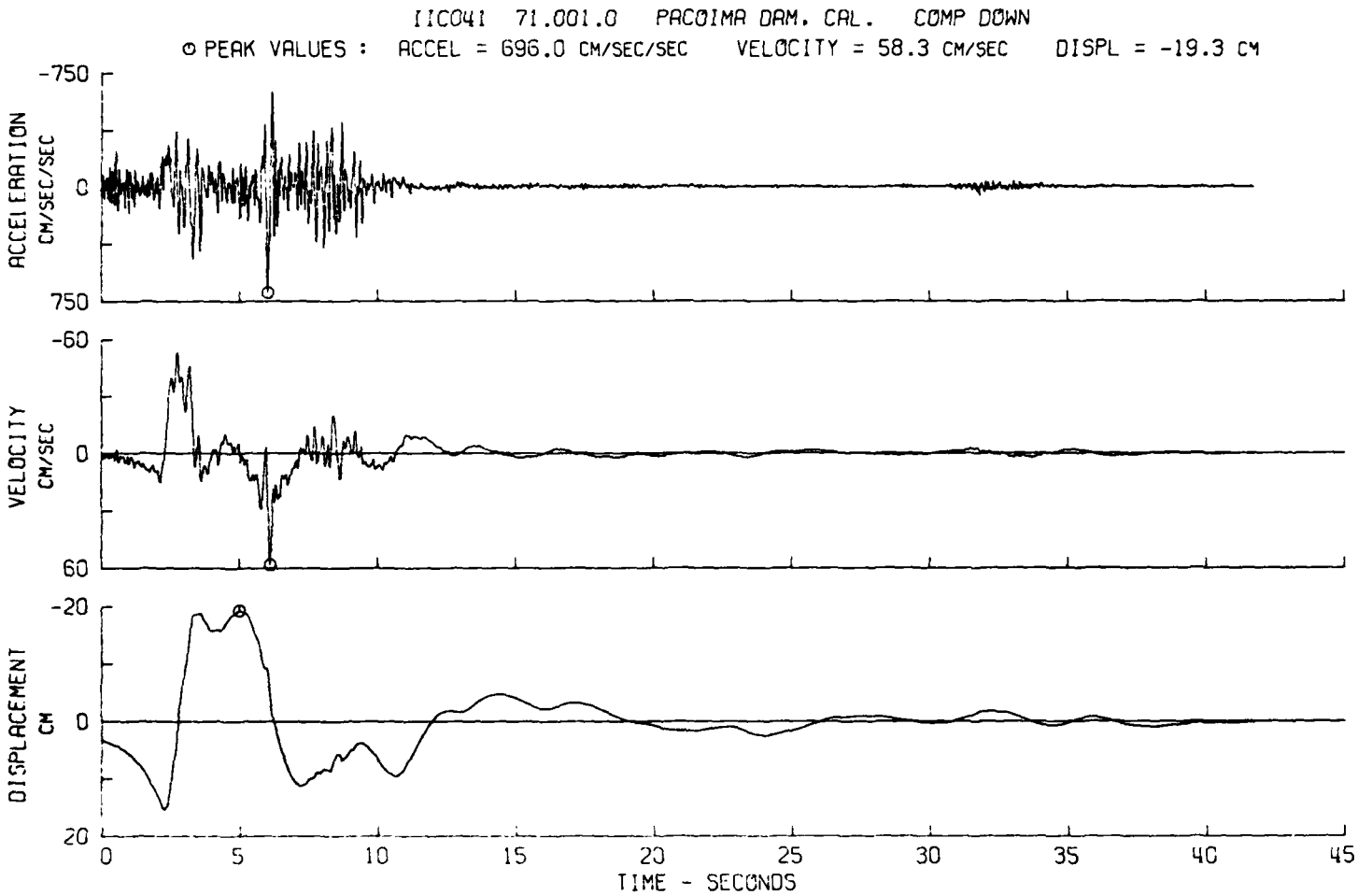

Figure 1.3. San Fernando Earthquake; Feb. 9, 1971 - 0600 pst (Sheet 1 of 3).

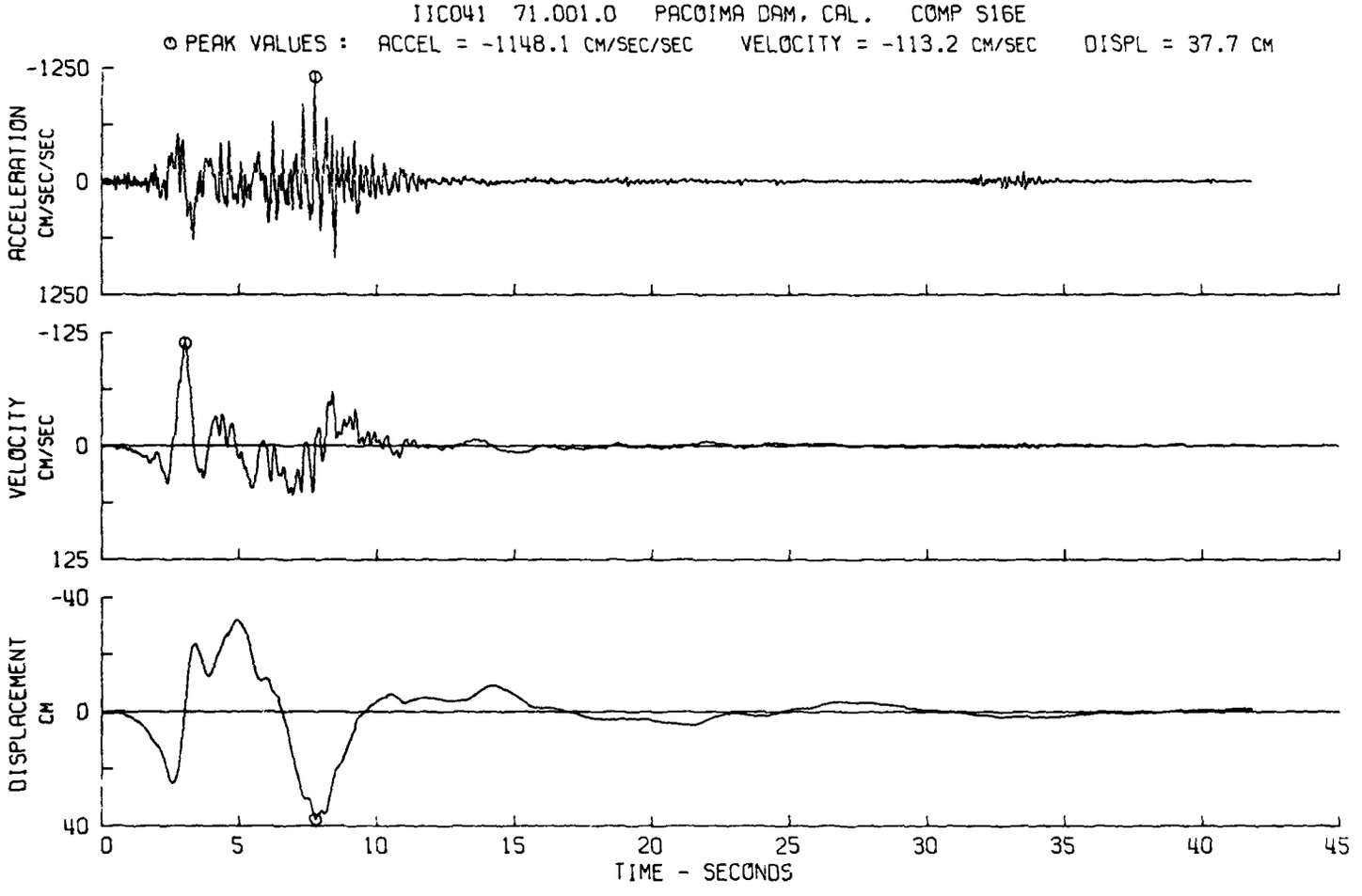

Figure 1.3. (Sheet 2 of 3).

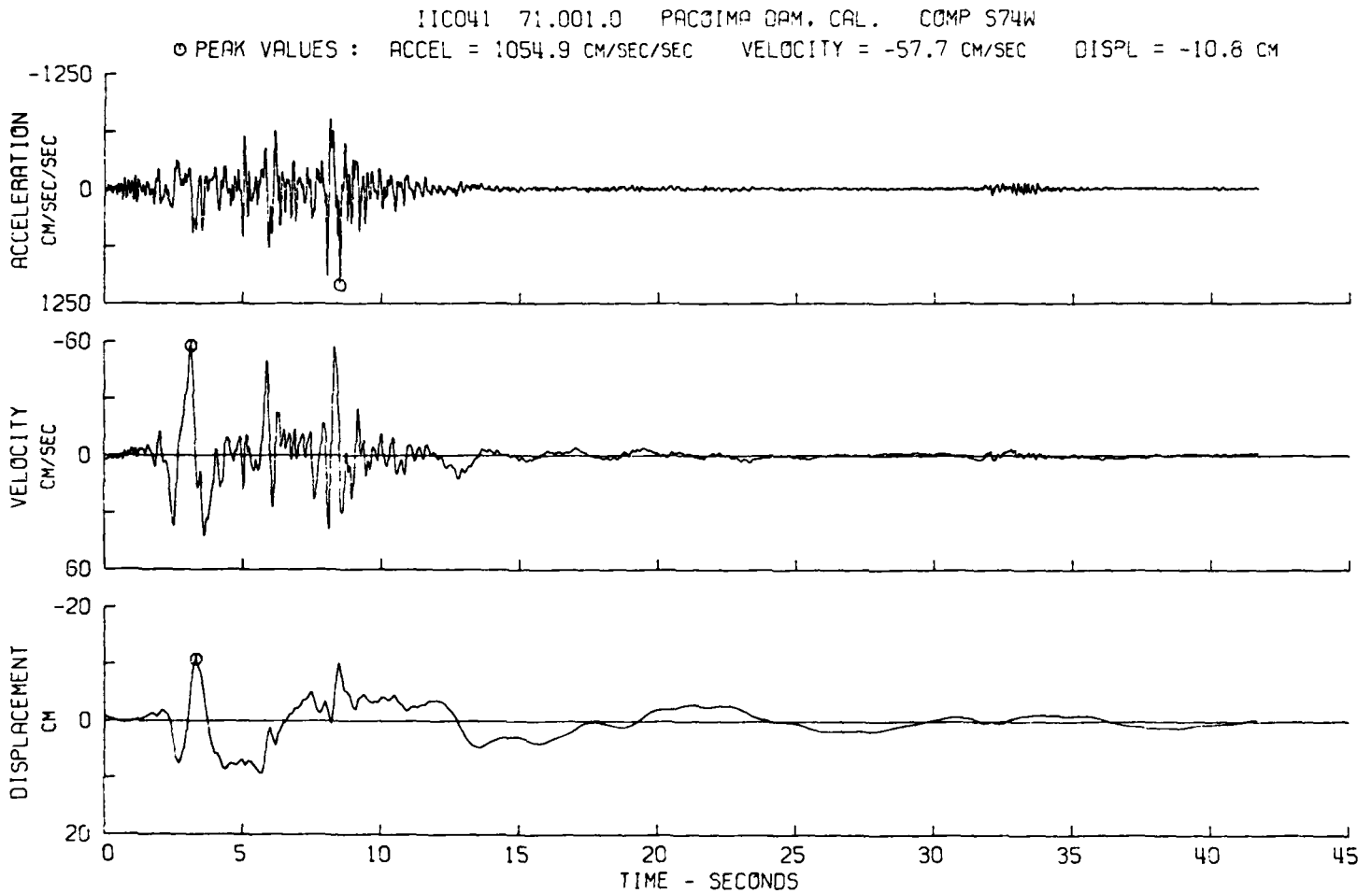

Figure 1.3. (Sheet 3 of 3).

transition and calculates the seismograms from the conservation equations of continuum mechanics. He has, for example, fitted the model predictions for near-field strong-motion data at Pacoima in the 1971 San Fernando earthquake. He was able to fit the first five to six seconds of the displacement record well (see Figure 1.3c). Deviations at later times, starting near seven seconds, are probably due to the omission from the model of near-surface faulting, as well as the neglect in the calculations of the contribution from surface waves generated at the free surface. Of importance, however, comparison of theoretical and observed velocities (e.g., see Figure 1.3b) clearly shows that a model which fits short-period far-field data well does not necessarily fit higher frequency near-field data very well at all. Thus, a model which fits the seismic data below 2 Hz can be constructed that does not provide an acceptable fit to the higher frequency accelerations near the fault. This present difficulty in most synthetic modeling remains the central problem in strong-motion prediction because, for engineering purposes, the concern is mainly with acceleration records, rather than with displacements (see Section 2.4).

The second procedure is the numerical solution of the equations by finite elements or finite differences. Such studies offer the inclusion of more realistic structure around the source, such as a weak zone of gouge material which occurs in most fault zones and a realistic crustal structure near the surface. An example is a study, again of a Pacoima record, by McCowan, Glover, and Alexander (1977). Finally, the moment tensor mentioned above has been used to calculate synthetic seismograms for small earthquakes and for underground nuclear explosions (Stump and Johnson, 1977). The numerical calculations were made by using many point sources on the fault, delaying

and summing their contributions at any given point on the surface. Successive approximations yield synthetic records which are close to the observed seismograms.

1.4 Aims of This Study

The principal aim of this study is to advance the abilities of seismologists and engineers to explain the wave patterns observed on strong-motion records obtained near to the earthquake source. The art of interpretation of seismograms is well advanced at earthquake observatories so far as seismic waves from distant and small earthquakes are concerned, but, to the present, few people are able to make much headway in the interpretation of accelerograms, for example, using seismological wave nomenclature.

The approach used in this study is to work through a number of the most important earthquakes known in earthquake engineering circles and examine the recorded strong ground motions in the light of available knowledge of faulting, intensity reports, and theoretical seismological considerations. The work differs from most recent seismological studies on synthetic strong-motion records in that the emphasis is not on explaining in detail every portion of the wave, using theory, but rather to identify the main waves on the record and, if possible, the place on the fault from which they come.

Finally, from the experience gained by working with actual strong-motion records, especially in the ten case histories (Part III), some general inferences are drawn about the broad principles of interpretation needed in the strong-motion field (see Section 4.1). Further, based on the interpretational analysis, some comments are made about the optimum set of parameters which are needed to provide a prediction of ground motions in specified circumstances.

Another objective of the work was to ascertain what types of records are needed if reliable predictions of strong ground motions are to be made. An illustration is given in Section 4.2 by developing rules for the construction of engineering seismograms. The weaknesses of attempting to interpret and extrapolate using records from independent single stations are well-illustrated

by this study. It also defines the constraints that the use of such data places on producing representative artificial motions. These ideas are worked out in Sections 4.5 and 4.6.

Finally, it is hoped that the analysis of the case studies made here in terms of simple physics and ray theory will assist a wide audience in earthquake engineering to be aware of what is feasible in strong-motion seismology at the present time. Of course, the simple theory used cannot give a full description of the complicated dynamic processes involved in large earthquake generation, but it is of interest to explore to what extent the principal seismological aspects can be described by an approach from first principles.

PART II

MAJOR NEAR-FIELD PROBLEMS OF ENGINEERING INTEREST

2.1 Maximum (Peak) Amplitudes

For some time, a key scaling parameter in the specification of ground motion for engineering purposes has been the maximum (peak) acceleration. These peak values are used to scale not only the seismograms (time histories), but also to anchor the high-frequency end of ground response spectral curves. The methodology was evolved in the 1960's when there were few strong-motion records for large to moderate earthquakes available and the maximum amplitudes seen on accelerograms were about 0.3g to 0.5g.

The situation has now changed for several reasons. First, many instrumental measurements have now been obtained of peak accelerations greater than 0.5g. Indeed, in the Imperial Valley, California, earthquake of October 15, 1979 (see Section 3.9), a peak acceleration of about 1.7g was observed in the vertical direction and on the Pacoima record (see Figure 1.1) a peak horizontal high-frequency amplitude of 1.2g was measured. At the same time, it is observed that these high-acceleration values often are represented on the record by only one or two spike-like features. In other words, they are not representative estimates of the accelerations which were being experienced through the strongest ground shaking. Indeed, in some cases they could be characterized as abnormal samples of a more typical frequency distribution of peak amplitudes.

A second observational property has also recently come to light. Near to the source of quite small earthquakes, strong-motion instruments often record high accelerations. Well-known examples of this are the Bear Valley, California, earthquake of September 4, 1972 (M_L = 4.7, peak horizontal

acceleration = 0.69g), and the Ancona earthquake of June 21, 1972, in Italy (M_L = 4.5, peak horizontal acceleration = 0.61g).

These observations of high peak accelerations at high frequencies from small-magnitude earthquakes show that raw peak acceleration taken alone can be a deceptive parameter so far as scaling ground motions for engineering purposes. Another aspect of the problem is that in synthesizing ground motions for engineering design it has been common practice to emphasize the peak acceleration parameter. For example, this procedure has been followed by the Nuclear Regulatory Agency in terms of the safe shutdown earthquake for a particular site. The procedure, of course, breaks down when it is accepted that a given peak acceleration (0.5g, say) could apply to strong ground motions of vastly different overall seismic energies and spectra.

Another difficulty with the emphasis on peak accelerations stems from the high-frequency nature of the observed peaks in almost all cases (see Figure 1.1). It is now realized that an engineering response spectrum can be drawn which would be anchored at the peak acceleration specified for the predicted earthquake at the site, while the spectral amplitudes at longer periods, say beyond one second, could be quite deficient for the predicted type of earthquake. For this reason, demand is growing for not just a peak acceleration as the dominant scale parameter, but also suitable scaling parameters for maximum velocity and even maximum displacement. An illustration comes from the recent ACT risk maps for the United States (Donovan, Bolt, and Whitman, 1976) where the free-field ground-motion response spectra were scaled at short periods to an effective acceleration parameter and at longer periods to an effective velocity parameter. Partly for this reason, in the analyses that follow, discussion will be given not only on acceleration records, but also to their first and second integrals (i.e., velocity and displacement).

Because of the central role that has been played by peak accelerations in estimating strong ground motions, they have been correlated against a number of parameters. One of the most important is the correlation of near-source acceleration with local magnitude. Figure 2.1 illustrates the marked differences in estimates due to different assumptions. A few observed values from actual strong-motion records are added to Figure 2.1 to indicate some of the scatter of data that went into these extrapolations. The dashed line comes from a study by Page et al. (1972) in which they give peak accelerations against magnitude for very near-source distances. The curve is fixed by extrapolations back from a few earthquakes of moderate size (generally up to about magnitude 7) at distances greater than 5 km from the ruptured fault. The assumptions used lead to a curve which rises rather steeply above magnitude 6 to about 1.2g for the largest earthquakes. The second curve on Figure 2.1 is based on attenuation curves (by Schnabel and Seed, 1973) for peak acceleration as a function of magnitude. The different assumptions used lead to an extrapolation with almost no increase in the horizontal peak acceleration at near-source distances for magnitudes above 6.5. It should be mentioned that the general physical properties of the source model discussed in Section 1.3 would seem to favor the second hypothesis over the first. This is because the amount of seismic energy produced in any frequency band along the rupturing fault would be a function of the elastic properties of the rocks near the dislocation at any time, rather than the summation at a given time of energies over the whole fault plane. In the former case, the emitted wave energy is limited above a threshold while in the latter it would be greater for larger magnitude earthquakes than for smaller magnitude earthquakes. This central problem of scaling from low-magnitude to high-magnitude earthquakes remains unresolved, but further

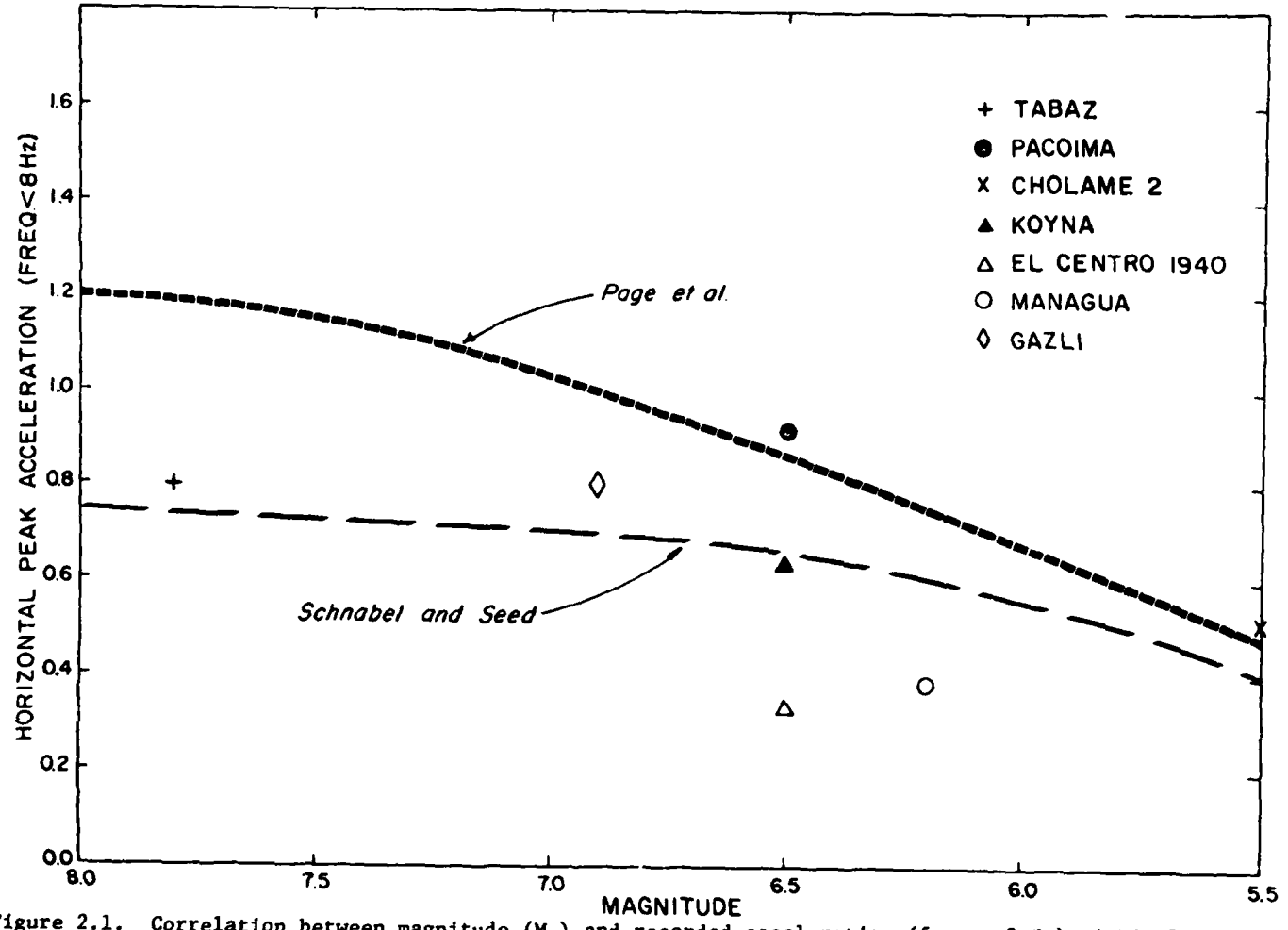

Figure 2.1. Correlation between magnitude (M_L) and recorded acceleration (freq. < 8 Hz) within 5 km of the causative fault. The curves are after Page et al. (1972) and Schnabel and Seed (1973).

evidence has come to hand recently which indicates that the threshold model is the more valid. First, the observations mentioned above of high peak accelerations obtained close to the source of small-magnitude earthquakes indicate that peak high-frequency energies do not depend strongly upon the ultimate total length and width of faulting.

Secondly, key evidence comes from a strong-motion record obtained in the city of Tabas in the Tabas, Iran,earthquake of September 16, 1968. The Geophysical Institute of Iran located the epicenter at 33.18°N latitude and 57.4°E longitude and the surface wave magnitude was assessed at 7.7. This earthquake is thus the largest as yet to have been recorded in the very near field. The surface faulting which occurred was, at its shortest distance, less than 10 km from the strong-motion instrument. As shown in Figure 2.1, the peak acceleration for this great earthquake (about 0.8g) fits well the threshold hypothesis. A working hypothesis is thus that the representative maximum acceleration values near to a fault are about the same at high frequencies for moderate magnitude earthquakes as for great magnitude earthquakes. We might expect that magnitude will show up as a more important parameter for wave amplitudes at longer wave length (periods greater than 2 sec , say) and will also be strongly correlated with the total duration of the shaking.

2.2 Duration

The concept of the duration of strong motion at a site is a crucial one in terms of understanding the dimension of the source and also in estimating the overall energy which should be incorporated in the input ground motions for any structure.

The physical model outlined in Section 1.3 predicts that the duration, if defined in a quantitative way, will be significantly dependent upon the dimensions of the faulted surface. The waves are radiated from the moving dislocation across the full dimensions of the plane; both magnitude and seismic moment reflect this dimension. (The magnitude estimate used for great earthquakes is the surface wave magnitude which is estimated from waves of period of 20 sec or even larger, which correspond to wavelengths of 50 km or greater. These wavelengths effectively sample the whole source dimension. The seismic moment defined by equation (1.2) is proportional to the dimensions of the faulted area.) Considerable weight can thus be given to the duration parameter in both the interpretation of strong-motion records and in the synthesis of time histories for a particular site.

Estimates for the bracketed duration (amplitudes greater than 0.05g) can be obtained from Figure 2.2. Three instrumental measurements (Bolt, 1973) are shown; a recent point is from the Tabas earthquake and is particularly important since it represents a measurement of duration of strong ground accelerations in the near field for a very large earthquake. (The end of the curve in Figure 2.2 for the large magnitudes was originally only weakly based on felt reports from large earthquakes.)

Deviations from the mean duration curve usually arise because of multiplicity of the earthquake source and also the special side effects of layering and soil conditions. Unfortunately, it is not possible to predict the

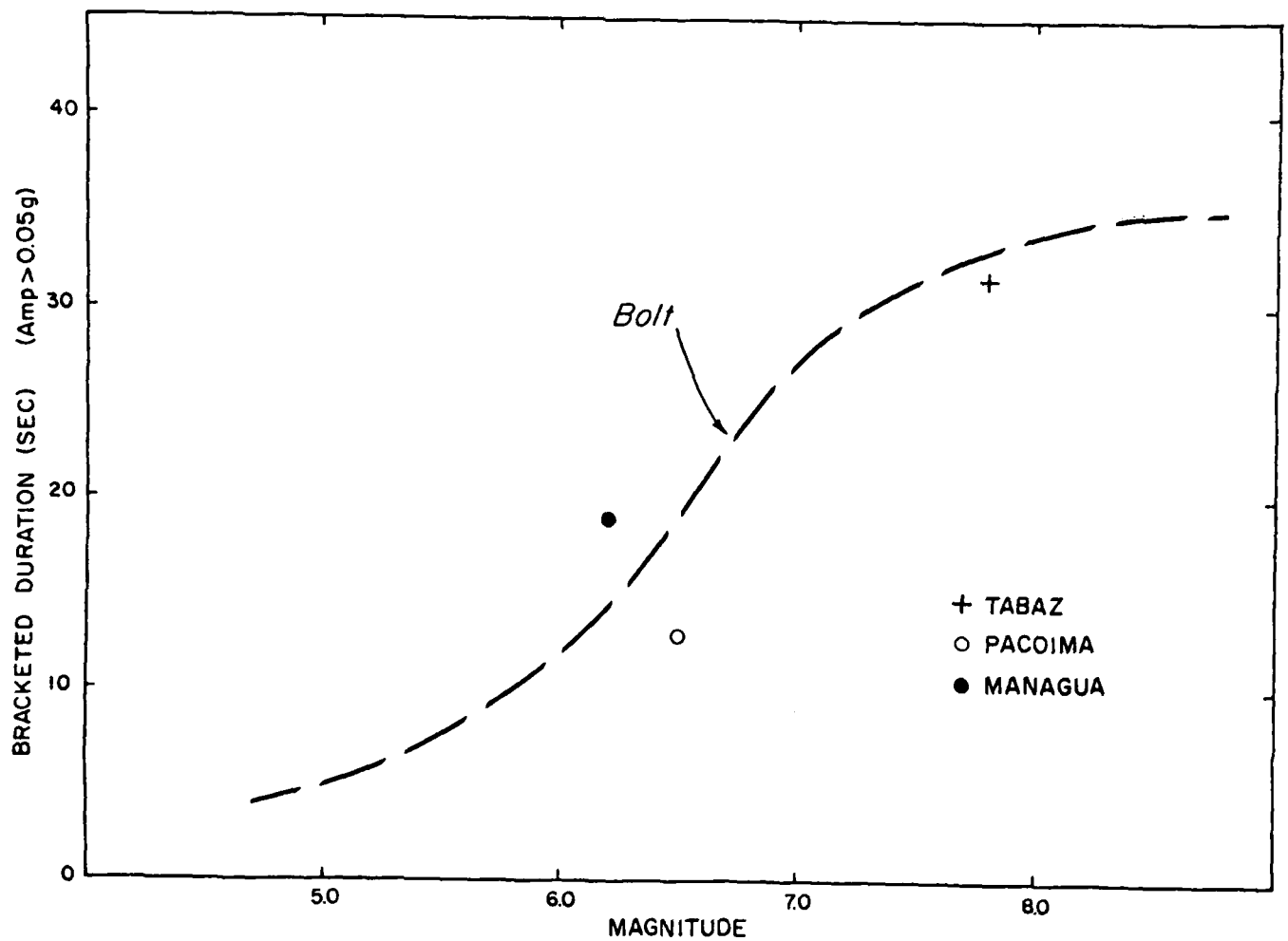

Figure 2.2. Correlation between magnitude (M_L) and bracketed duration (seconds) for amplitudes >0.05g. The curve is after Bolt (1973).

occurrence of a multiple earthquake in which the total motion is made up of two or three decisively distinct episodes of motion separated by some seconds. Such multiple shocks can be explained in terms of the model of Section 1.3 in the case when the dislocation breaks through rough spots or barriers on the fault plane.

In the case studies of Part III, the durations of the strong-motion records will be considered. Generally, the bracketed durations agree within 10 percent with the curve given in Figure 2.2 but, under certain special seismological circumstances (for example, the deep-focus Romanian earthquake, Section 3.7), deviations can be greater.

2.3 Patterns of Arrivals - Deterministic and Stochastic

After the appropriate duration of a strong-motion record is estimated, based on the seismic moment M_o or magnitude M_L of the earthquake, it remains to analyze the detailed patterns of groups of waves on the strong-motion record. An observatory seismologist becomes efficient at recognizing patterns of arrival of P and S body waves and surface waves when working with seismograms from distant earthquakes or small local ones. The question is to what extent can similar sets of stable patterns be recognized for strong ground motions in the near field. Let us consider four aspects of the problem.

(a) We have available three types of records. The primary seismogram in most cases is the accelerogram since such instruments are designed to record ground accelerations in the frequency range normally of interest to engineers. We also have the complementary records of wave velocity and displacement (see Figure 1.3). There thus could be three different dominant patterns, one for each of the three variables - acceleration, velocity, and displacement. In fact, the availability of these three time functions is of great assistance in the interpretation of strong-motion records. Accelerograms appear more structured, with many high-frequency pulses and considerable variability in amplitudes. The first integration to wave velocity considerably smooths these records and emphasizes frequencies in the middle range of interest. A third integration produces usually quite smooth displacement-grams with fewer fluctuations and a simpler pattern of dominant waves, usually with periods beyond one second. Sometimes, however, because of problems with baseline corrections and instrumental drift, the integrations produce large long-period bays and variations in the displacement records which may or may not be physically related to the seismic waves themselves. This type of long-period noise makes interpretation almost impossible.

(b) It has been known for some time that the general shape of strong-motion records can be simplified into three parts. The first is an increase in amplitude which is the envelope of the (largely) P-wave motion rising from zero up to the longer amplitudes. A middle section follows where the amplitude fluctuation remains more-or-less the same and which can be bounded by lines parallel to the base line. The final part of the pattern is a descending taper which encompasses the coda of the record and whose slope may be small. These attempts at simplification of the pattern certainly work for certain records (see, e.g., Figure 3.12)but are not very satisfactory in characterizing other important strong-motion records (see, e.g., Figure 1.1). Nevertheless, as the cases considered in Part III show, this tripartite division is a useful one (see Section 4.2). Deviations are not likely to seriously affect the overall spectrum of the time history for engineering design purposes.

(c) By analogy with regular seismograms of smaller ground motions we would expect there to be a wave pattern which follows the following properties. There should be an initial portion of ground motion made up mainly of the longitudinal P waves. Depending on the distance between the site and the source, there will then be an onset of S waves which will be superimposed on P waves still arriving from other parts of the moving dislocation. Greatly enhanced shaking will continue, consisting of an unknown mixture of S and P waves, but with the S motions becoming richer as the duration increases.

Later in the horizontal component records there will be surface waves of both Rayleigh and Love type, in general mixed with S body waves (see Figure 2.3). Again, depending on the distance of the site from the causative fault and also on the structure of the intervening rocks and soils, the surface waves will be dispersed into trains with certain frequency

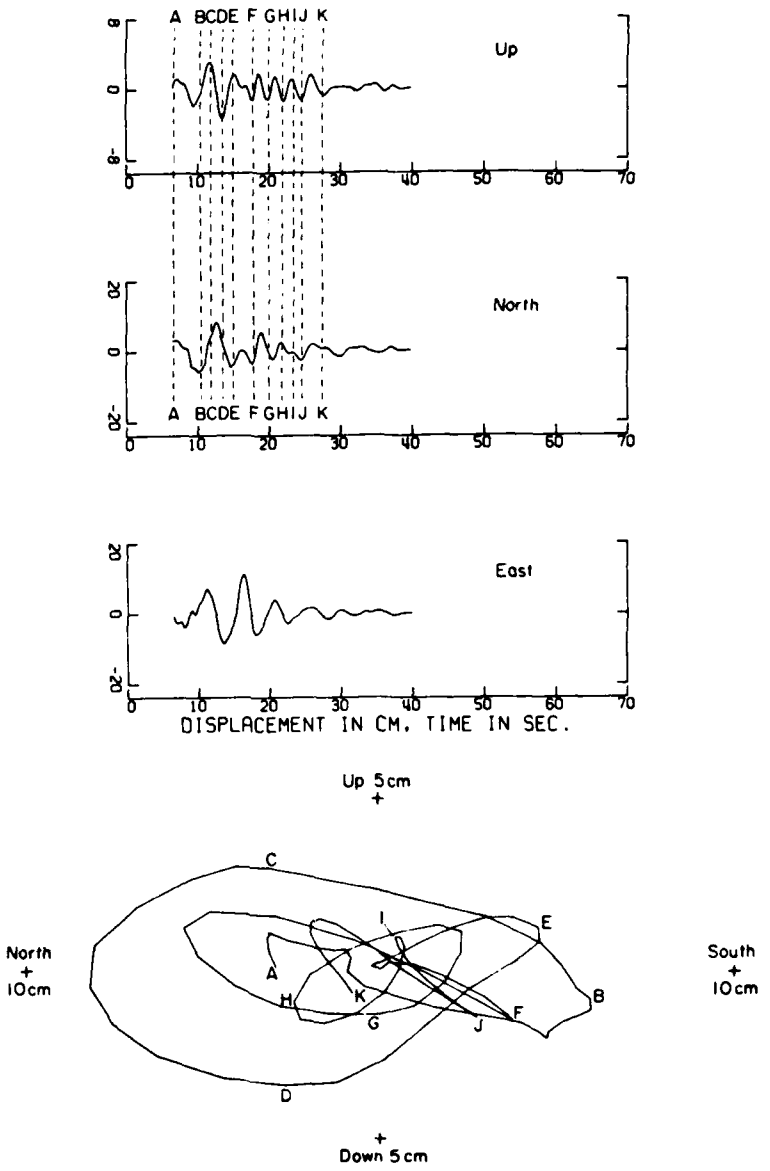

Figure 2.3. Three components of ground displacement obtained by summing several displacement records at strong-motion instrument sites about 20 km from the San Fernando fault rupture, 1971. The UP and NORTH components correlate well and give the particle motion plotted at the bottom. The motion is retrograde elliptical - typical of Rayleigh waves. The EAST (transverse) component does not correlate and may be interpreted as a Love wave train (after Hanks, 1975).

characteristics as a function of time (Hanks, 1975). This record coda is likely to be significantly affected by the focal depth of the faulted surface; the greater the depth, the less likely that a significant train of surface waves will be contained in the strong motions.

As we will see in the discussions in Part III, other portions of the record will contain pulses which can be explained in terms of special properties of the finite but extended source of the motions. If the dimensions and dynamic properties of the source were known, then the appropriate patterns could be built up in the time history for such wave pulses as the "break-out phase" and "stopping phase" (see Section 1.3). Since this is not likely to be the case *a priori*, these details are often not included.

(d) One pattern should be an ingredient of any realistic strong ground motion near to the causative fault. As mentioned in Section 1.3, there is seismological evidence that near to a ruptured fault a pulse of approximately one-second duration propagates outwards and affects structures on the surface (see Section 3.2). This pulse, however, may not have the largest accelerations on the record, although it may be associated with the greatest kinetic energy. It has been pointed out from studies of the damaged Olive View Hospital in California in the 1971 San Fernando earthquake (Bertero *et al.*, 1978) that failures in that structure apparently occurred during the long-duration pulse that can be seen in the Pacoima velocity record (see Figure 1.3) about 3 seconds after the instrument triggered. The hospital structure was forced out of its elastic range of response by this motion, with significant damage to the supporting columns of the lower floors. The subsequent strong ground motion of higher frequency (peak acceleration greater than 1.0g) then shook the damaged buildings without further significant inelastic displacements.

It must be regarded as good practice, therefore, to include at an appropriate portion of a near-source record (see Section 4.2) a longer period pulse which corresponds to the elastic rebound or "fling" along the fault as the dislocation passes by the site. The effects of this in engineering terms are important since the presence of this fling ensures that the longer period parts of the response spectrum are realistically energetic (see Section 2.1).

The above expectations have been based largely on the theoretical model. Such deterministic explanations of the observed wave patterns will normally be found to leave a residual portion of the record unexplained. These unexplained residuals are found particularly in studies with synthetic displacement records for wave frequencies above 1 Hz and for acceleration records. The unexplained portion must be dealt with stochastically, as suggested, for example, by Haskell (1964). An example of the problem is discussed in Section 3.4. From a theoretical point of view, this random component of strong ground motion can be thought of as arising primarily from the unknown distribution of roughness along the fault and, consequently, the unknown roughness distribution density $\Phi(\underset{\sim}{x})$. If this could be specified, then the stochastic problem would become a deterministic one. This stochastic component of strong ground motion has been one reason why one approach to modeling artificial time histories has been by random number generators (Penzien, 1970).

As yet, no roughness distribution densities have been proposed for different classes of earthquakes. In their recent barrier model for the earthquake source, Aki et al., (1977) propose three ways to estimate the interval between the significant barriers along an extended fault of the

area. The methods are a) surface measurement of the slip across the fault breaks, b) fitting the model with observed near- and far-field seismograms, and c) using data from small earthquakes in the region to scale upwards for the larger fault rupture. In general, we might assume on general physical grounds that each major type of fault has its own roughness distribution density $\Phi(\underset{\sim}{x})$. Thus, along the San Andreas fault, with its special tectonic history and mechanism, the function would be of one kind, whereas a fault like that that ruptured in the 1971 San Fernando earthquake might have a quite different roughness distribution function. In Section 4.2, a theoretical suggestion is made which might be helpful in the effort to specify and evaluate functions of this kind and test their utility.

2.4 Spectral Content

In this report, emphasis is given to the time histories of the strong ground motions. By contrast, in engineering practice at the present time, design requirements usually demand the provision of response spectra representing the ground motion at the site or its effect on a harmonic oscillation. Time histories, however, are also used, particularly for mechanical engineering tests and special analysis of critical structures. In the mathematical sense, the treatment of ground motion in either the time domain or the frequency domain is a matter of convenience and in certain interpretation problems it is essential to compare the representations in both domains (see Section 4.2). While in this work no general comparison is given between spectra of strong ground motions, there are two points about the spectral content of strong ground motions that are important in interpreting strong-motion records.

First, the spectrum from any artificial strong-motion record should not contain either gaps at certain frequencies or should not be deficient in energy at the longer period end of the spectrum. Of course, comparison of actual Fourier amplitude spectra from strong ground-motion records indicates significant fluctuations in the amplitude peaks of the spectra. For some time "average" design ground motions, however, have been used to avoid this problem.

There is also a measurement deficiency with many widely-used analog strong-motion accelerometers. Statistical analysis of the strong-motion records from the 1966 Parkfield earthquake and the 1952 Taft earthquake (Shoja-Taheri, 1977) indicates that the useful limit of long periods of velocity and displacement calculated by integration of analog accelerogram

records is restricted by human reading and by baseline correction errors. The long-period limits due to the combined errors vary between 7 and 14 sec. Beyond these limits, components of displacement spectra from the present analog accelerograms are not a reliable measure of ground motion. It has also been found that the usuable long-period limit with the standard analog paper records, T_c, varies (increases) with record length L. For L equal to 40, 50, and 60 sec, T_c is estimated to be about 10, 12, and 14 sec, respectively. At a period of about 16 sec, the combined errors for the majority of cases of strong-motion records studied exceed 25 per cent of the accumulative displacement amplitude spectrum. Digital records, however, from the newly available digital strong-motion accelerometers (see Section 4.5) should allow the above limit to be significantly extended.

Secondly, the spectrum of strong ground motions is in two parts. The first is the amplitude spectrum, which is normally all that is considered in strong-motion seismology and earthquake engineering. The second part, however, is the phase spectrum, and this phase defines the pattern of seismic waves, which is the subject of these interpretation studies. This property has not been as widely used in the construction of artificial strong ground motions as it deserves. For example, an amplitude spectrum from a magnitude 7.5 earthquake with adequate maximum amplitudes can be combined with the phase spectrum from another earthquake (with smaller amplitudes, say, than required) but with a phase spectrum appropriate to the wave pattern for very near-fault motions.

A computed illustration is given in Figure 2.4 which shows a horizontal component spectrum of the Pacoima record combined with the phase spectrum from the horizontal record from Parkfield (Station 2). In this

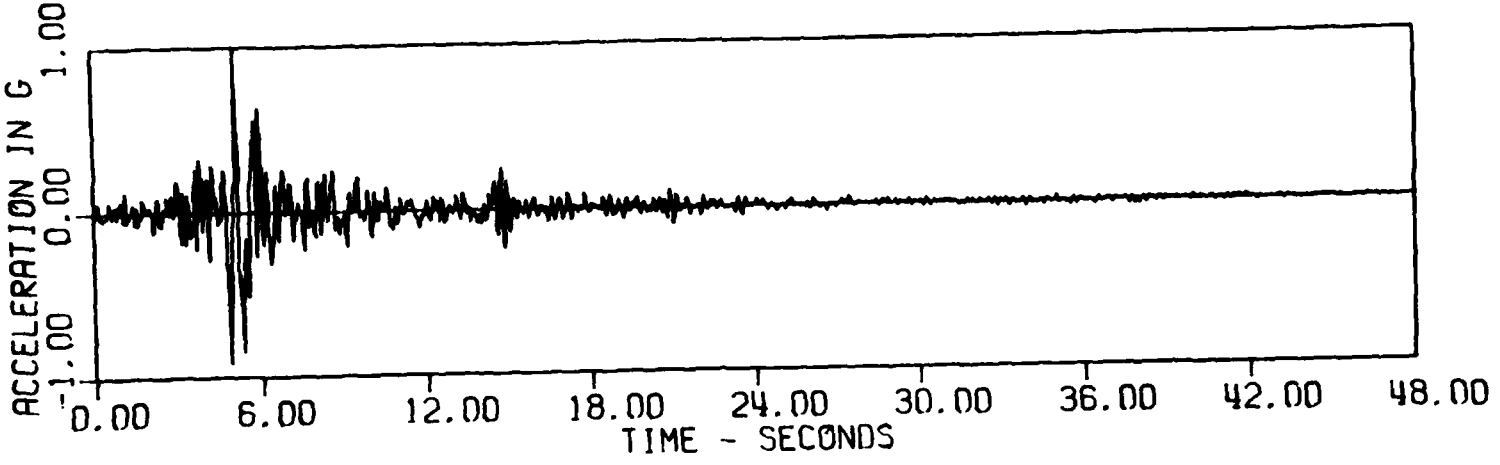

Figure 2.4. Synthetic accelerogram constructed from the Fourier amplitude spectrum of the S16E horizontal component Pacoima record (Figure 1.1) and the phase spectrum of the Parkfield Station 2 record (Figure 3.4).

way, a more realistic time history is obtained (in terms of the arrivals of specific seismic waves and the inclusion of fling) for a near-field earthquake (M_L = 6.5) produced by strike-slip faulting. (Compare the records in Figures 1.1 and 3.4). This idea has been incorporated in the construction of the artificial record which is given in Section 4.2.

In theoretical terms, a permanent offset along a fault occurring in a few seconds must produce seismic waves which are rich in longer period waves. Spectral curves from near-field records will show displacement amplitudes inversely proportional to frequency. As the seismic waves travel away from the seismic source, the very long-period amplitudes (static offsets) are reduced, thus enhancing relatively the higher frequencies. An example of amplitude spectra of strong-motion records is given in Figure 2.5.

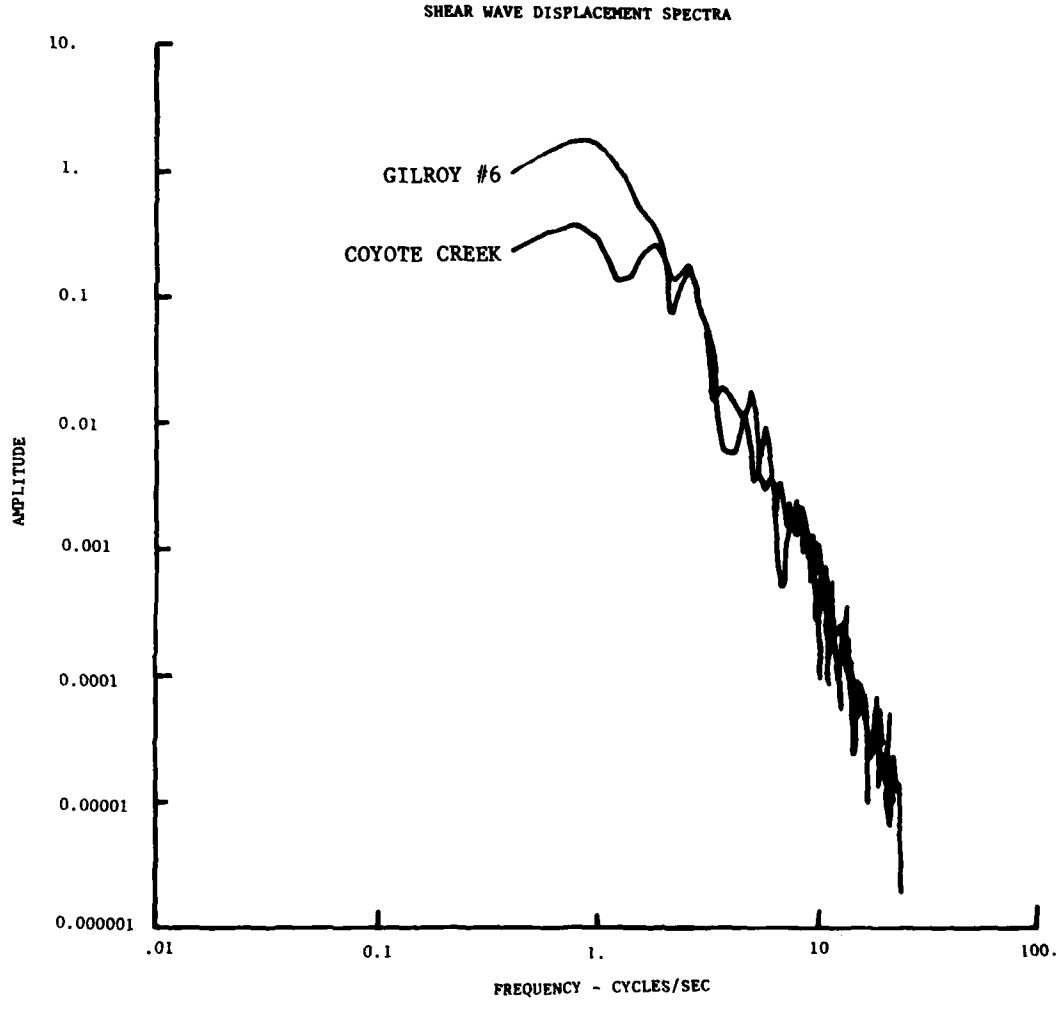

Figure 2.5. Wave displacement Fourier spectra calculated from two strong-motion records of the August 6, 1979, Coyote Lake, California earthquake (after Singh, 1981).

2.5 Effect of Fault Properties

An indication has already been given in Section 1.3 of some of the ways in which the geometrical and physical properties of the fault source enter into the generation of seismic waves. Let us consider here in a little more detail the way that fault properties complicate both the interpretation of strong-motion records and the prediction of ground motions for engineering design purposes.

In the first place, theoretical calculations show that the mechanism of faulting affects significantly the seismic ground motion produced. Thus, dislocation models for strike-slip faults produce different synthetic ground motions than models for dip-slip faulting. In some circumstances, the predominant nature of faulting is known, as, for example, the source mechanism of large earthquakes along the San Andreas fault system (right-lateral strike-slip). It must be observed, however, that most faulting tends to be complicated and composite. Evidence of this comes both from fault plane solutions (see Figure 3.30) which usually show components of both vertical and horizontal motions, and also the geological field evidence for fault offset at the surface.

As yet, there are insufficient theoretical cases solved to provide a comparative set of synthetic ground motions for the main types of earthquake mechanisms. On the observational side, again there are insufficient detailed case studies to confirm major inferences. It seems reasonably clear, however, that fault dislocations with predominant vertical motions give rise to larger vertical components of strong ground motion near to the source (made up largely of P and SV motion) than do fault dislocations with predominantly horizontal slip (producing mainly SH motions). The case histories in Part III are generally in agreement with this proposition with the sharp

exception of the 1979 Imperial Valley earthquake which, although seemingly predominantly strike-slip, had high vertical accelerations (see Section 3.9). Other effects such as surficial soil and rock structure near the fault can clearly mask the effect of the earthquake mechanism.

It has been observed that seismic waves are markedly refracted laterally in certain circumstances near to major faults (Uhrhammer, 1981). For example, very close to the San Andreas fault in central California, P waves have been observed refracted by 30° away from linear paths. The reason for this lateral refraction is the existence of low-velocity material in the fault zone. This material consists of shattered rock, subsidiary faults, and layers of fault gouge (a clay produced by the crushing of rock by repeated fault movements). The seismic wave velocities in the gouge material are relatively low (as low as 1 km/sec) and have the effect of sharply refracting the waves as they pass through the gouge into the more rigid country rock. The width of the gouge zone may extend horizontally up to one or two km and several km with depth. Indeed, gouge material might extend to considerable depth under high temperature and pressure along all major fault zones. The gouge may make up a mosaic patchwork producing the roughness or barrier model (see Section 1.3).

The presence of weak and shattered material-like gouge in the zone of the earthquake source also has other implications in the use of mathematical models for predicting the onset of phases, since, in viscoelastic materials, separation between pure P and pure S motions may not occur. The variation in properties of the shear gouge may also produce zones where anisotropy is significant and this also may complicate wave motions.

Perhaps the most important aspect, however, of the presence of shear zones of low rigidity rock along the fault zones is the damping character-

istics of the viscoelastic material. There is likely to be much more damping of high-frequency waves propagating through this material than for waves propagating through the elastic country rock. Some measurements of the attenuation parameter Q (defined as the number of oscillations for a decaying sinusoid to fall to $100/\exp \pi = 4.3$ percent of its initial value) indicate values as low as 10 and 20 in the fault zone. The implications of this damping are important in terms of putting an upper bound to the peak high-frequency acceleration amplitudes (see Section 2.1) near to the earthquake source and in limiting the duration of shaking from the fault rupture (see Section 2.2) and in controlling and limiting the extent of kinematical focussing due to the moving dislocation (see Section 2.6).

2.6 Directivity and Focussing

A major practical question in strong-motion interpretation and construction of artificial time histories is to what extent the time history at a particular site is dependent upon the location of the rupture on a given fault. It is known both theoretically and observationally that each seismic wave type has a directivity function which depends on the azimuth relative to the center of the earthquake source (see Figure 4.7).

Consider the seismic sources in the form of superimposed force couples (or a seismic moment tensor). This representation entails that each type of seismic wave has its own radiation pattern. Thus, for example, a vertical strike-slip fault can be represented by a double couple with center at the focus; the radiation pattern for SH waves will consist of a four-lobed pattern with maximum amplitudes at directions normal and along the faulting. Similarly, P waves and Rayleigh waves will have appropriate radiation patterns (Aki and Richards, 1980). Because the intensity of ground shaking is the effect of all the waves that arrive at a point, these radiation patterns are not always obvious by looking at isoseismals based on the assessed intensity. Nevertheless, in the interpretation of accelerograms and numerical modeling of synthetic strong-motion records, seismic radiation patterns are essential ingredients.

In the case of large earthquakes where the rupture length L is significant compared with the wave lengths considered, the radiation pattern becomes more complicated. Rather than the usual symmetric pattern typical of a stationary point source, the radiation pattern lobes for the various seismic waves become retracted or extended, depending on the direction of rupture along the fault. There are now published a number of reasonably representative radiation patterns for moving earthquake sources which are helpful in

the interpretation of strong-motion records (see, e. g., Ben-Menahem and Singh, 1972). This effect of rupture velocity is called dynamical directivity, and it is an important matter to detect this directivity on strong-motion near-field records. Because of the various complications, this has not yet been yet been clearly accomplished in the near field, although these patterns are widely verified in the far field.

Another aspect of the moving seismic source is the occurrence of a Doppler-like effect analogous to sound radiation on an acoustic point source that moves in a medium at rest. If, when stationary, the source has a symmetric radiation pattern, its radiation would be expected to be focussed in the direction of motion when it is moving with a finite velocity. The amount of focussing, in general, will be different for the case when the source velocity V is subsonic ($V < \alpha$ for P waves) or supersonic ($V > \alpha$ for P waves). A purely geometrical argument (Morse and Ingard, 1968) gives rise to the well-known focussing factor

$$F = (1 - M\cos\theta)^{-1} \tag{2.1}$$

where θ is the angle subtended by the direction of the wave from the source and rupture direction and M is the Mach number V/α. The result is that, depending on the angle θ, there is a Doppler shift in both the wave amplitude and frequency.

Various examples have been cited by seismologists (e.g., Benioff, 1955) that strong-motion data obtained from stations along the direction of the ruptured fault evidence the focussing of earthquake motions. Reasonable values for the parameters in the above formula indicate that the focussing effect might (for a perfectly elastic non-attenuating medium) change the wave amplitude by a factor of up to 10, with an increase in front of the rupture

and with a decrease behind. There will similarly be an increase in frequency in front of the rupture and a decrease behind.

Evidence for directivity focussing in actual earthquakes is discussed in Part III (see Sections 3.1, 3.8, 3.9, and 3.10). The effect on strong ground motion is important in both interpretation and prediction of strong ground motions for design, since, if a structure is built close to a fault, motions may differ depending on the direction of rupture relative to the structure.

2.7 Effect of Complex Propagation Paths in Ground Structure

In Sections 1.2 and 1.3, the effect of horizontal layering in the crustal rocks on seismic waves has been outlined. In many situations, however, particularly in fault zones, the variations in soil and rock structure are not restricted to plain parallel horizontal layering. Particularly in sedimentary basins there will be significant lateral variations and often irregular shaped and sloping rock structures. The behavior of elastic waves encountering such physical obstacles is mathematically complicated and only a few special cases have been treated theoretically. Indeed, mode conversions, scattering, diffraction, and resonance make even numerical estimates for standard procedures extremely difficult. In these circumstances, the elementary ray approximation may perhaps be misleading, so that the simple approaches must be used with caution wherever there is evidence of marked inhomogeneities in structure.

The problem is that normally the presence or absence of seismic structural anomalies is unknown. Even with deep borehole data and geophysical profiling, large-scale anomalous bodies of arbitrary shape along active fault zones may not be well defined. Nevertheless, it has been common for seismologists and engineers to call on this hypothesis to explain rapid variations in intensity in areas of heavy shaking. It is one way to explain, for example, the reason why a pocket of high intensity is seen at one place and yet no damage occurred to similar structures in another part of the area about the same distance from the earthquake source. The explanation, therefore, is usually open to question even though such structurally anomalous bodies would certainly focus seismic waves by refraction in the same way that light waves are focussed by a lens. This mechanism of seismic focussing is, of course, quite different from that in the previous section.

The prediction of strong ground motion in circumstances where the rock structure is complicated depends upon the use of numerical methods to solve the differential equations. The finite element method of approximation is one such scheme. In the last six years, it has been shown to be applicable for the computation of surface wave excitation of geologically complicated structures (Drake,1972a,b; Bolt and Smith, 1976). A number of problems have been solved to demonstrate the effect of surface topography and varied structures on plain or cylindrically propagating P and S waves and dynamic finite element models of fault rupture have been used to compute fault ruptures (McCowan, et al., 1977).

An illustration of the use of such calculations to help explain strong motion is the case of the Pacoima strong-motion record (Figure 1.1). Because the recording instrument was on a ridge which connected with the abutment of the dam, the question arose whether this rapid variation in topography might not explain the high accelerations observed in this case. A number of calculations (Boore, 1973; Smith,1975a,b)indicated that, indeed, ridge topography could cause variations in the amplitudes of SH, SV, and P waves of over 100 per cent in certain frequency ranges. It was also demonstrated that a unique deterministic explanation of a particular peak along these lines was not yet possible.

A long-standing problem in seismology and earthquake engineering is the effect that deep trenches, canyons, and scarps have on seismic waves incident on the topographic feature. Studies on two-dimensional mountain scarps and canyons, using analytical and numerical methods (Boore, 1970; Smith, 1975b;Bolt and Smith, 1976), indicate that topography can have significant effects on wave patterns and spectral content.

On the engineering side, there have been suggestions that deliberately engineered barriers, such as trenches or zones of rock shattered by explosives, might be used to reduce the intensity of shaking at a particular site for certain frequency ranges (Lysmer and Waas, 1972). The basic idea is that a ringed zone of altered rock whose average elastic parameters differ appreciably from those of the unaltered rock on either side may reduce seismic motion (see Figure 2.6) by reflection,scattering,and wave conversion. In this way, wave energy would be screened from the internal site and geophones within the ringed zone would show lower wave energy than if the barrier were not present.

The investigation of seismic barriers is not new, but only limited results have so far been published. The main aim of the study undertaken here,related to this program of research,was to extend and test the results of previous investigations, the layered crustal models with trenches, but using a more general seismic wave input. Another aim was to obtain theoretical results for a more realistic model by including the effect of damping on the seismic waves. A more complete account of the work may be found in the paper by May and Bolt (1981).

The numerical code used for this study was the dynamic finite element program developed by Smith (1975a). The method employs integration in time and, under certain conditions, provides cancellation of unwanted reflections from the sides of the finite element mesh. Like other finite element schemes, the response of the code is severely wave-length limited. The original program was modified to provide up to 7,000 nodes (6,831 elements) for the P-SV case and 10,000 nodes (9,801 elements) for the SH case. Programs were also modified to produce snapshots of the propagating wave field throughout the

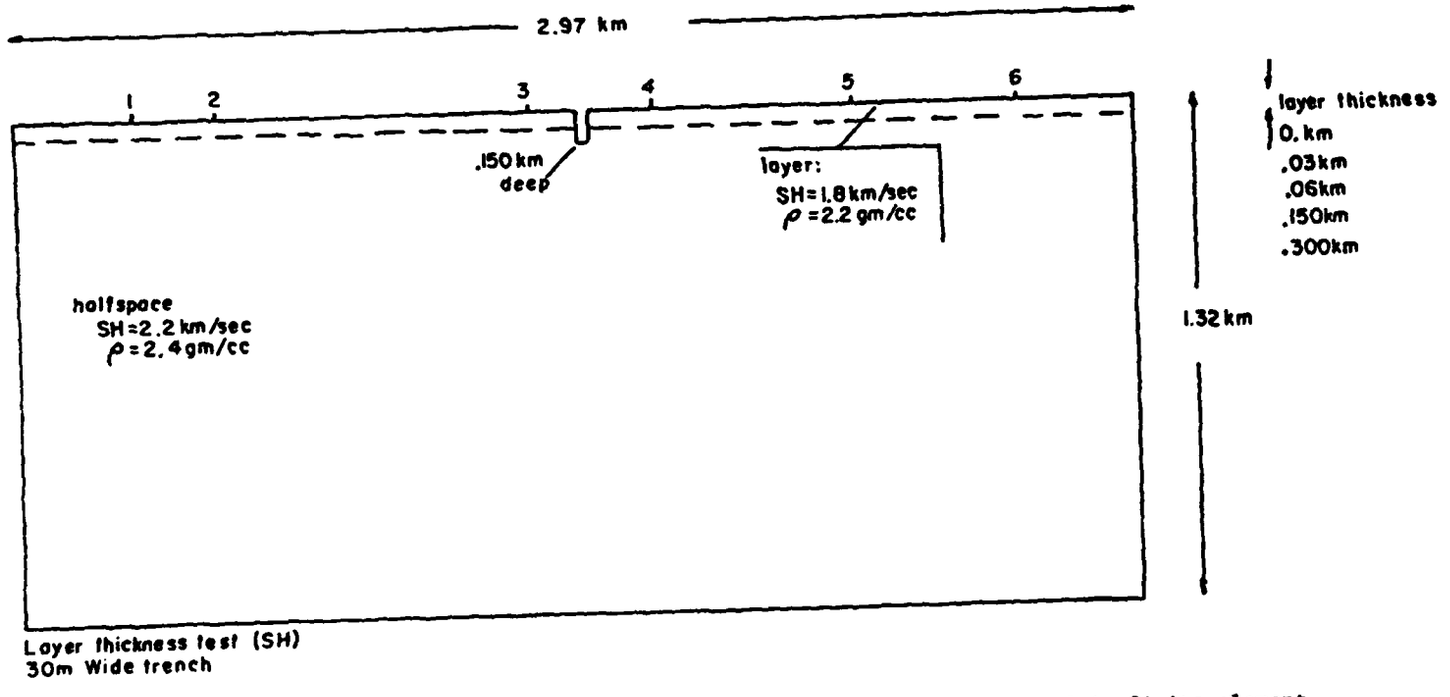

Figure 2.6. Model of an elastic half-space with trench and surficial layers used in finite element calculations. The thicker the layer relative to the depth of the barrier, the more surface wave energy passes around the barrier.

mesh at selected time intervals. Input to the finite element grid was a constant 10-cm displacement lasting 0.1 sec at the upper left-hand corner of the grid. One illustration of the results is reported here in the case of SH waves. In Figure 2.6 is shown the case of a single open-air trench (30 meters wide by 150 meters deep). A crustal model was simulated by a grid containing 4,500 nodes. Each element was a square 30 meters on a side. The layer thicknesses included a half-space model with zero layer thicknesses and thicknesses of 30 meters, 60 meters, 150 meters, and 300 meters.

Figure 2.7 is a computer-generated contour map showing the advancing wave front (labeled a), an incoherent zone (labeled b) of energy due to dispersion introduced by the finite element approximation, and a reflection from the left-hand bottom corner of the grid which was not cancelled. Of interest is the early formation of a reflected wave field with opposite nodal motion at the trench boundary (labeled c). At a later time, the reflected wave field was enlarged in width and extended deeper into the model. The reflection travels with the same velocity as the incident wave field. Except the disturbances caused by the upgoing mesh reflection, the lower part of the incident wave field (labeled d) has not been significantly changed by interaction with the trench.

From studies of this kind and also studies of the spectra at various points along the top of the mesh, certain important conclusions concerning the effect of trenches and scarps on strong ground motion were obtained. First, as might be expected, it was found that as the thickness of the layer increases for fixed trench depth, significant differences in wave fields appear. The surface portion of the wave field slows and broadens, especially after encountering the trench, and the transmitted and diffracted part of the incident wave field that occupies the space behind the trench is modified

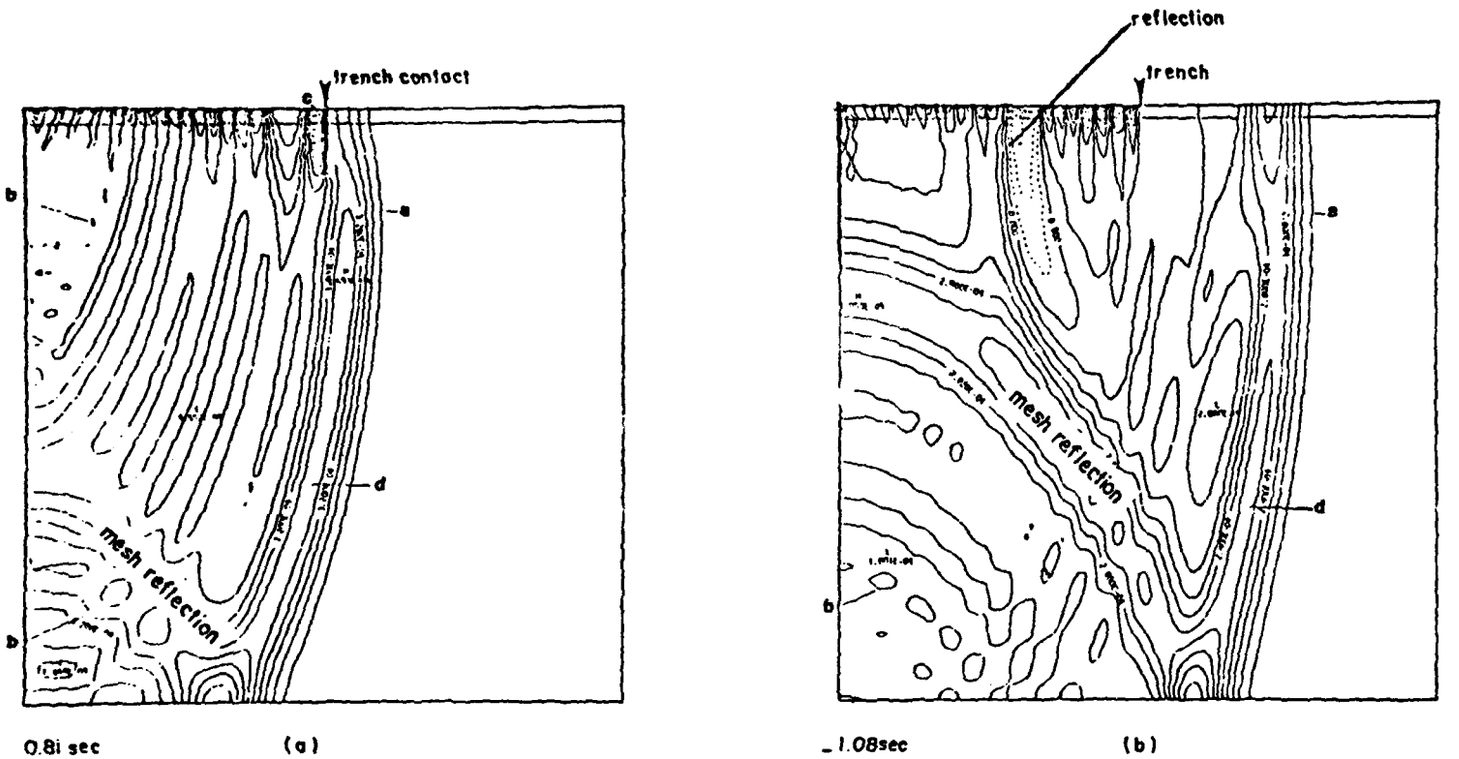

Figure 2.7. Computed SH wave fields for the model defined in Figure 2.6. Contours show lines of equal mesh displacement at two times after the application of an SH pulse at the upper left corner of the model. Vertical exaggeration is 2.25 and the surface layer width gives the linear scale.

less and less. And, lastly, the back reflections from the trench are less pronounced.

Calculations brought to light the marked role of surficial layering in attenuation properties of the surface rocks or soils on the effectiveness of seismic trench barriers. Barrier models without these features cannot, in general, reliably predict seismic wave fields at the surface. In the range of cases studied, trench depth d, rather than width, is the most sensitive parameter. When the ratio d/λ, the ratio of trench depth to the wave length of shear waves, is greater than about 0.6, spectral ratios of 0.06 and less are found for SH waves for frequencies of 4 to 6 Hz. By contrast, for frequencies less than 3 to 4 Hz, power spectral ratios from unity to about 2 and greater are observed, indicating amplification for the horizontal component of wave motion. Spectral ratios calculated at some locations in front of the barrier system show over two-fold amplification. The spectral ratios also changed significantly with the relative location of the free surface observation point.

PART III

CASE STUDIES

Ten earthquakes have been selected for exploratory analysis because of the availability of clear strong-motion records and considerable seismological information. As well, the records interpreted represent a rather broad sample of source types and observation situations.

3.1 Kern County, California - July 21, 1952

References: Gutenberg (1955a); Bolt (1978); Hanks (1978)

Location:
- Earthquake: 35°00'N, 119°02'W
- Accelerometer: Lincoln School, Taft AR-250 (USCGS)
- Foundation: 8-m-thick alluvium, overlying sandstone

Size:
- Magnitude: M_L = 7.2 (revised)
- Moment: $M_o = 2 \times 10^{27}$ dyne cm
- Mean Stress Drop: Δp = 60 bars

Fault Source Characteristics:
- Faulting: A number of small segments of left-lateral, steep reverse faulting observed along 31 km of White Wolf Fault. Maximum slip rates observed:
  - 1.2 m vertical (south block up)
  - 1.0 m left-lateral
- Focal Mechanism:
  - Strike N50°E
  - Dip 60-66°SE
  - Motion reverse, left-lateral
- Parameters:
  - L = 31 km
  - W = 25 km
  - D = 1.1 m
- Mean Rupture Velocity: 2.2 km/sec

Peak Wave Amplitude Values:

	VERT	S69E	N21E
Acceleration (cm/sec^2):	102.9	175.9	152.7
Velocity (cm/sec):	6.7	-17.7	-15.7
Displacement (cm):	-5.0	-9.2	-6.7

Bracketed Acceleration Duration (Acc. > 0.05g):

d = 19.5 sec

General Aspects:

The Kern County earthquake was the strongest (M ≈ 7.7) in California since the San Francisco earthquake, 1906, with major damage occurring in the Bakersfield-Arvin-Tehachapi region.

Geologically, the region consists primarily of crystalline and granitic rocks which rise to the E and SE to form the Sierra Nevada and Transverse Ranges and plunge steeply to the SW, forming the bottom of the elongated San Joaquin Basin. Within this basin has been deposited a heterogeneous series of sediments which at places attain the thickness of 8 km.

The earthquake originated on the White Wolf fault along the margin of the northern foothills of the Transverse Ranges with an ENE-WSW direction. This fault, being a northern subsidiary of the Garlock fault, is one of the shortest known to have been responsible for a major earthquake in California. Although it manifested a considerable horizontal (left-lateral) displacement, it is essentially a reverse fault which has experienced a large vertical component of movement (about 3000 m) in the geological past.

Interpretation (Taft records):

Extensive surface faulting was observed in this earthquake, which may have extended a total length of over 60 km. The fault trace showed considerable curvature and en echelon offsets. (A map of the faulting is available in Richter, 1958, Figure 28-27.) The most continuous portion of the fault had a length of about 51 km of surface rupture. The faulting was dip-slip with downthrow to the west, but there were small segments of left-lateral motion.

A very simplified model of the fault surface in relation to the Taft record is shown in Figure 3.2. The distance of the epicenter from Taft is 40 km, the focal distance is about 45.5 km, and the distance to the extreme northerly point B of the surface faulting is about 88.5 km. The southwesterly extent of the surface rupture is not known, but in Figure 3.2 is shown as perhaps extending southwest well beyond the focus.

The records to be interpreted (Figures 3.1a, 3.1b, and 3.1c) are the widely used strong-motion Taft accelerograms and the corresponding velocity and displacement records. It should be remembered that there are difficulties in obtaining the integration constants with analog records of the kind obtained at Taft and some of the longer period motions appearing on the displacement records may be an artifact of the numerical algorithm used. Also note that the vertical scales differ from component to component.

In Part III, unless otherwise specified, we assume a mean rupture velocity of 2.2 km/sec, a shear velocity beneath the surface alluvium of 3.3 km/sec, and a corresponding P velocity of 5.5 km/sec.

Consider first the P waves. With a velocity of 5.5 km/sec, the first P wave to arrive at Taft from the focus would travel for 8.2 sec. and the corresponding S wave would arrive after 13.6 sec, giving an S-P interval of 5.4 sec. We interpret the onset of the first large motion associated with the peak acceleration on the S69°E record (see Figure 3.1b) as the onset of the S wave from the focus. Although this onset occurs on both horizontal components, it is not clear on the vertical component, in agreement with the properties of the S wave traveling rather steeply upwards from depth (see Figure 3.1a).

The S wave onset time is 3 sec in Figure 3.1b. If we assume the instrumental start-up time to be 0.1 - 0.2 sec (see Hudson, 1970), there is a delay of 5.4 - 3.2 = 2.2 sec. Thus, the instrument may have triggered late, the velocities may need adjustment, or possibly the focus was nearer to Taft. (Given the care in the location of the focus by Cal Tech investigators, the latter seems unlikely.)

The last S wave to arrive at Taft would probably radiate from the dislocation as it comes to rest at points below B. An S wave from B would take about 50 sec to arrive at Taft. The interval, therefore, between the S wave from the focus and the S wave from the northeast edge of the rupture would be about 37 sec. This arrival time is marked with an arrow in Figure 3.1b and corresponds approximately with the cessation of high-frequency shaking in the horizontal direction. In this interval, the amplitude of the ground velocities is relatively high and their periods are of the order of one sec. (Note on Figure 3.1a the uneven long-period motion on the velocity record in the vertical component. This motion might represent P waves, but the wave pattern is complicated and not readily subject to theoretical explanation. It may be that the longer period motion is an artifact of the numerical method used to obtain these rather low velocities.)

As we move down the record, the accelerations decay but, beyond a time of 30 sec, the velocity displacements records on all three components show the development of a relatively large monochromatic wave train. Indeed, it has the largest displacements on all three components. One explanation is that this is a surface wave train (mainly Rayleigh waves because of its presence on the vertical component) which is being guided

by the surficial alluvial layers between the White Wolf fault and Taft. Given the geometry shown in Figure 3.2, the velocity of such a Rayleigh wave train would be rather low, approximately 1 km/sec, with periods of 5-10 sec. Such a surface wave train is quite compatible with theoretical considerations. For example, Mooney and Bolt (1966) have shown that for a sedimentary basin, thickness 3 km, the fundamental Rayleigh mode has a minimum group velocity at a period of about 5 sec at a velocity of about 1 km/sec.

Finally, the bracketed duration (above acceleration 0.05g) is about 20 sec. For a total length of faulting of 60 km and a rupture velocity of 2.2 km/sec, we would expect waves to continue to be radiated from the moving dislocation for about 25.5 sec. Because an allowance has to be made for the attenuation of the seismic wave from the fault surface to Taft, there is an adjustment of about +5 sec to the observed value (Bolt, 1973). There is thus reasonable agreement with the observed bracketed duration. In other words, the assumed dimensions of the fault surface and a rupture velocity of about 2.2 km/sec are consistent with the duration of strong acceleration on the Taft record.

The above interpretations are, of course, subject to many uncertainties because of the undoubted complexity of the crustal structure and the faulting process in this earthquake. It has been pointed out, for example, that about 120-meter length of vertical faulting was observed on the Garlock fault after this earthquake. The latter fault offset is about 30 km from the White Wolf fault, which undoubtedly was the primary seismic source, but "sympathetic" dislocation of other faults in the region may also have occurred.

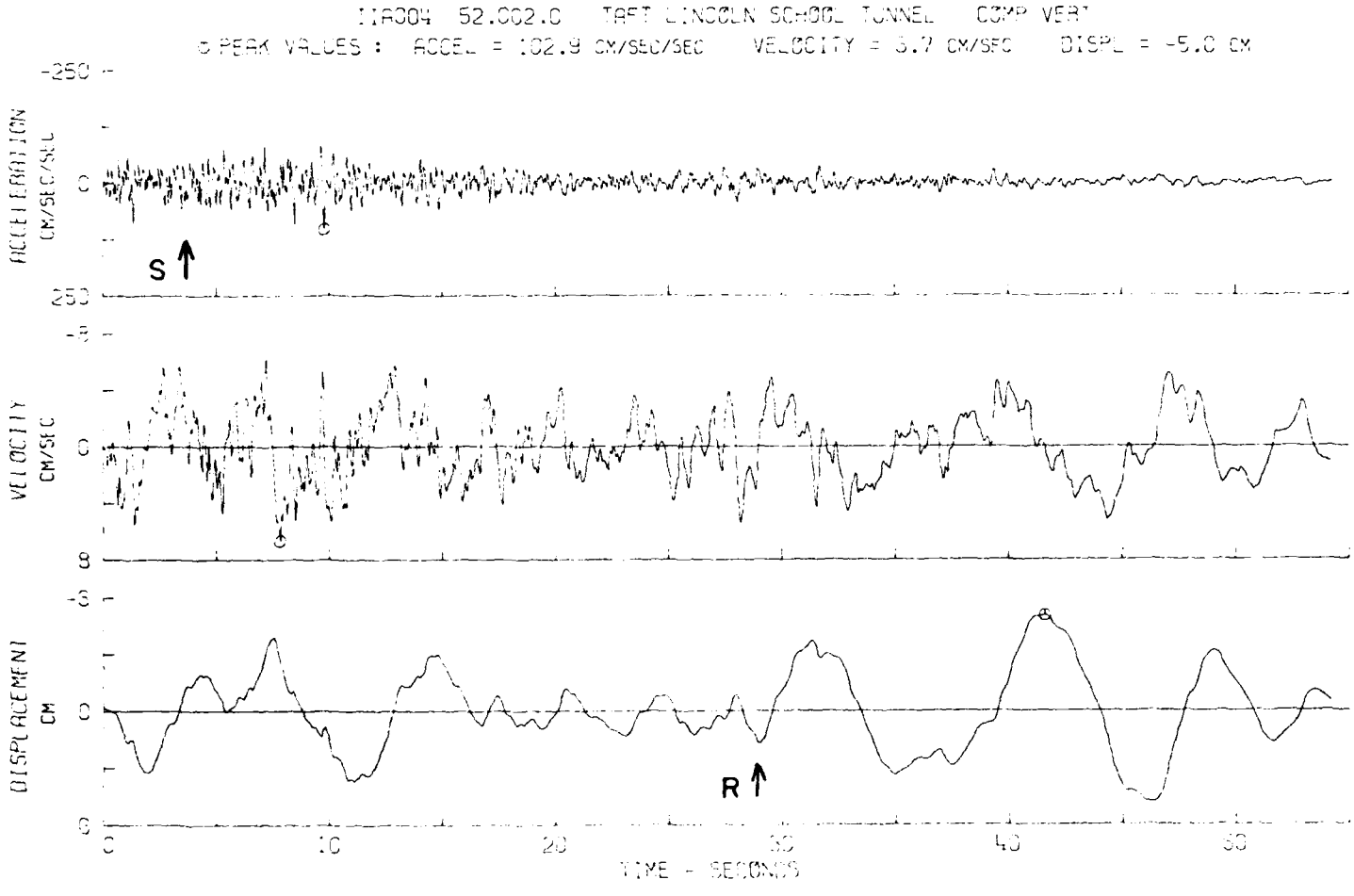

Figure 3.1. Kern County, California, earthquake; July 21, 1952 - 0453 pdt (Sheet 1 of 3).

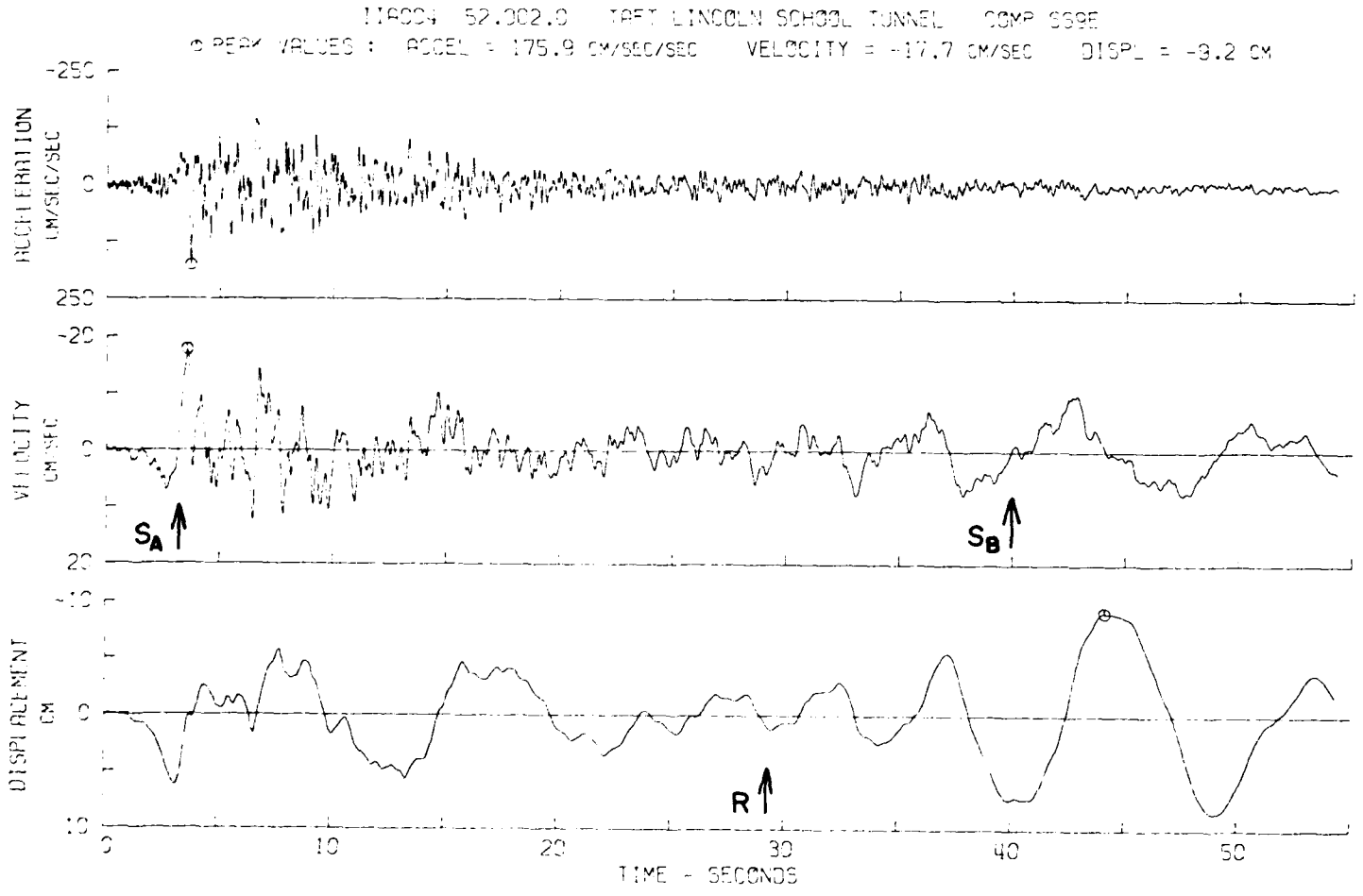

Figure 3.1. (Sheet 2 of 3).

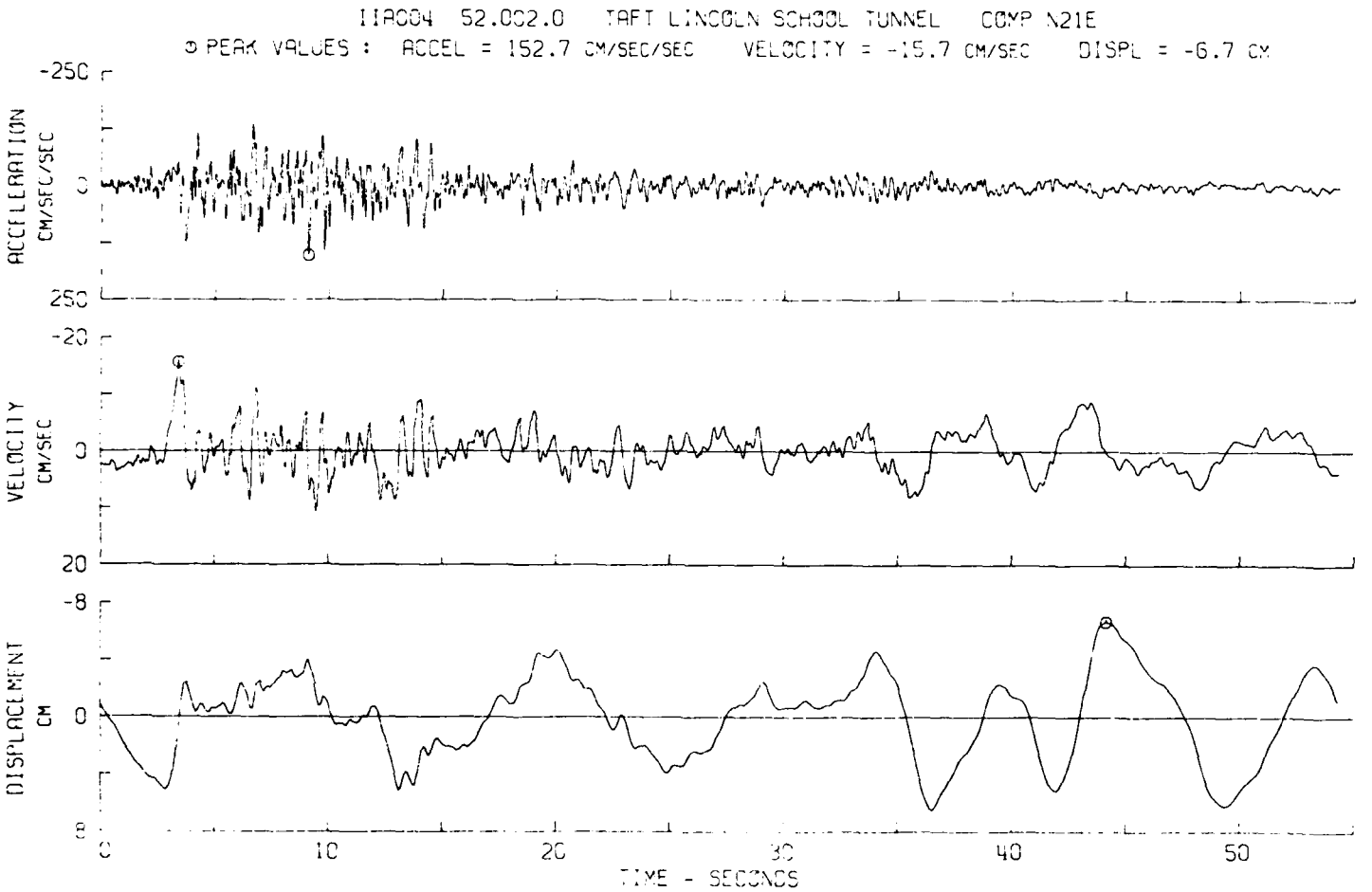

Figure 3.1. (Sheet 3 of 3).

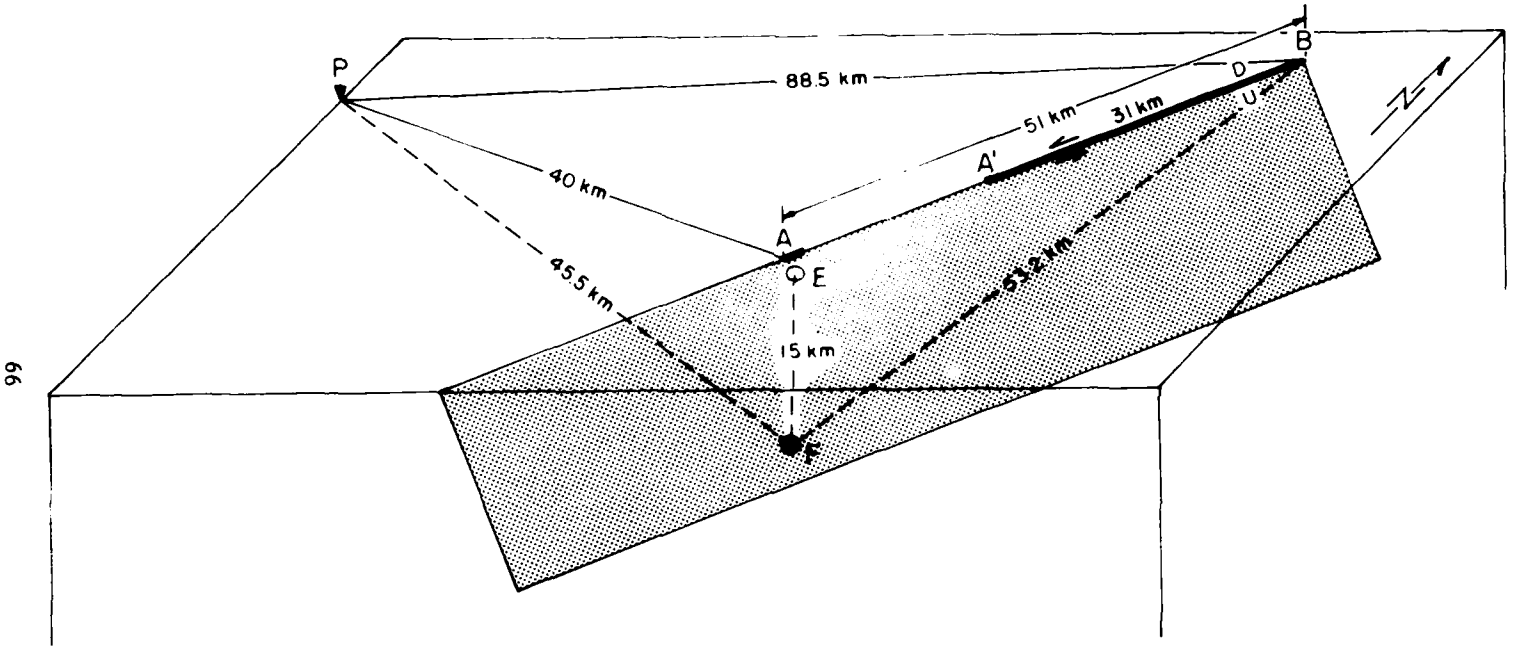

Figure 3.2. Simplified model of the rupture surface in relation to surface faulting, Taft station (P), epicenter (E), and focus (F) for the 1952 Kern County, California earthquake.

3.2 Parkfield, California - June 28, 1966

References: Coffman (1966); McEvilly et al. (1967); Aki (1968); Eaton et al. (1970); Anderson (1974)

Location: Earthquake: 35°57.3'N, 120°29.9'W

Accelerometers:

1. Temblor AR-240
2. No. 5 AR-240
3. No. 2 AR-240

Foundation:

1. On sandstone
2. On alluvium
3. On alluvium

Size:

Magnitude: $M_L = 5.5$

Moment: $M_o = 1.9 \times 10^{25}$ dyne cm

Mean Stress Drop: $\Delta p = 3.1$ bars (estimated from parameters below and equation 1.1.)

Fault Source Characteristics:

Faulting: Rupture observed predominantly along a central segment of the San Andreas fault. Strike is N33° - 39°W; dip is 86° - 90°E. Predominant right-lateral motion with maximum slip of 21-25 cm.

Focal Mechanism: Strike N29° - 35°W; dip 85°SW - 88°NE. Motion was right-lateral, 26° to 13° upward component on SW block.

Parameters:

L = 40 km

W = 12 km

D = .21 - .25 m

Mean Rupture Velocity:

2.5 - 2.9 km/sec

Peak Wave Amplitude Values:

1. Temblor	DOWN	N65W	S25W
Acceleration (cm/sec^2):	-129.8	-264.3	-340.8
Velocity (cm/sec):	4.4	-14.5	22.5
Displacement (cm):	1.4	4.7	-5.5

2. No. 5		DOWN	N05W	N85E
	Acceleration (cm/sec^2):	-116.9	-347.8	-425.7
	Velocity (cm/sec):	-6.8	-22.5	-25.4
	Displacement (cm):	-3.4	-5.2	-7.1
3. No. 2		DOWN	N25W	N65E
	Acceleration (cm/sec^2):	-202.2	out	-479.6
	Velocity (cm/sec):	-14.1	out	-77.9
	Displacement (cm):	4.3	out	26.3

Bracketed Acceleration Duration (Acc. > 0.05g):

1. Temblor d = 3.9 sec
2. No. 5 d = 8.6 sec
3. No. 2 d = 12.2 sec

General Aspects:

The epicentral region lies within the narrow NW-SE trending Cholame Valley which is a segment of the San Andreas fault.

The basement of the valley at the western flank of the San Andreas fault zone is composed of granites and gneisses, located under 3.5 km thick Quaternary and Tertiary sediments, while at the eastern flank it consists of the Franciscan melange under a 4.2-km-thick sedimentary overburden. These basement conditions entail a complicated elastic medium for seismic wave propagation.

The Parkfield earthquake is of particular interest because of the large accelerations recorded on near-field instruments, and because of the considerably long surface breakage, with respect to its moderate size.

Another interesting point is the rapid decrease of the ground motion with distance from the causative fault. The maximum acceleration (50% at the fault) reduced to 1/10th at a distance of 16 km away from it. The strong-motion seismograms lost their pulse-like character with distance from the fault, becoming isotropic (Housner and Trifunac, 1967).

The epicenter lies near the ruptured fault trace and within the aftershock zone. This location means that a bilateral rupture propagated both to the NW and SE.

Interpretation (Stations 2, 5 and Temblor):

Quite a number of papers have been written interpreting the important set of records obtained in the near field from the Parkfield earthquake of 1966. It is not possible to go into detail of these treatments here (Trifunac and Udwadia, 1974; Boore and Zoback, 1974: Aki, 1968; Bouchon, 1980a,b; and Shoja-Taheri, 1977). Rather, we consider only three stations. One important theoretical result is that the surficial layer of sediments over the granitic basement plays a very important role in the form of the strong-motion records obtained in the Parkfield array.

The source-station geometry is given in Figure 3.6. The average velocities in the sediments and basement rock are shown as well as distances between the focus and the ends of the dislocation marked as AD to the north and BC to the south. The faulting surface was essentially vertical and displacements were right-lateral strike-slip.

The three records come from Stations No. 2, within the fault zone itself, Temblor, and Array Station No. 5. These three stations are denoted by the notation R1, R2, and R3, respectively, in Figure 3.6. The record at Station No. 2 is of particular importance (see Figure 3.4). First, we see the usual relatively low level of shaking representing the P-wave motion that triggered the instrument. This continues until there is a significant onset containing both high-frequency and longer period motion marked with an arrow S in Figures 3.4a and 3.4b. Unfortunately, at this station, the second horizontal component N25°W did not trigger, which puts severe constraints on the interpretation that can be made.

For interpretation purposes, it is desirable to rotate the horizontal particle velocities and displacements in a coordinate system which corresponds to the components parallel and normal to the fault. The directions S33°E and N57°E were chosen as the parallel and normal components to the fault. (To convert the instrumentally recorded traces to the actual ground motions, the vertical and horizontal components were also reversed in direction.) The velocity records are shown in Figures 3.5a, 3.5b, and 3.5c. For calculations of travel time, an average P velocity of 5.7 km/sec has been adopted and the S velocity obtained by assuming a Poisson's ratio of 0.25. The S-P times for Stations 2, 5, and Temblor are then 3.9, 4.0, and 5.3, respectively.

In Figure 3.5, the observed arrival of the direct S wave at each station is shown. At all stations, the velocity amplitudes on the normal components N57°E are larger than those for the parallel components S33°E. This is expected from the radiation pattern of a double couple source.

There are two or three onsets shown prior to the arrival of the S_1 wave on the vertical component of velocity at Station 5. These arrivals are probably the P waves of small earthquakes that occurred immediately after the main shock on the fractured fault (within about 3 sec).

Next, let us consider the onsets designated S_2 in Figures 3.5a, 3.5b, and 3.5c. These onsets are related to the waves with peak accelerations recorded on the corresponding accelerograms. They are not likely to be predominantly surface waves because they have short durations and non-dispersive features. The amplitudes decrease rather sharply

with distance from the source of the energy release (compare the amplitudes at Stations 2, 5, and Temblor), whereas near to the source of energy release the surface waves should increase in amplitude with source distance. Furthermore, the arrival times are at least a few seconds earlier than expected if they are assumed to be surface waves. Shoja-Taheri (1977) has worked out diagrams showing particle motions of the ground during the passage of the S_2 waves. On the basis of this work, he interprets the S_2 waves as S waves generated by termination of the rupture within a few km northwest of Station 2. In other words, these waves are associated with the stopping phase for this earthquake source. For a source rupture length of 29 km, the average rupture velocity is about 0.2 km/sec smaller than the average shear velocity along the wave paths between the initial source and the stations. If the length of faulting was only 20 km, so that the dislocation stopped before it reached Point B in Figure 3.6, a rupture velocity of about 2.5 km/sec is entailed. Based on other seismological work, the lower velocity is perhaps to be preferred.

Let us now consider the recorded surface waves on the records of Figure 3.3 and Figure 3.5. A significant portion of the total energy which arrives following the stopping phase in Figure 3.5 (S_2) is no doubt contributed by surface waves (mainly Love waves because the amplitudes of the horizontal components at each station are generally larger than those on the corresponding vertical component). It will be seen from the velocity records that the Love waves following the stopping wave suffer dispersion as they travel towards the further stations. Times of arrival of the surface waves indicate that they

propagate with rather small velocities (about 1.5 km/sec). These low velocities suggest that the crustal model with the low velocity surficial layers is appropriate.

The N65°E component of Station 2 recorded Love waves whose amplitudes are, in general, comparable with the amplitudes of the corresponding waves at Station 5. On the other hand, the amplitudes of the Love waves at Temblor are considerably smaller than the amplitudes of those recorded at Station 5. Shoja-Taheri has also drawn particle-motion diagrams for the surface wave portions of the records discussed here, and he finds some elliptical motion on the vertical plane with both retrograde and prograde motions. He concludes that, at Stations 2 and 5, the Rayleigh waves are noticeably less energetic than the Love waves but, by comparison, the recorded Rayleigh waves at Temblor seem to carry more energy than the Love waves.

A distinguishing feature of Figure 3.4 is the pulse-like displacement on the horizontal record which arrives at about 3 sec on the record. If this wave is related back to the focus, the velocity for that travel path would be about 2.9 km/sec. This is rather a high, but not impossible, value for the dislocation to travel through the granitic rocks and propagate up through a few km of sediments. Our interpretation is that this is the wave associated with the fling of the fault as the dislocation approaches and passes. The dislocation here involves unilateral rupture to the south approaching the stations and would obviously involve Doppler effects associated with a moving source (mentioned in Section 2.6).

Finally, the duration of motion for a rupture of 2.9 km/sec over a distance of 29 km is about 10 sec. The measured bracketed duration in this earthquake at Temblor is about 4 sec, while that at Station 5 is about 9 sec. In this case, there is a smaller duration than predicted by the total time of rupture because of the concentration of the pulse as it moves down the fault towards the station.

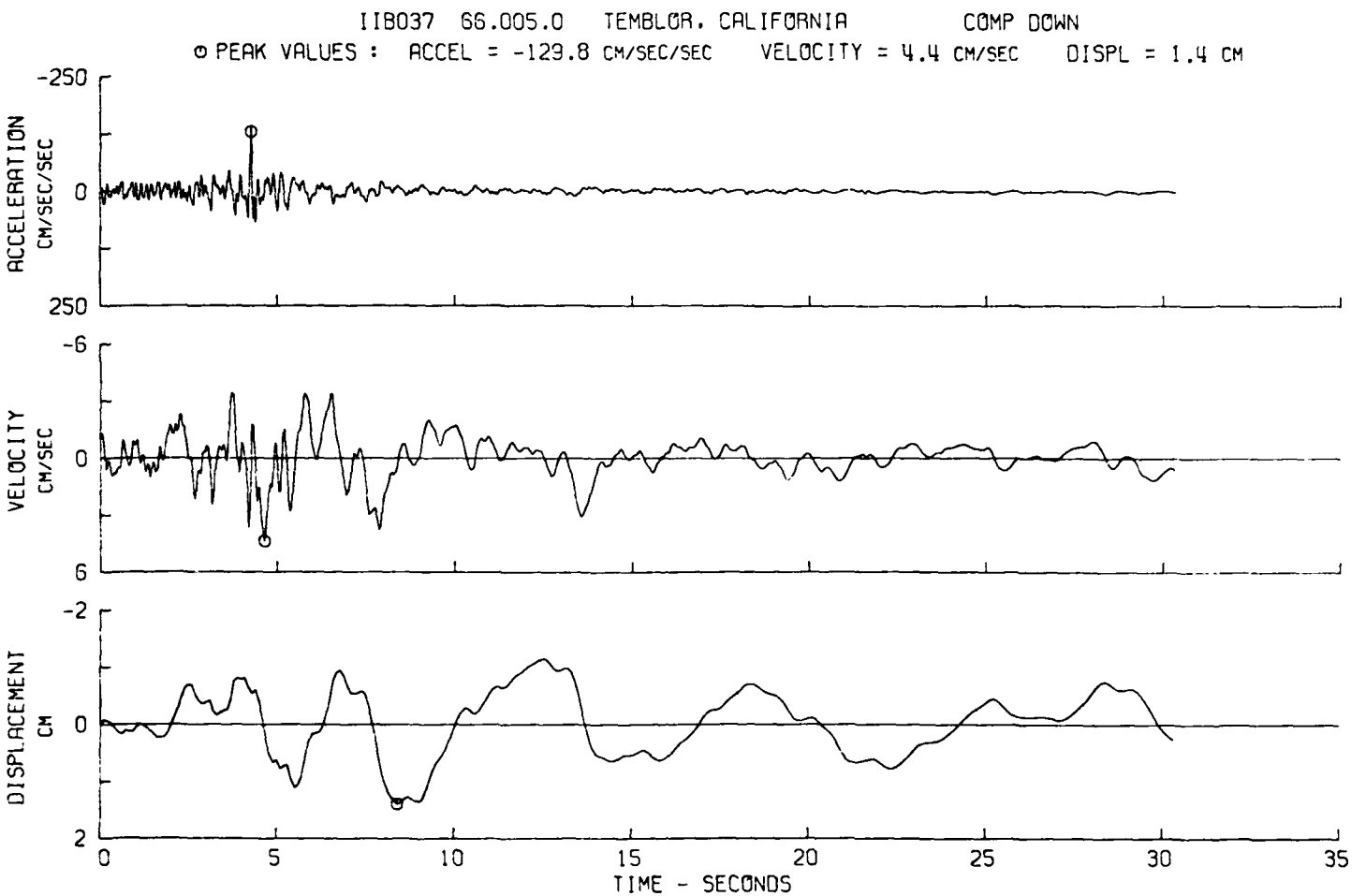

Figure 3.3. Parkfield, California, earthquake; June 27, 1966 - 2026 pst (Sheet 1 of 6).

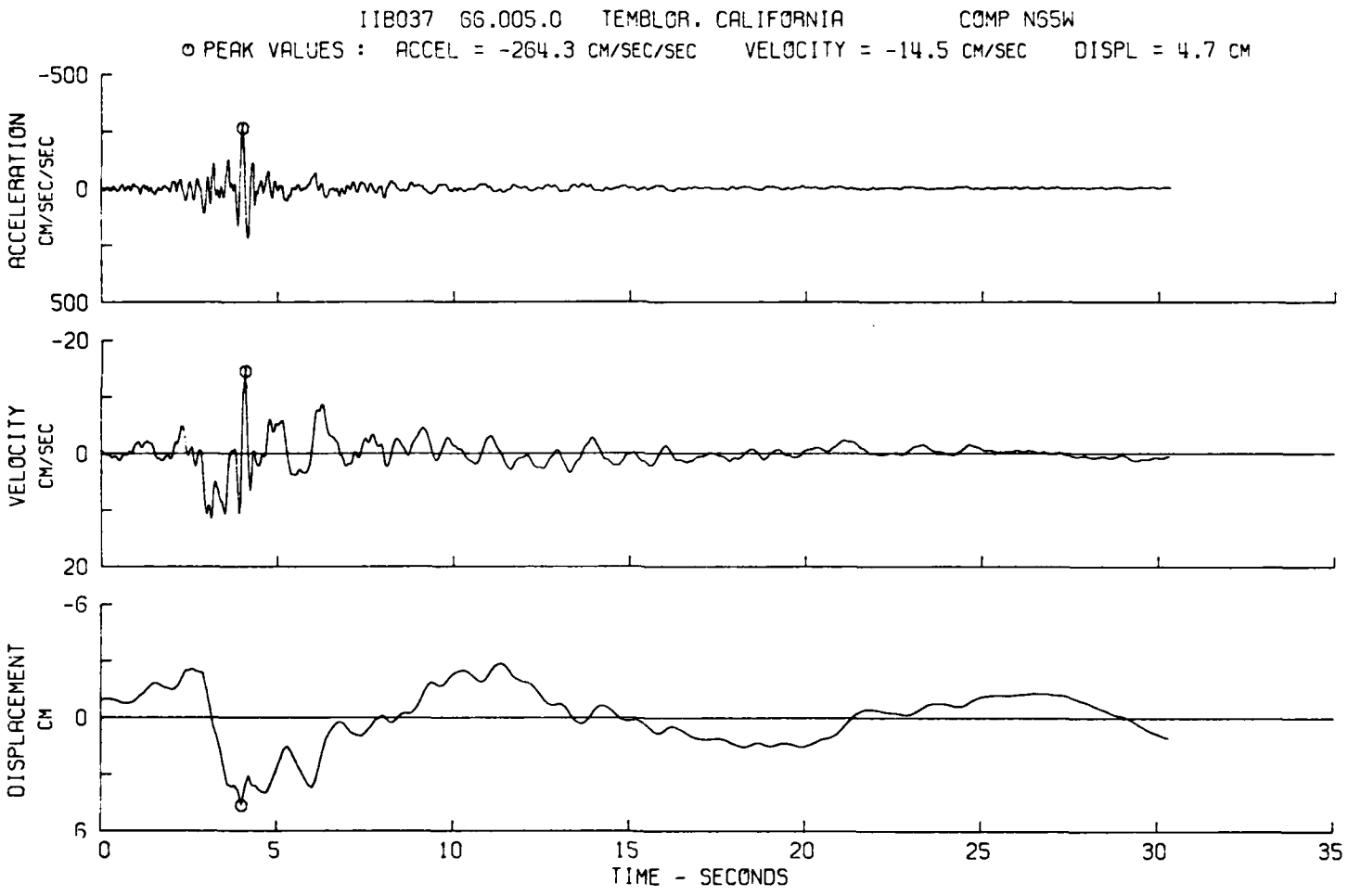

Figure 3.3. (Sheet 2 of 6).

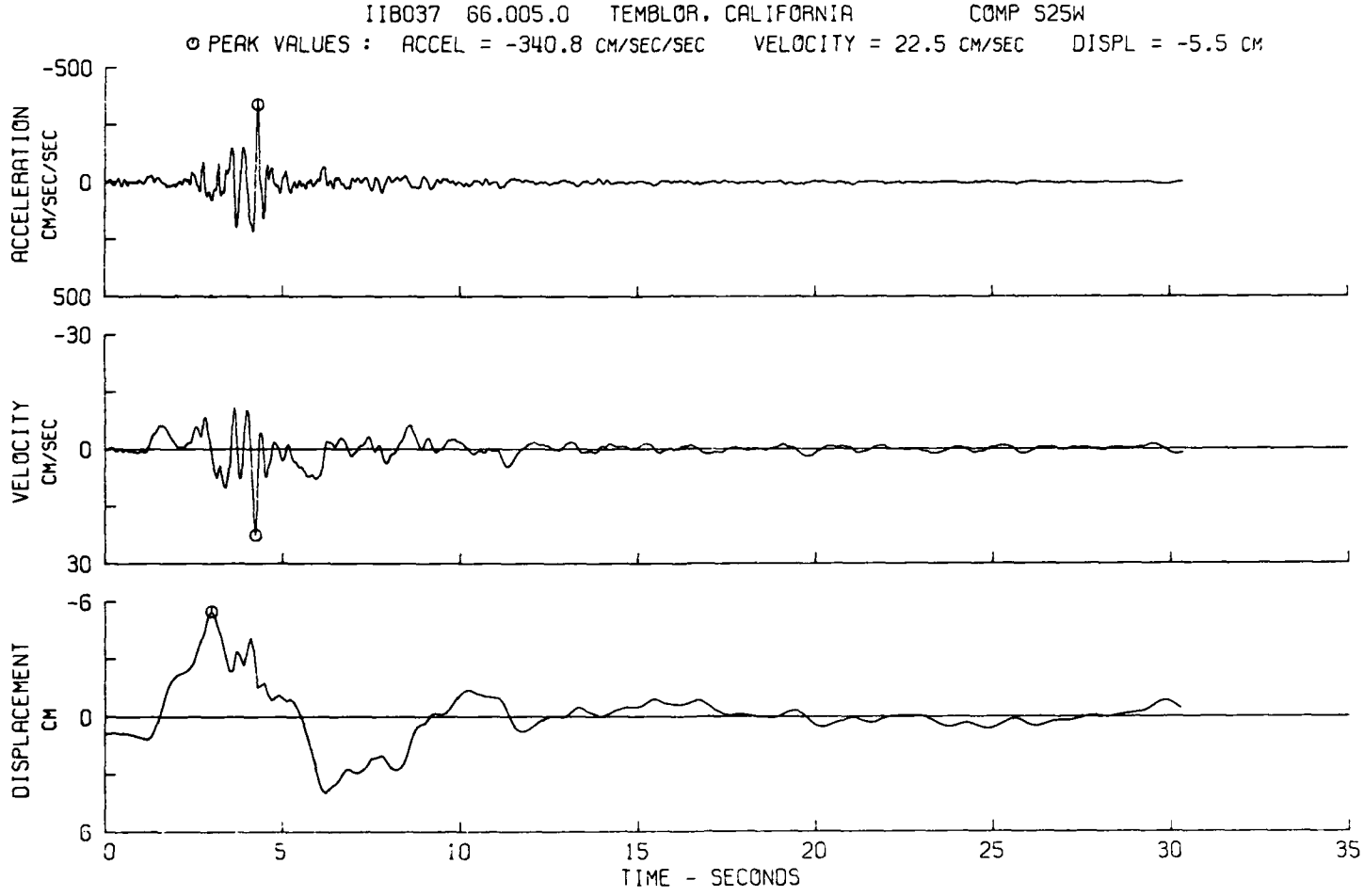

Figure 3.3. (Sheet 3 of 6).

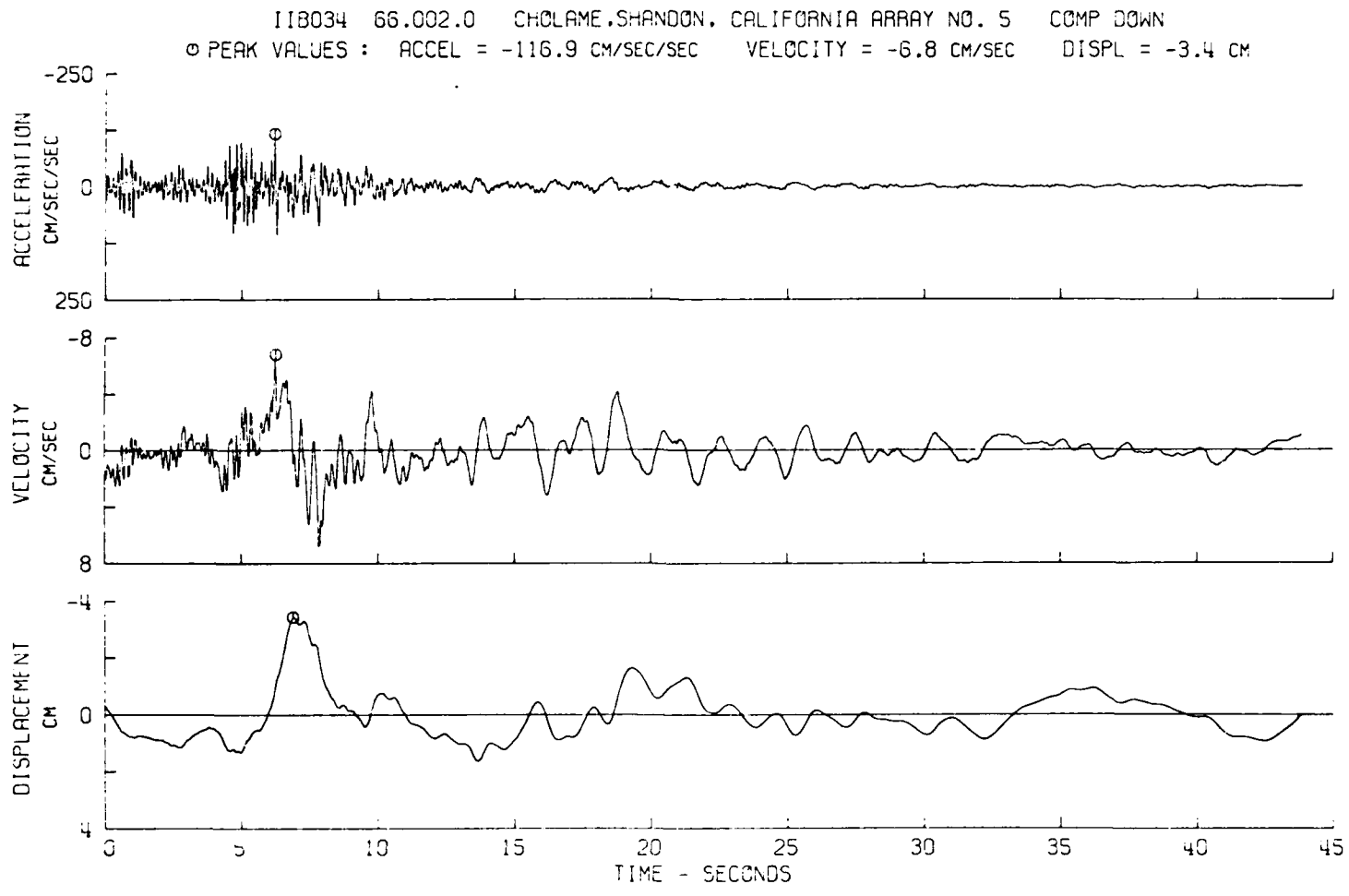

Figure 3.3. (Sheet 4 of 6).

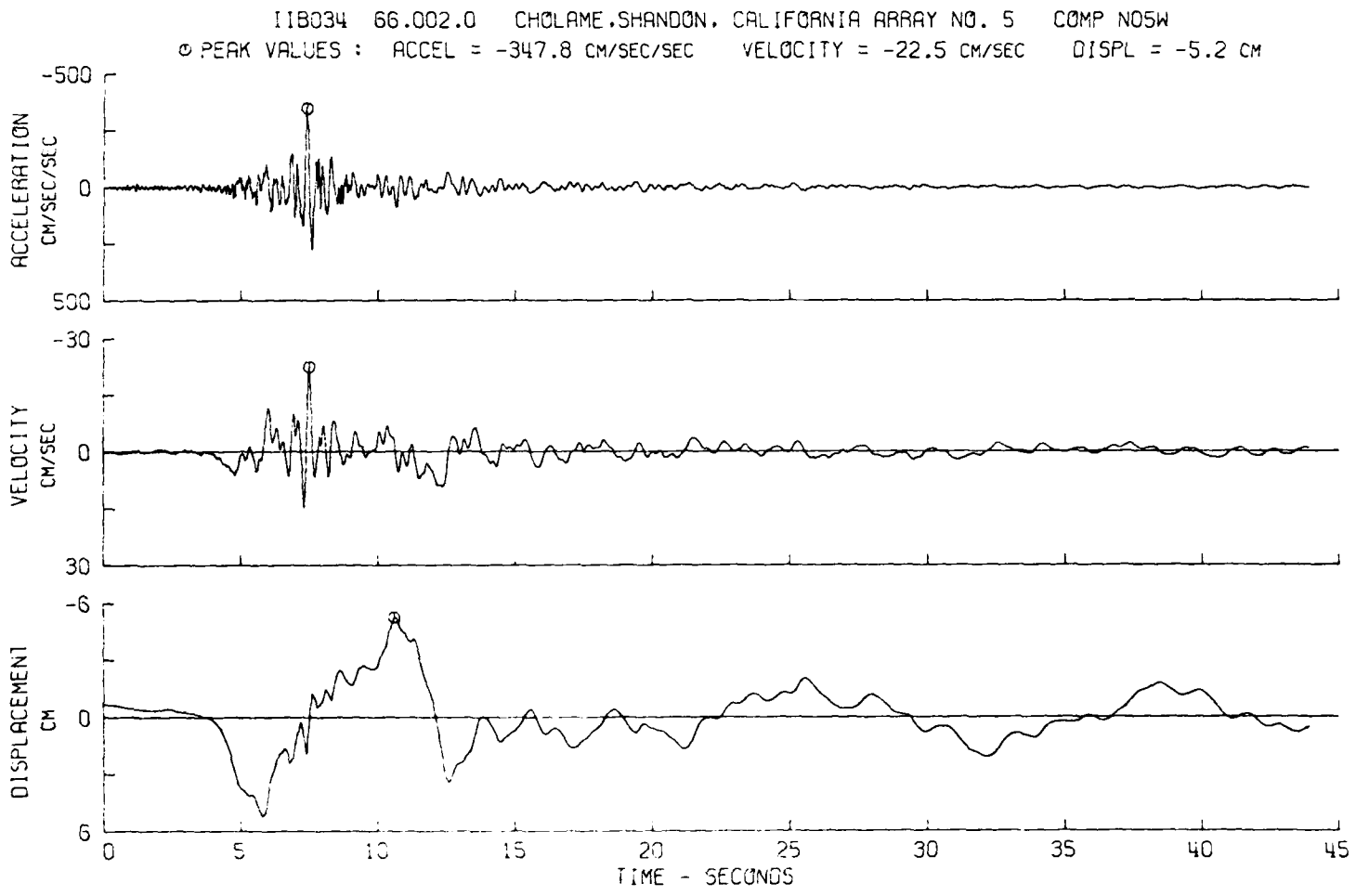

Figure 3.3. (Sheet 5 of 6).

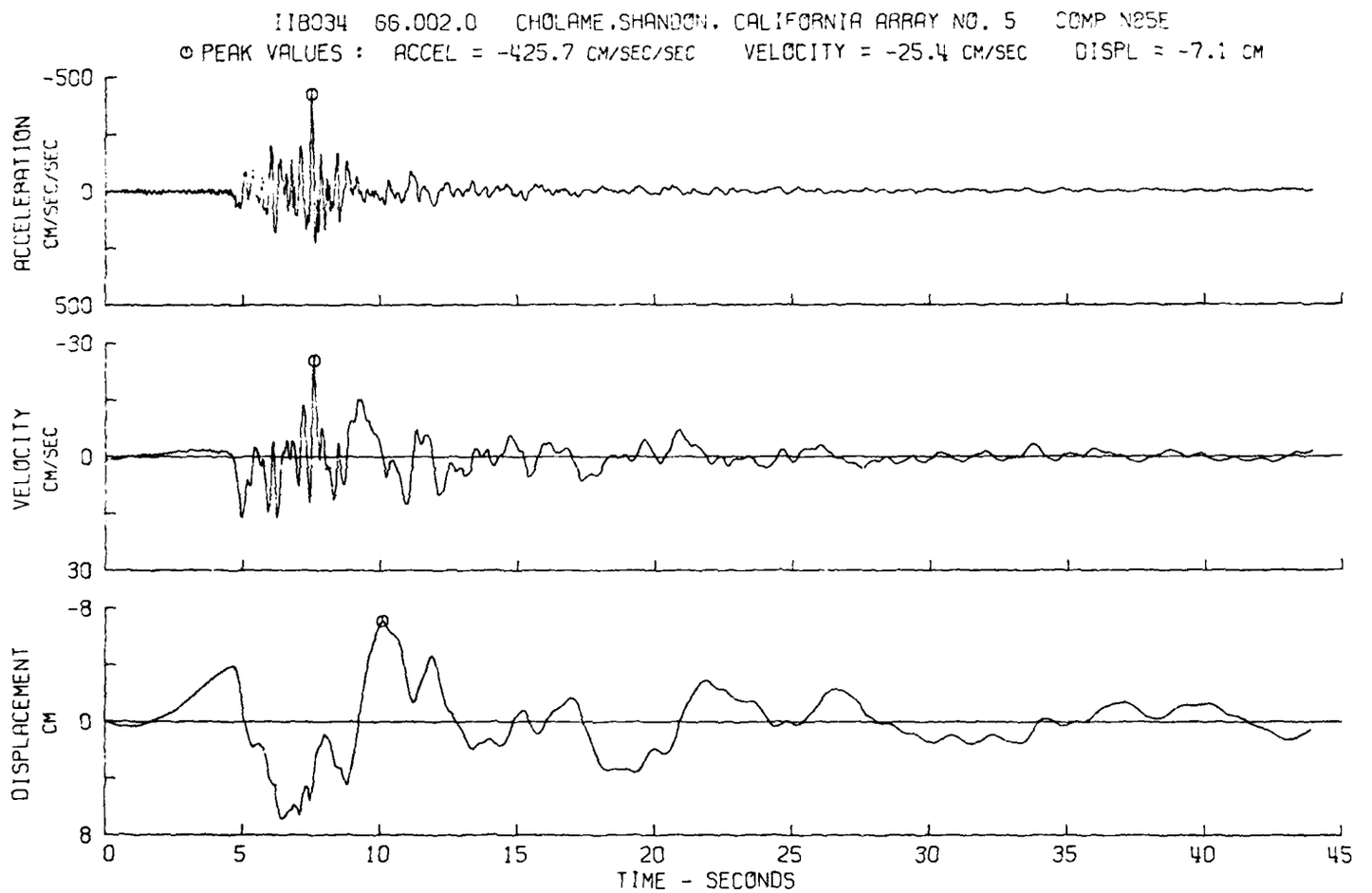

Figure 3.3. (Sheet 6 of 6).

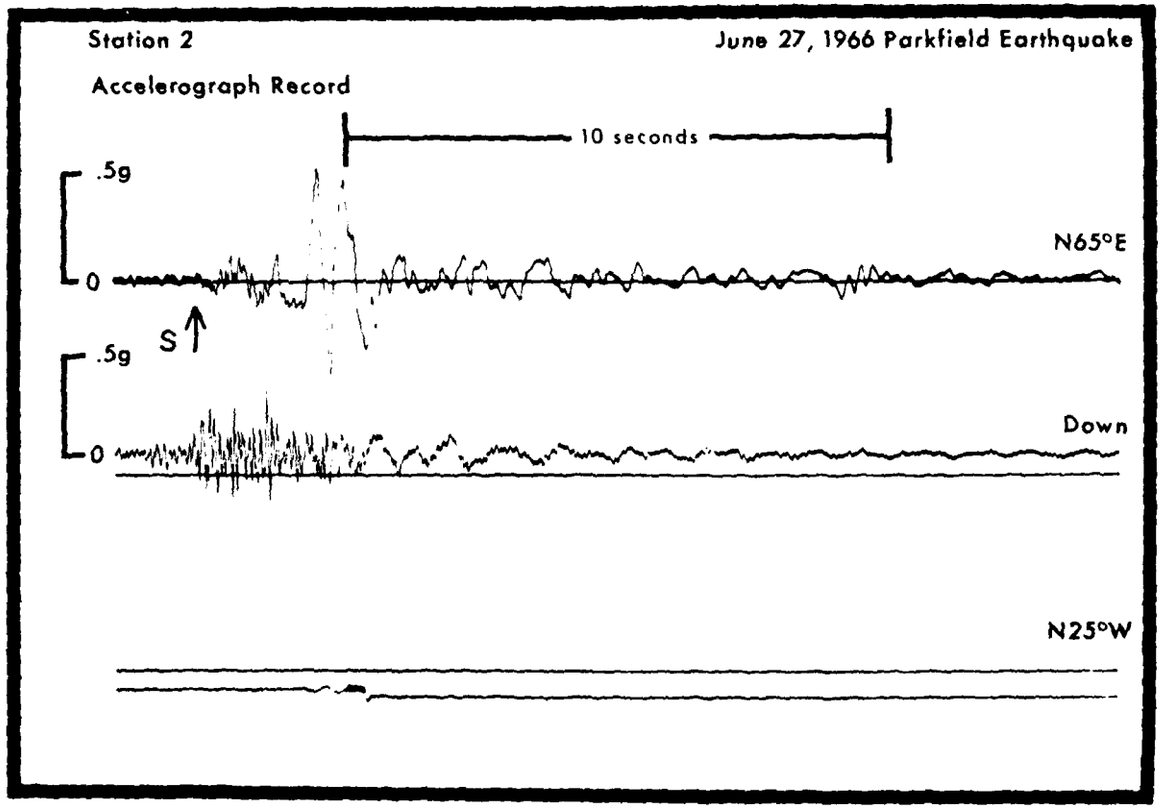

a. Three components of acceleration

Figure 3.4. Recordings made at Cholame-Shandon Station No. 2 during the 1966 Parkfield, California, earthquake (Continued).

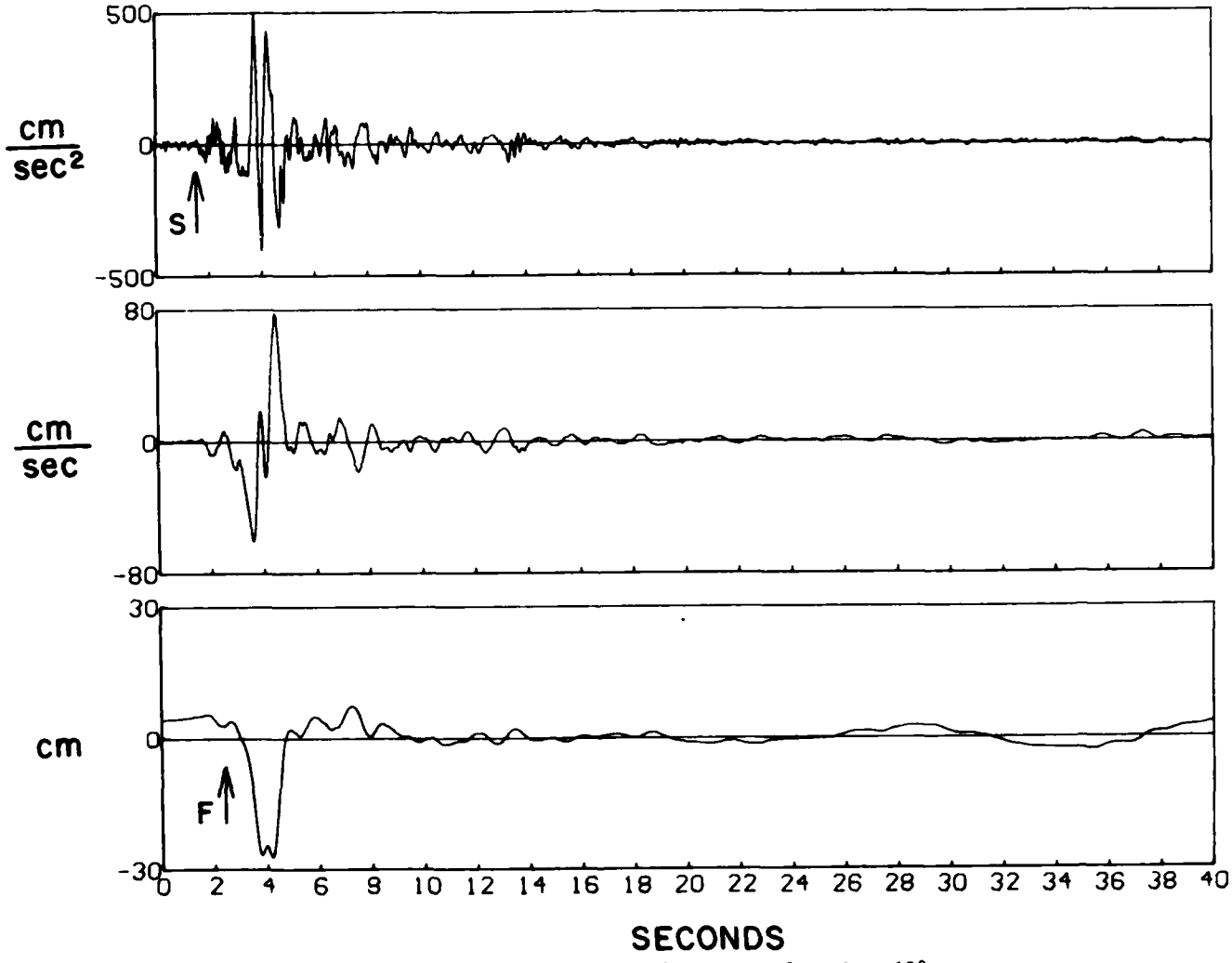

b. Accelerations, velocities, and displacements for the N65°E components

Figure 3.4. (Concluded)

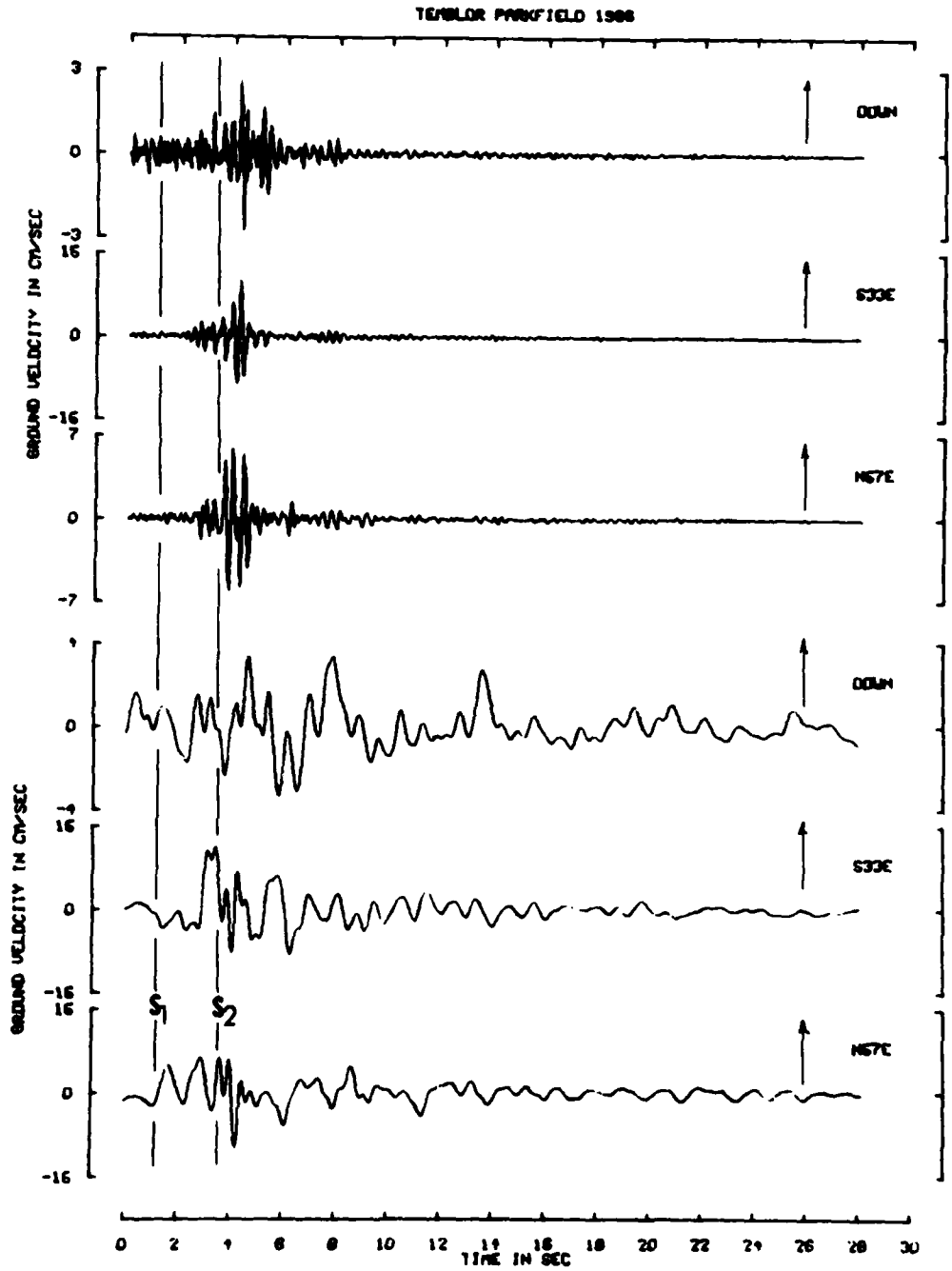

Figure 3.5. Velocity components for Stations Temblor, No. 5, and No. 2, high-pass and low-pass filtered using 4-pole Butterworth filters with 3-Hz corner frequencies (Sheet 1 of 3) (after Shoja-Taheri, 1977).

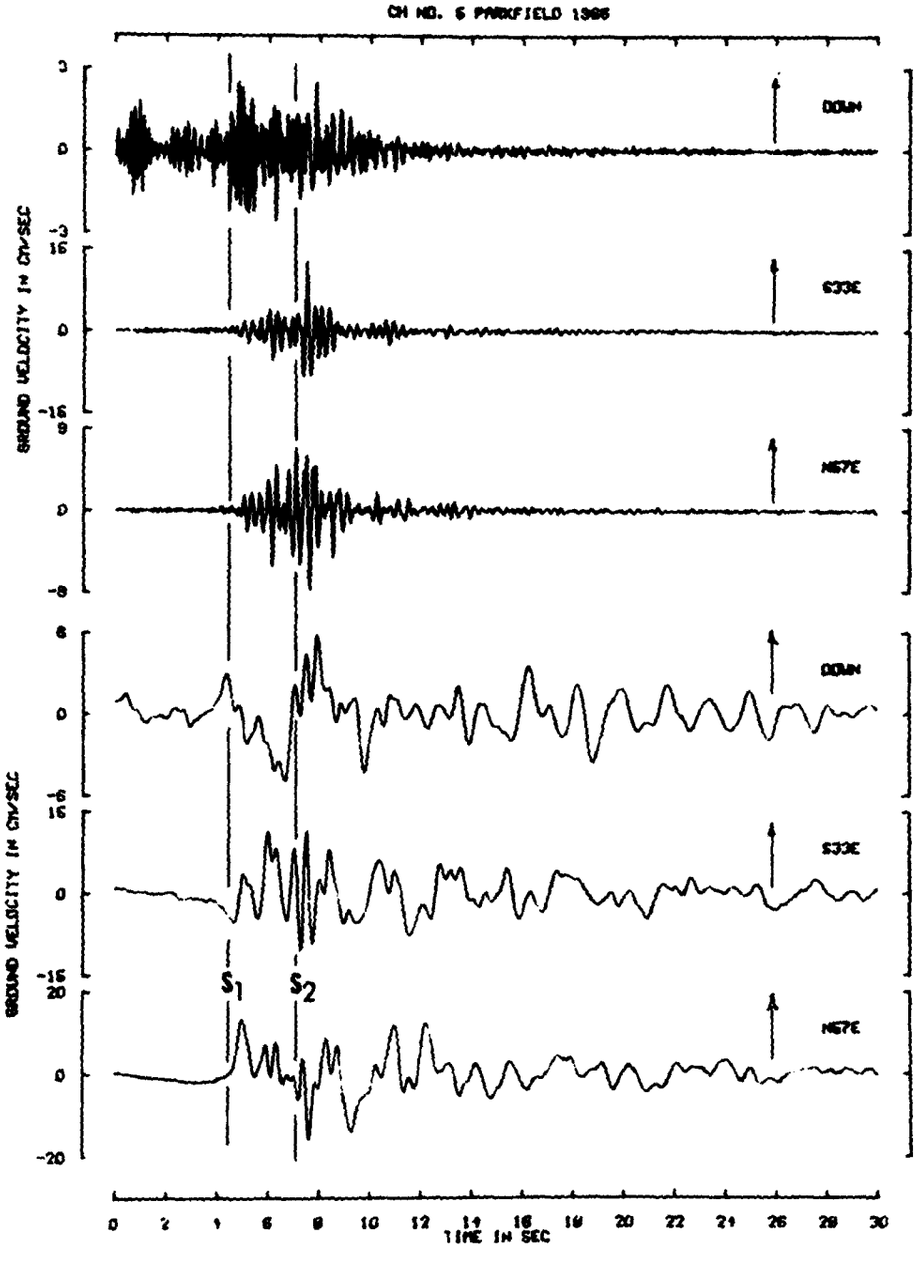

Figure 3.5. (Sheet 2 of 3).

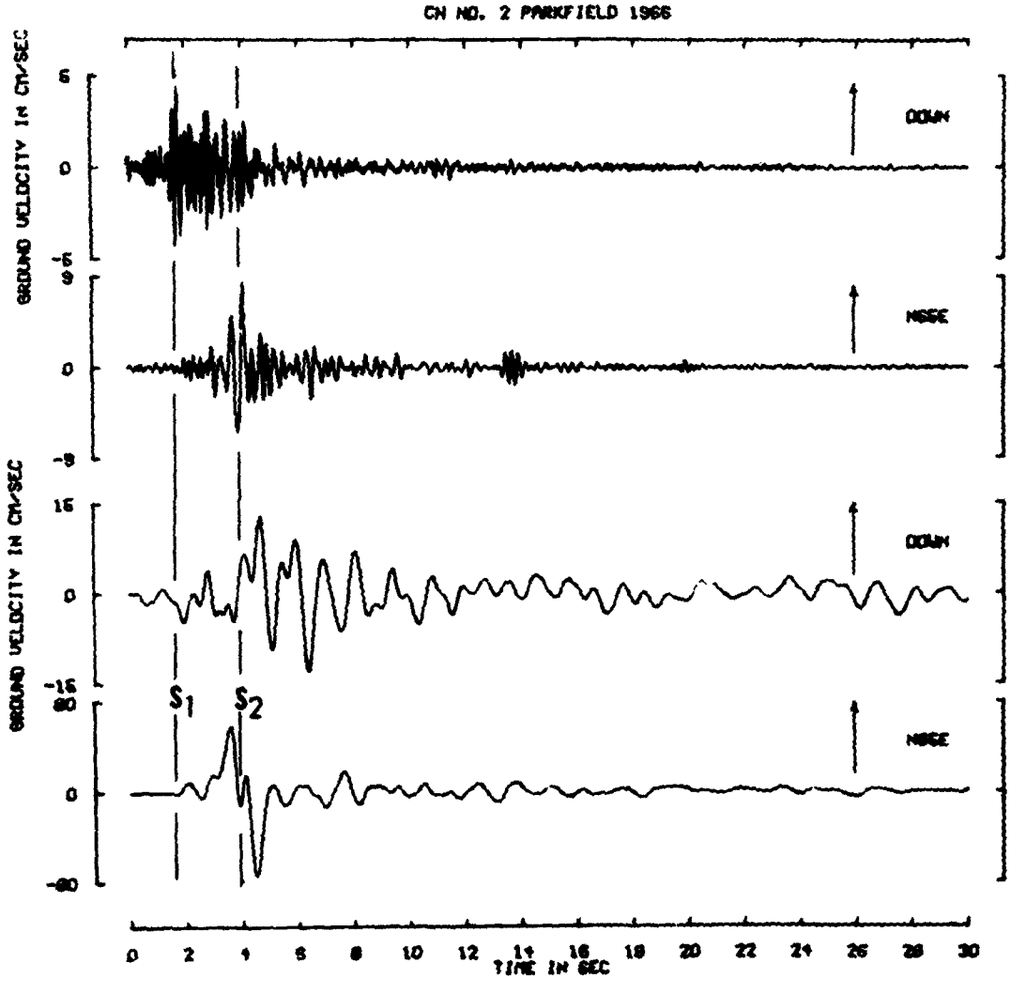

Figure 3.5. (Sheet 3 of 3).

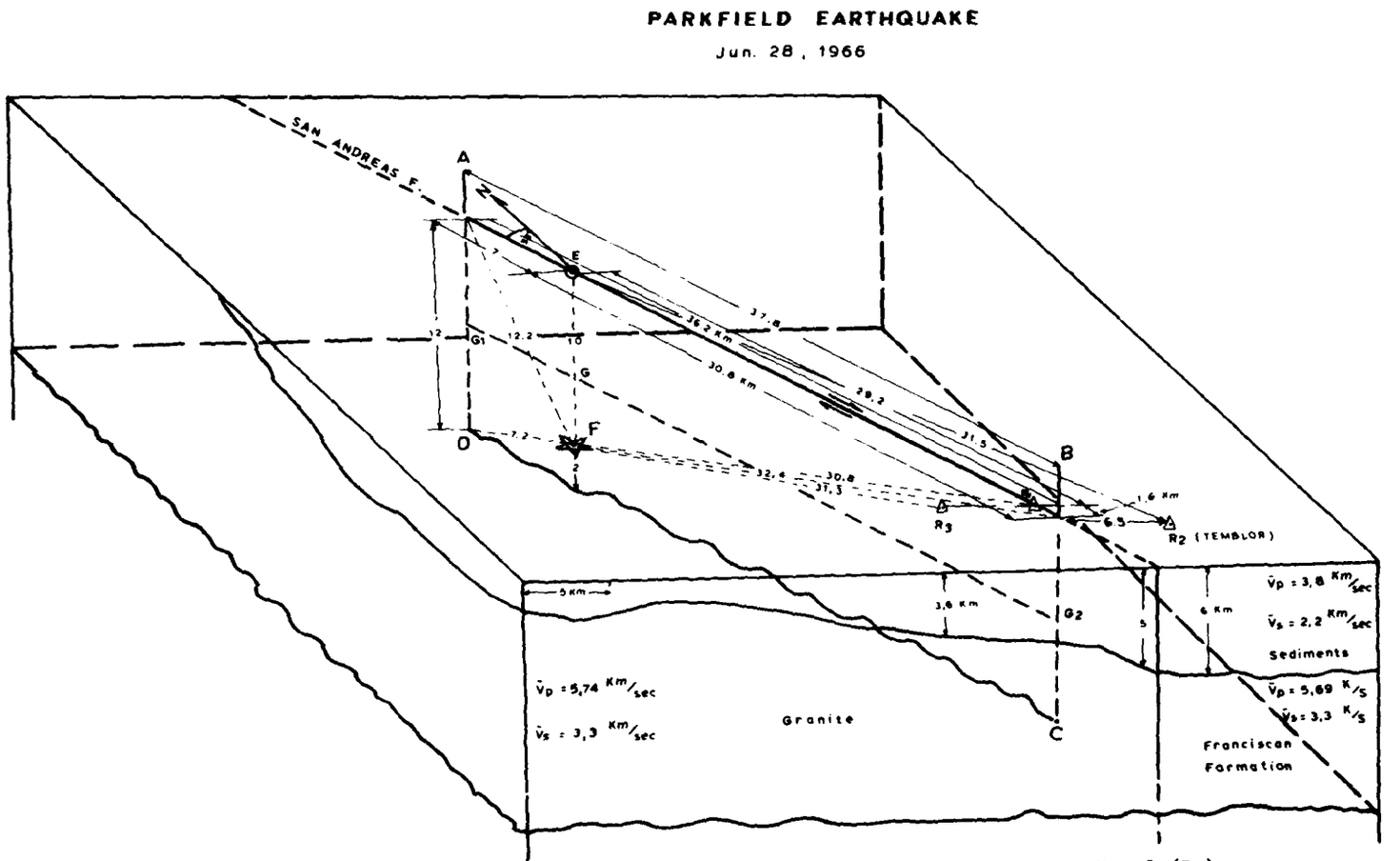

Figure 3.6. Model of the rupture surface in relation to surface faulting, Station No. 2 (R_1), Station No. 5 (R_3), Temblor station (R_2), epicenter (E), and focus (F) for the 1966 Parkfield, California, earthquake.

3.3 Borrego Mountain, California - April 9, 1968

References: Allen and Nordquist (1972); Heaton and Helmberger (1977)

Location:

Earthquake:	33°11.4'N, 116°07.7'W
Accelerometer:	El Centro Site No. 117 Imperial Valley Irrigation District
Foundation:	650 m of alluvium, ground water table close to the surface

Size:

Magnitude:	M_L = 6.4
Moment:	M_o = 7 x 10^{25} dyne cm
Mean Stress Drop	Δp = 500 bars

Fault Source Characteristics:

Faulting:	Approximately 33 km along the Coyote Creek Fault, a major branch of the San Jacinto Fault zone. Rupture dominantly right-lateral strike-slip, consisting of two N35°W trending en echelon segments. Maximum observed displacements: 38 cm on NW segment 20 cm on SE segment Dip of fault plane is nearly vertical - rare vertical displacements did not exceed 20 cm.
Focal Mechanism:	Fault plane: strike S48°E, dip 83°NE Auxilliary plane: strike N42°E, dip 90°
Parameters:	L = 33 km W = 12 km D = 0.20 - 0.38 m
Mean Rupture Velocity:	2.5 - 3.0 km/sec

Peak Wave Amplitude Values:

	VERT	S90W	S00W
Acceleration (cm/sec^2):	-29.7	-56.3	-127.8
Velocity (cm/sec):	3.4	-14.7	25.8
Displacement (cm):	-3.9	-11.0	-12.2

Bracketed Acceleration Duration (Acc. > 0.05g):

d = 1.7 sec

General Aspects:

The meizoseismal area is approximately at sea level and consists mainly of sand dunes. It lies within the Salton Trough which is a depression formed and bounded by crystalline rocks and filled with Tertiary and Quaternary sediments. These sediments, overlying a strongly undulating crystalline basement which at places outcrops at the surface, attain a thickness of as much as 6 km (Heaton and Helmberger, 1977).

Present in the Trough are several major, active, right-lateral fault zones. These features suggest great variability to the uppermost crustal structure and explain the strong variation of the observed wave motions.

The earthquake ranks among the larger shocks recorded in the U.S. as well as the largest to occur from 1959 to 1968. A most surprising phenomenon associated with it is the small displacements that triggered on a number of distant faults, far outside its aftershock area.

The epicenter lies on the western side of the Salton Trough and roughly midway along the zone of aftershock activity (see Figure 3.8). Like the Parkfield earthquake, it thus has a bilateral faulting process with the fracture propagating both NW and SE from the point of the initial rupture.

Interpretation (El Centro records):

The strong-motion records for this case are shown in Figures 3.7a, 3.7b, and 3.7c. There is no doubt from the vertical component accelerogram (Figure 3.7a) that this instrument triggered relatively late in the P motion, since the record begins with high-amplitude, high-frequency

motions which are sustained for about 15 sec. It should be noted that the horizontal component accelerations (allowing for the different scales) remain relatively small (see Figures 3.7b and 3.7c) until the onset of a larger motion at a time marked by the arrow S about 6 sec after the triggering of the instrument.

The geometry of the source and station configuration is shown in Figure 3.8. Here the total length of faulting is about 33 km with right-lateral strike-slip motion on a nearly vertical fault. The distance of the epicenter from the El Centro station is about 67 km and the end of the assumed faulting at point C is 47 km from the station. The faulting was bilateral, but the BC portion ruptured towards the station.

The S-P time for travel from the focus to El Centro is 8.2 sec. Again allowing for start-up time of the instrument, the arrow marked S most probably shows the onset of the first S waves from the focus. Calculations of travel times of P and S waves indicate that the duration of the strongest high-frequency vertical wave motion, approximately 20 sec, is associated largely with high-frequency P waves (associated with some SV motion) radiating from the moving dislocations. (We note that high-frequency vertical component P waves were prominent on records from the 1979 Imperial Valley earthquake near El Centro, c.f., Case 3.9). On the other hand, the largest horizontal strong motion is associated with SH waves and constitutes most of the record between 6 sec and 40 sec.

The wave train marked R is no doubt associated with Love waves with some Rayleigh waves perhaps present since, while very clear on the two horizontal components, associated motion may well be present in the

noisy vertical component record. For the onset time marked R on Figure 3.7b, the velocity of this train, if it began at the focus F, would be about 1.3 km/sec for a period of 6-sec waves. This is a plausible velocity for fundamental Love and Rayleigh waves propagating across the sedimentary structures between Borrego Mountains and El Centro in the Imperial Valley (Mooney and Bolt, 1966). A modeling study of the strong motion in this earthquake has been done by Heaton and Helmberger (1977). They also conclude the El Centro record is dominated by SH-type motion, and they explain this by the presence of a thick sedimentary layer (2-9 km) near El Centro that enhances formation of Love waves. An average rupture velocity of 2.5 to 3.0 km/sec appeared to fit the data.

The calculated duration of the strong ground motion for a rupture velocity of 2.5 km/sec and a rupture length L of 33 km is about 13 sec for a near-source site. The observed duration at El Centro, however, is only 2 sec. We must add to this about 11 sec to allow for the attenuation of the wave train over a distance of 67 km (Bolt, 1973). The result is then fair agreement between the observed duration and the probable time to complete the rupture along the causative fault.

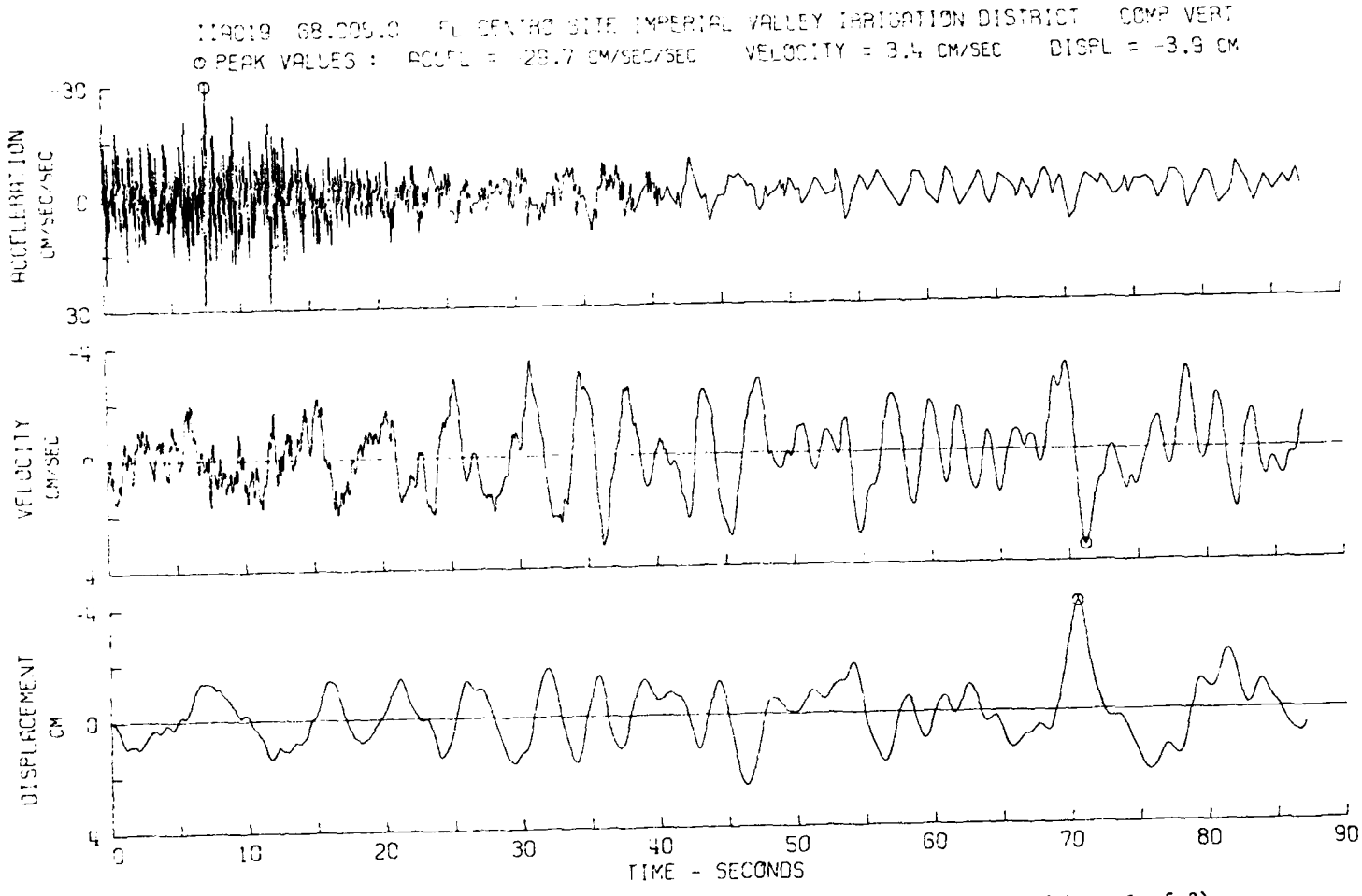

Figure 3.7. Borrego Mountain earthquake; Apr. 8, 1968 - 1830 pst (Sheet 1 of 3).

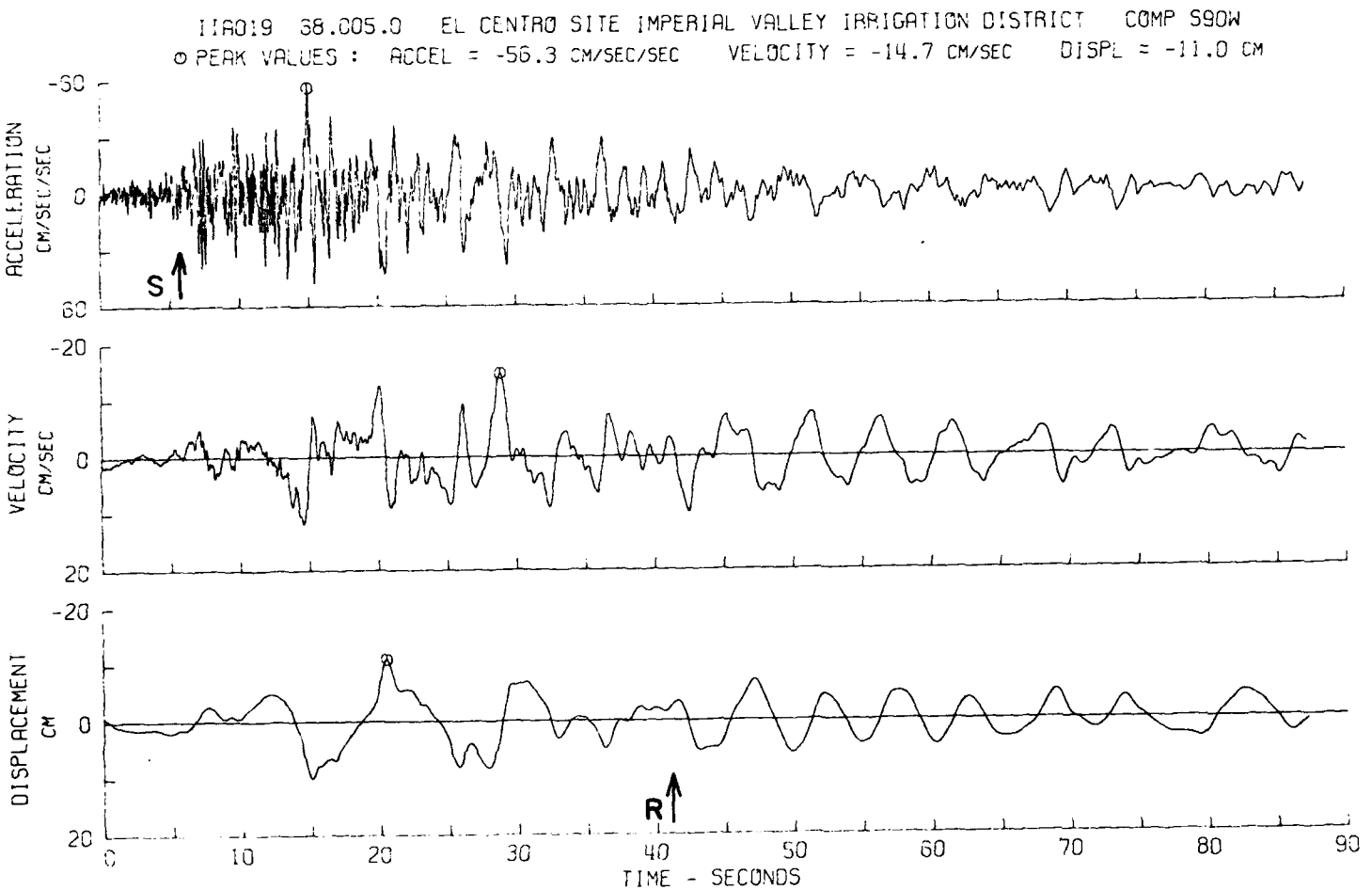

Figure 3.7. (Sheet 2 of 3).

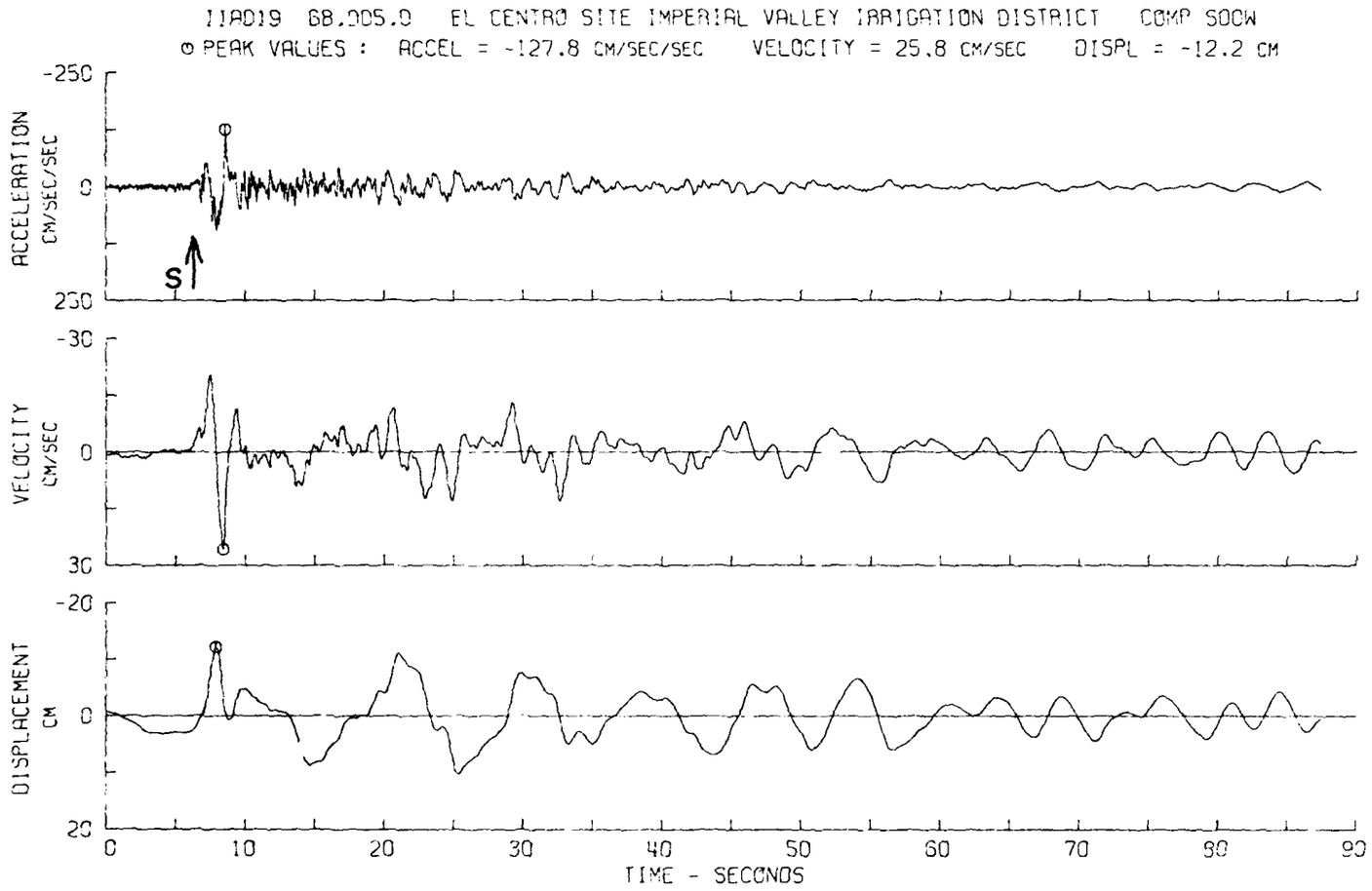

Figure 3.7. (Sheet 3 of 3).

AD-A108 615 CALIFORNIA UNIV BERKELEY DEPT OF GEOLOGY AND GEOPHYSICS F/G 8/11
STATE-OF-THE-ART FOR ASSESSING EARTHQUAKE HAZARDS IN THE UNITED--ETC(U)
OCT 81 B A BOLT DACW39-78-C-0061

UNCLASSIFIED WES-MP-S-73-1-17 NL

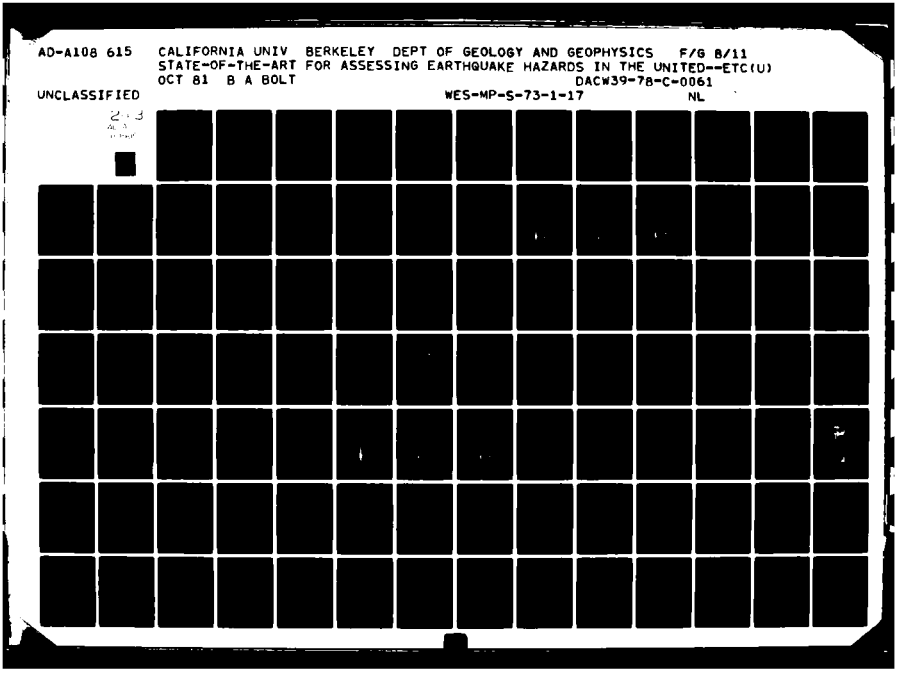

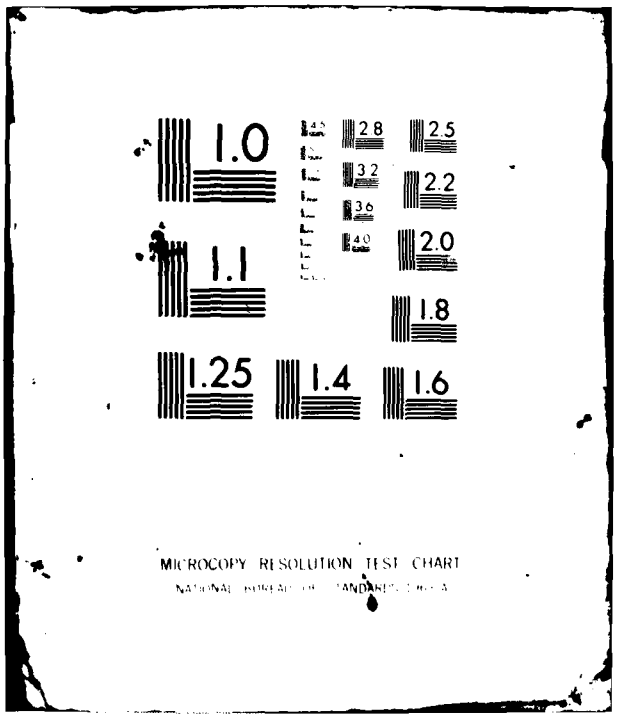
1.0
1.1
1.25
1.4
1.6
1.8
2.0
2.2
2.5
2.8
3.2
3.6
4.0
MICROCOPY RESOLUTION TEST CHART

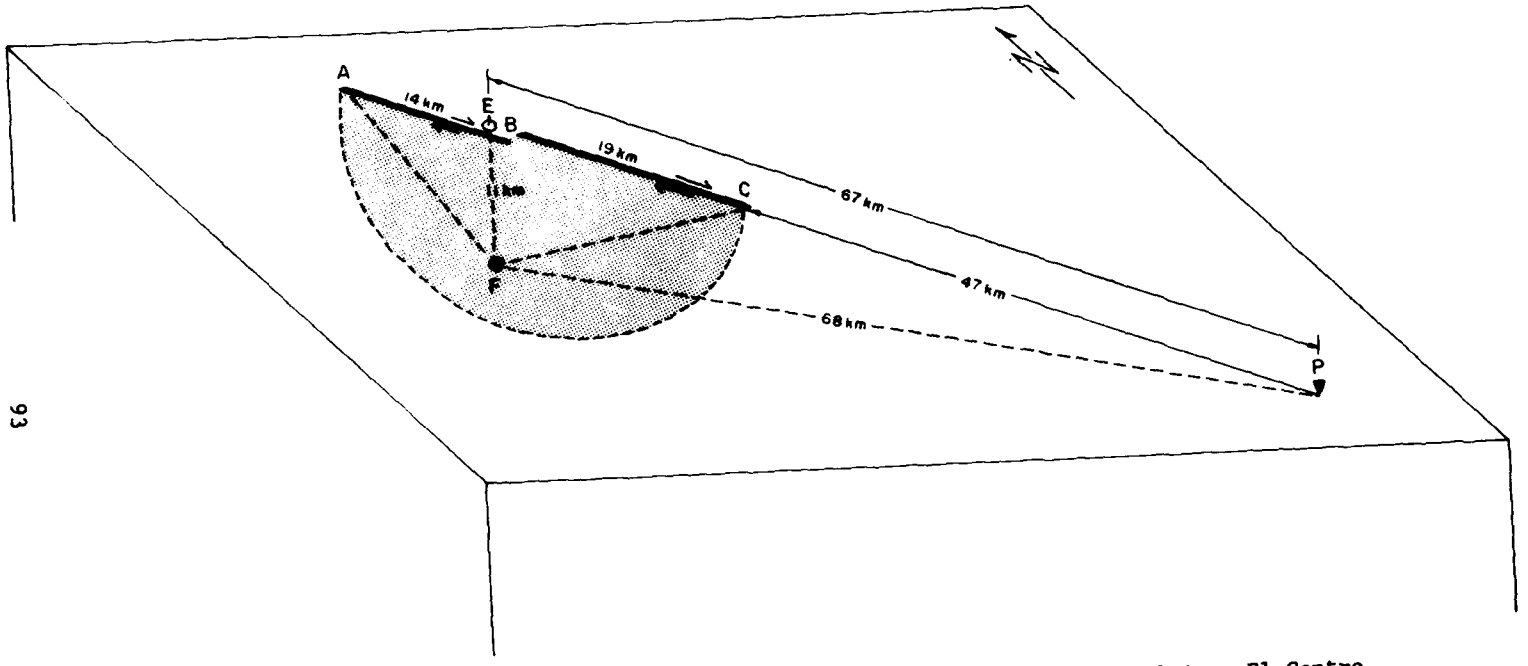

Figure 3.8. Simplified model of the rupture surface in relation to surface faulting, El Centro station (P), epicenter (E), and focus (F) for the 1968 Borrego Mountain, California, earthquake.

3.4 San Fernando, California - February 9, 1971

References: Allen et al. (1971); Kamb et al. (1971); Whitcomb (1971): Bolt (1972); Hanks (1978)

Location:

Earthquake: 34°24.0'N, 118°23.7'W

Accelerometer: Pacoima Dam

Foundation: Dam abutment

Size:

Magnitude: $M_L = 6.5$

Moment: $M_o = 1.5 \times 10^{26}$ dyne cm

Mean Stress Drop $\Delta p = 50$ bars

Fault Source Characteristics:

Faulting: Mean strike was N70°W; dip was 45°NE. Surface faulting extended 12 to 15 km with combined thrusting and left-lateral motion.

Focal Mechanism:

Strike	N64°W
Dip	52°NE
Motion	Predominantly reverse faulting, with left-lateral strike-slip component.

Parameters:

L = 12-15 km

W = 13 km

D = 1.6 m

Mean Rupture Velocity:

3.0 km/sec

Peak Wave Amplitude Values:

	DOWN	S16E	S74W
Acceleration (cm/sec^2)	696.0	-1148.1	1054.9
Velocity (cm/sec)	58.3	-113.2	-57.7
Displacement (cm)	-19.3	37.7	-10.8

Bracketed Acceleration Duration (Acc. > 0.05g):

d = 13.4 sec

General Aspects:

The Pacoima strong-motion accelerograms present an unequaled opportunity to test the predictive power of seismological theory for the near field. For strong motions in crystalline rock, elastic wave theory should be adequate for even the largest earthquakes. The non-linear treatment for the overlying unconsolidated alluvium and soils can then be applied as a correction if the required physical properties are known. One of the main challenges of future research is, in fact, to produce on request by an engineer the full time history of the ground motion at a site with specified geology and position relative to a defined rupture mechanism on a nearby fault.

A provisional solution by Allen et al. (1971) gave an origin time of $14^h00^m41.6^s$ (GMT), with a latitude 34°24.0' North and longitude 118°23.7' West. The focal depth was 13 km. (In a later revision Allen et al. (1972) computed a depth of 8.4±4 km. The difference is relatively unimportant for the arguments in this paper.) The magnitude of the earthquake, calculated from the Berkeley network of Wood-Anderson seismographs, was 6.48±0.15. Use of a Richter magnitude of 6.5 satisfies all of the seismographic evidence.

Surface faulting occurred in the San Fernando Valley and along the foothills of the San Gabriel Mountains, crossing Little Tujunga Canyon, south to Sunland. This faulting indicated both thrusting and left-lateral motion. The strike varied from place to place, with a mean value of N70°W and a dip of 45°. The total length of surface faulting, established from field studies, was approximately 12 to 15 km. There is a discontinuity in the western half of the arc, with an offset. The thrusting was such that the San Gabriel Mountains moved southward over

the San Fernando Valley. En echelon fractures were mapped in the mountains as far north as the Veterans fault.

A zone of aftershocks occurred roughly in the form of a horseshoe, with the center near the main shock and the ends of the crescent running southeast under the San Gabriel Mountains and under the Sylmar region.

The overall seismological and geological evidence together shows that the detailed faulting is somewhat complicated, with at least different dips to the upper and lower portions of the fault plane. Nevertheless, the main effect can be modeled in terms of a single fault zone which dips from the surface San Fernando fault at an angle of about 45° under the San Gabriel Mountains to intersect the focus. This simplified model is shown in Figure 3.10. The dimensions of the dislocated zone are such that Pacoima is approximately 5 km to the north of the surface rupture and the epicenter lies approximately 10 km to the north, along the same line. The line PE in Figure 3.10 intersects the fault AC at B.

A feature of the tectonic setting is that the upthrust block consists of crystalline basement rocks of the San Gabriel Mountains. These consist of dense igneous and metaigneous rocks, chiefly diorite. The Pacoima instrument was located on this crystalline basement. The fault surface, from its attitude, must have dipped through the zone of contact of the crystalline rocks with the Cenozoic sediments of the valley northward to a region at depth where crystalline rocks were in contact across the fault rupture.

Interpretation (Pacoima records):

Many aftershocks show an interval of 1.7 sec between the P-wave onset and a large 3 to 5-Hz onset. This later wave packet is probably the arrival of the S waves. The same interval, 1.7 sec, occurs on the strong-motion record of the main shock. It can, therefore,be safely assumed that the Pacoima instrument was triggered by the first P wave.

The three components of recorded acceleration, S74°W, vertical, and S16°E, were placed in digital form (sample interval 0.02 sec) on magnetic tape. The digital samples were then converted into continuous analogue form. In order to make a direct comparison with the earthquake mechanism, the recorded orthogonal components were resolved, using an analogue device, along the strike, down the dip,and along the upward normal to the fault plane.

The first three traces in Figure 3.11 are the resulting resolved components of strong acceleration at Pacoima. The three resolved components are labeled ξ, η, ζ, respectively.

If the faulting were entirely of the thrust type, the resolved motion along the strike of the fault would represent transverse seismic waves. These would be mainly of SH and Love type. Their amplitudes would be small. As seen in Figure 3.11 , however, there are significant wave motions in the transverse direction, although the overall amplitudes are less than those on the other two components. These motions, no doubt, arise mainly from the strike-slip components of faulting in this earthquake.

It should also be noticed that the transverse components of acceleration have a different appearance to the longitudinal and normal components. In particular, the amplitude of the first 5 sec of the transverse component does not contain such obvious long-period components as the other components.

There is a general correlation between the motions η and ζ in the vertical plane PEF (see Figure 3.11). The wave motion, therefore, is presumably of longitudinal (P) type, polarized S type, and various Rayleigh-mode motion. In particular, clear correlation may be seen between the longitudinal and normal particle motion in the relative long-period motion beginning at 2.5 sec from the wave onset. There are also noticeable correlations in amplitude and phase in the wave coda at 6 and 8 sec after P.

The continuous records were next filtered through Krohn-hite filters to obtain the time history as a function of frequency. The signals were passed at frequencies of 0.5, 0.75, 1.0, 1.5, 2, 4, and 10 Hz. The results of 10-Hz filtering are shown in the last three traces of Figure 3.11. In this case, to allow direct intercomparison, the accelerograms are arranged in parallel so that the onset time corresponding to the first P motion is aligned down the paper.

An attempt will now be made to explain the features of Figures 3.9 and 3.11 in terms of the rupture dynamics for the fault model shown in Figure 3.10.

For the simple model considered here, assume first that the rupture progresses up the fault plane at an average speed of 2.5 km/sec. (The offset across the fault from the elastic rebound may increase upward from near the focus to the surface.) Assume further that in the crystalline rocks of the crust, the P and S velocities are 5.5 and 3.3 km/sec, respectively. For simplicity, no allowance is made for the reduction in velocity near the surface because of weathering, cracking of the rocks, and other effects.

Seismic waves will leave the upper surface of the fault plane and travel through the crystalline rocks to Pacoima. The first wave to reach Pacoima is the P compressional wave from the focus; travel time is 2.7 sec. This is followed by the direct shear wave, called S_1 in Figure 3.11, which arrives 1.7 sec after the first P. As can be seen from Figure 3.11, S_1 coincides with the beginning of the longer-period motion on the accelerograms.

Consider the rupture progressing up the fault plane from F to D. At D, the dislocation is at its nearest point to Pacoima. The effect of the dislocation is to annihilate the double couple which is causing the thrusting motion.

The total travel time from F to D, at a fault rupture speed 2.5 km/sec, and D to P, as an S wave (say S_2), is 6.5 sec. By the time of arrival of this computed S_2, Figure 3.11 shows that the longer period acceleration pulse on the strong-motion record has ended. This suggests that the assumed rupture velocity is too low.

An allowable increase in rupture velocity to 3.0 km/sec would entail the arrival of S_2 one sec earlier. As Figure 3.11 then shows, S_2 would arrive at the same time as the longer period pulse which is reasonable. (See especially the normal 10-Hz trace of Figure 3.11.) The ray theory hence agrees with the notion that the ground displacement has occurred in a single episode. The displacement record (Figure 3.9) obtained by integrating the Pacoima accelerograms (Trifunac and Hudson, 1971) shows that it is in the interval S_1 to S_2 that the major ground displacement occurs.

When the rupture reaches the surface at B, a breakout phase will occur

This may be associated with the production of Rayleigh-type waves of various modes and frequencies (ground roll). The time for a surface wave to reach Pacoima from this source is 4.3 sec after the arrival of P. After the point marked R on Figure 3.11 , Rayleigh-type waves of various frequencies and amplitudes arrived at Pacoima from progressively more distant sections of the near-surface San Fernando fault. The theory of Rayleigh waves indicates that only at considerable distance from the source will true Rayleigh amplitudes become large compared with those of the body waves.

The remaining part of the accelerograms contains the high-frequency components with some of the highest amplitudes. Yet, on the above explanation, the dislocation source has already passed under Pacoima and reached the surface at B. The question, then, is what is the source of the large high-frequency motions in the remaining part of the record?

Of the alternative explanations only one has much likelihood. [The Pacoima displacement *record* (*Trifunac* and Hudson, 1971) shows clearly only one major increment, suggesting that the fault displacement was not multiple in a low-frequency sense.]

The source of the latter half of the accelerograms, which contain several spikes of about 1g acceleration, can be found in terms of the model shown in Figure 3.10. As the rupture front moves up the fault zone, there will be regions where the rock fracture involves the release of bursts of high-frequency energy (see Bolt, 1970). In some places the strike slip will be different from others. One can conceive, therefore, of a stochastic release of bursts of high-frequency energy from domains near to the rupture front. Because, in this case, the rupture is partly through crystalline rock, the high-frequency energy may contain relatively high amplitudes (see Figure 3.11; also Sections 2.7 and 4.4).

Consider the path FMP shown in Figure 3.10. The time of travel of the waves from this source would be

$$\frac{FM}{2.5} + \frac{MP}{3.3} = \frac{8}{2.5} + \frac{17}{3.3} = 3.2 + 5.2 = 8.4 \text{ sec}$$

The shear wave marked S_m on Figure 3.10 would then arrive approximately 5.7 sec after the P onset. Even greater delays are possible from high-frequency sources of this kind. An extreme case would be a burst of high-frequency energy just below A at the southern end of the San Fernando fault. In this case, the time of onset after P is approximately 8 sec. The onset would arrive at about the position marked S_A in Figure 3.11.

This explanation directly relates the duration of the Pacoima record to the extent of propagation on the fault. We have shown that the known dimensions of the rupture plane are reasonably in accord with the length of record actually obtained (10 sec at 10 Hz).

It is important to check the model on both frequency content and amplitude. The farther the source from the recording station, the greater will be the attenuation of high-frequency waves. Suppose the attenuation is proportional to an exponential law

$$\exp\left(-\omega d/2 c Q\right) \qquad (3.1)$$

For the diorite, suppose Q equals 150. Then, for 10 Hz S waves traveling a distance of 10 km, the amplitude would diminish (neglecting geometric spreading) by a factor 0.5. On the other hand, waves of frequency 4 Hz would diminish only by a factor of 0.8.

As Figure 3.11 shows, the recorded waves of greatest mean duration at Pacoima have frequencies in the spectral range of from 2 to 4 Hz.

If Pacoima had not been situated on the crystalline block, but on material with a lower Q, the high-frequency coda obtained at Pacoima would have occurred with much lower amplitudes.

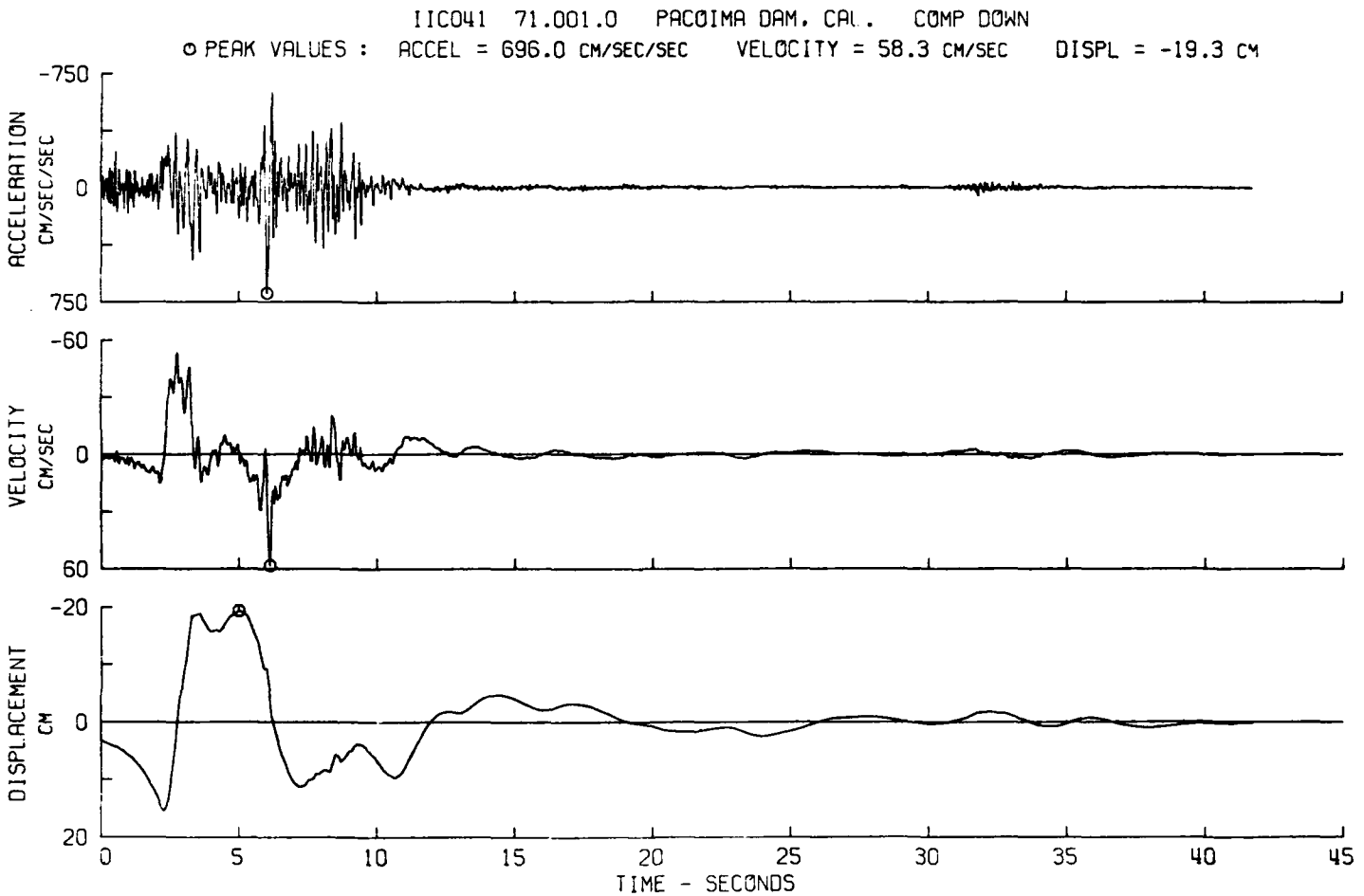

Figure 3.9. San Fernando earthquake; Feb. 9, 1971 - 0600 pst (Sheet 1 of 3).

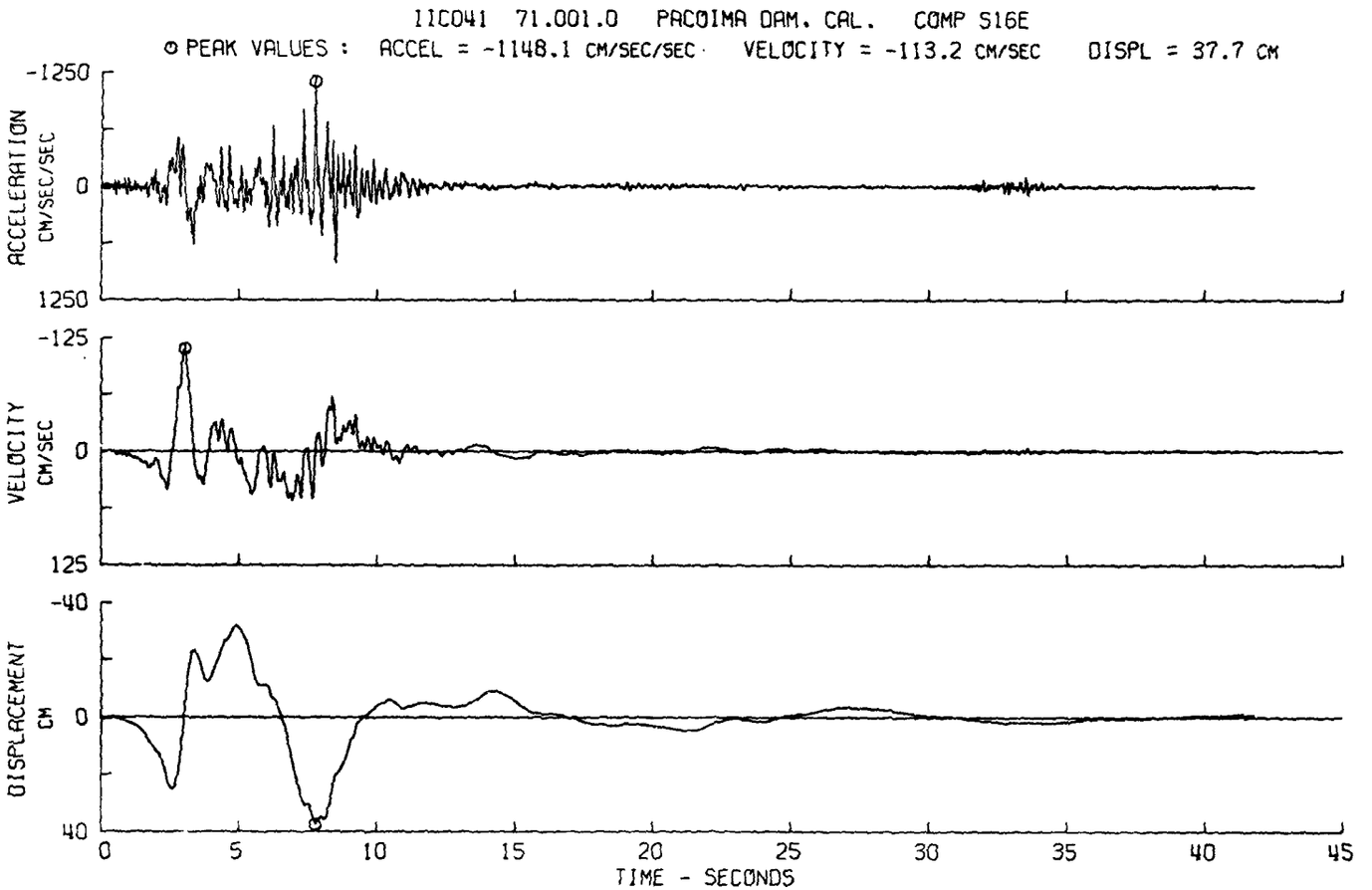

Figure 3.9. (Sheet 2 of 3).

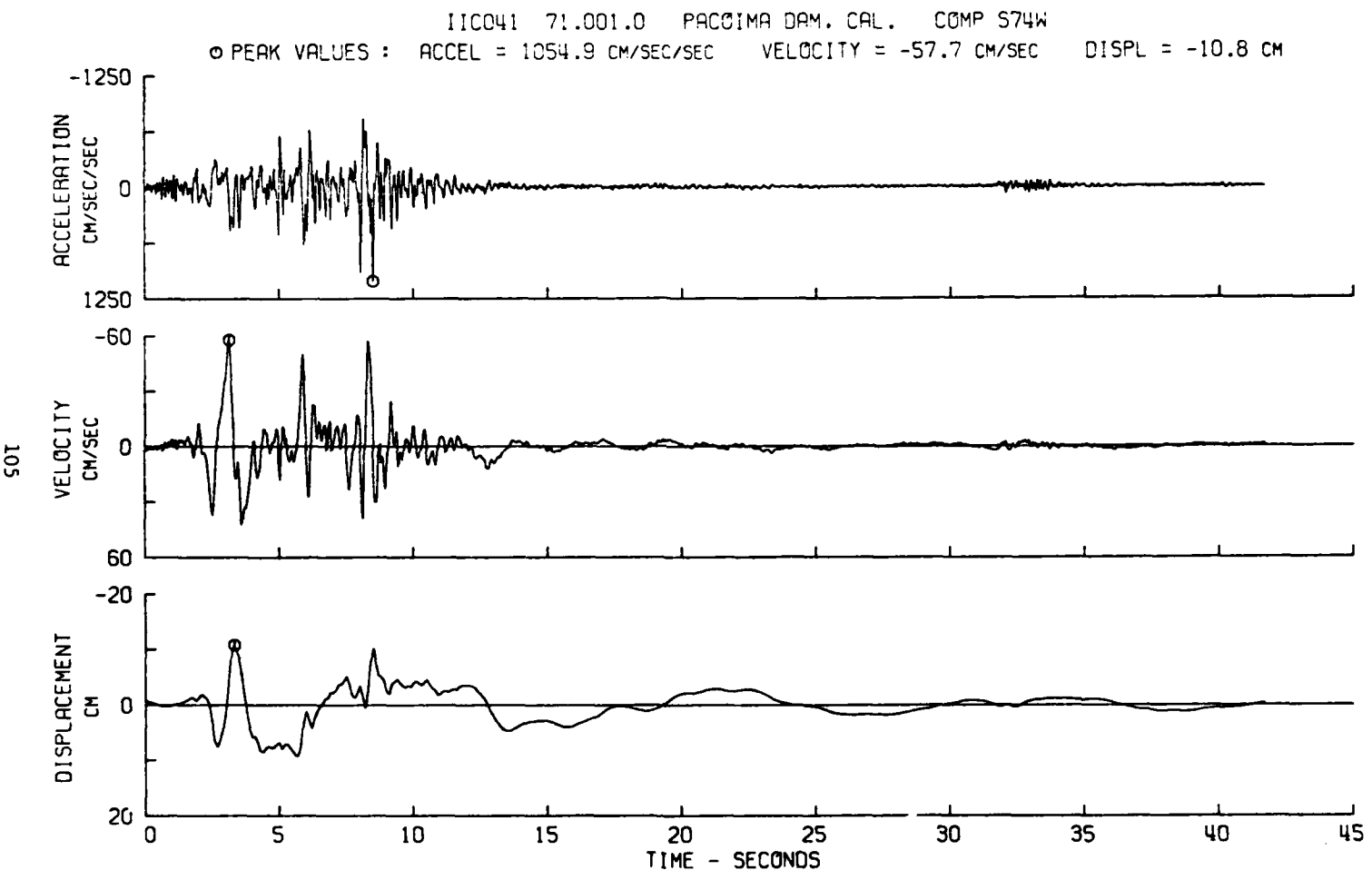

Figure 3.9. (Sheet 3 of 3).

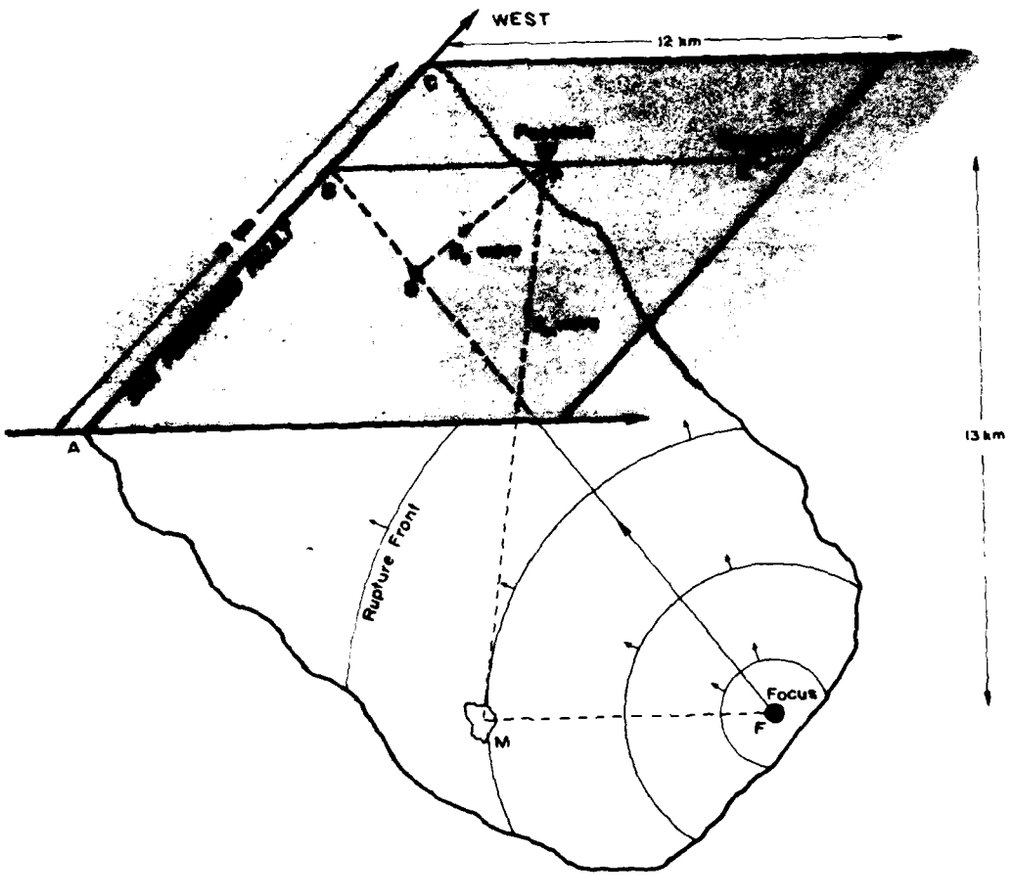

Figure 3.10. Simplified model of the rupture surface in relation to the San Fernando surface faulting, Pacoima Dam station (P), epicenter (E), and focus (F). The dip is taken as 45° and the strike N72°W. DP is the shortest ray path for waves from the rupture. MP is a general ray path from the dislocation to Pacoima through the mountain rocks (from Bolt, 1972).

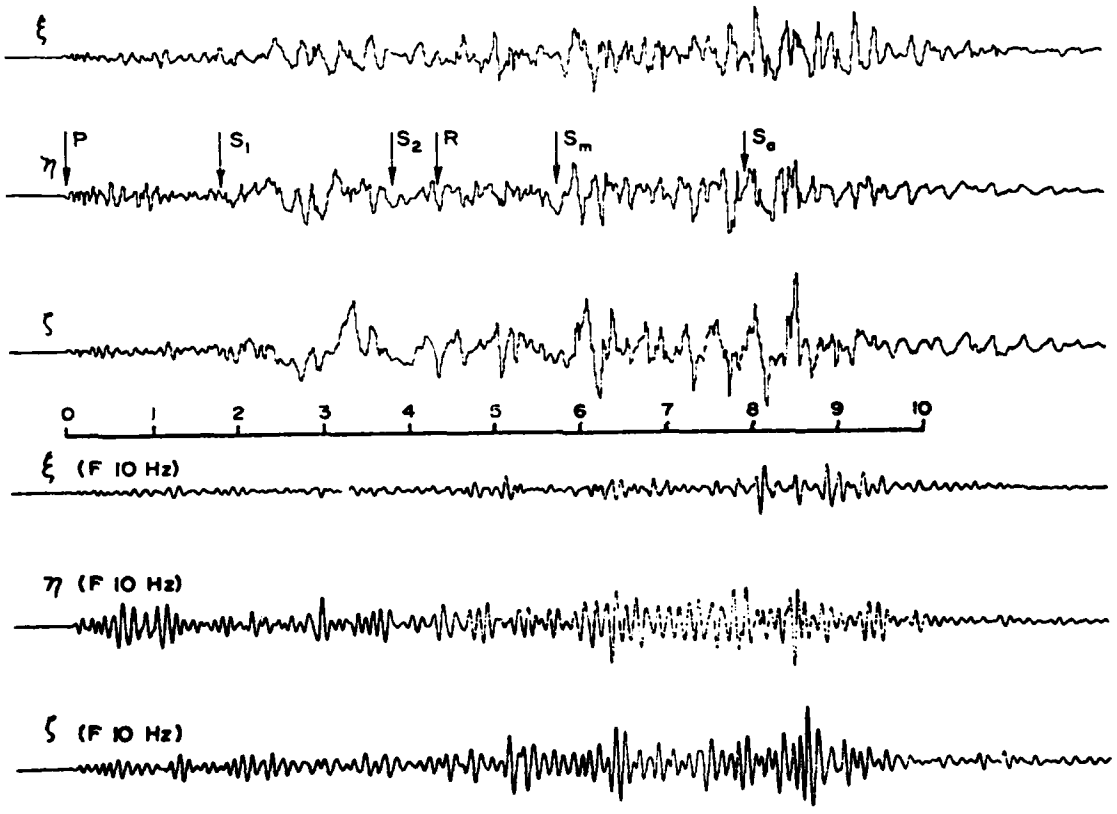

Figure 3.11. Components of ground acceleration at Pacoima resolved from original records: ξ, along strike; η, down dip; ζ, normal to fault plane. The lower three traces are the result of passing the top three through a notch filter at 10 Hz (from Bolt, 1972).

3.5 Managua, Nicaragua - December 23, 1972

References: Algermissen et al. (1974); Langer et al. (1974); Brown et al.(1974); Knudson et al. (1974); Sozen & Matthiesen (1975)

Location:

Earthquake: 12°20'N, 86°08'W

Accelerometer: ESSO Refinery
AR-240

Foundation: -

Size:

Magnitude $m_b = 5.6$

Moment: $M_o = 2.7 \times 10^{25}$ dyne cm

Mean Stress Drop $\Delta p = 4.8$ bars*

Fault Source Characteristics:

Faulting: Four faults observed to be activated, striking N35°-40°E. Maximum length of rupture observed was 6 km along the Tiscapa Fault.

Focal Mechanism: Strike N42° - 52°E
Dip 74°NW - 82°SE
Motion left-lateral

Parameters: L = 20 km
W = 8-12 km
D = .38 m

Mean Rupture Velocity:

1.7 km/sec

Peak Wave Amplitude Values:

	DOWN	EAST	SOUTH
Acceleration (cm/sec^2):	-299.9	-351.0	318.5
Velocity (cm/sec):	17.5	37.7	-30.0
Displacement (cm):	-8.7	14.9	-6.2

Bracketed Acceleration Duration (Acc. > 0.05g):

d = 14.0 sec

---

* Mean stress drop estimated from parameters below and using equation 1.1.

General Aspects:

The earthquake was located a few kilometers to the east of the SW margin of the Nicaraguan Depression and greatly damaged the city of Managua. The event has been defined as a "shallow-focus volcanic" earthquake and belongs to that class of earthquakes that occur within or near regions of contemporary volcanism (Dewey et al., 1973, 1974).

The meizoseismal area (area within the isoseismal VIII) measures about 100 km^2 and covers the region to the south of the Managua Lake, including the city of Managua. Geologically, the area constitutes a relatively flat plain, sloping gently towards the lake and consists of volcanic rocks overlain by low-density and high-porosity alluvial deposits. Fault rupture, due to the earthquake, occurred on four subparallel faults, traceable on the ground surface across the urban area of Managua. Its trend was on all four from SW to NE and the displacement was dominantly left lateral (see Figure 3.13).

From the tectonic point of view, the activated faults may be interpreted to be a multiple surficial expression of a single fault lying deeper under the unconsolidated alluvial deposits and having the same direction to its exposed components. This fault, according to the aftershock distribution, extends for at least 15 km (horizontally) into the Managua Lake.

Interpretation (ESSO Refinery Records):

The focus of this earthquake lay beneath the center of Managua at a depth of about 5 km. Of particular interest, the location of the focus was estimated by seismologists using the characteristics of the waves recorded by the strong-motion accelerometer at the ESSO refinery (see

Figure 3.12) on deep alluvium about 10 km from the center of the city. The instrument is marked R in Figure 3.13, which gives a schematic view of the seismic sources.

The four faults shown were identified by field geologic studies in Managua as having displacement during the earthquake sequences. The slip was mostly horizontal with left-lateral motion. The maximum aggregate displacement on two of the faults reached about 30 cm. Thus, the surface evidence points to a complicated composite structure. For the sake of simplicity, we will assume that the surface ruptures connect together at a depth of a few km beneath the surface to a primary fault plane.

Based on the geometry in Figure 3.13, the S-P time to the receiver R is about 1 sec. This corresponds closely with the arrival of the S phase marked on Figure 3.12b. (It is assumed that the instrument triggered on the arrival of the first P motion,which is likely for an instrument so close to the primary source of the waves.) In this case, P and S seismic waves should be propagating almost vertically by the time they reach the ESSO station. This is well borne out by the quite large amplitudes of vertical motion seen on Figure 3.12a which consists undoubtedly of mainly P and SV polarized motion.

The P wave from the assumed furthest portion of the faulting under the lake (point C) should follow the first P arrival from the focus by about 12.6 sec for a rupture velocity of 1.7 km/sec and average compressional velocity of 4.5 km/sec. This arrival time corresponds to the arrow marked P_c on the velocity plot (Figure 3.12a). Similarly, the S wave from the same point C for an average shear velocity of

2.1 km/sec would arrive about 18.4 sec after the first P arrival (S_c, Figure 3.12c). With the above assumptions, these phases may mark the end of the total rupturing process; however, there is a distinctive cessation of high-frequency ground motion at about 7.7 sec. Using the above velocities, this time may correspond to the generation of shear wave energy from the furthest point of rupture (D) propagating toward the station, i.e., toward the southwest.

The total duration of movement of the dislocation for length L = 20 km and a rupture velocity of 1.7 km/sec is 11.8 sec. The observed duration of 14 sec of strong shaking is, by comparison, longer. Because the site is so close to the fault, no correction here is necessary for attenuation of the motion, so there is a discrepancy of about 2 sec. As suggested in the previous paragraph, however, the rupture velocity in this earthquake may be somewhat less than in the California earthquakes, and there is also the possibility that the fault rupture was not confined to one plane.

Finally, the large displacements and velocities of the waves arriving on both the vertical and horizontal records at about 2-1/2 sec from the onset are worthy of comment. These have been marked by the arrow F on Figure 3.12b. In the circumstances of Figure 3.12 , the dislocation would move upward from the focus and break out into the surface, giving rise to a long-period fling, according to the hypothesis described in Section 1.3. Tentatively, therefore, we associate this long-period motion after F with this elastic rebound effect. Finally, we note that the Managua records contain no evidence of significant surface waves in sharp comparison with the Borrego Mountains case, but similar to the Parkfield

Station 2 recordings. This is to be expected since the recording is taken essentially over the dislocation wh re theory predicts surface waves are not developed.

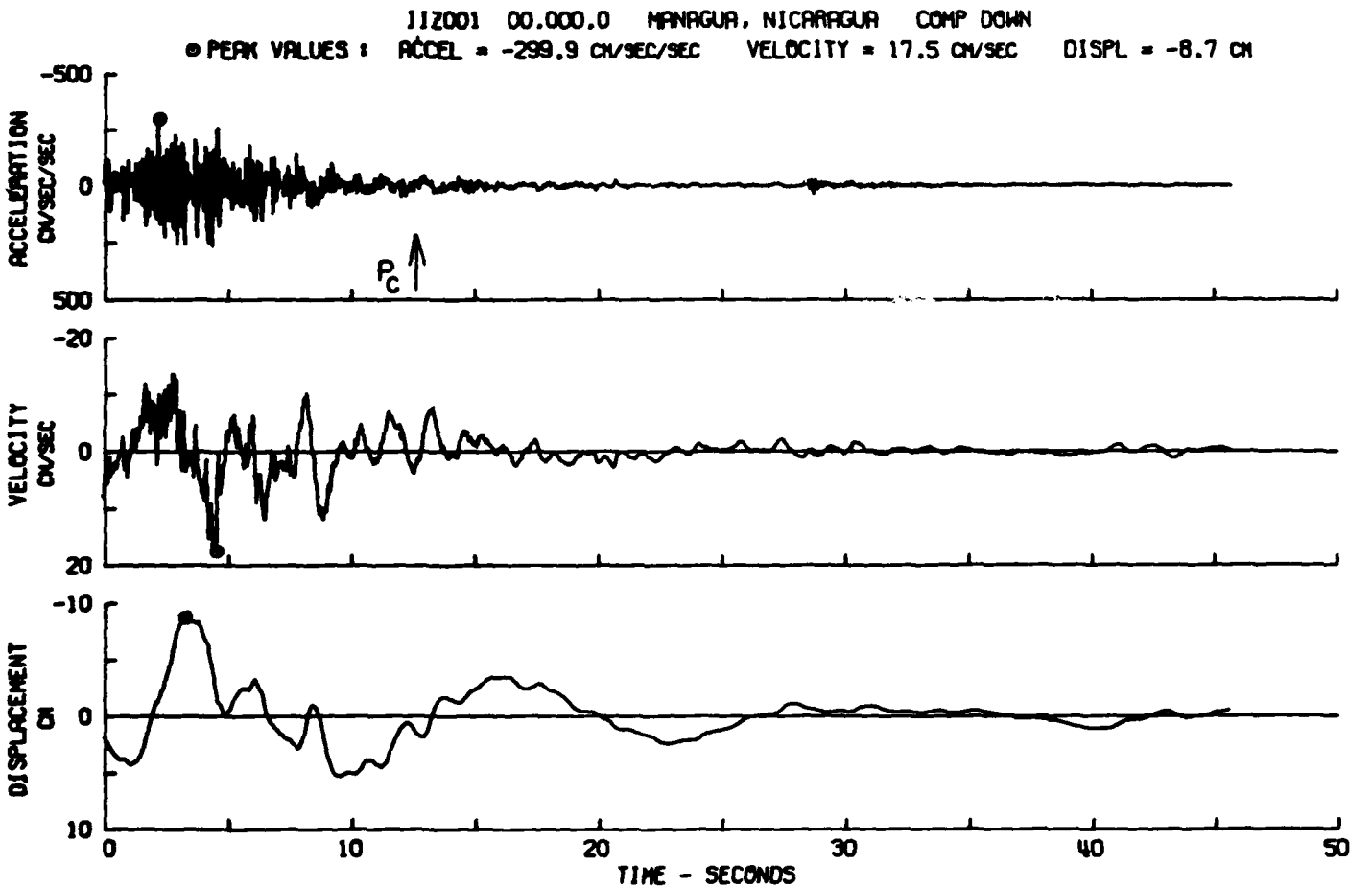

Figure 3.12. Managua earthquake; Dec. 23, 1972 - 0629 gmt (Sheet 1 of 3).

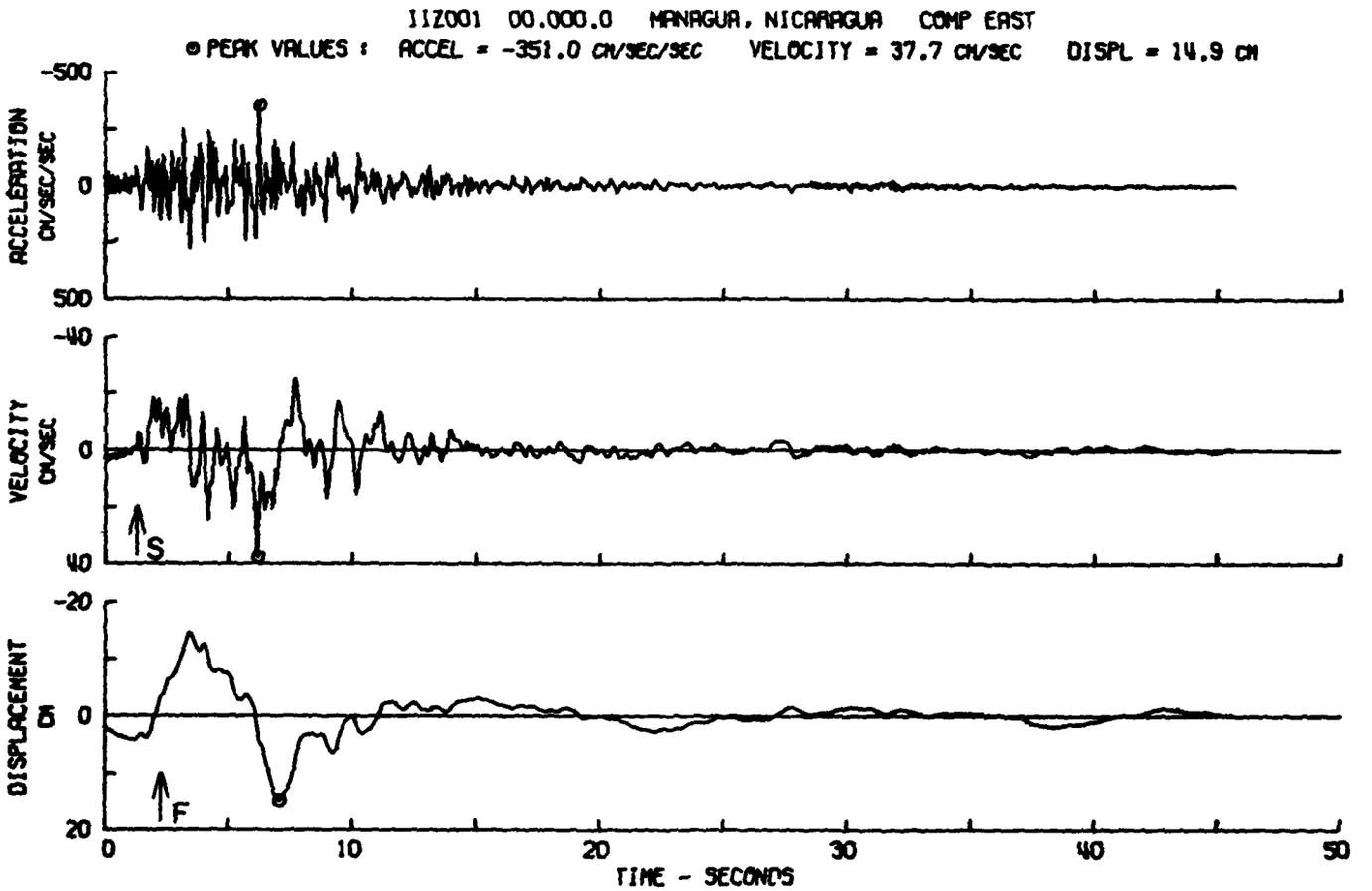

Figure 3.12. (Sheet 2 of 3).

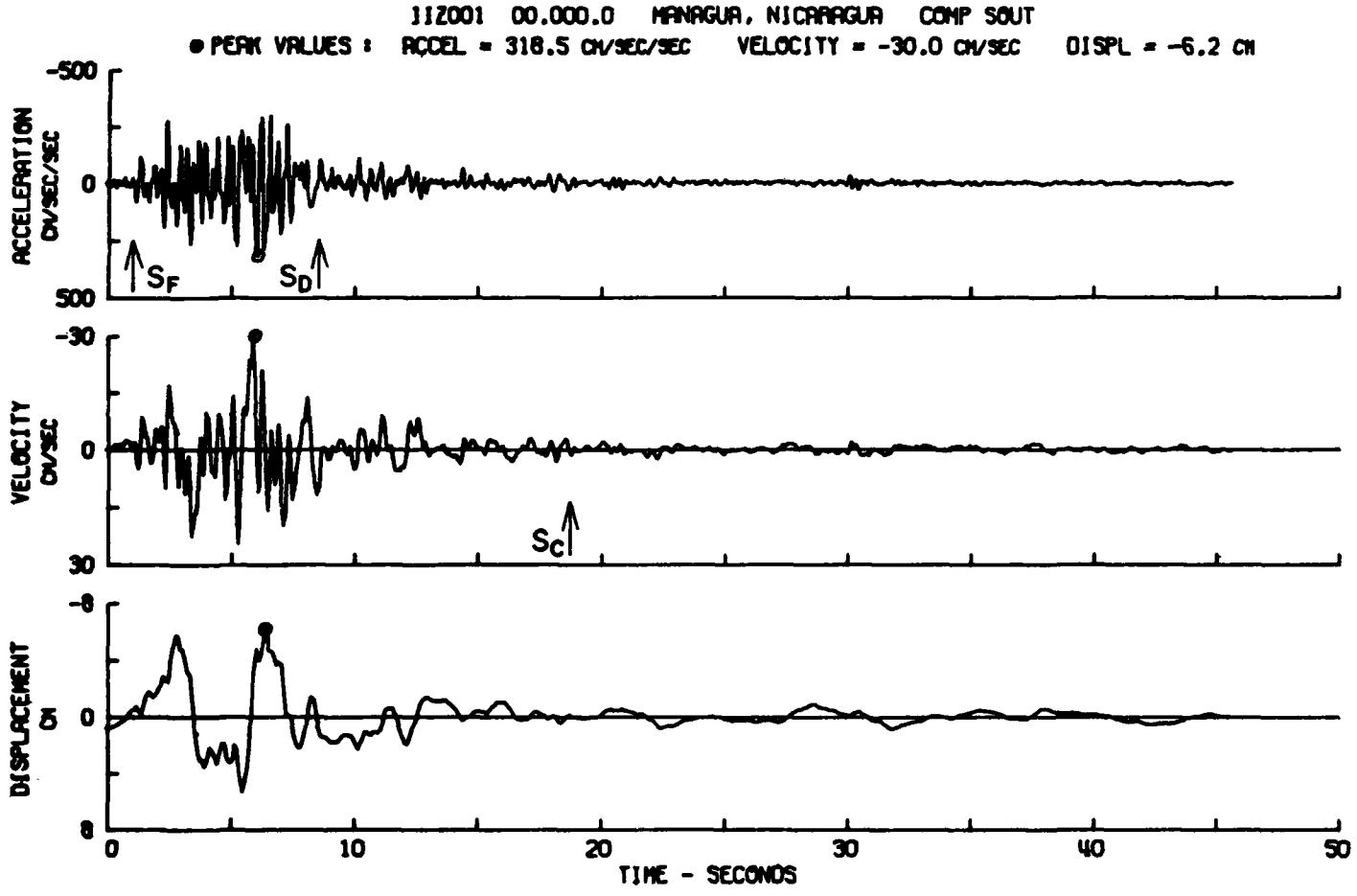

Figure 3.12. (Sheet 3 of 3).

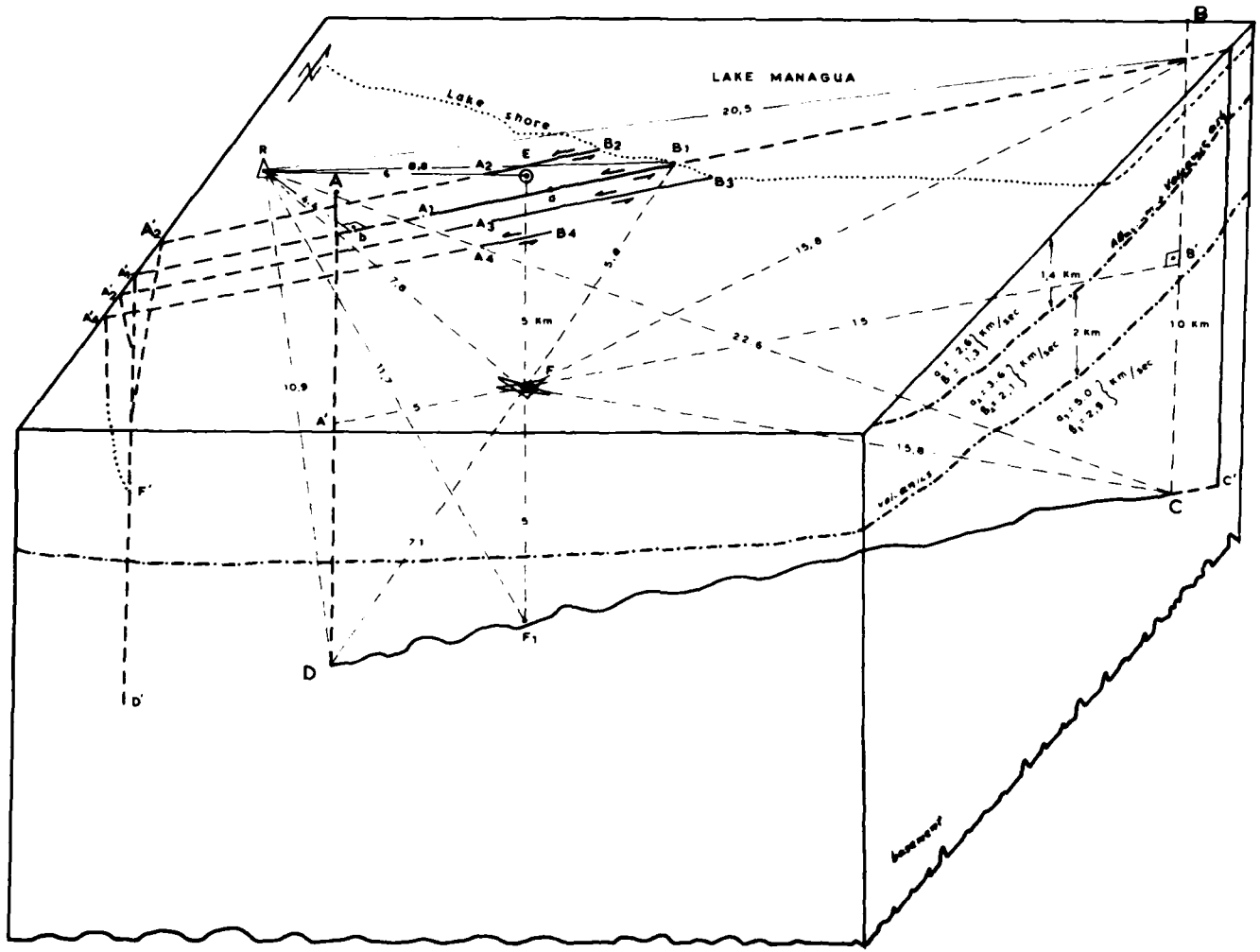

Figure 3.13. Model of the rupture surface in relation to surface faulting, ESSO station (R), epicenter (E), and focus (F) for the 1972 Managua, Nicaragua, earthquake.

3.6 Gazli, Uzbek, USSR - May 17, 1976

References: Aptekman et al. (1978); Hartzell (1980)

Location:

Earthquake:	40°21'N, 63°27'E
Accelerometer:	Karakyr Point SSRZ
Foundation:	-

Size:

Magnitude:	M_L = 6.35
Moment:	M_o = 1.6 x 10^{26} dyne cm
Mean Stress Drop:	Δp = 200 bars

Fault Source Characteristics:

Faulting: Rupture plane did not clearly break the surface. Only ground slumping and accompanying local surface cracking was observed.

Focal Mechanism: Thrust mechanism with

strike	N40°E
dip	54°SE
rake	78°

Parameters:

L = 54

W = 8-15 km

D = 3.3 m

Mean Rupture Velocity:

2.0 to 2.5 km/sec

Peak Wave Amplitude Values:

	VERT	NS	EW
Acceleration (cm/sec^2):	1300.0	656.0	738.0
Velocity (cm/sec):	49.0	44.0	54.0
Displacement (cm):	7.1	9.0	10.0

Bracketed Acceleration Duration (Acc. > 0.05g):

d ~ 14 sec

General Aspects:

The earthquake in this case history is actually one of a pair which considerably damaged the town of Gazli in Uzbekistan, USSR. The first earthquake occurred on April 8, 1976, and in the days that followed a strong-motion instrument was placed at Karakyr Point, near Gazli, by the Institute of the Physics of the Earth (USSR Academy of Sciences). This instrument was thus in place and recorded the second earthquake on May 17, 1976 (M_S = 7.0), and it is the second earthquake only that is discussed further in this section.

The locations of the seismic source and the recording stations are shown in Figure 3.15 (Aptekman et al., 1978, and Hartzell, 1980). The strong-motion accelerometer was an SSRZ three-component instrument with optical recording, and the records have been made available by the Institute of the Physics of the Earth. The peak accelerations recorded were 1.3, 0.7, and 0.8g for the vertical, N-S and E-W components. Because this was the highest vertical component ever recorded before the 1979 Imperial Valley earthquake (see Section 3.9), the high vertical acceleration measured in this case was at first viewed with some suspicion. For this reason, the recording instrument was carefully checked by the Institute, but no malfunction or misscaling of the records was found.

According to a fault plane solution study made by Hartzell (1980), the earthquake had a thrust mechanism with an average dislocation of about 3.3 meters. The rupture is thought to have started at a depth of 15 km, which is about the same, or a little deeper, as maximum rupture depths in California. The dip of the fault plane is given as 54° to the southeast with the strike N40°E. We may, therefore, use Figure 3.10 for the fault plane for the San Fernando earthquake in 1971 as a reasonabl approximation for the source surface in the Gazli earthquake.

Interpretation (Karakyr Point records):

Although details of the rupture surface in the Gazli earthquake are not as firm as those for the San Fernando earthquake, the situation is reasonably similar (see Figure 3.10). The recording station was above the thrust surface, which must have had a dimension of approximately the same value (150 to 200 km^2).

If the instrument is assumed to be triggered on the first P wave from the focus (depth 15 km), with a velocity of P of above 6 km/sec, the direct S wave from the focus would arrive about 2.5 sec after the triggered time. This time of arrival is shown as S on the horizontal components of the record and the vertical component (Figure 3.14). A little later, at about 3 sec, the horizontal records show an increase in both amplitude and period of acceleration and velocity (particularly the N-S component) and is slightly reminiscent of the early pulse-like motion on the Pacoima record. However, the dominant pulse does not arrive on the horizontal components until 5.5 sec after onset. The horizontal motions then remain large up to about 12 sec after the record begins.

The vertical component record which gives clues on SV and Rayleigh wave motion shows a long-period pulse in the velocity record approximately 7.5 sec after the onset of triggering. This pulse of over 1 sec in duration is strongly correlated with a similar motion on the N-S component.

The shortest distance from the rupture plane to the Karakyr Point station is about 11.6 km. Considering seismic energy generated from this point and assuming a rupture velocity of 2.0 km/sec, the first pulse at 5.5 sec on the horizontal instruments would correspond to a

P wave with a velocity of about 6.0 km/sec, and the pulse at 7.5 sec on the vertical instrument would correspond to an SV wave with a velocity of about 3.5 km/sec.

Hartzell (1980) points out that from the amplitudes of the teleseismic P and pP phases (the P wave that travels upward first and is reflected back into the Earth at the free surface) there is evidence of strong vertical directivity in the propagation rupture. This is consistent with the strong vertical motions recorded on the vertical component instrument. He also infers from the study of the distant records that there was an average rupture velocity of between 2.0 and 2.5 km/sec. The synthetic Wood-Anderson records computed from the accelerograms give a local magnitude M_L of 6.35.

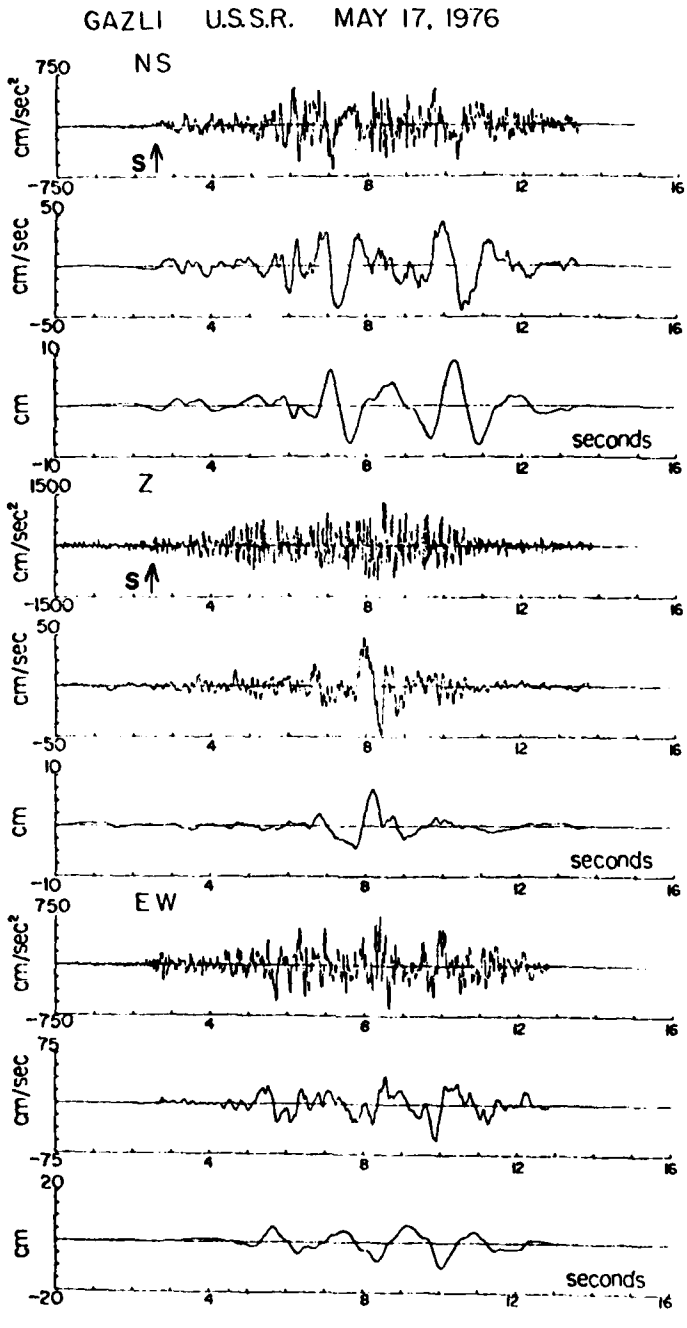

Figure 3.14. Accelerations, velocities, and displacements from the Karakyr Point accelerograph (from Hartzell, 1980).

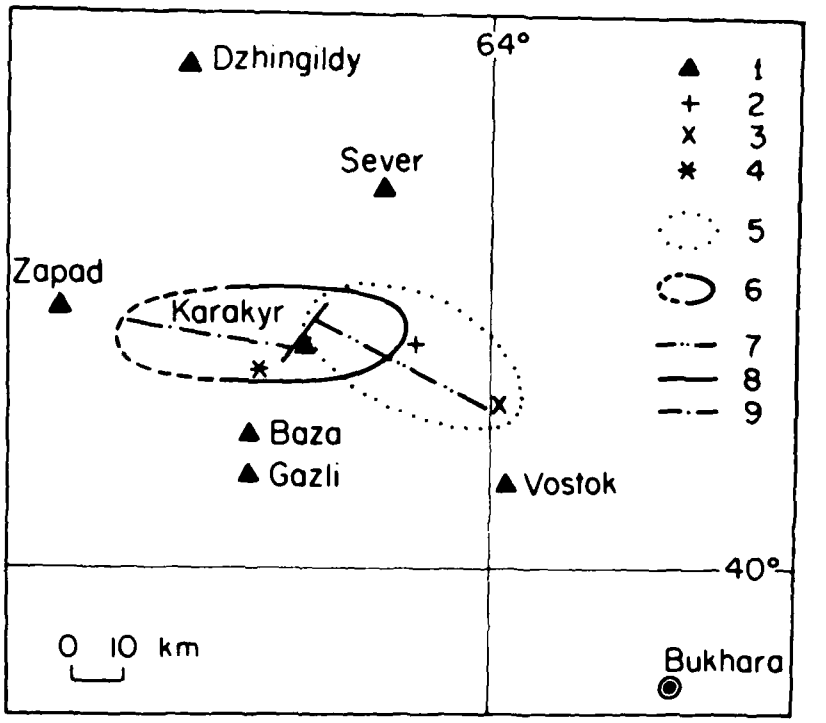

Figure 3.15. Epicentral region of the April 8 and May 17, 1976 Gazli earthquakes after Aptekman et al. (1978). The symbols are defined as follows:

1 - seismographic stations
2 - epicenter of April 8 event
3 - supposed epicentral location of large aftershock of April 8 event
4 - epicenter of May 17 event
5 - approximate location of aftershocks of April 8 event
6 - approximate location of aftershocks of May 17 event
7 - approximate location of the fault break for the April 8 event
8 - approximate location of the fault break in the initial stages of breaking for the May 17 event
9 - approximate location of the major fault break for the May 17 event

(from Hartzell, 1980)

3.7 Bucharest, Romania - March 4, 1977

References: Müller et al. (1978); Hartzell (1979); Berg et al. (1980)

Location:

Earthquake: 45°52'N, 26°45'E

Accelerometer: Bucharest
Single-story reinforced concrete frame building; basement
SMAC-B

Foundation: 12 m of clay over deep loess and alluvial deposits

Size:

Magnitude: m_b = 6.8 (BRK)

Moment: $M_o = 2.0 \times 10^{27}$ dyne cm

Mean Stress Drop: Δp = 57 bars

Fault Source Characteristics:

Faulting: no surface rupture observed

Focal Mechanism: predominantly thrusting motion
strike N40°E
dip 70°NW
rake 99.4° (Hartzell, 1979)

Parameters: L = 50 km
W = 50-65 km
D = 1.5 m

Mean Rupture Velocity:

3.8 km/sec

Peak Wave Amplitude Values:

	VERT	NS	EW
Acceleration (cm/sec^2):	100.0	221.0	187.0
Velocity (cm/sec):	13.0	82.0	37.0
Displacement (cm):	3.8	27.0	13.0

Bracketed Acceleration Duration (Acc. > 0.05g):

d = 10 sec

General Aspects:

This earthquake differs from the other case studies in having a much deeper focus, about 100 km. We thus have an example of seismic waves traveling from a source well beneath the depths characteristic of California earthquake sources. Sufficient energy was generated, however, to cause considerable damage in central and southeastern Romania.

The epicenter was located in the Vrancea region of the Carpathian Mountains, approximately 170 km north-northeast of the capital city of Bucharest. A peculiar feature of the historical earthquake pattern in the Carpathians is a persistent pocket of intermediate focus sources under the Carpathian bend at depths of between 100 and 160 km.

Nine strong-motion accelerographs and two seismoscopes were installed in Romania at the time of the earthquake. Records were recovered from the ground-level accelerographs in Focsani, Vrincioaia, and Bucharest, from the accelerograph at the top of one of the two instrumented buildings in Bucharest and from both seismoscopes, but only the two seismoscope records and two accelerograms from Bucharest are intact. The complete Bucharest ground record is shown in Figure 3.16. The recording accelerograph was located in the basement of a one-story, reinforced concrete frame building at the Buildings Research Institute in the eastern part of the city. The accelerogram was recorded on a Japanese-built, three-component SMAC-B accelerograph with 10-Hz natural frequency accelerometers that are critically damped.

Damage caused by strong ground shaking was most severe in Bucharest, where 35 buildings collapsed and numerous other buildings sustained

structural and architectural damage and damage to contents. The isoseismal lines (see Berg et al., 1980) show an asymmetric pattern which stretches essentially to the south, southeast, and southwest of the epicentral region. For example, Focsani, between the epicentral area and Bucharest, had collapsed unreinforced masonry walls, and the cities of Craiova and Alexandria, located to the west and southwest of Bucharest, contained unreinforced masonry walls in low-rise construction which collapsed, some partly and some totally. By contrast, the effects of strong ground shaking in Brasov, to the west of the epicenter, and in Bacau, to the north, was slight. This asymmetric pattern of strong ground motion has been noticed in earlier Romanian earthquakes from the Vrancea zone, for example, in the November 10, 1940 earthquake, M_S = 6.4, with focal depth of 150 km.

The intensity of shaking (MM) could be rated between VIII and IX in Bucharest. Bucharest is both the capital and largest city in Romania. Thirty-five buildings collapsed, most of them near the heart of the city. Some buildings collapsed in the 1977 earthquake that survived the 1940 earthquake. However, strong motion in the 1940 earthquake was, of course, not recorded.

Interpretation (Bucharest records):

Seismological studies since the 1977 earthquake have provided both fault-plane solutions and the study of the seismograms of distant and near stations. The fault mechanism is a thrust type, with rupture propagating mainly towards the southwest. It has also been demonstrated that the earthquake consisted of multiple ruptures of at least three episodes. For example, Iosif and Iosif (1977) have examined closely the

records of insensitive, mechanical instruments of the Romanian seismic network and inferred that there were four separate shocks within a 9-sec interval, of which three (M_L = 6 to 6.9) are the major components of the earthquake. The type of evidence available is shown in Figure 3.17. There, three separate onsets, marked P1, P3, and P4, are shown for the station Echery, at a distance of about 1,400 km from the epicenter.

Based on such studies, a plausible simplified rupture surface for the March 4, 1977 earthquake is sketched in Figure 3.18. Although the actual source mechanism appears to be complex, the inferred rupture surface, shown by arrows in the figure, would involve thrusting of the mountains over the deep alluvial plains to the southeast, with the rupture traveling a distance of approximately 100 km mainly to the south. This rupture pattern is consistent with the distribution of aftershocks that were recorded by sensitive seismographic stations after the main shock was complete.

According to Müller et al.(1978), the third shock of the multiple event was the strongest,and they present evidence for a strong bending of the rupture surface as shown in Figure 3.18 and also a reversal of the motions of elastic rebound on the rupture plain. They also find evidence for abrupt termination of the rupture, producing strong stopping signals. They have the rupture plane dipping northwest with a dip angle of 70°.

The SMAC-B strong-motion accelerogram recorded in Bucharest is shown in Figure 3.16. The strong-motion instrument was evidently triggered by a P wave from one of the multiple events (perhaps the third) that made up the whole earthquake. The most notable features after the

triggering are the large-amplitude (0.16g and 0.20g) pulses (periods 1.1 and 1.6 sec) that occur in the E-W and N-S components about 20 sec after the instrument was triggered (trigger level is 0.01g vertical acceleration). Such solitary pulses would be unusual at this epicentral distance for shallow-focus earthquakes. After each pulse, the accelerations are lower in amplitude and higher in frequency.

By contrast, there are no long-period pulses in the vertical component, where accelerations are generally in the 8- to 10-Hz frequency range, with the maximum acceleration being about 0.12g. The interpretation is that, after about 20 sec of predominantly P wave motion, a large S pulse of predominantly SH type arrived from the main rupture. The velocity of this pulse to travel a distance of approximately 160 km is about 4 km/sec. This value is reasonable for S waves in this region.

It will be noted that no wave motion can be read that is coherent between the vertical and horizontal component instruments, indicating that almost no Rayleigh waves were generated. This is to be expected from the theory of the generation of surface waves which require sources to be near the surface for efficient generation. A final note of importance is that the long S minus P warning duration allowed time for some persons to escape from buildings that finally collapsed.

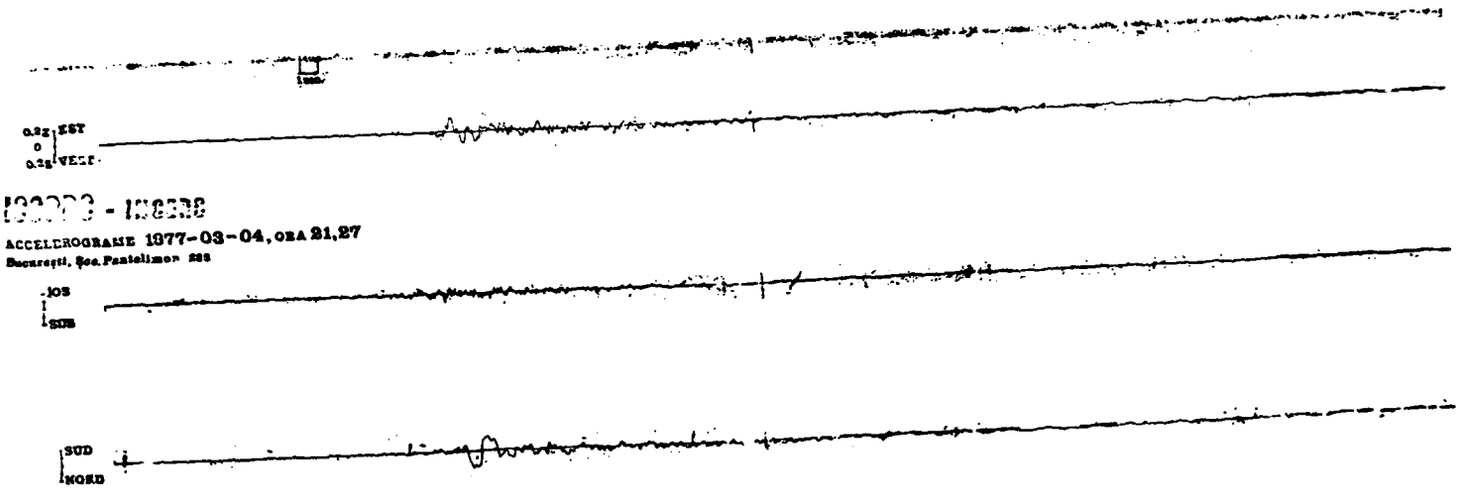

Figure 3.16. Accelerogram recorded in Bucharest in the 1977 Romanian earthquake.

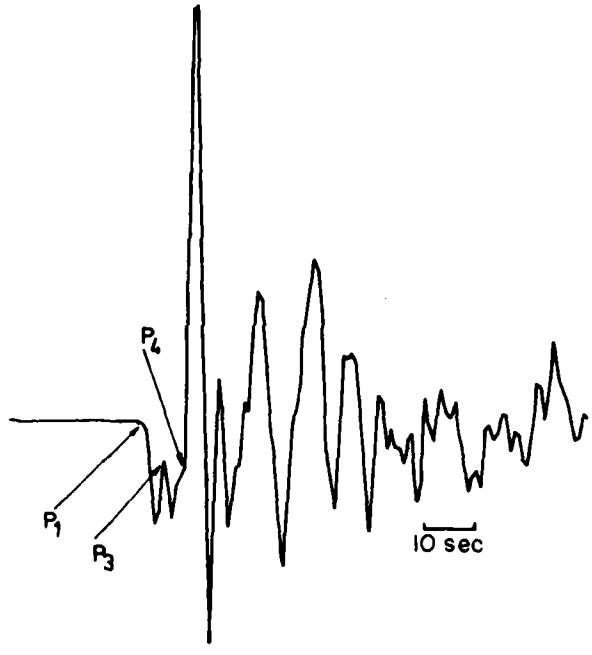

Figure 3.17. Accelerometer record for Echery station, located about 1400 km from the epicenter of the 1977 Romanian earthquake. (from Iosif and Iosif, 1977)

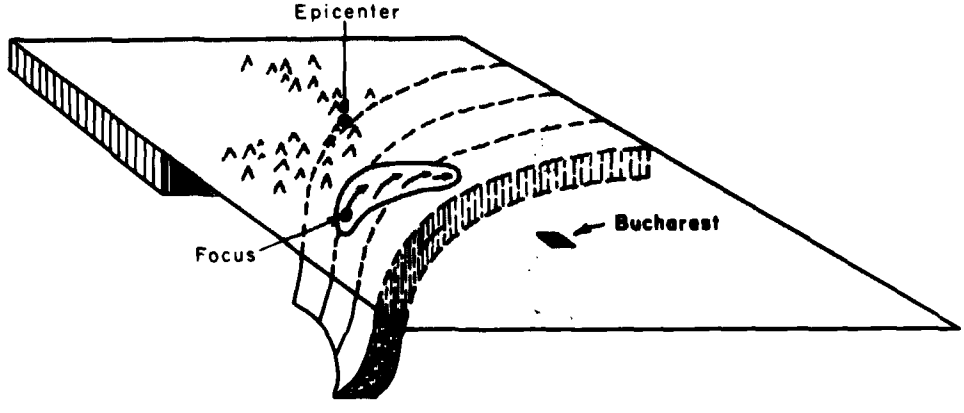

Figure 3.18. Simplified model of the rupture surface for the 1977 Bucharest, Romania, earthquake.

3.8 Coyote Lake, California - August 6, 1979

References: Porcella et al. (1979); Uhrhammer (1980)

Location:
- Earthquake: 37°6.12'N, 121°30.2'W
- Accelerometer: 1. Coyote Creek C217/SMA-1T
  2. Gilroy Array #6 1413/SMA-1
- Foundation: both instruments on conglomeratic sediments

Size:
- Magnitude: $M_L = 5.9$
- Moment: $M_o = 6 \times 10^{24}$ dyne cm
- Mean Stress Drop: $\Delta p = 18 \pm 5.6$ bars

Fault Source Characteristics:

- Faulting: Minor breaks and cracks along about 8-10 km of the Calaveras Fault, which strikes N30W. Right-lateral displacements up to 5 mm were observed.
- Focal Mechanism: Strike N(27±7)°W
  Dip (90±15)°
- Parameters: L = 23.1 km
  W = 5 km
  D = 0.21 ± 0.066 m (from M_o)
  = 0.005 m (observed at surface)
- Mean Rupture Velocity:
  2.2 km/sec

Peak Wave Amplitude Values:

1. Coyote Creek	UP	S70W	S20E
Acceleration (cm/sec^2):	98	225	157
Velocity (cm/sec):	-	-	-
Displacement (cm):	-	-	-
2. Gilroy Array No. 6	**UP**	**N40W**	**S50W**
Acceleration (cm/sec^2):	167	333	412
Velocity (cm/sec):	-	-	-
Displacement (cm):	-	-	-

Bracketed Acceleration Duration (Acc. > 0.05g):

1. Coyote Creek
   d = 4.3 sec
2. Gilroy Array No. 6
   d = 7.7 sec

General Aspects:

This moderate size earthquake occurred within the region of the western foothills of the Diablo Range and affected the southern half of Santa Clara Valley. Its epicenter was instrumentally located at the eastern flank of the Coyote Lake while its meizoseismal area was centered at the southeast end of the same valley, roughly between the towns of Hollister and Gilroy (Uhrhammer, 1980).

The earthquake is the largest to occur in this province since the one of 1911 and was generated on the Calaveras fault zone. This feature, which is a principal branch of the San Andreas fault system, has an overall length of 160 km and a NW - SE direction.

The fault segment that was activated during the earthquake has a length of about 23 km (considering both the length of the aftershock area and the ground rupture) starting from the NW edge of the Coyote Lake. Further SE, it runs along the eastern margin of Santa Clara Valley while midway bends slightly south-westwards and crosses the SE end of the same valley, up to the NW outskirts of Hollister.

Geologically, the region along the fault consists of strongly faulted and deformed sandstones, mudstones, conglomerates, volcanics, and contemporary deposits. These formations further to the east are in tectonic contact with the Franciscan formation. The general picture of a highly

complicated terrain presents difficulties for seismological interpretation (i.e., source parameters, wave propagation evaluations, and site effects).

Interpretation (Coyote Creek and Gilroy Array No. 6 Records):

This earthquake is of special interest (Uhrhammer, 1980) because 24 strong-motion accelerometers triggered, located within 50 km of the fault rupture, with several very near to the Calaveras fault. Peak ground accelerations of about 0.4g (both horizontal and vertical) were observed (see Figures 3.19 and 3.20). These provide a valuable set of strong-motion records for studies of fault mechanisms, wave generation, and directivity. Full analyses of the records from this earthquake have not yet been made, and we mention here only the two obtained at each end of the fault rupture (Figures 3.19 and 3.20).

The geometry of the faulting is speculated on in Figure 3.21. There is field evidence for small surface slip in the right-lateral sense towards the southern end of the fault, but the evidence to the north towards Coyote Lake (Point A) is much more tenuous. The assumption is that the rupture commenced at the focus under Point E and traveled partly to the north but mainly to the south towards Point B, where it broke out at the surface. The total horizontal dimension of faulting would thus be about 23 km. The focus of the earthquake is well determined at about 6 km.

A plan showing the distribution of near-field accelerometers is given in Figure 3.22. The distribution was in the form of a profile at right angles to the fault, and the figure shows the comparison of acceleration, velocity, and displacement at each of the stations (in the usual metric units). The attenuation of all the three parameters away

from the fault can be clearly seen after allowance for variations due to soil and crustal structure. According to the rupture model adopted, the dislocation moved from the north to the south away from the Coyote Creek Station towards the Station No. 6. Enhanced acceleration, velocity, and displacement recorded at Station No. 6 compared with the Coyote Creek Station (both close to the ruptured fault) were in agreement with directivity focussing (see Section 2.6).

As an illustration of the value of transforming strong-motion instrument records to more familiar ones, Figures 3.19 and 3.20 show comparisons between accelerograms and computed equivalent Wood-Anderson records (see Appendix A). It can be seen that the Wood-Anderson response has filtered out some of the higher frequencies present in the accelerograms and thus interpretation is easier. On both these Wood-Anderson records we mark the onset of two phases, called S_1 and S_2. These would be interpreted in normal seismological practice as the arrival of two S phases from the focus, taking different paths due to the structure in the crustal rocks.

It is of interest also to compare the coda for both the Coyote Lake and the Gilroy instruments. The motions on the Wood-Anderson records in the Coyote Creek case (Figure 3.19b) extend to 20 sec after the onset of the S wave. On the other hand, in the case of the southern station, Gilroy No. 6 (Figure 3.20b), the ground motion is much compressed in time with a smaller coda. This compression of wave energy in time is consistent with a fault rupturing towards the south. The effect on the displacement spectra of the moving source can be seen in Figure 2.5.

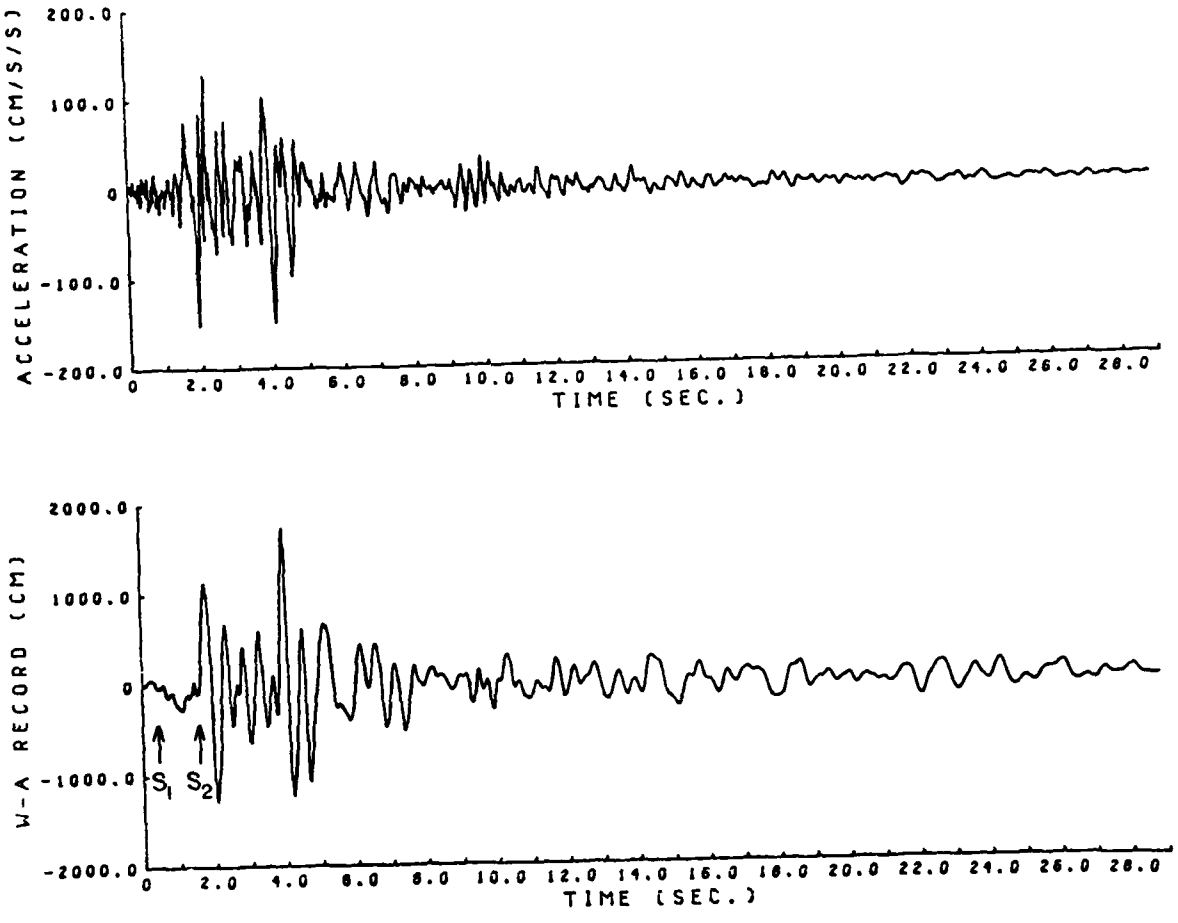

a. N-S component

Figure 3.19. Coyote Creek; N-S and E-W components (Continued).

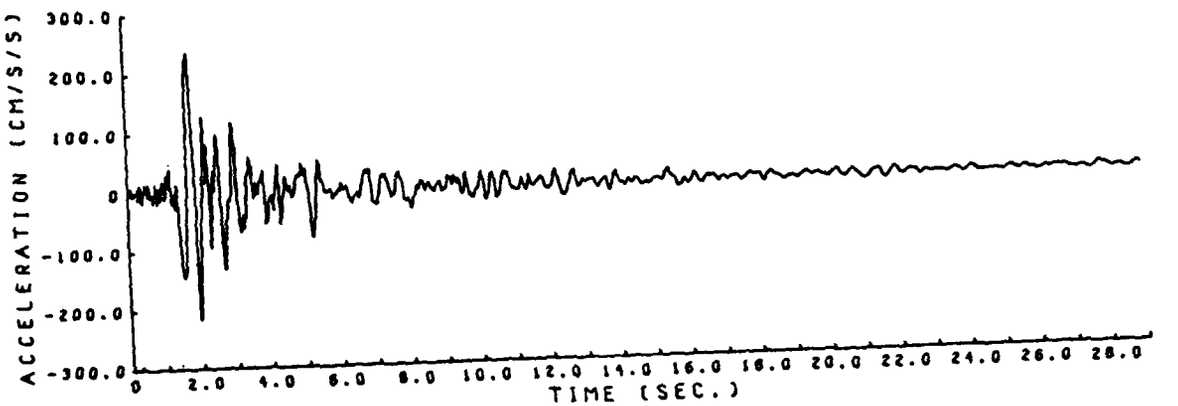

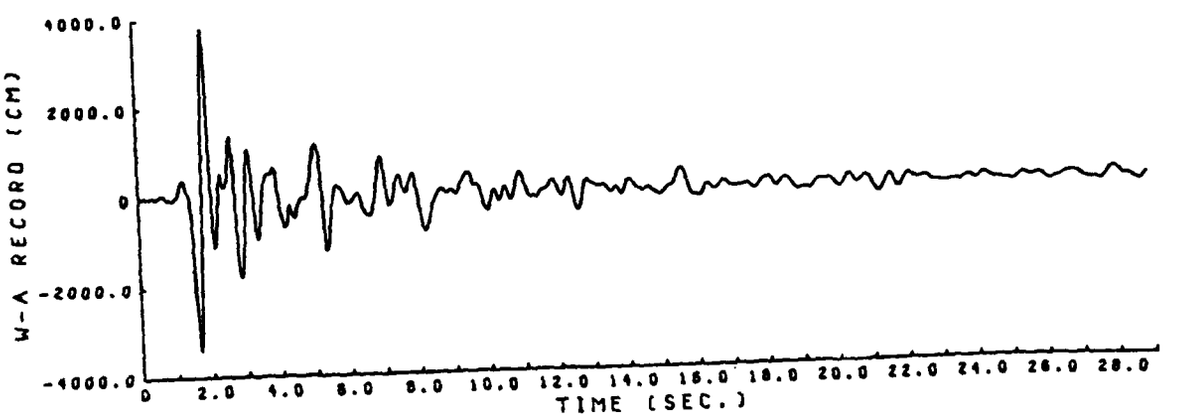

b. E-W component

Figure 3.19. (Concluded).

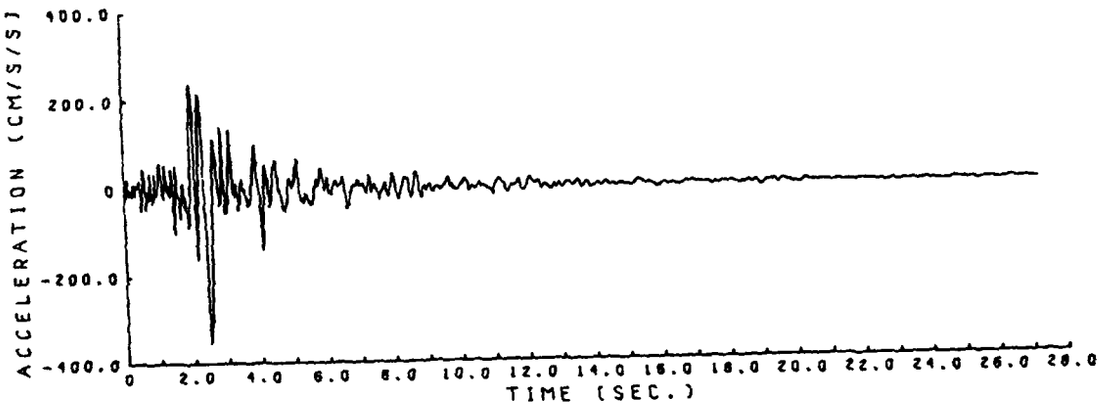

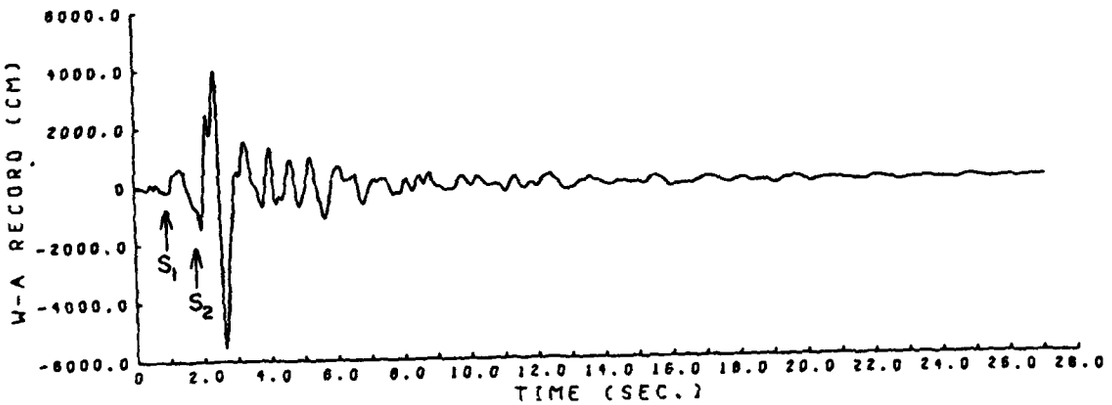

a. N-S component

Figure 3.20. Gilroy No. 6; N-S and E-W components (Continued).

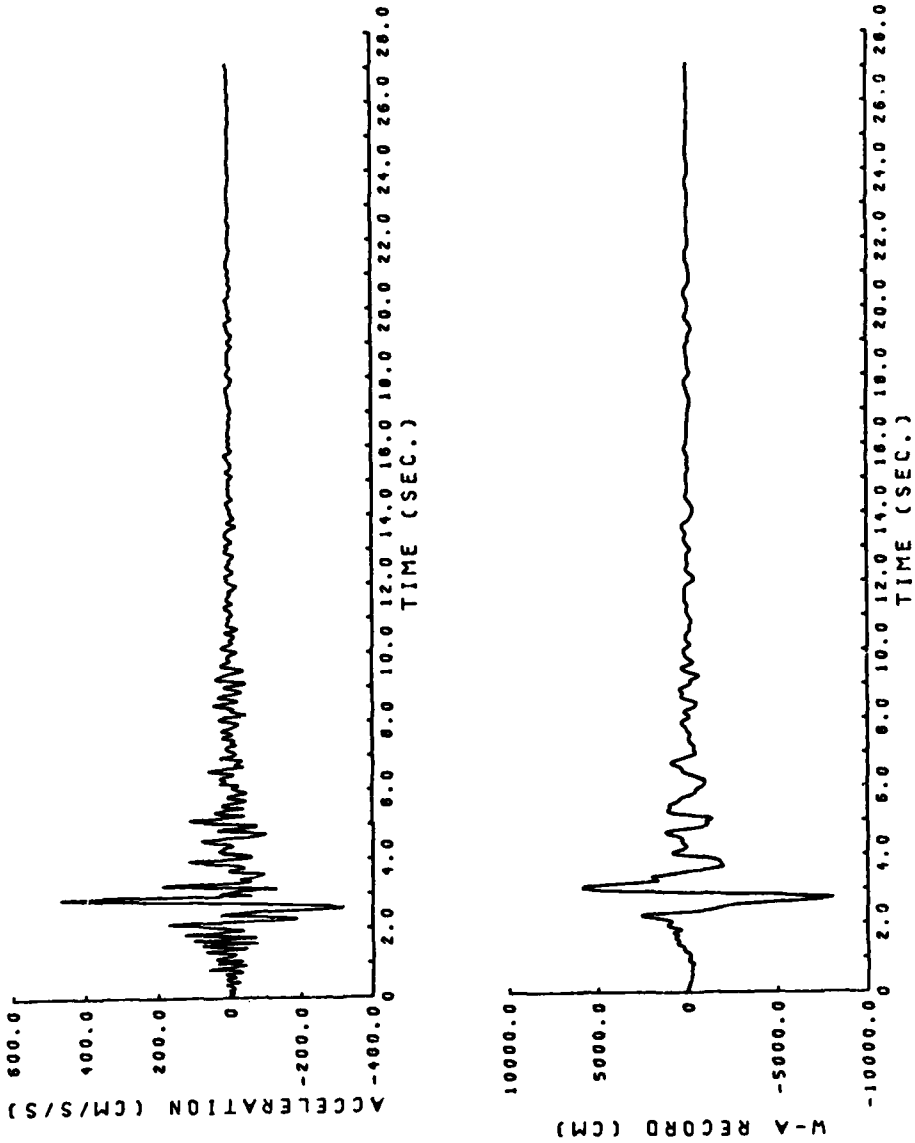

b. E-W component

Figure 3.20. (Concluded).

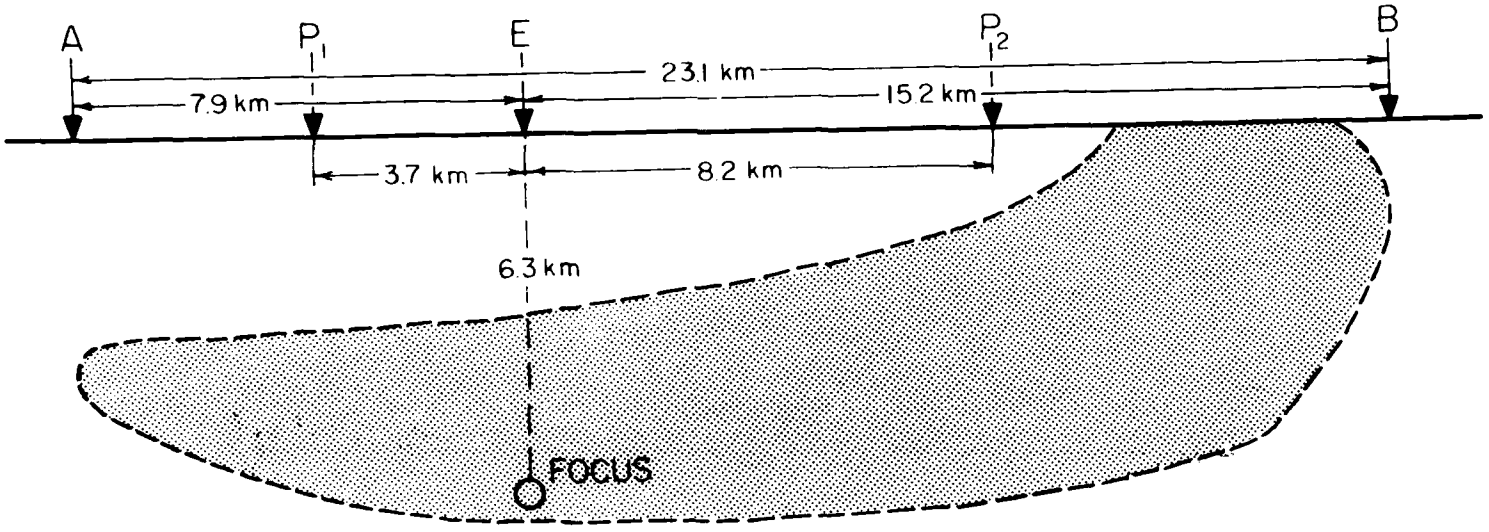

Figure 3.21. Simplified model of the rupture surface in relation to the Coyote Creek station (P_1), Gilroy No. 6 station (P_2), epicenter (E), and focus for the 1979 Coyote Lake, California, earthquake.

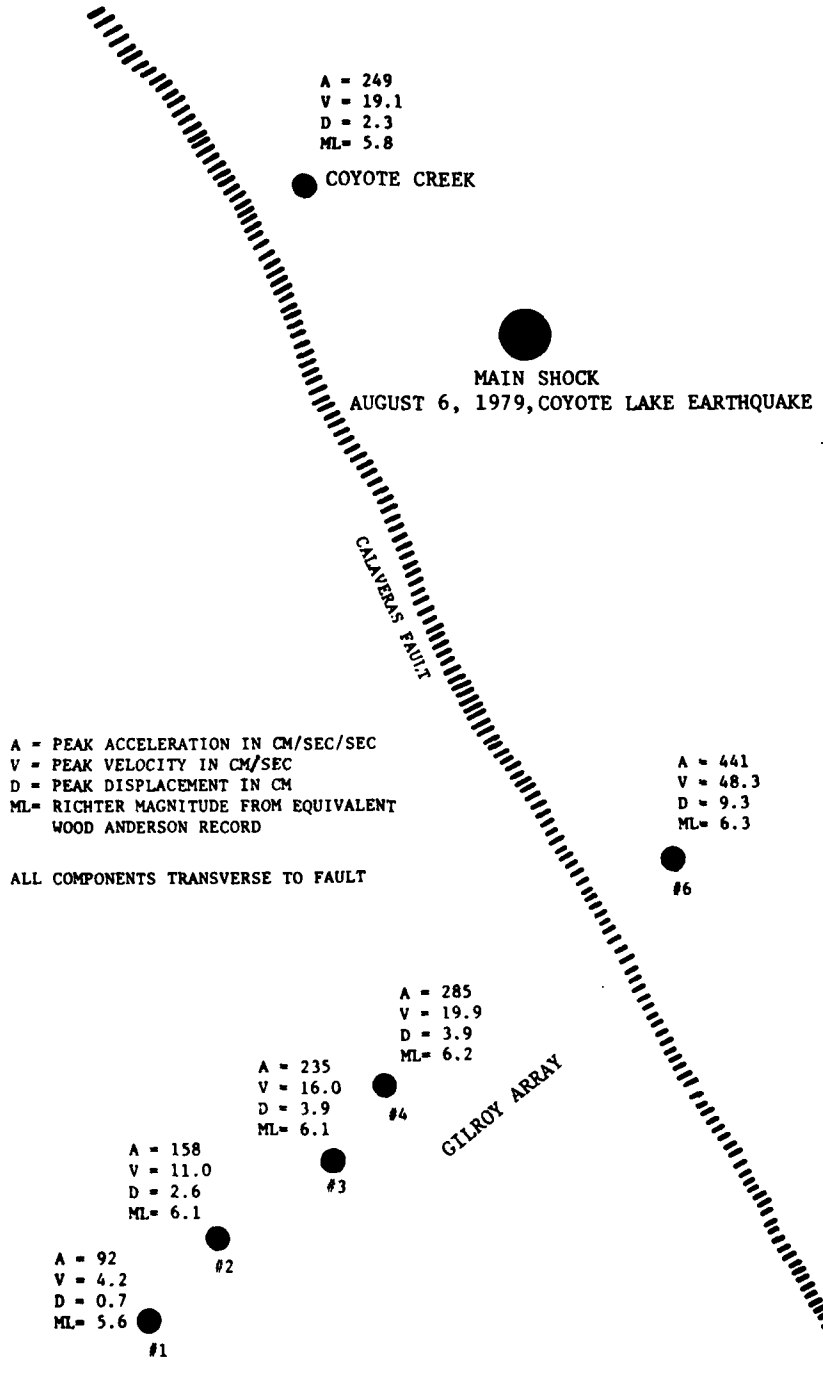

Figure 3.22. Map of Calaveras fault and accelerometer stations for the Coyote Lake earthquake. Peak accelerations, velocities, and displacements are given for component transverse to the fault (from Singh, 1981).

3.9 Imperial Valley, California - October 15, 1979

References: Porcella and Matthiesen (1979); Rojahn (1981)

Location:
- Earthquake: 32°38'N, 115°20'W
- Accelerometer: Bond's Corner SMA-1T
- Foundation: 1-story building, ground level

Size:
- Magnitude: M_L = 6.6 (CIT)
- Moment: $M_o = 8.7 \times 10^{25}$ dyne-cm*
- Mean Stress Drop: Δp = 5.5 bars*

Fault Source Characteristics:
- Faulting: Rupture observed along approximately 35 km of the Imperial and Brawley Faults. Motion was right-lateral strike-slip (up to 55 cm) with some dip-slip offsets (up to 19 cm) down to the east.
- Focal Mechanism: -
- Parameters: L = 35 km; W = 15 km; D = 0.55 m
- Mean Rupture Velocity: 2.0 to 3.0 km/sec

Peak Wave Amplitude Values:

	UP	S40E	S50W
Acceleration (cm/sec^2):	461	-575.7	770.4
Velocity (cm/sec):	-	-43.6	44.1
Displacement (cm):	-	12.2	-14.6

Bracketed Acceleration Duration (Acc. > 0.05g)

d = 19.1 sec

* Moment and stress drop estimated from parameters below and using equation 1.1.

General Aspects:

The October 15, 1979, Imperial Valley earthquake provided an extensive and important set of strong-motion records in the near field. Detailed interpretation, based on adequate theoretical modelling, of the main peaks on the accelerograms will, of course, take many years. For the present purpose, we list only the problems of interpretation on which this set of observations throws particular light.

(a). Variations of wave patterns with distance from the seismic source. As shown in Figure 3.23, a linear array of strong-motion accelerometers (many with absolute radio time marks) recorded the seismic waves along a profile at right angles to the fault. In Figure 3.23 are marked preliminary values of peak acceleration, velocity, and displacement. These simple parameters (cf. the discussion in Section 4.1) give an indication of the way the waves attentuate in the near field (see Figure 3.24). More significant information is given by the seismograms themselves. They have been studied but are not reproduced here (see USGS OFR 79-1604) except the record at Bond's Corner (Figure 3.26).

(b). Directivity focussing in the near field. The 1979 Imperial Valley strong-motion records are from reasonably well-distributed sites (Figure 3.23) and help test the hypotheses concerning source of radiation effects, including the effect of a moving dislocation. The preliminary conclusion is that the effect can be detected in the wave displacements, but is small relative to other sources of variation in the wave acceleration.

Theoretical modelling of wave focussing due to a moving source suggests that the zone of focussing is concentrated into a narrow lobe

in the direction of the velocity of rupture. Some work suggests that the highest velocities would occur in the direction of rupture propagation in a focussing lobe of width approximately $\pm$ 5° from the direction of the dislocation (Figure 3.25). On these models, the small areal extent of directivity focussing could be missed observationally unless there are a large number of strong-motion instruments in the near field. Nevertheless, in the case of the 1979 Imperial Valley faulting, Bond's Corner and Station No. 2 should be within the lobe and, as Figure 3.23 shows, there is no indication of higher than average accelerations and velocities at these stations.

(c). The ratio of energy in the vertical and horizontal components of the seismic waves. In part of the near field of the faulting that produced the October 15, 1979, Imperial Valley earthquake some recorded ground acceleration have peak vertical values greater than 0.7 times the peak horizontal values.

In particular, Stations 5, 6, 7, 8, and 9 show ratios of 1.27, 2.41, 1.25, 0.86, and 0.95, respectively (USGS OFR 79-1654). The amplitudes of the Fourier spectra from these stations reflect these ratios by showing comparable values for vertical and horizontal response at frequencies greater than about 5 Hz. The spectra also show that, in the relevant frequency band, the exceedence of vertical amplitude over horizontal is most marked for frequencies of 10 Hz or higher (e.g., Stations 6 and 7).

However, there is variability. Station 4 of the El Centro array (see Figure 3.23), situated 7 km from the ruptured fault, has a V/H ratio of only 0.52: at Bond's Corner station, where the maximum peak horizontal acceleration (0.77g) was measured (Brady, et al., 1980),

the ratio is 0.7. It should also be noted that at stations beyond 11 km from the fault source, peak vertical accelerations were comparable or fell short of horizontal ones in many cases, with V/H ratios less than 2/3.

In summary, ground accelerations in the near field of the fault dislocation in its northern section are, in a frequency band near 10 Hz (but not near 1 Hz), rich in vertical component seismic waves. At Bond's Corner, near the southern end of the fault zone, more usual values of V/H were observed.

(d). Effects of focal mechanism on the strong motion. The shallow focus earthquake (focal depth about 10 km) was produced by predominantly unilateral rupture of the Imperial fault. The associated surface rupture ($\sim$ 35 km long) had both right-lateral strike-slip offsets (up to 55 cm) and dip-slip offsets (up to 19 cm) down to the east. The maximum lateral displacement occurred near the international border about 20 km south of the El Centro array, and the maximum vertical displacements occurred near Mesquite Depression (Figure 3.23), about 5 km north of the El Centro array.

Significant "subsidiary" faulting occurred along the Brawley fault ($\sim$ 10 km of surface rupture) to the east of Mesquite Depression. The maximum displacement measured was 15 cm of dip-slip (down to the west) and 3 cm of right-lateral slip. The El Centro array profile crosses both the dislocated Imperial and Brawley faults.

It is clear that the fault-rupture source was a mixture of lateral and vertical elastic rebound with the proportion of each changing from south to north. More than one fault dislocated in the

energy release. Sympathetic dislocation of the Imperial and Brawley faults would produce quite complex superposition of seismic waves of various types and hence complicated accelerograms at Stations 8, 7, 6, and 5 in particular.

The source mechanism and position of the near-field array stations are favorable to the generation of vertically polarized ground motions at these sites. The main dislocation moved upwards and to the northwest from about 10-km depth with both lateral and vertical elastic rebound (see Figure 3.27). The first result of importance is that such a source would continuously produce a significant amount of vertically directed (P) compressional waves and polarized (SV) shear waves.

Secondly, the dislocation first penetrates through the basement rock (vertical travel distance about 6 km) and then through the sedimentary layers (thickness about 4 km) and, finally, through the surficial alluvium and soil (about 300 meters thick) where it breaks out at the surface. It is known from many theoretical studies that, as the dislocation breaks from one layer to another, the partitioning of seismic energy into various types of seismic waves changes markedly -- as might be expected on general physical grounds. There is considerable published work on this result, particularly recent studies (M. Bouchon and K. Aki, 1977; M. Bouchon, 1980a,b). Further references can be found in Aki and Richards (1980).

Interpretation (Bond's Corner)

The interpretation of the main features of the strong-motion records is based upon the simplified source dislocation model sketched in Figure 3.27. The model is based on the limited available information on the structure of the upper crust in the Imperial Valley.

The main assumptions are that (i) the dislocation surface is essentially restricted to a fault plane of width about 10 km, (ii) the crust is strongly layered (two layers L_1 and L_2 are shown) with significant velocity gradients in L_1, and (iii) there is a surficial layer of relatively low-velocity alluvium. Some simple ray paths for such a structure are shown in Figure 3.27, and we can calculate expected travel times of such principal wave onsets and seek to identify them on the various records.

Typically, the alluvium and underlying sediments consist of more or less horizontal layers with local variations in thickness and strong velocity gradients (see Helberger and Hadley, 1981). For the present purpose, we assume a surficial layer of recent alluvium (known to be about 300 m thick in the vicinity of El Centro), overlying a sedimentary layer (or layers) from 4 to 6 km thick (see Leivas et al., EERI Report, February 1980). Beneath these sediments is basement crustal rock. Average P and S velocities in these representative layers are resonably well known from seismic surveys.

As a consequence of this structure, P and S waves generated near the focus at the onset of the dislocation would be refracted sharply upward (Snell's law) both at the bottom of the Quaternary sediments and the bottom of the alluvium. At each interface, some P wave energy will convert to SV (vertically polarized shear) wave energy and vice versa. When these P and SV waves strike the surface at steep angles of incidence, there will be downward reflection and P and SV waves will be "trapped" by multiple reflection in the surficial layers. The degree of the reverberation is, of course, a function of frequency, but from the theory of wave guides it is known that waves (both body and surface waves) with wave lengths that are sub-multiples of layer thicknesses produce resonant peaks of energy. For P or SV waves of

frequency 10 Hz in the alluvial layer (seismic velocities of 600 to 200 meters per sec), the wave lengths are 60 to 20 meters. The position of the spectral amplification observed in the vertical response curves for some El Centro array stations is thus to be expected.

It must be pointed out, however, that the propagating P and SV waves of frequencies near 10 Hz are damped relatively strongly in the surficial sediments. In this earthquake, however, as the dislocation spreads from the focus, energy is continually being fed as trapped high-frequency P and SV waves into the surficial layer, thus sustaining strong ground motion in the vertical plane.

The above explanation is in accord with the seismic phases (onsets) read from the three components of accelerograms at each near-field station (see Figures 3.26a, 3.26b, 3.26c). An analysis of these time histories (not given here) shows onsets of high-frequency P (mixed withSV) waves about 2.5 to 3 sec after triggering. (As expected for strike-slip faulting, the SV wave amplitudes are greater than those of SH waves.) About 3 sec later, the records show a strong but longer period pulse-like motion beginning, mainly on the horizontal records. This predominantly SH wave motion denotes the onset of "fling" produced by the elastic rebound of the dislocation as it passes near the array.

Several possible velocity models were analyzed and compared to the data. The model used here gives

L_1 = 2 km/sec $\quad$ L_2 = 8 km
α_1 = 4.0 km/sec $\quad$ α_2 = 5.8 km/sec
β_1 = 2.5 km/sec $\quad$ β_2 = 3.5 km/sec

Consider the record at Bond's Corner recorded about 8 km north of the focus. The dislocation spreads upwards towards the station at progressively

slower velocities (say, starting at 3.0 and ending at 2.0 km/sec at the top of L_1). The time of rupture to Bond's Corner is thus about 4.2 sec. On the other hand, the P wave from F reaches the station after 2.3 sec and the direct refracted S (called S_1 in Figure 3.26b) after about 3.5 sec. The interpretation for Bond's Corner is thus an initial 2 sec of P waves, followed by relatively high-frequency SV waves (onset S_1). Then, in about one sec of elapsed time, the dislocation breakout pulse (the fling) arrives at S_2. The wave train follows with Rayleigh surface waves developing (R in Figure 3.26a).

Let us now consider the energetic high-frequency vertical motions that were recorded in this earthquake (see Figure 3.26a). There are a number of explanations of these (unexpected) motions, including crustal structure, local amplification due to structure and soils at the instruments and, perhaps, directivity focussing. The two most plausible explanations would appear to be that (a) the high-frequency motions are P waves that were refracted sharply upwards through the surficial sedimentary layers or (b) they are produced by local ground amplification. In any event, most tentative analyses to the present agree that they are the result of the concentration of vertical motion in a rather narrow zone around the causative Imperial fault. At the northern end, where the vertical motion was greatest, there is the further possibility that vertical block faulting took place between the Imperial fault and the Brawley fault. The surface evidence showed that there was downward vertical motion around the Mesquite depression, and this may have resulted in the generation of high vertical accelerations at the El Centro stations near the intersection of the Brawley and Imperial faults.

The above explanations given of the near-field motions in the 1979 Imperial Valley earthquake are based on first seismological principles, and

more refined analyses are needed. It seems unlikely, however, that the main conclusions will be altered; i.e., that the high V/H energy ratios at high frequencies observed on some El Centro array stations are a consequence of (a) the trapping in surficial alluvial and sedimentary layers of steeply reflected P and SV waves, strongly generated by fault dislocation almost vertically upwards through the sedimentary layers, and (b) the focussing of P energy because of strong gradients in elastic properties of the upper layers.

There are site specific implications for estimation of ground motion using the Imperial Valley record. Consider for comparison a site in the east of San Francisco Bay near the Hayward fault (see Section 4.2). The Hayward fault passes by such a site as a long more-or-less continuous linear feature. It is classified as strike-slip and does not terminate or change strike significantly nearby. This contrasts with the observed dip-slip component of fault offset and the major lateral translation of the Imperial fault south of Brawley. There is no major bifurcation of the Hayward fault in the East Bay like that of the Imperial and Brawley faults. Consequently, there is no mechanical mechanism available for generating the mix of P and SV waves observed on the El Centro array.

Of even greater importance, however, is the difference in surficial crustal structure. There is no basin structure along the Hayward fault equivalent to the Tertiary and Quaternary sedimentary deposits overlain by alluvium and soil that occur in the Imperial Valley. Layering in sedimentary basins has dramatic effects on the amplitudes, phase partitioning,and spectral patterns of propagating seismic waves. There is also strong evidence that similar effects occur when the fault rupture penetrates through surficial alluvial layers. Both conditions are conducive to the generation of enhanced vertical accelerations.

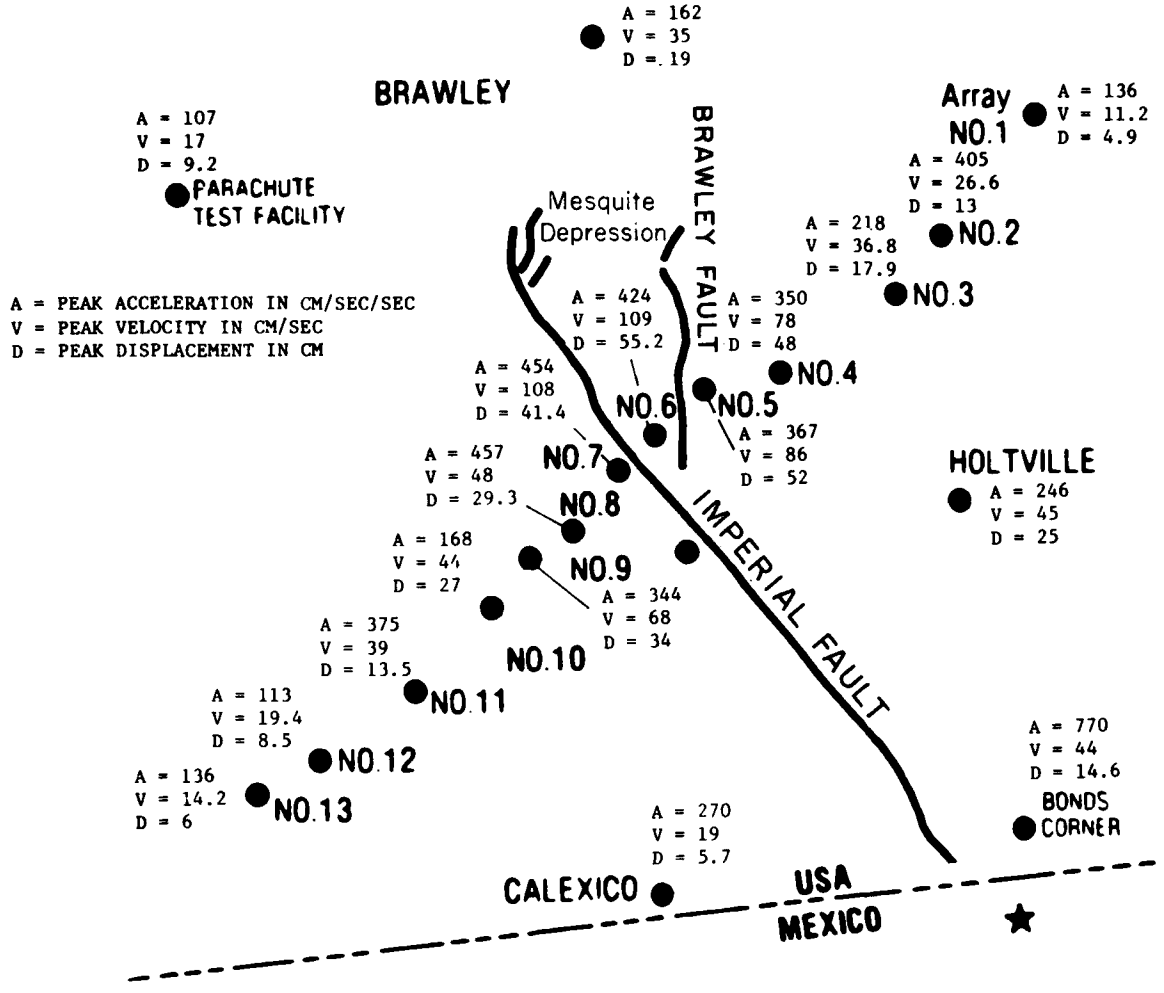

Figure 3.23. Map of surface faulting and accelerometer stations for the 1979 Imperial Valley earthquake. Peak accelerations, velocities, and displacements are given for the component transverse to the fault.

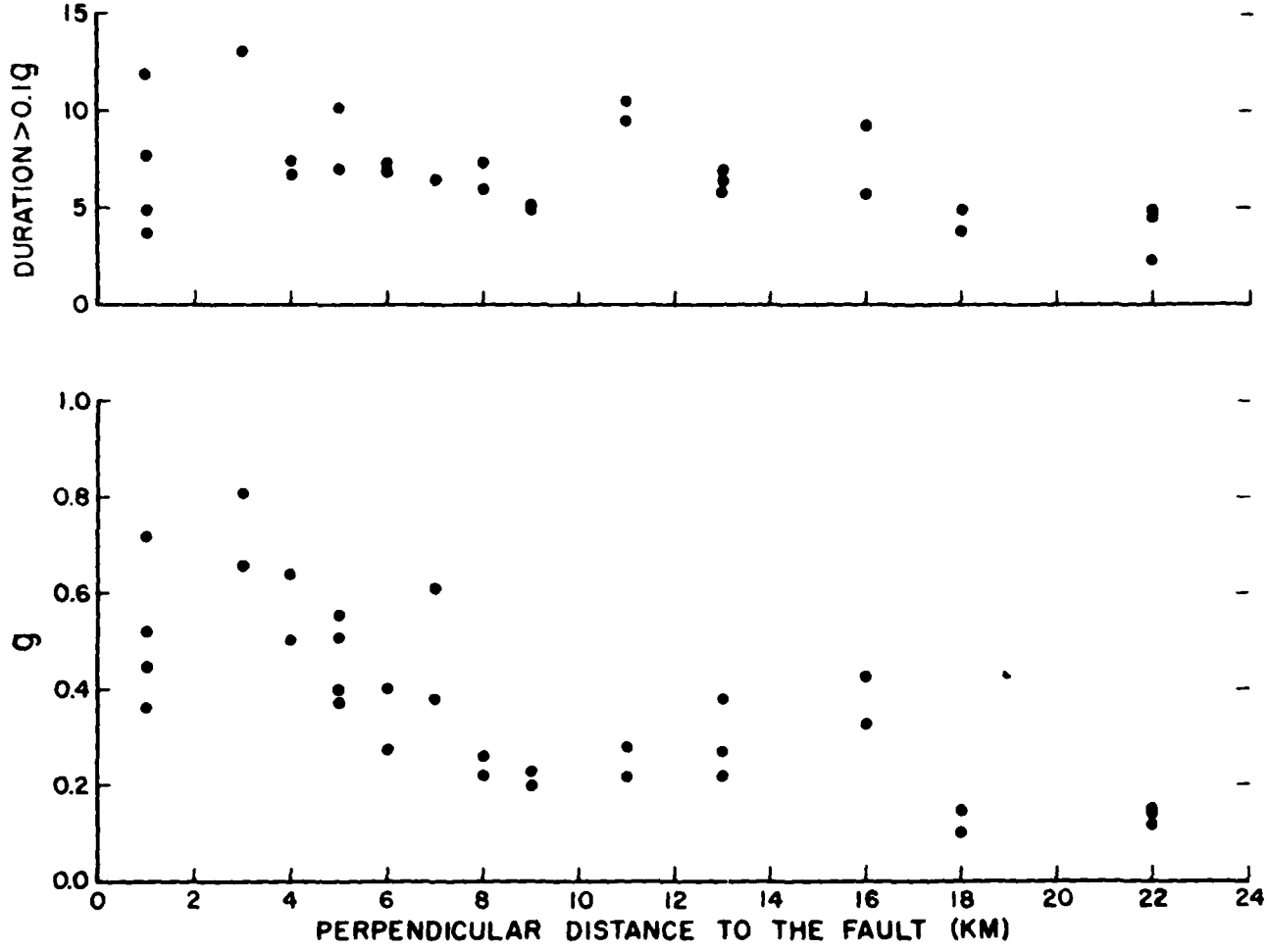

Figure 3.24. Bracketed duration (acc. > 0.1g) and peak accelerations as a function of distance to the fault.

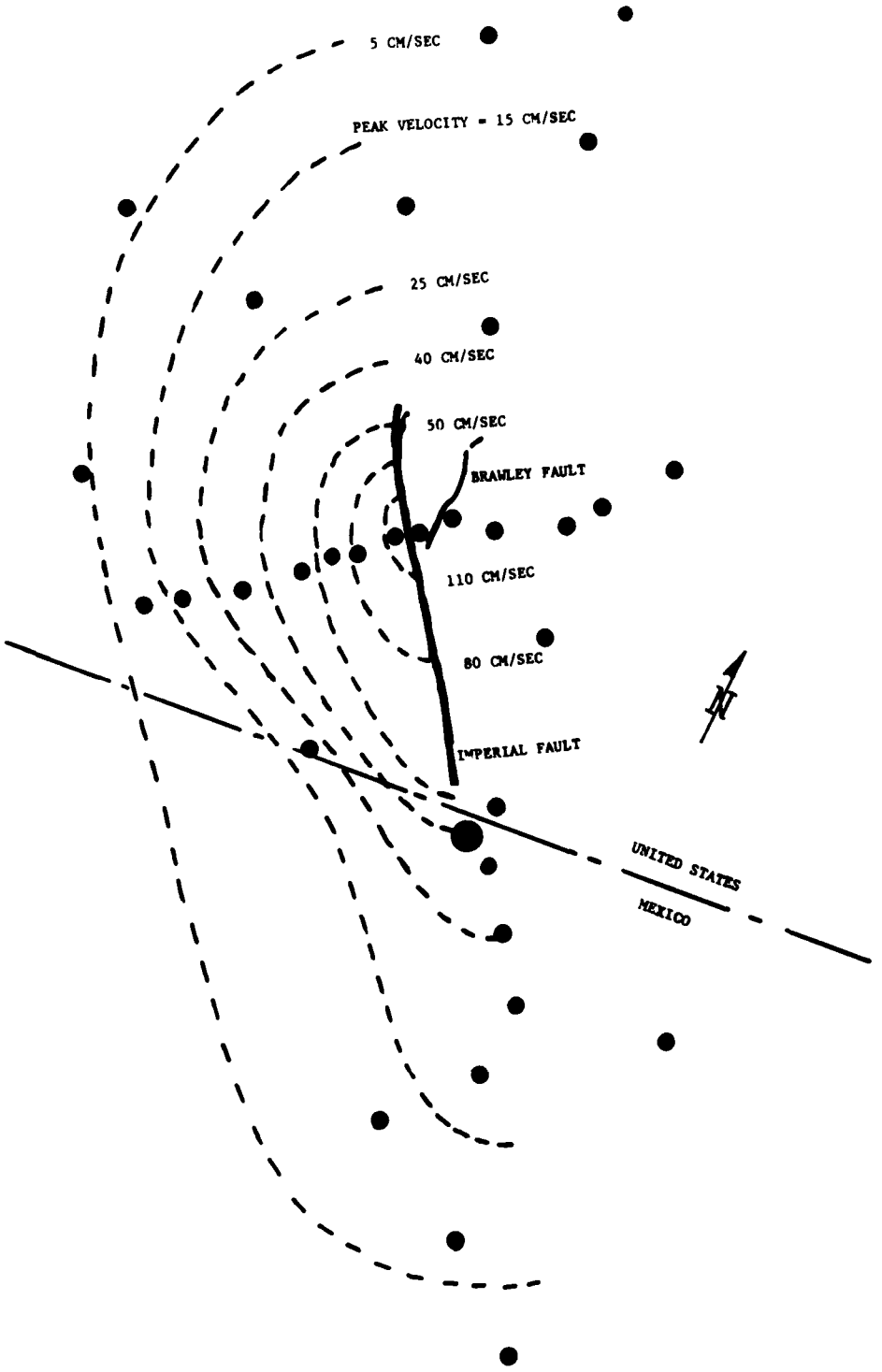

Figure 3.25. Contour map of peak velocity (transverse component) for the 1979 Imperial Valley earthquake.

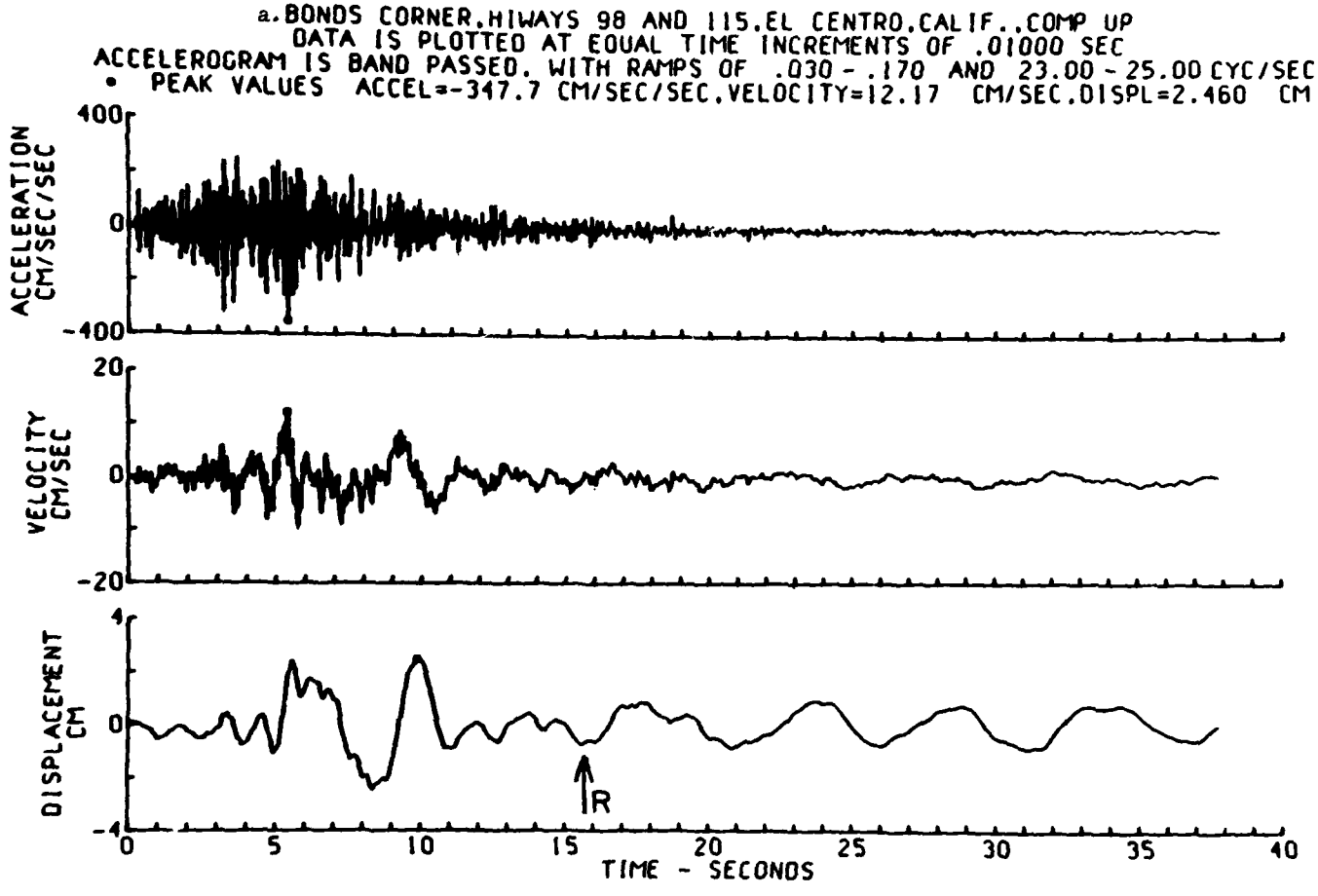

Figure 3.26. Corrected acceleration, velocity, and displacement for the Imperial Valley earthquake of October 15, 1979 - 2317 utc (Sheet 1 of 3).

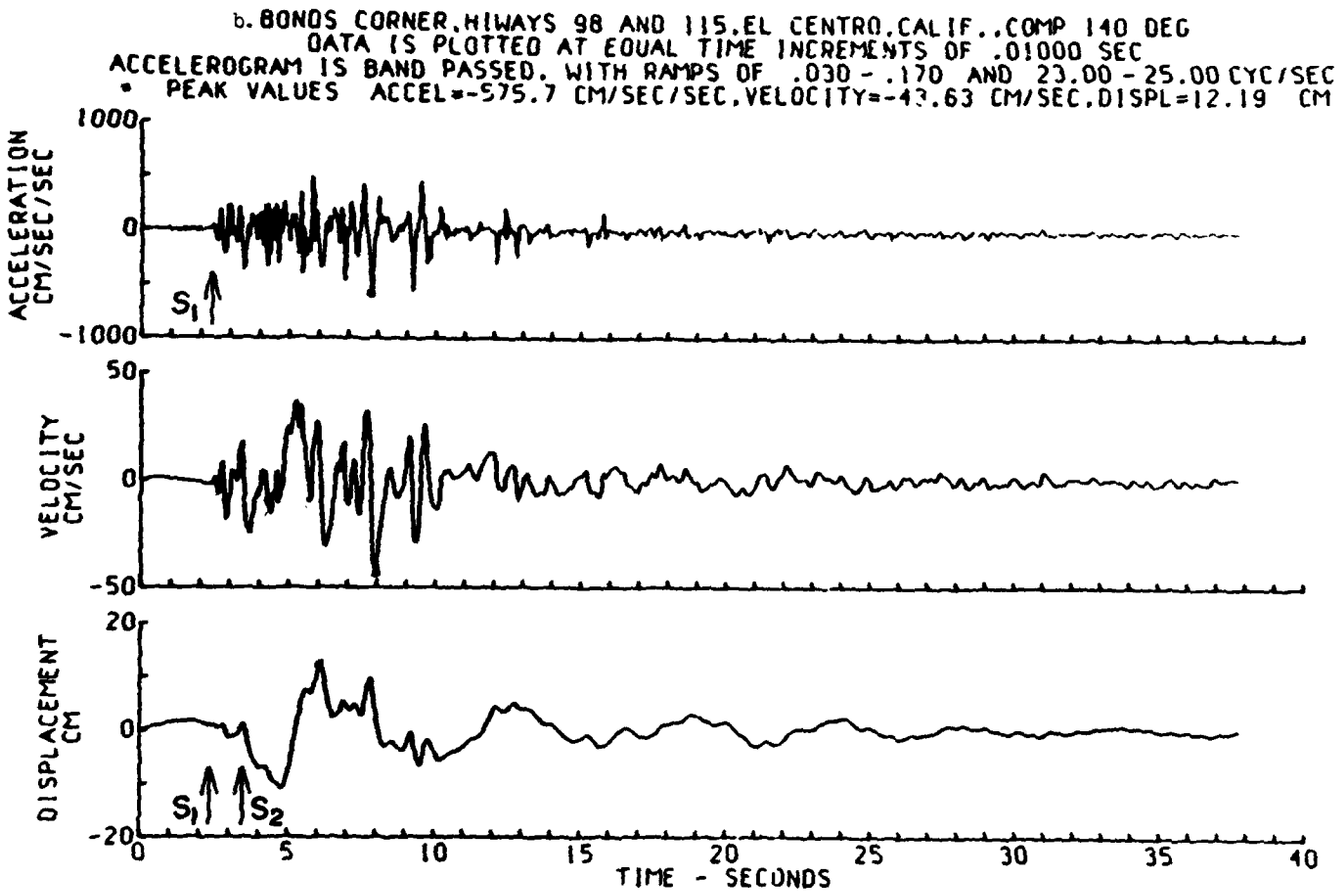

Figure 3.26. (Sheet 2 of 3).

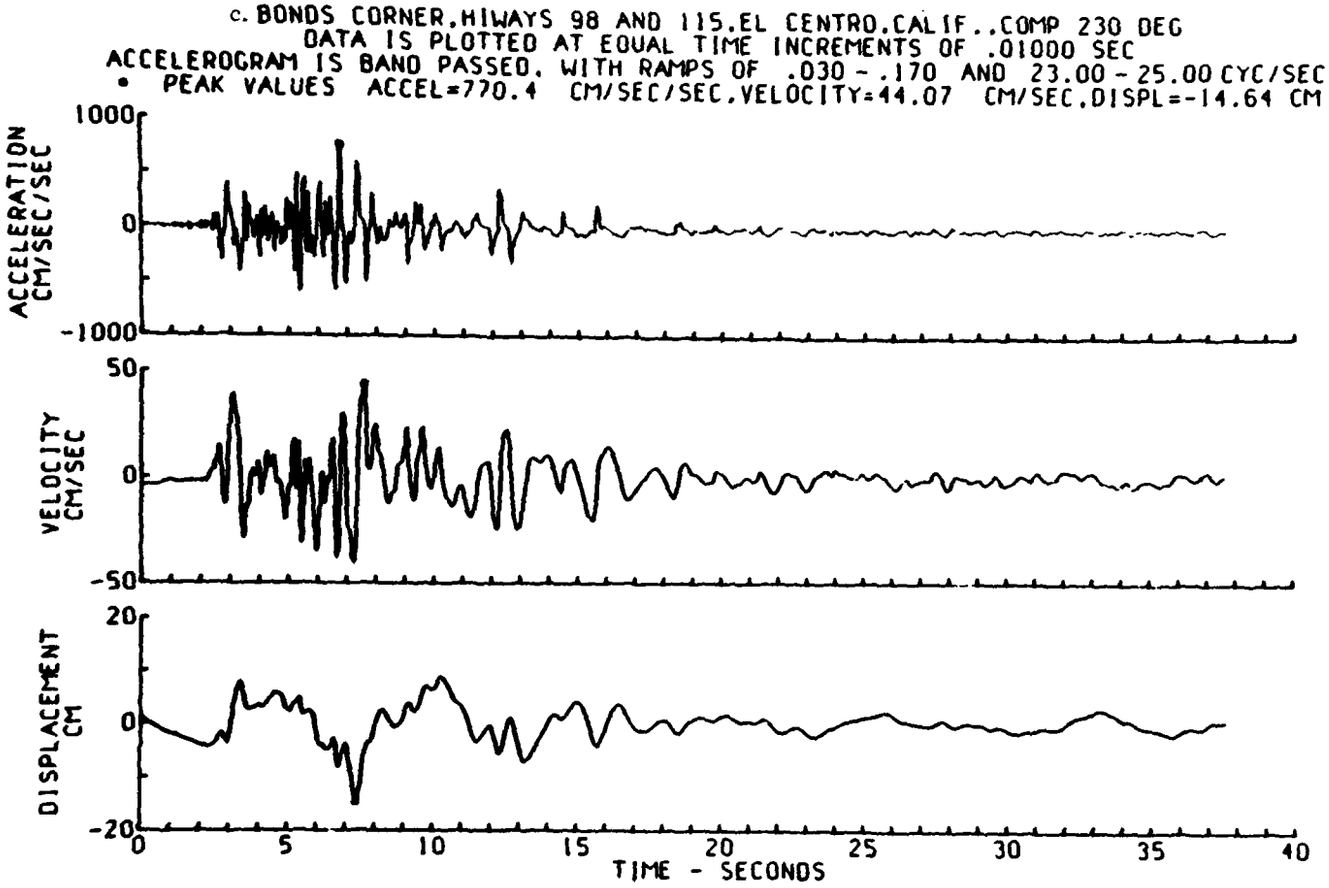

Figure 3.26. (Sheet 3 of 3).

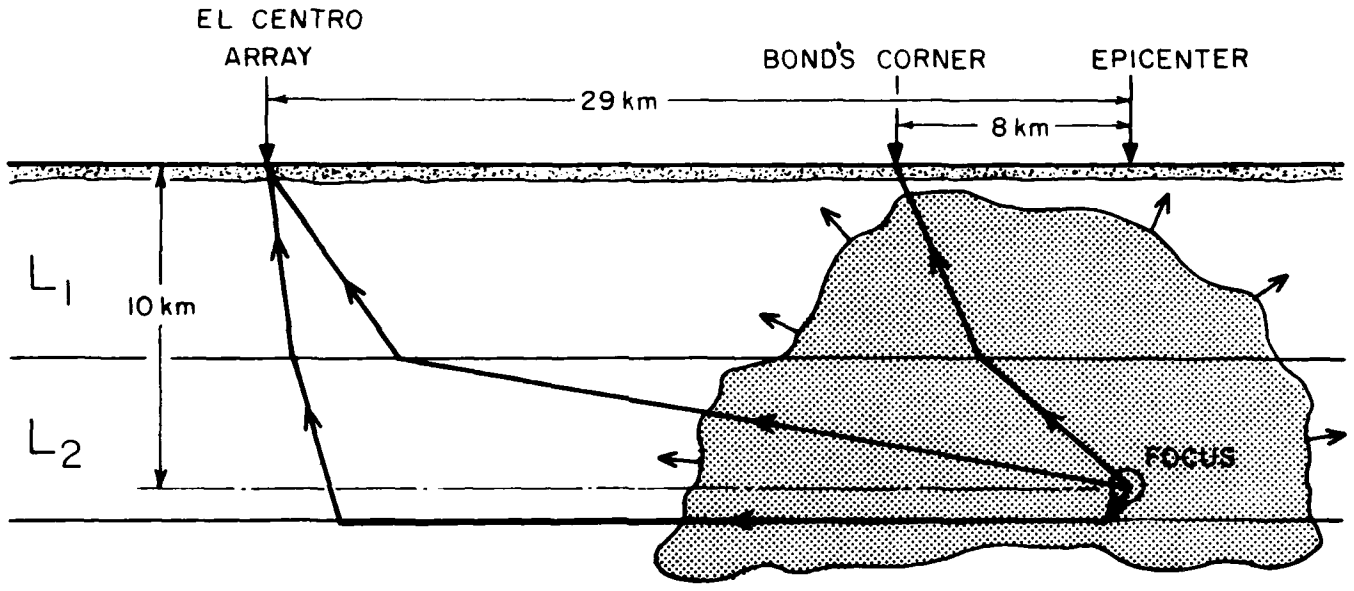

Figure 3.27. Simplified model of the expanding rupture surface in relation to the Bond's Corner and El Centro array stations, the epicenter, and the focus for the 1979 Imperial Valley, California, earthquake. Note that the rupture probably did not continue much below the depth of the focus.

3.10 Livermore Valley, California - January 24, 1980

Reference: Bolt et al. (1981)

Location: Earthquake: 37°51.0'N, 121°48.9'W

Accelerometer: Livermore Veterans Administration Hospital

Foundation: basement of the hospital

Size: Magnitude: $M_L = 5.5$

Moment: $M_o = 6 \times 10^{24}$ dyne cm

Mean Stress Drop: $\Delta p = 0.5$ bars*

Fault Source Characteristics:

Faulting: Surface rupture observed along at least 6 km of the Greenville Fault. Predominant offsets were right-lateral of 0 to 5 cm, sometimes accompanied by comparable vertical offsets with the northeast side up, on average.

Focal Mechanism: Right-lateral, strike-slip
Strike N13°W
Dip 85°W

Parameters: L = 25 km

W = 18 km

D = 0.05 m

Mean Rupture Velocity:

-

Peak Wave Amplitude Values:	VERT	S52E	N38E
Acceleration (cm/sec^2):	-	-	167
Velocity (cm/sec):	-	-	-
Displacement (cm):	-	-	-

Bracketed Acceleration Duration (Acc. > 0.05g):

d = 3.7 sec

---

* Mean stress drop estimated from parameters below and using equation 1.1.

·eral Aspects:

On the morning of January 24, 1980, a moderate earthquake (M_L = 5.5) was felt widely in central California from Lake Tahoe to Monterey Bay. The earthquake occurred north of Livermore Valley about 12 km to the southeast of Mount Diablo, and was associated with surface rupture along the Greenville fault (Figure 3.28). Some damage was reported. There was a foreshock (M_L = 2.7) a minute and a half earlier and a sequence of 59 events ($M_L \geq 2.5$) in the ensuing six days. On the evening of January 26 (January 27 GMT) a larger magnitude earthquake occurred in the sequence (M_L = 5.6); see Figure 3.29. This second principal shock was located 14 km to the south of the first principal earthquake towards the southern end of the Greenville fault. Preliminary estimates of the seismic moments of the two principal shocks are 6 x 10^{24} dyne cm, respectively. The January 24 event will be the emphasis in this study.

The rupture propagated over 15 km to the southeast along the Marsh Creek-Greenville faults on January 24 and stopped in the vicinity of Highway 580. This direction of propagation may explain to some extent the relatively high intensities reported near the southeast end of the Greenville fault compared with intensities to the northwest.

Field investigations after the January 24 event indicated surface rupture along the Greenville fault zone for at least 6 km, with both right-lateral strike-slip and some dip-slip motion with the northside up. Figure 3.30 shows the fault-plane solution (upper hemisphere projection) where the causative fault strikes N13°W and dips 85°SW. Variable offsets on surface cracks suggested displacements of a few centimeters.

Interpretation (Veterans Administration Hospital Records):

This earthquake has been included in Part III because it was the

subject of detailed seismological analysis by the author and colleagues at the Seismographic Station, Berkeley (Bolt et al., 1981). The nearest strong-motion instrument to record the earthquake, however, was that at the Veterans Administration Hospital at a distance of 25 km from the focus and 10 km from the southern end (Point B) of the known faulting. The record is reproduced in Figure 3.31. The peak acceleration of 0.1g was small.

This small amplitude record has a relatively simple pattern and is an example of a case which resembles a normal seismogram. First, we assume that the instrument did not trigger on the onset of the first P wave from the focus with an overall delay of about 2 sec before the trace appeared.

The S-P time for this distance from the focus corresponds to 3.1 sec. This would correspond to the onset of the high frequency motion (called S_1) which can be seen clearly on the vertical component, but is also present on the two horizontal components. The largest motion, however, is a pulse-like motion, marked S_2 on the record. S_2 occurs predominantly on the two horizontal components and, therefore, corresponds to SH polarized motion or Love wave motion. The corresponding surface wave velocity is 1.5 km/sec, from which we infer that the wave is controlled by the sediments in Livermore Valley.

Finally, it should be mentioned that surface intensity in the first principal shock was rated higher towards the south of the rupture (e.g., at Livermore) than to the north (e.g.. Concord). Although there are other explanations, directivity of the fault rupture may have contributed to this pattern. Unfortunately, we cannot draw inferences on this matter from the single V.A. record.

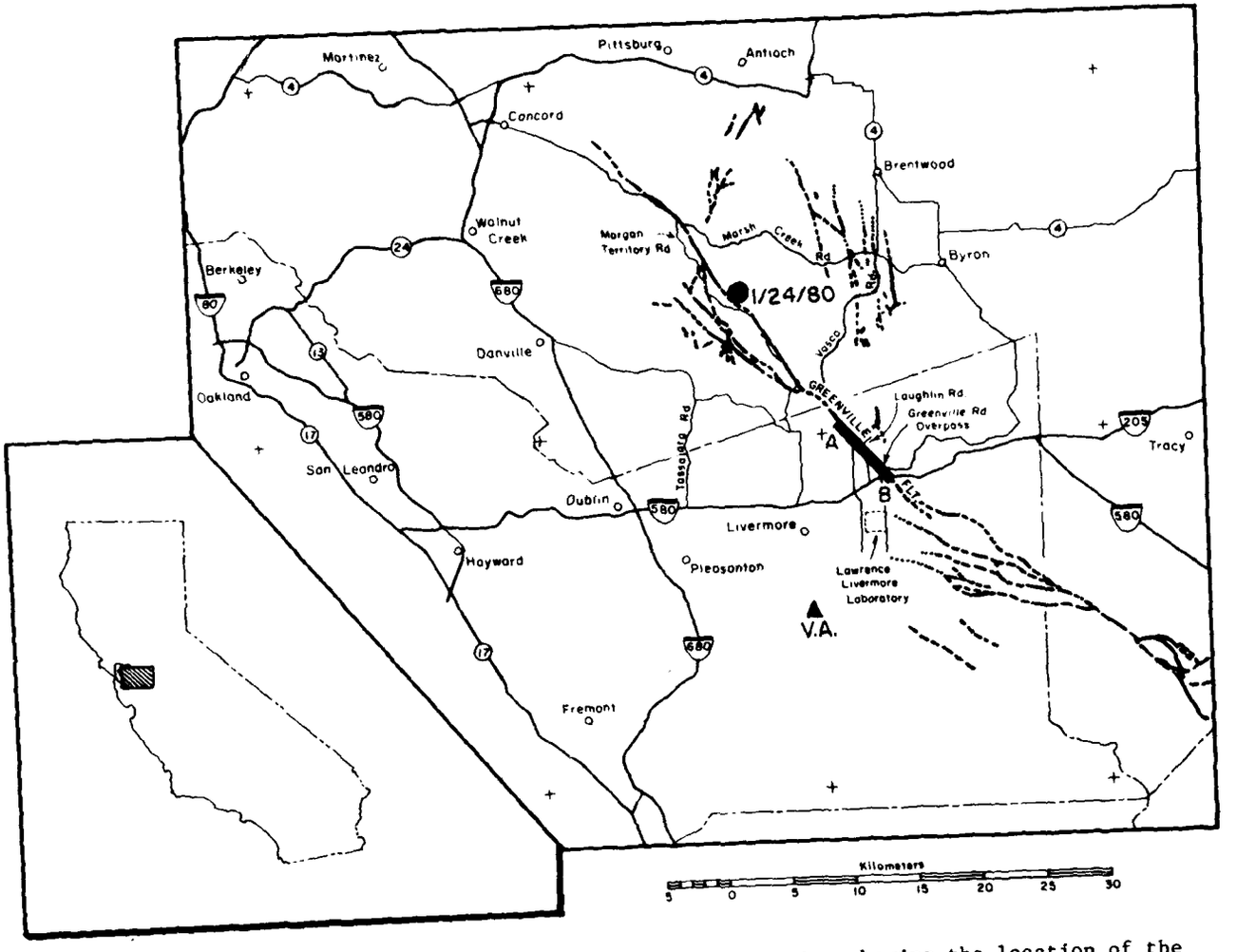

Figure 3.28. Map of the Livermore Valley, California, region showing the location of the Veterans Administration Hospital, epicenter, and surface faulting (AB) associated with the earthquake on January 24, 1980.

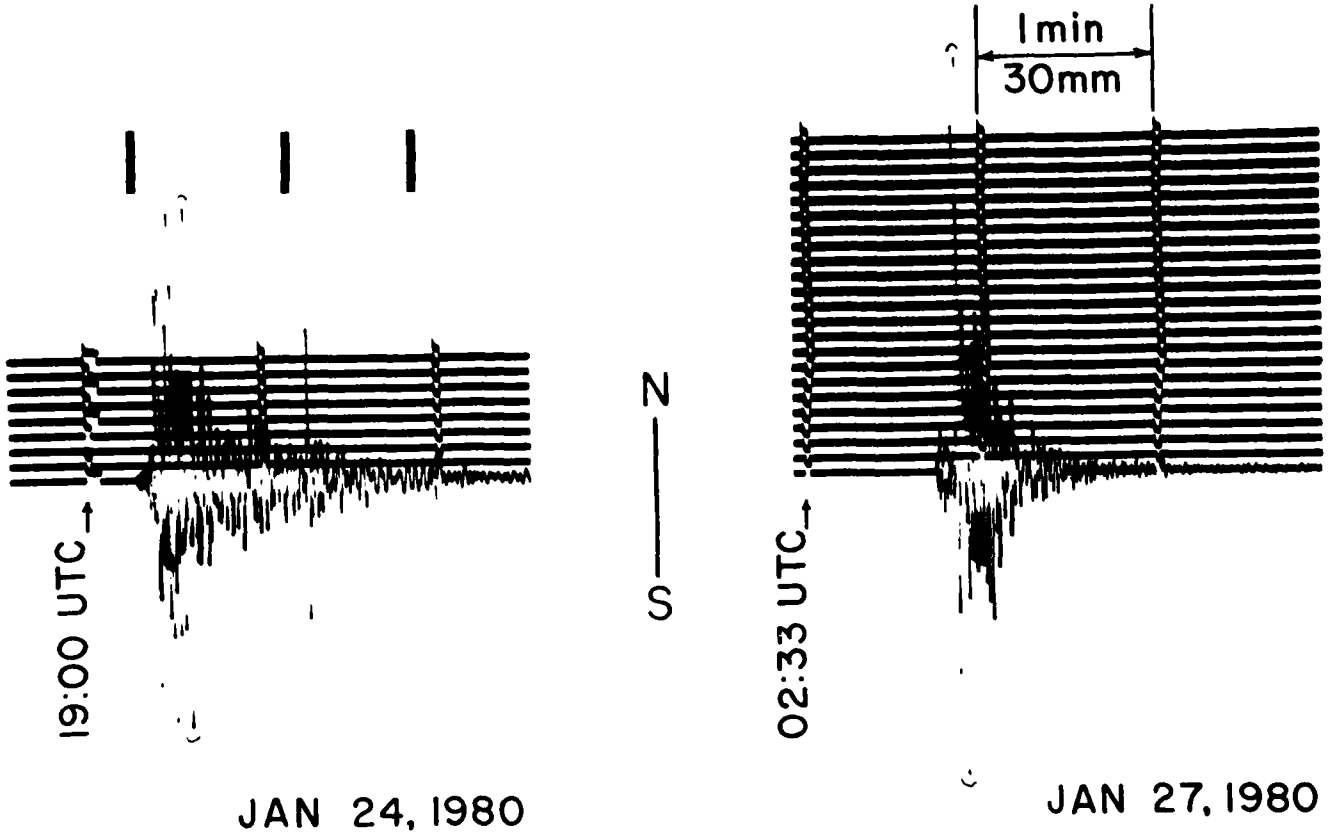

Figure 3.29. Seismograms (100X torsion) recorded at Berkeley for the Livermore Valley earthquakes of January 24 (M_L = 5.5) and January 27 (M_L = 5.6).

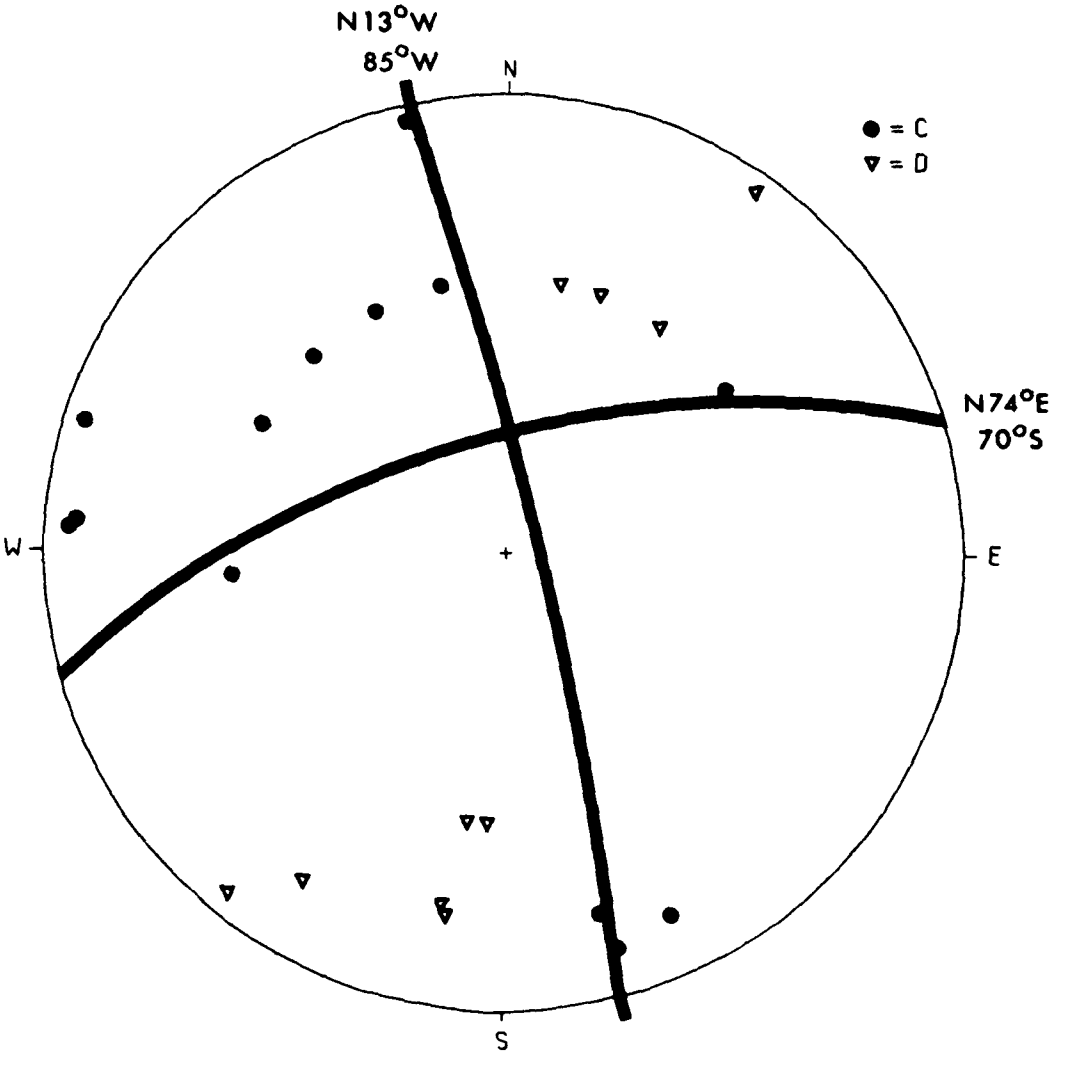

Figure 3.30. Fault plane solution for the January 24, 1980, Livermore Valley earthquake.

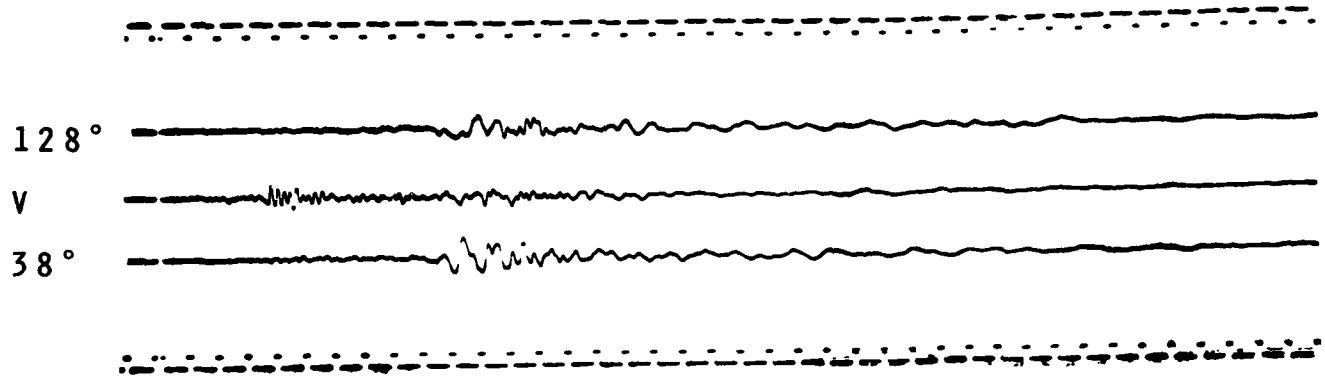

Figure 3.31. Accelerograms for the January 24, 1980,Livermore Valley earthquake recorded at the V.A. Hospital. Time ticks mark 0.5-sec intervals.

PART IV

DISCUSSION

4.1 Broad Principles of Interpretation

The detailed case studies for the ten earthquakes given in Part III together with analyses of other strong-motion records from the same earthquakes and from other earthquakes, allow some inferences to be drawn concerning the problem of seismological interpretation of strong-motion records. The principles that are outlined in what follows are among the first to be attempted in strong-motion seismology and are necessarily tentative and subject to revision and refinement as more experience of this kind of work comes to hand. The main discriminants and diagnostics that have been found useful can be summarized under five headings.

4.1.1 Vector decomposition into three components of ground motion

Unless there is an instrument malfunction, three components of ground motion are usually available after a modern strong-motion instrument (accelerometer) triggers. This provides perhaps the most valuable tool for discrimination of the wave types. This special decomposition is one that is much utilized in ordinary observatory seismology, although not in all cases are there matched three components of ground motion available. For example, the standard Wood-Anderson instruments (see Figure 3.29), upon which the local (Richter) magnitude scale is based, have only two horizontal components with no matched vertical-component instrument to accompany them to provided essential information about particle motions in the vertical direction (e.g., Rayleigh waves).

We have seen that in most cases the vertical component record looks different from the horizontal record in frequency content and in wave pattern (see Figure 3.7). The explanation is that the vertical component contains mainly P waves, SV waves, and higher mode Rayleigh waves, whereas the horizontal ground motion contains significant SH components. A closer look at this diagnostic can be obtained by rotation of the recording axes (often essentially arbitrary lines of field convenience) so that the (two horizontal) components represent a dynamically meaningful vector resolution (see Figure 3.4). The most usual effective resolution is to align the transverse and longitudinal components of ground motion relative to the strike of the earthquake source. This is reasonably easy in the case of a small to moderate earthquake, but for a great earthquake, the concept of transverse and radial components of ground motion in the near field loses much of its meaning. Simple orthogonal transformations are easily programmed and the transformed horizontal components can be plotted out on the same scale, or a more convenient one, as the original records (see Section 3.4).

Some of the controversies in earthquake engineering, particularly in the applicability of methods developed in soils engineering that assume predominantly vertically propagating waves, are affected by the interpretation. Although there is no question that there will be in general seismic waves of various types that propagate horizontally through any site, it is also the case that in the presence of the low velocity layers (such as soils) incident waves from below will be refracted sharply upwards so that vertical component energy in the

record may well dominate. For a given strong-motion set of three component records, the point can be checked by calculating particle orbits spatially in the computer. These orbital motions can now be easily displayed as a function of time on a video screen.

4.1.2 The use of acceleration, velocity, and displacement

Unlike the usual situation in conventional seismology, in working with strong-motion instruments we have a nine-dimensional rather than a three-dimensional field in which to seek discriminants. The comments made above on the three components of strong acceleration hold equally well for the three components of ground velocity and three components of seismic ground displacement. As we have seen, because each integration smooths the higher and more erratic components of wave motion, often the velocity and displacement records are simpler and enable more straightforward interpretations of the wave patterns to be made. The integrations, in effect, remove much of the stochastic part of the motion discussed in Section 2.3. Thus, on many velocity records the onset of the first major S motion is often quite unequivocal (see Figure 3.7c), and on the displacement records in the near field the presence of a long-period pulse associated with the passage of the dislocation near to the site (the fling) can be clearly seen (see Figure 3.4b).

There is also more opportunity with velocity and displacement records to make comparisons with synthetic records, since most numerical modelling succeeds best at periods greater than one second (c.f., Section 1.3).

4.1.3 Transformation to familiar instrumental response

Most seismologists who do observational work develop their ability by continual reading of seismograms from small and moderate earthquakes. They are, thus, familiar with seismograms produced by such instruments as Wood-Anderson instruments, Benioff short-period instruments, and so on. Because this experience now exists, it is, therefore, valuable to transform the ground motions recorded on the less familiar and less productive strong-motion accelerometers to one of the more common instruments so that comparisons with more familiar patterns can be made.

Recently, Kanamori and Jennings (1978) demonstrated that local magnitude M_L could be determined fairly reliably from strong-motion accelerograms. In effect, the accelerogram records were used as an input to the equation of motion of the Wood-Anderson torsion seismograph, thus producing a synthetic seismogram which could be read in the standard way. They applied the method to 14 records from the San Fernando earthquake and obtained a mean local magnitude of 6.3, in agreement with a previously reported value of 6.3 based on Wood-Anderson records only. They point out that the method of finding local magnitude is useful in the determination of engineering design criteria. Thus, if accelerograms are selected representative of the design earthquake in terms of duration and frequency content, the accelerograms can be scaled to produce synthetic Wood-Anderson responses that are consistent, at a given distance, with the local magnitude of the design earthquake.

In the present study, the technique has been applied to a number of earthquakes, including particularly the Coyote Lake (Section 3.8) and the 1940 Imperial Valley events (see Figure A1). The algorithm

used is outlined in Appendix A. Figure 4.1 gives an example of a strong-motion record which has been transformed into the equivalent Wood-Anderson record. It was found that the artificially generated Wood-Anderson records were often very helpful in seismological interpretation of the wave pattern.

4.1.4 Use of arrays

Even when the full power of the nine-dimensional information space mentioned in Section 4.1.2 is used to find diagnostics for interpretation, it sometimes happens that there will still be considerable questions involving uniqueness and resolution of records from a single three-component instrument.

The best proposal to remove these difficulties is to cross correlate recordings between accelerometers at nearby sites. A common time base between neighboring accelerometers in an array of strong-motion instruments allows the actual phases of the seismic waves to be correlated in space as well as in time, thus facilitating identification of wave types (as well as the direction of propagation). Discussion of this matter is postponed to Section 4.5.

4.1.5 Interaction between record and model

In conventional seismology, identification of seismic onsets can be accomplished in some circumstances by determining the wave properties on the seismogram independently of any knowledge of the source. However, in most cases interpretation is much facilitated when there is at least a rough idea of the distance and direction of the source from the

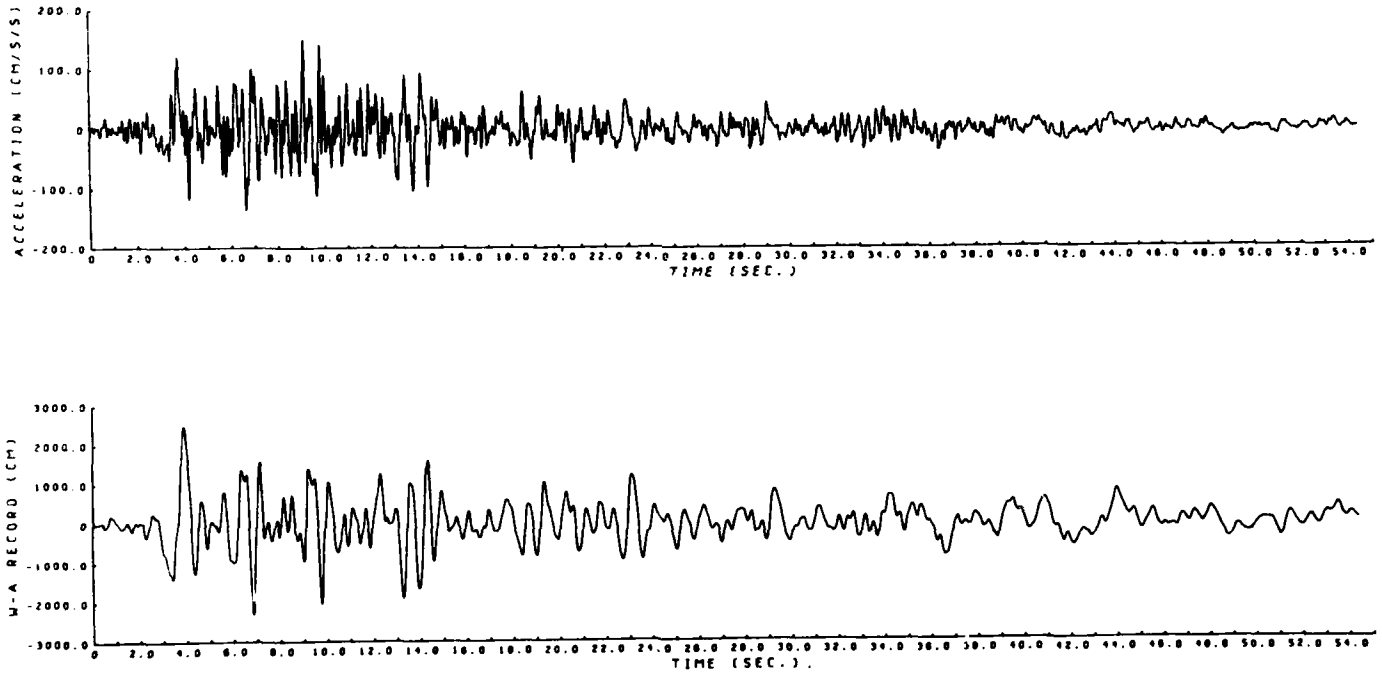

Figure 4.1. Corresponding accelerogram and Wood-Anderson seismogram for the N21°E and S69°E horizontal components of ground motion at Taft School station in the 1952 Kern County, California, earthquake (Continued).

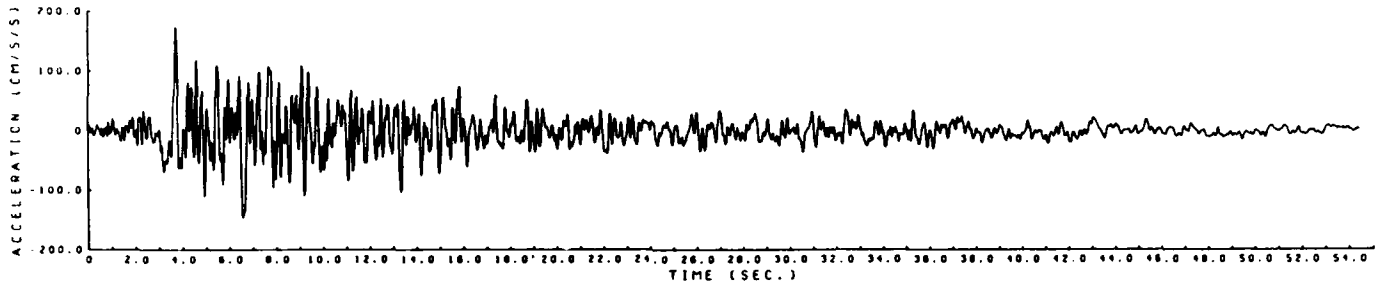

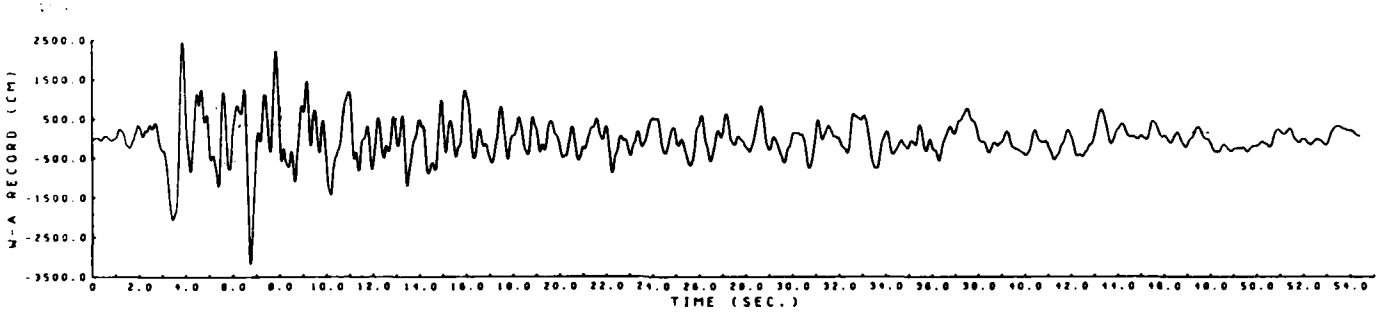

b. Taft School Tunnel components S69°E

Figure 4.1. (Concluded).

instrument. Often, a seismologist will make successive approximations between these two aspects of the diagnosis.

In the interpretation of strong-motion records, it is clear, for example, from the assessments in Part III that the interpreter is going to need all the clues available concerning the larger variety of significant waves that may occur on a strong-motion accelerogram. It is thus almost a requirement for explanation that something be known on the nature of the seismic source, its distance from the site, and its size. Then, using plausible values for P, S, and surface wave velocities, some bounds can be put on the times of arrival of the phases and the total duration of the record (see e.g., Section 3.4). Of course, there is feedback between this interpretative analysis and the development of a knowledge of the source itself.

There are, moreover, no standard travel-time curves available for the interpreter of strong ground motion records (such as are available as standard tools for the interpreter of seismograms of teleseisms and small local earthquakes). What is needed are suites of representative synthetic records which are defined by standard parameters, such as fault length (magnitude dependence), focal depth, source mechanism, and distance from the fault. Such standard synthetic records could then be used as templates to guide the interpretation and, with experience, interpolations between templates should give rather reliable discrimination.

4.2 Robust Estimation of Parameters

What are required for both interpretation and prediction of strong ground motion are both parameters and methods of estimation of them that are not seriously dependent on abnormal values. We, therefore, seek robust parameters and robust algorithms with a high performance even with very diverse sampling. (The mode and median in statistics are often more robust estimates of central tendency than the mean).

An example of a nonrobust parameter is the raw peak acceleration taken from an accelerograph, as discussed in Section 2.1. There have been various proposals to provide a more stable scaling parameter, such as filtering the record, say above 8 Hz, and using the maximum amplitude on the filtered record as a representative upper bound on acceleration. Another proposal is to take an average, say, of the five maximum peaks and the five minimum troughs. It might be mentioned that rather than the sample mean, the mode of these values is likely to be the most dependable estimate.

In recent years, the laudable use of uncertainties along with mean values has become more widespread in strong-motion seismology. For example, in dealing with response spectra, the mean spectrum and spectra representing one or two standard deviations are often considered. The weakness is, however, that little attention is given to the sampling distribution of the data, which are often quite scattered and not consistent with, say, a normal distribution. As part of the present research, some attention has been given to the fundmental problem of estimating the probability density function of strong-motion parameters from samples of the observations themselves. The most promising approach seems to be by nonparametric estimation. Some details of this theoretical work will be reported later elsewhere, and only an outline is given here.

We start with the histogram from the observations or residuals. These could be, for example, the differences $\underset{\sim}{x}$ between an actual strong-motion record and the corresponding synthetic strong-motion record. The problem is to estimate the density function $f(\underset{\sim}{x})$ of an m-dimensional vector $\underset{\sim}{x}$, given N observations (Good and Gaskins, 1972). The construction of $f(\underset{\sim}{x})$ proceeds by maximum likelihood, i.e., maximize a score ω which is defined by

$$\omega = \sum_{i}^{m} \log f(x_i) - P(f) , \qquad (4.1)$$

where the roughness penalty P is a functional of f. An example of a penalty function is an integral due to R.A. Fisher,

$$P = \int (f'^2 / f)\, dx . \qquad (4.2)$$

An example will now be given, not of interpretation, but the complementary aspect of the work involving construction of a strong-motion record. The record is meant to represent a large earthquake as recorded within one km of the active Hayward fault zone in central California. In historical times, two large earthquakes have been reported centered on the Hayward fault, the first on June 10, 1836, and the second on October 21, 1868, both with fissures on what is now called the Hayward fault. Of course, no instrumental record of the ground motion was obtained at that time. Based on the reports available of historical earthquakes and the present geological knowledge of the dimensions of the right-lateral strike-slip Hayward fault, the magnitude of the maximum earthquake generated is taken to lie between 6.75 and 7.25. This entails a rupture length of L = 40 km and rupture depth of h = 15 km.

With these specifications, (horizontal) components of earthquake ground motions were constructed that satisfied simultaneously the following criteria: a) peak ground acceleration at about 0.7g with frequencies less

than 10 Hz. b) a peak ground velocity of about 100 cm/sec, c) a peak displacement associated with the seismic waves (i.e., nonstatic displacement, such as landslides) of about 50 cm, d) a bracketed duration of acceleration above 0.05g (at frequencies less than 10 Hz) of 20 to 30 seconds, e) an interval between the P and S wave onsets of about 5 seconds, corresponding to an assumed focal distance of 25 km, f) a longer period pulse following the first S wave arrivals that models the fling of the fault rebound as the rupture goes by the site, and g) a psuedo-velocity spectrum (2 per cent damping) that resembles in shape and level similar spectra obtained by combining seismic ground motions from many sources (Housner and Jennings, 1964).

The acceleration, velocity, and displacement records were built up by first drawing general envelopes with required shape, amplitudes, and duration (see Section 2.3). Then 20-term Fourier series were used to represent the wave motion within these envelopes. The coefficients of the sine and cosine terms were varied in order to obtain allowable spectra for frequencies from 8 to 0.5 Hz and phase relations (see Section 2.4) that modeled the P and S onsets, the fling pulse, and the decaying coda. Finally, additional higher frequency motion was superimposed randomly (see Section 2.3) to produce a more "realistic looking" accelerogram (i.e., one with a more continuous energy distribution through all frequencies of concern).

From the suite of records thus obtained, the record reproduced in Figure 4.2 was selected as meeting criteria (a) to (g). In the actual record shown, the peak acceleration (horizontal shaking) is 0.70g, the peak velocity is 90 cm/sec, and the peak displacement is 54 cm. In Figures 4.3 to to Figure 4.6, various response spectra for the time history shown in 4.2 are also given for comparison.

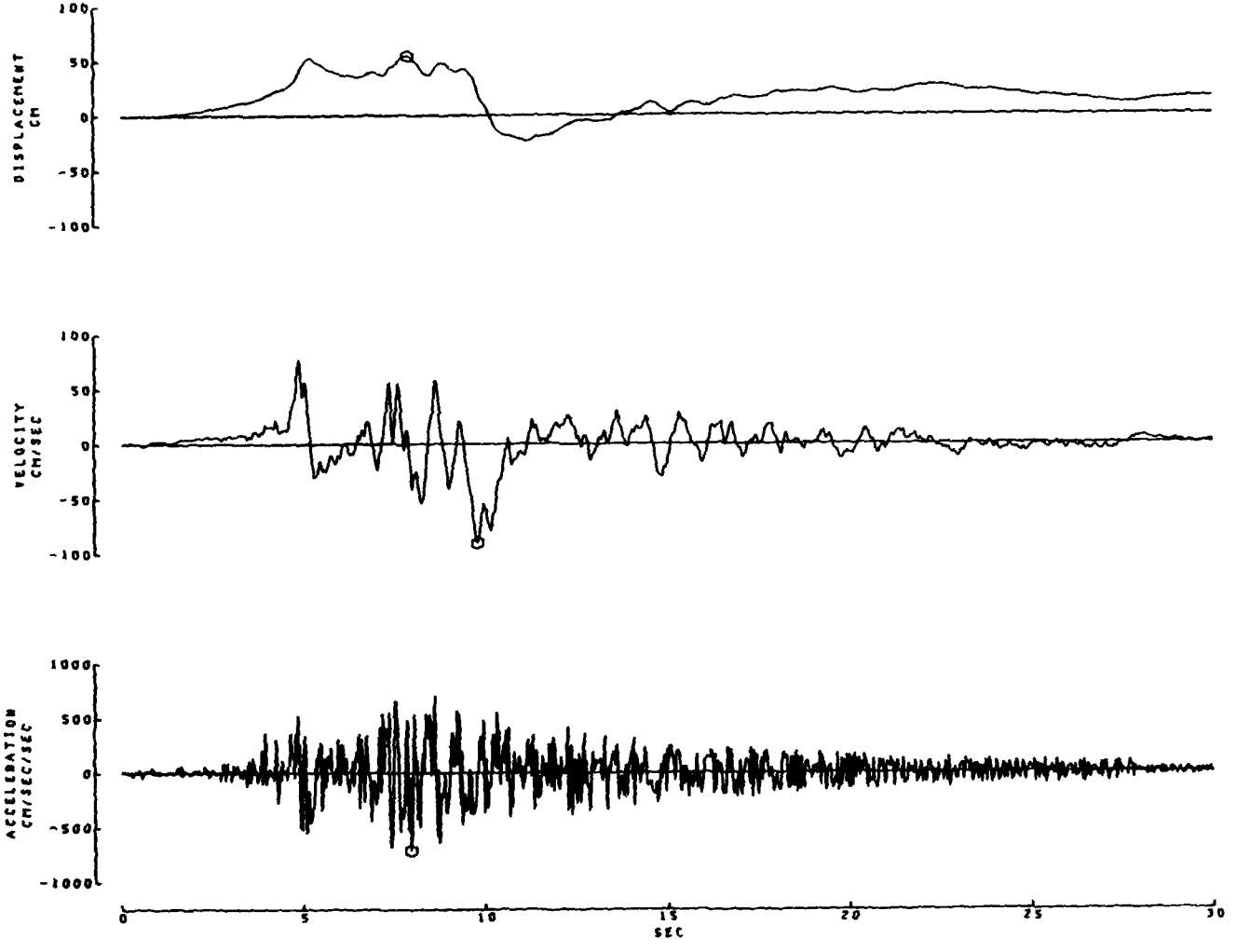

Figure 4.2. Synthetic horizontal component ground motions predicted for a near-fault site in a magnitude 7.0 earthquake produced by adjacent rupture of the Hayward fault ("BOLTSHOCK").

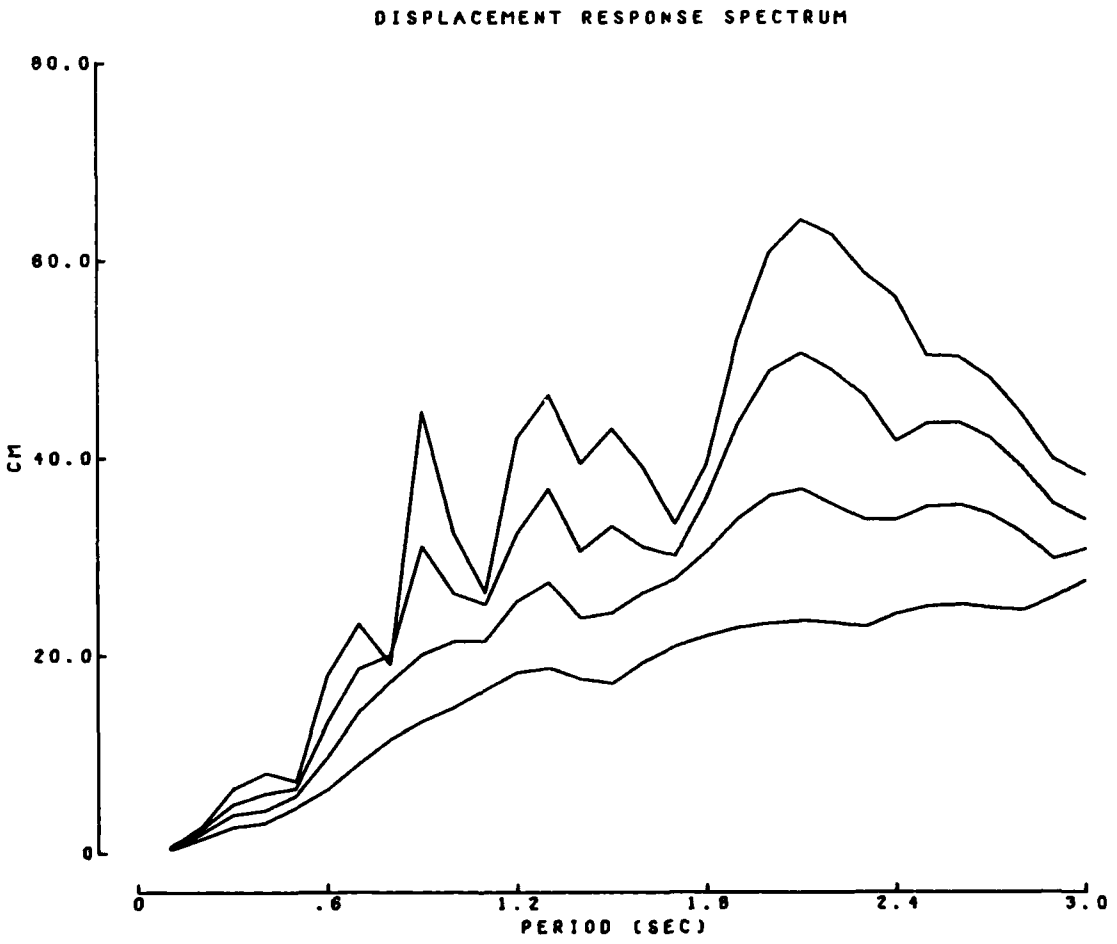

Figure 4.3. Displacement response spectrum for ground motion in Figure 4.2. (from top: 2, 5, 10, and 20 per cent damping)

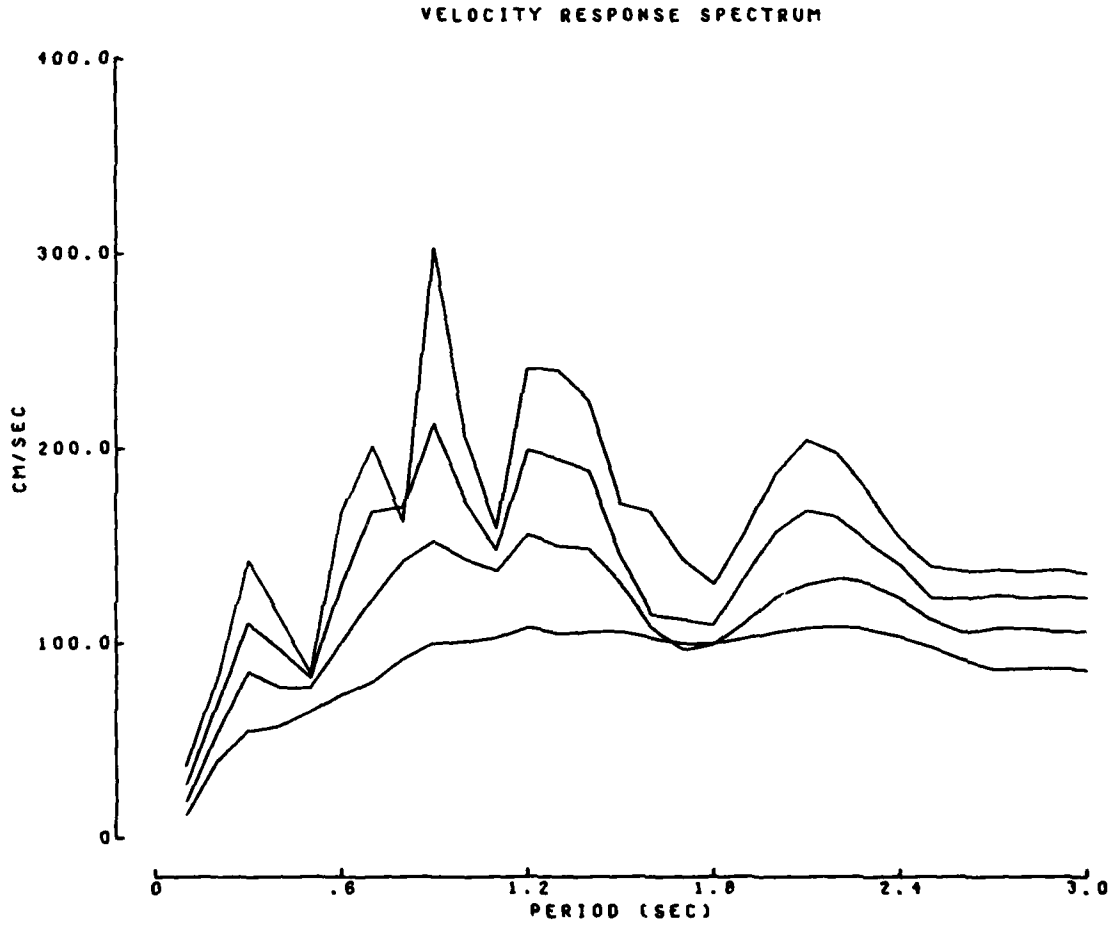

Figure 4.4. Velocity response spectrum for ground motion in Figure 4.2. (from top: 2, 5, 10, and 20 per cent damping)

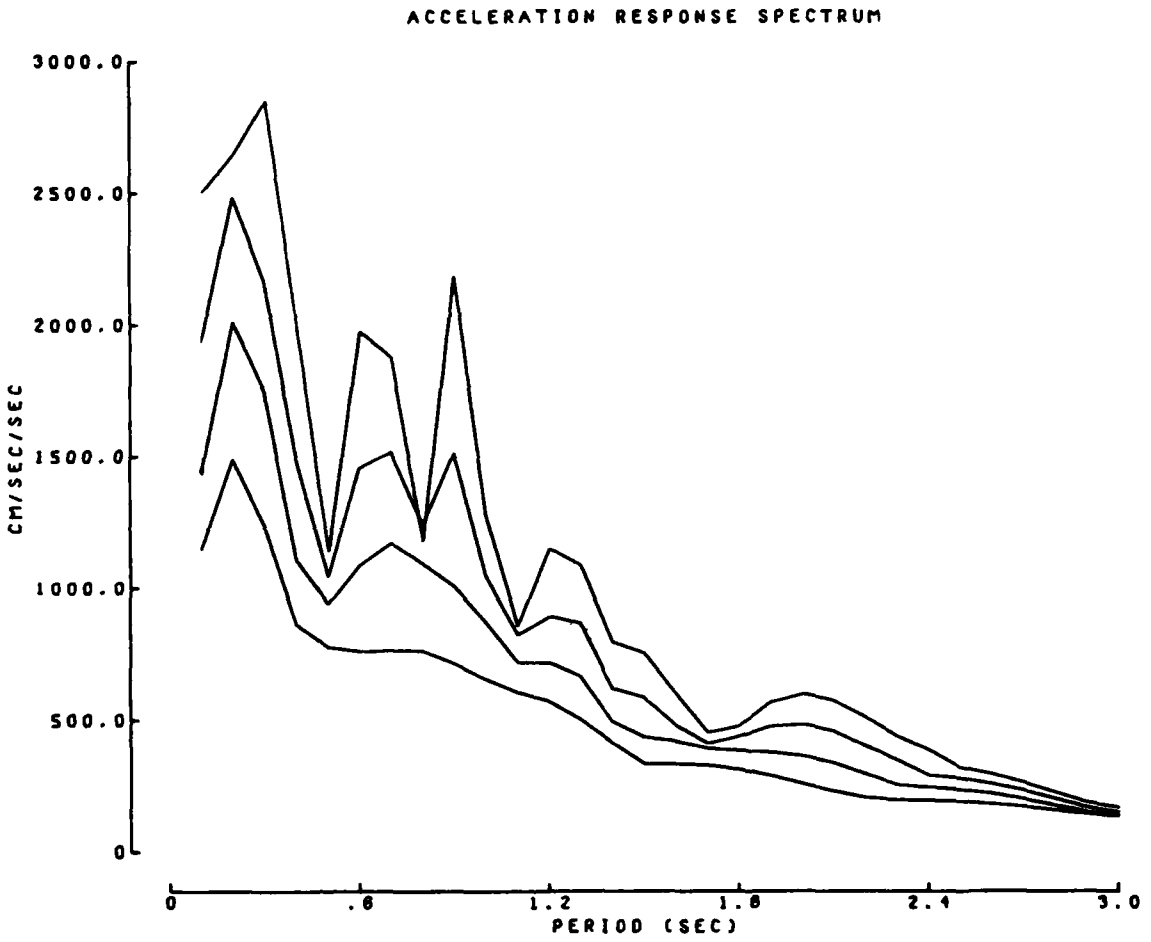

Figure 4.5. Acceleration response spectrum for ground motion in Figure 4.2. (from top: 2, 5, 10, 20 per cent damping)

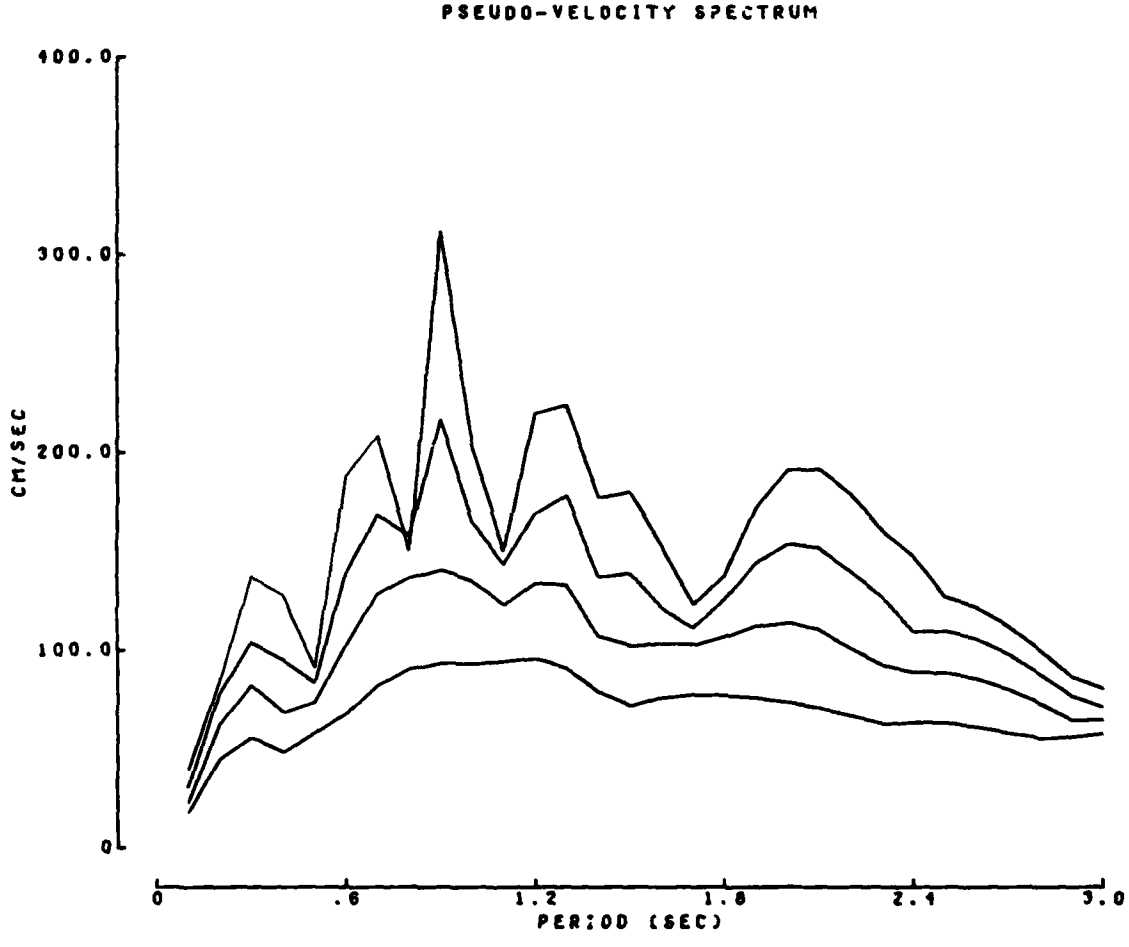

Figure 4.6. Pseudo-velocity spectrum for ground motion in Figure 4.2. (from top: 2, 5, 10, and 20 per cent damping)

When compared with various published time histories and spectra for the largest earthquake now observed, the motions are consistent with the spectral energy and duration measured elsewhere. This method of construction, based on general seismological theory and the earthquake mechanism, makes it likely that the synthetic ground motions will be close to any actually recorded on the weathered rock near to this site in a repetition, say, of the 1868 earthquake on the Hayward fault.

4.3 Some Remarks on High-Acceleration Values

The first inference to be drawn from the case studies in Part III concerning peak accelerations is that this parameter is not robust. The implication is that some other measure of energy or amplitude of seismic waves should be adopted to specify size of strong ground shaking in critical situations. So far as the construction of strong ground motions for design purposes is concerned, it should be mentioned that it is easily demonstrated that the high-frequency peak of acceleration can be changed by 10 per cent or so without significantly changing the spectral curves or the overall energy. This result is evident also from the construction of the Hayward fault earthquake given in the previous section.

Secondly, consideration of the horizontal components of acceleration given in the case studies demonstrates that these are made up of superposition of many wave types radiating from an extended and moving source. As a consequence, the peak accelerations depend on the phasing of the various harmonic components of the motion and do not necessarily coincide in time on the horizontal components. An example is the horizontal components recorded at Taft (see Figure 3.1). (In this case, the direction of instrumental orientation correlates with the strike of the rupturing fault.) As the accelerograms show (see Figure 3.1), the maximum amplitudes of acceleration occurred at quite different times during the motion and are not the result of any vectorial combination. Not only does this observation have important consequences for accelerogram interpretations, but it also has practical consequences for earthquake engineering design. As an illustration, consider the complete representation of average earthquake excitation at a site. It is not usually appropriate ab initio to resolve the motions in a particular direction

because it is not known just what section of nearby faults will rupture. In an earthquake, the seismic waves can be of various types from various fault sections, traveling various paths in the crustal rocks and superimposed in a complicated way.

Penzien and Watabe (1975) deal with the problem completely in the time domain by designing a set of principal directions (with three components) for which the variances of the component ground motions are stationary values. Another approach to optimal spectral combination and representative time histories has been worked out by Shoja-Taheri and Bolt (1977). The spectra of the two recorded horizontal components in a given earthquake are combined to maximize the resultant spectrum independently of azimuthal orientation. The phases of the two components play an important role. In this way, the significant dependence of the parameters of strong-motion records on the arbitrary azimuthal components is removed.

The final inference from the present study on high peak accelerations concerns the use of the stress drop as a parameter. It is sometimes suggested that this parameter is a key to understanding the seismic motions and to modeling numerically the ground motions. The parameter defined in Section 1.3 is, from a physical point of view, an important one. However, the usual stress drop calculated from the formula given in Section 1.3 (or from the spectra of the ground motion, see Aki and Richards, 1980) is the average stress drop for the whole dislocation episode. That is to say, the stress drop is averaged over the whole dimension of the fault. When high-frequency accelerations are concerned (frequencies of about 10 Hz), we must think instead of rapid variations in stress drop from one place to another along the fault. Unfortunately, there is as yet no way of assessing

these delta function-like occurrences. Most earthquakes have stress drops of less than 100 bars. There is evidence, however, that in some circumstances, such as localized dislocations in highly stressed and rigid rock, stress drops of well over 100 bars occur.

Again, we arrive at the idea of a roughness distribution density function discussed in Sections 1.3 and 2.5. There it was pointed out that local increases in roughness or friction along the fault (fault barriers) would give rise to local stress concentrations of a few kilometers in extent. The marked variation of stress drops (relative to the overall mean value) at points along the fault surface could give rise to jumps in acceleration superimposed on the overall deterministic wave motion. The best approach seems to be to treat these localized stress drops in terms of a stochastic distribution. With additional work, this stochastic distribution might be estimated in a nonparametric sense, using the method sketched in Section 4.2.

4.4 The Focussing Controversy

In at least seven of the earthquakes studied in Part III, there was evidence for a variation in intensity with azimuth relative to the seismic source (i.e., Kern County, Parkfield, San Fernando, Bucharest, Coyote Lake, Imperial Valley, and Livermore Valley). Because seismic intensities are of a qualitative rather than a quantitative measure, there is some difficulty in determining the cause for this variation in the directivity of intensity.

Three candidate mechanisms which could generate the effect have already been mentioned (see Section 2.6). The first, which is undoubtedly dominant in certain circumstances, is the variation in crustal structure and in near-surface alluvium and soil properties. These pockets of high intensity were clearly obvious in the isoseismal diagrams following the 1906 San Francisco earthquake and correlated closely with recent alluvial valley deposits in central California. The two other causes are the radiation pattern associated with the earthquake mechanism and the Doppler focussing of the waves due to the motion of the source. The first of these mechanisms is well confirmed by seismological measurements over many years, based, initially, on the ideas of the Byerly fault-plane solutions (see Figure 3.30) in the far field. The detailed effect in the near field is not yet so well determined, but is certainly present.

It is, however, the role and extent of the effectiveness of geometrical focussing due to the source motion which has come to the fore in recent years. For example, the Nuclear Regulatory Commission, in some recent hearings on licensing of nuclear power stations, has been concerned to consider evidence for the effect of such focussing on predicted ground motions for the design of nuclear reactors. Thus, in a recent case before the Atomic

Safety and Licensing Appeal Board (Docket No. 50-2750L and 50-3230L), a question raised by the Appeal Board (No. 7) stated, in part:

> "Interveners and the applicant have suggested that the strong-motion data obtained from stations along the direction of the Imperial fault evidence the 'focussing of earthquake motion.' Yet, when the acceleration data of two such stations, El Centro Arrays Nos. 6 and 7, are plotted as a function of distance from the fault, the horizontal acceleration values fall well below the regression mean line for one km distance. The vertical acceleration values were also lower than the mean in such a fault. To the extent possible, the party should analyze the seismic records for this earthquake as they pertain to the focussing phenomena and relate the results of such analyses to the likelihood that focussing might result in amplified seismic motion."

This question generated considerable work in the special context raised by the Nuclear Regulatory Commission's Atomic Safety and Licensing Appeal Board. The general conclusion from both the studies in Part III given above and also from recent publications is that focussing due to rupture propagation probably occurs to some degree in all earthquakes. In those cases where there are enough strong-motion instruments to allow correlations along the fault of the ground motions in a quantitative way, the evidence does not, however, support the predictions of very high amplifications and phase shifts (see Section 2.6) predicted by the theory of a moving source

It has been shown that one explanation for the large ground motions at Pacoima Dam (Heaton and Helmberger, 1979) is, in part, the focussing phenomena. (We also indicate (Section 3.4) other reasons for the large amplitudes at Pacoima, including the topography on which the instrument was operated.) As the above quotation indicates, some near-field accelerations in the 1979 Imperial Valley earthquake do not show any obvious indication of focussing in wave acceleration. Some recent work carried out by Singh (1981) in connection with the present study brings to light some important results concerning focussing and directivity. Singh has found that evidence for kinematical focussing, while difficult to find with accelerations, is often present when

the peak velocities of ground motion are plotted. In particular, for the 1979 Coyote Lake earthquake and the 1979 Imperial Valley earthquake, there is definite evidence from recorded wave velocities of directivity (see Figure 4.7). The contours of the peak ground displacement shown in Figure 4.7 are, in contrast to the corresponding acceleration contours, pear-shaped relative to the fault rupture, with enhanced motion northward in the direction of source rupture. The shape of the lobes is similar to the shape that would be predicted from simple moving source models (see Section 2.6).

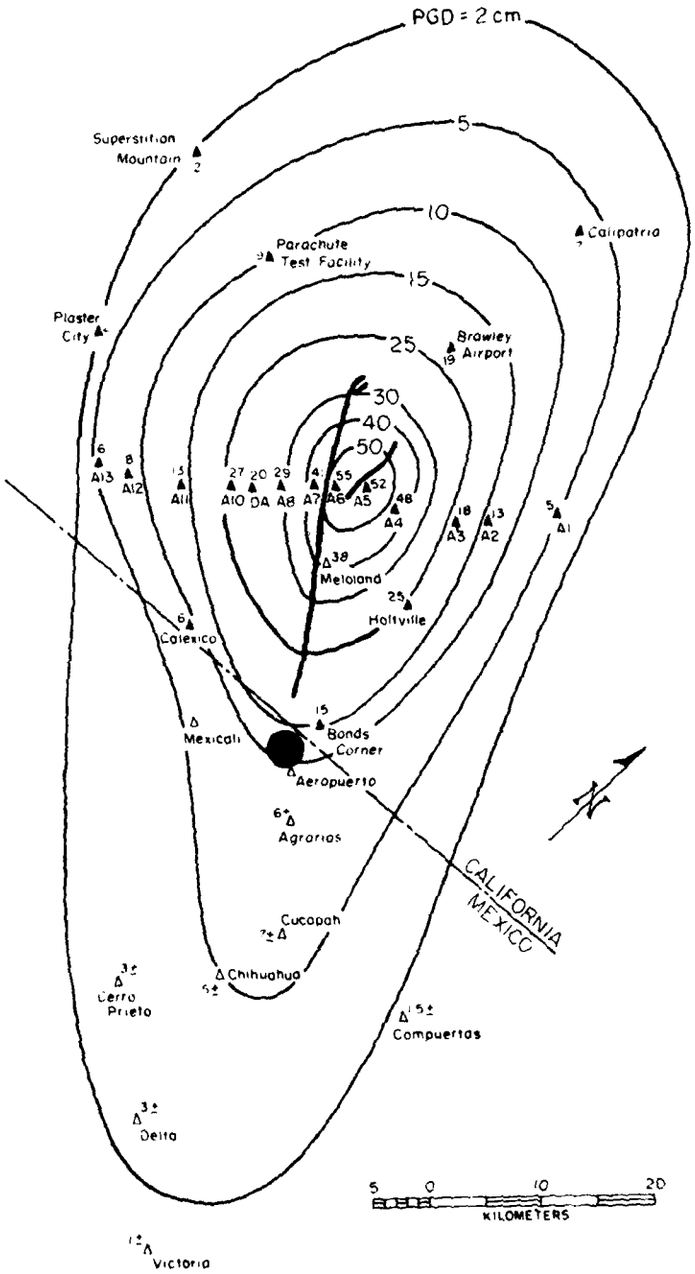

Figure 4.7. Peak ground displacement contours, Imperial Valley earthquake, 1979 (after J. P. Singh, 1981).

4.5 Need for Strong-Motion Instrument Arrays

Many of the problems encountered in the previous sections in securing a unique interpretation of recorded ground motions require more advanced instrumentation than the single three-component analog accelerometer that has been used in the past. A significant advance in resolution can be obtained by the use of an array of strong-motion instruments in a geometrical configuration, with each accelerometer having a common time base (see Figure 4.8). The latter property allows the actual phases of the seismic waves to be correlated between recording elements. It also permits the identification of the wave types by the scrutiny of the orbits of the particles of ground motion. The first improvement step is to equip individual strong-motion accelerometers with radio receivers which enable absolute time (from WWV, say) to be marked on the record. The linear array of accelerometers at right angles to the Imperial fault which triggered in the October 5, 1979, Imperial Valley earthquake (see Figure 3.23) contained instruments with this feature.

A proposal for the establishment of an international network of special research arrays for the measurement of strong shaking earthquakes grew out of a workshop in Hawaii in May, 1978, sponsored by the International Association of Earthquake Engineering and the International Association of Seismology and Physics of the Earth's Interior. Among the designs considered were source mechanism arrays and wave propagation arrays. Consider an analogy between a seismic array, like that in Figure 4.8, and an array of radio telescopes. The seismic wave front propagates across the array and triggers each element in a sequence that depends upon the azimuth of arrival and the wave velocity. Thus, both the direction of the approach of each wave type and its apparent velocity can be determined by cross-correlating

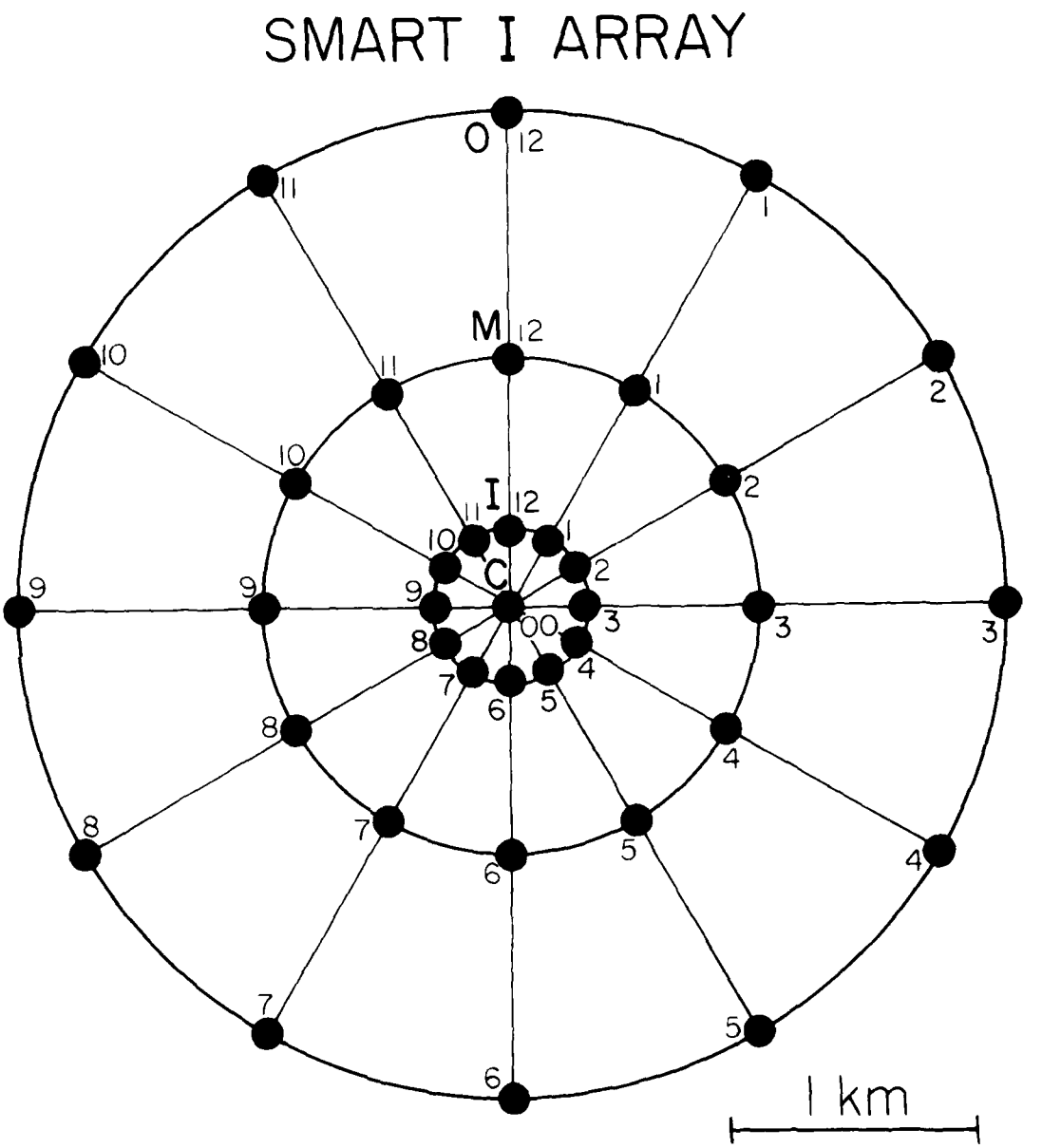

Figure 4.8. Configuration of the SMART1 array of digital strong-motion accelerometers in Taiwan.

AD-A108 615 CALIFORNIA UNIV BERKELEY DEPT OF GEOLOGY AND GEOPHYSICS F/G 8/11
STATE-OF-THE-ART FOR ASSESSING EARTHQUAKE HAZARDS IN THE UNITED--ETC(U)
OCT 81 B A BOLT DACW39-78-C-0061

UNCLASSIFIED WES-MP-S-73-1-17 NL

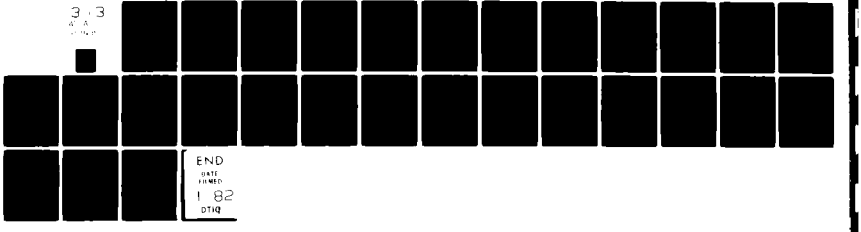

END
DATE FILMED
1 82
DTIC

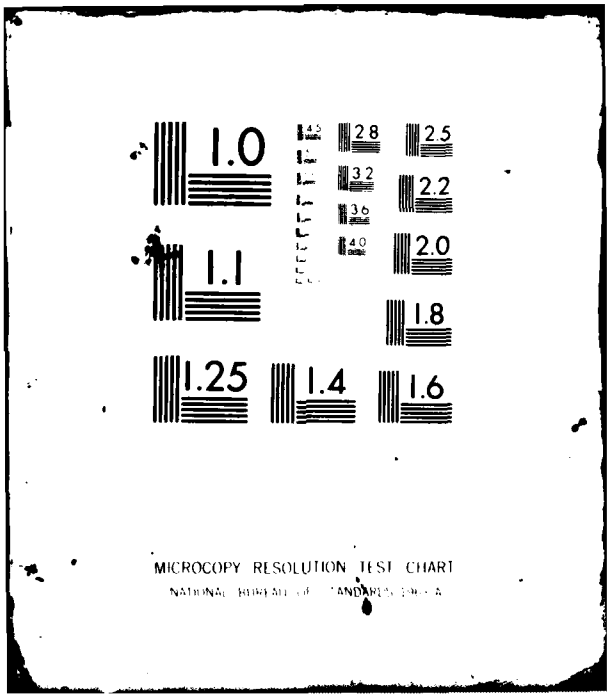
1.0
1.1
1.25
1.4
1.6
1.8
2.0
2.2
2.5
2.8
3.2
3.6
4.0
MICROCOPY RESOLUTION TEST CHART

the times of arrival of peaks and troughs of the various array elements. In different terms, we can use a computer to "steer the array" towards a particular section of the nearby rupturing fault and determine what type and amount of seismic energy is, at that time, radiating from that section of the fault. Indeed, the computer can lock the array response onto the rupture front itself and follow the dislocation as it moves from one end of the fault break to the other.

Geometrical spacing in surface arrays must be designed to resolve as much of the source of propagation details as possible. Design of source mechanism arrays would differ for strike-slip, subduction, and dip-slip faulting. Some of the arrays might be narrow, such as that constructed in the Imperial Valley, extending parallel or normal to the active fault for tens or even hundreds of kilometers. In order to remove both frequency and spatial aliasing, individual elements in the arrays have to be properly placed, so that waves of the frequency bands of interest can be resolved.

Another type of array considered is a local laboratory array (or local effect array). These might range from simple to relatively complex configurations of elements to provide data for the gradients of ground motion and the nature of wave propagation through a restricted site. They would contain 25 to 40 instruments arranged over an area of about one square kilometer and they would exist alone or in conjunction with source mechanism and wave propagation arrays. In practice, a specific site would present its own opportunities and it would be often advantageous to work with a hybrid array capable of treating several strong-motion problems.

The first such hybrid array to commence operation is located in the Lanyang plain of northeast Taiwan. This array, called SMART 1, has 37 digital strong-motion accelerographs located in the configuration shown in

Figure 4.8. There are three rings, each with 12 instruments, with radii of 200 m, 1 km, and 2 km, respectively. These dimensions and configuration minimize aliasing problems for strong ground motions with frequencies in the range between 5 Hz and 2 sec. The omni-directional nature of circular arrays best suits the general azimuthal distribution of likely sources of strong earthquakes in the vicinity of the Lanyang plain.

Each element consists of a triaxial force balance accelerometer capable of recording plus or minus 2g acceleration connected to a digital event recorder. These digital event recorders (DR-100) are low-powered digital recording systems that have been successfully used by a number of seismological groups in the last few years in the field to record microearthquakes. Power is from batteries with a battery charger to external electric power. The recorder uses a magnetic tape cassette of conventional type. The accelerometers will trigger on both vertical and horizontal components of ground motion. Signals are digitized as 12-bit words at 100 samples/sec. There is a digital delay memory which stores the output from the forced balance accelerometers for approximately 2.5 sec. This memory is an important advance over conventional instruments and assures that the first ground motion, consisting of the first P wave, is not missed. Each DR-100 has a separate crystal clock and time code generator which provides day, hour, minute, and second information. These clocks are synchronized with highly precise time signals by manual adjustments in the field using a portable time comparator.

Twenty-one elements of the array were installed in the fall of 1980 and, by good fortune, two moderate earthquakes were recorded near to the array. The first earthquake (M_L = 5.8) occurred on October 18, 1980, at a distance of 50 km from the array, while the second, recorded on November 14, 1980 (M_L = 5.9), recorded just under the array at a depth of about 65 km.

A copy of three components of acceleration at one of the elements of SMART 1 in the second earthquake is shown in Figure 4.9.

Several important points immediately emerge from this type of recording: first, the true onset of the first P wave can be seen on the record and also the typical background noise before the arrival of the seismic wave; secondly, because the time of any digital sample is known to about 1/100th of a sec, cross-correlations between ray elements can be performed reliably up to frequencies of at least 15 Hz. Such spatial variations of ground motions are essential for engineering design purposes for structures such as dams and bridges which have large base dimensions.

It will be seen that this ability to correlate wave patterns across a small spatial dimension makes interpretation of the strong-motion seismogram much more straightforward and removes much of the non-uniqueness which has been present in past interpretations. We might expect that the problem of interference of wave trains coming from different parts of the dislocated fault can be studied by focussing the array response at various azimuths. Detailed analyses of the earthquakes mentioned above will be reported elsewhere with specific examples of the use of SMART 1 as an interpretive tool. It can be mentioned here, however, that a preliminary comparison between traces such as Figure 4.9 recorded at various elements of the array indicates similarities in waveforms (after taking account of the requisite time lags due to station element spacing) but also indicates clear departures from repetition of the waveforms at various intervals of the record. In the next section, an introductory account is given of the way in which correlations with arrays can be performed for interpretation purposes.

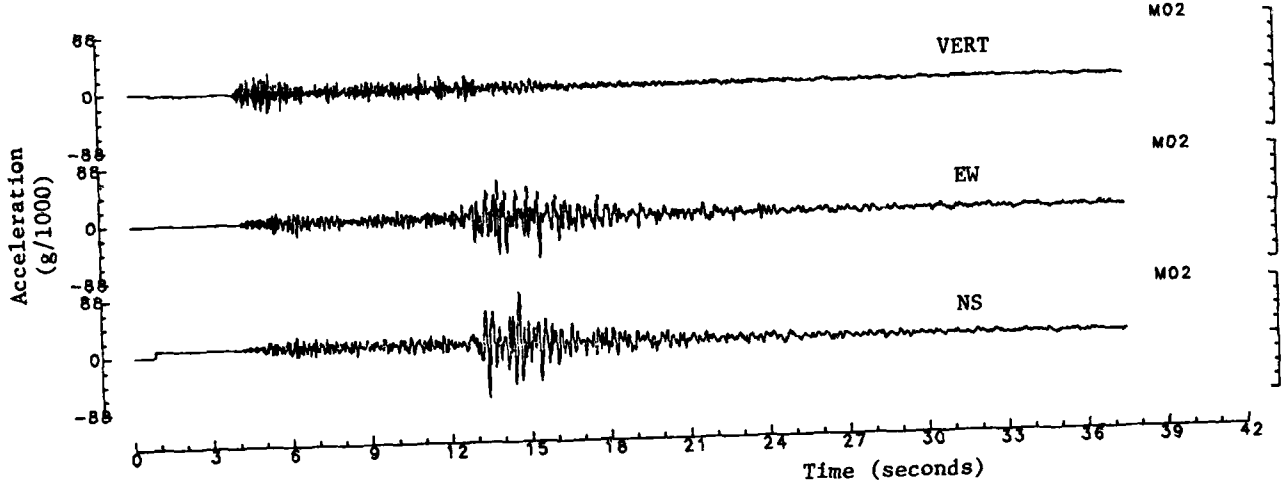

Figure 4.9. Examples of first accelerograms recorded by SMART1 (plotted from magnetic tape digital recordings). The accelerations are at site M02 (see Figure 4.8) for the November 14, 1980, earthquake.

4.6 Use of Mathematical Response Transformations

Consider a strong motion array located on a horizontal plane on "ideal rock," i.e., a basement that does not scatter or convert the incident large-amplitude seismic waves. A seismic wave front from a point on the rupturing fault some distance to the side and below the array will arrive as a circular front with a velocity V appropriate to the wave in question (P, S, or surface wave velocity). Let us assume for simplicity (but certainly not true for very near source arrays, like El Centro, Figure A1) that the wave front is a plane. This front will have an apparent surface velocity of $V/\sin \alpha$, where α is the angle between the wave front and the ground surface.

A coherent seismic wave is propagated across such an array (e.g., SMART 1 or El Centro) at its apparent ground velocity. Clearly, the order at which it is detected at each element of the array is a function of the azimuth of approach and the apparent velocity. In other words, phase shifts (time increments) exist for this wave onset at each accelerometer, and a computer can be programmed to measure these phase shifts and relate them to an arbitrary point of the array (usually the center element E(0)).

More generally, wave peaks (or troughs) are separated on the ground surface by a distance λ, corresponding to the wavelength. Thus, if the polar coordinates of the ith element of SMART 1, say, are r_i, θ_i, then the phase shift for an incoming seismic wave with azimuth θ and wavelength λ is

$$\phi_i = 2\pi \, (r_i/\lambda) \cos (\theta - \theta_i) \quad .$$

The recorded wave onset of the ith seismometer can thus be represented by a vector of amplitude a_i and phase angle ϕ_i .

The "output" or "response" of the array is given by the vector sum of the individual element records. If a wave front arrives instantaneously (vertically from below with SMART 1, or perpendicular to the fault traces

for the Gilroy and El Centro arrays) the accelerometer outputs are all in phase and the response is unity. Otherwise the response is less than unity.

We can use these simple concepts to have the computer insert incremental delays in the actual records from each element in order to maximize the response for sequential portions of the records. In other words, the strong-motion array can be "tuned" in the data analysis process to scan a range of wave velocities and wave approach azimuths. (Because strong-motion records contain many frequencies, this must be done frequency-by-frequency, introducing a third dimension.)

In order, for example, to estimate the direction from which a portion of the record has come (position on the rupturing fault) delays are inserted, assuming an apparent wave velocity for the full azimuth range. The approach azimuth at that time is the one that gives the maximum response of the array. The scheme is illustrated in Figure 4.10 for the SMART1 circular configuration. (The sharpest azimuth response is obtained with a circular array and is symmetrical.) For a wave length of 1 km, there is a peak response (the sum of the 37 equal elements of SMART 1) when the array delays are set to the correct direction of approach. If the delays are in error, then the resolution falls, as shown, with fluctuations (or side-lobes) in response.

The accuracy of determination of approach azimuth and wave velocity depends upon the sharpness of the array response, which in turn depends on the array dimensions and configuration. This is why each strong-motion array must in the future be designed carefully, with the local tectonic conditions and the specific seismological and engineering goals in mind. Care must be taken to avoid "aliasing" in both time and space. For digital record samples at time intervals Δt seconds, it is well known that it is

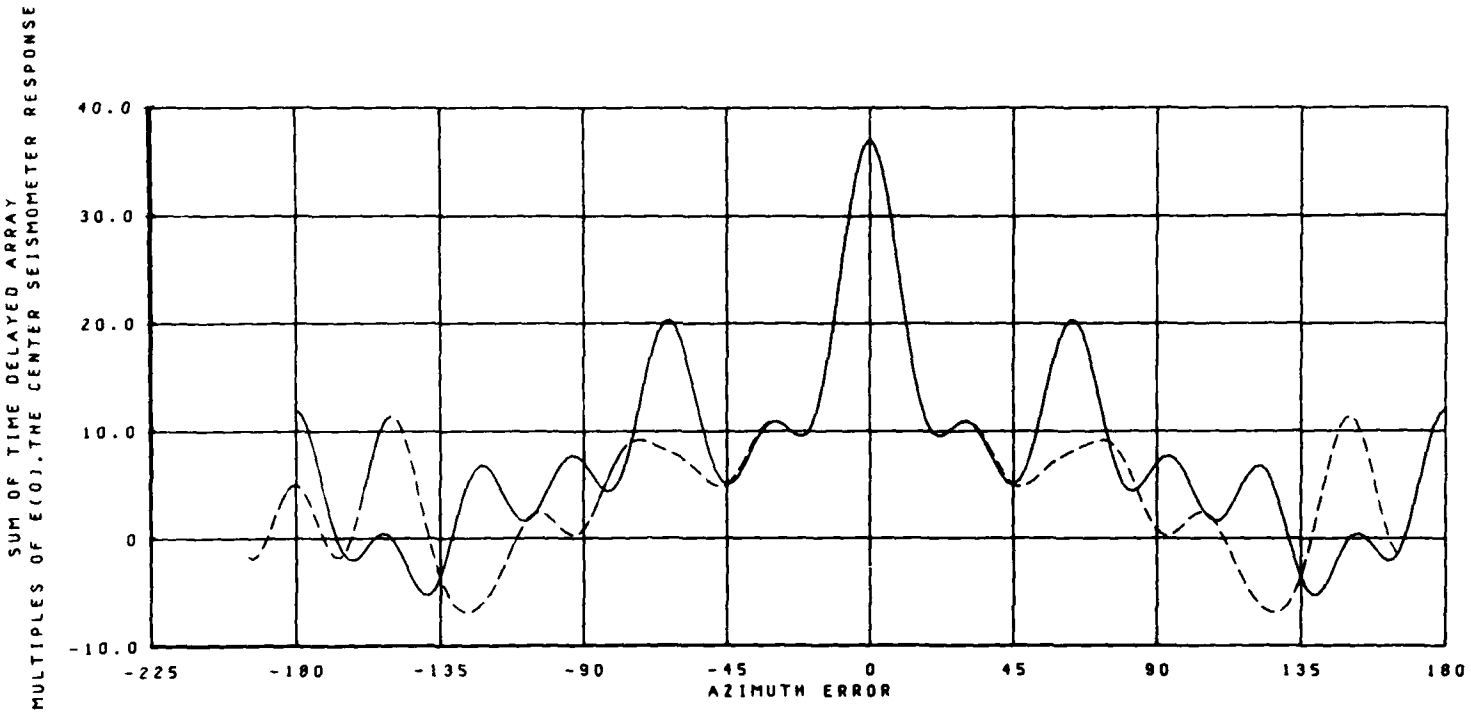

Figure 4.10. SMART 1 response, the effect of azimuth error in time delayed array for apparent wavelength of 1.0 km.

impossible to distinguish frequencies above the frequency $f_N = 1/2\ \Delta t$. This is because at least 2 samples are needed to detect any frequency component. The effect is that the energy of ground motions with frequencies greater than f_N will be added (or aliased) into the ground motion spectrum at lower frequencies.

For an array that is spatially distributed like SMART 1, there is an analogous sampling problem in terms of wave length. Suppose the array element spacing is Δx. Then the shortest wavelength detectable is $2\Delta x$ and the corresponding aliasing frequency is $V/2\Delta x$. Thus, for a seismic motion with velocity 2 km/sec and Δx = 200 m (the inner ring of SMART 1 has a radius of 200 m) the aliasing frequency is 5 Hz. In this case, the ground motion spectrum for 5 Hz and lower frequencies would be able to be computed satisfactorily.

REFERENCES

Aki, K. (1968). Seismic displacements near a fault, Bull. Seism. Soc. Am. 73, 5359-5376.

Aki, K., M. Bouchon, B. Chouet, and S. Das (1977). Quantitative prediction of strong motion for a potential earthquake fault, Annali di Geofisica 30, 341-368.

Aki, K. and P.G. Richards (1980). Quantitative Seismology, Theory and Methods, W.H. Freeman and Company, San Francisco, 948 p. (two volumes).

Algermissen, S.T., J.W. Dewey, C.J. Langer, and W.H. Dillinger (1974). The Managua, Nicaragua, earthquake of December 23, 1972: location, focal mechanism, and intensity distribution, Bull. Seism. Soc. Am. 64, 993-1004.

Allen, C.R., G.R. Engen, T.C. Hanks, J.M. Nordquist, and W. Thatcher (1971). Main shock and larger aftershocks of the San Fernando earthquake, February 9 through March 1, 1971, Joint Report, U.S. Geological Survey and NOAA, 17-20.

Allen, C.R. and J.M. Nordquist (1972). Foreshock, main shock and larger aftershocks of the Borrego Mountain earthquake, U.S. Geol. Surv. Prof. Paper 787, 16-23.

Anderson, J. (1974). A dislocation model for the Parkfield earthquake, Bull. Seism. Soc. Am. 64, 671-686.

Anderson, J.G. and P.G. Richards (1975). Comparison of strong ground motion from several dislocation models, Geophys. J. Roy. Astr. Soc. 42, 347-373.

Aptekman, Kh. Ya, V.M. Graiser, K.G. Pletnev, D.N. Rustanovich, N.V. Shebalin, and V.V. Shteinberg (1978). Some data on processes in the epicentral zone of the 1976 Gazli earthquakes, in Epicentral Zones of Earthquakes, 19, Questions in engineering seismology, Nanka, Moscow, 149-166 (in Russian).

Archambeau, C.B. (1968). General theory of elasto-dynamic source fields, Rev. Geophys. 16, 241-288.

Backus, G.E. (1977a). Interpreting the seismic glut moment of total degree two or less, Geophys. J. Roy. Astr. Soc. 51, 1-25

Backus, G.E. (1977b). Seismic sources with observable glut moment of spatial degree two, Geophys. J. Roy. Astr. Soc. 51, 27-45.

Benioff, H. (1955). Mechanism and strain characteristics of the White Wolf fault as indicated by the aftershock sequence, Calif. Div. Mines Geol., Bulletin 171, 199-202.

Ben-Menahem, A. and S.J. Singh (1972). Computation of models of elastic dislocations in the earth, in Methods of Computational Physics, V.12, B.A. Bolt (ed.), Academic Press, New York.

Berg, G.V., B.A. Bolt, M.A. Sozen, and C. Rojahn (1980). Earthquake in Romania, March 4, 1977: An Engineering Report, National Academy Press, Washington, D.C.

Bertero, V.V., S.A. Mahin, and R.A. Herrera (1978). Aseismic design implications of near-fault San Fernando records. J. of Earthquake Eng. and Struct. Dynamics 6, 31-42.

Bolt, B.A. (1970). Elastic waves in the vicinity of the earthquake source, in Earthquake Engineering, R.L. Wiegel (ed.), Prentice-Hall, Englewood Cliffs, New Jersey.

Bolt, B.A. (1972). San Fernando rupture mechanism and the Pacoima strong-motion record, Bull. Seism. Soc. Am. 62, 1053-1061.

Bolt, B.A. (1973). Duration of strong ground motion, Fifth World Conf. Earthquake Engineering, Rome.

Bolt, B.A. (1978). The local magnitude M_L of the Kern County earthquake of July 21, 1952, Bull. Seism. Soc. Am. 68, 513-515.

Bolt, B.A. and W.D. Smith (1976). Finite-element computation of seismic anomalies for bodies of arbitrary shape, Geophysics 41, 145-150.

Bolt, B.A., T.V. McEvilly, and R.A. Uhrhammer (1981). The Livermore Valley, California, sequence of January, 1980, Bull. Seism. Soc. Am., in press.

Boore, D.M. (1970). Love waves in a nonuniform waveguide: finite difference calculations. J. Geophys. Res. 75, 1512-1527.

Boore, D.M. (1973). The effect of simple topography on seismic waves: implications for the accelerations recorded at Pacoima dam, San Fernando Valley, California, Bull. Seism. Soc. Am. 63, 1603-1609.

Boore, D.M. and W.B. Joyner (1978). The influence of rupture incoherence on seismic directivity, Bull. Seism. Soc. Am. 68, 283-300.

Boore, D.M. and M.D. Zoback (1974). Two dimensional kinematic fault modeling of the Pacoima dam strong-motion recordings of the February 9, 1971, San Fernando earthquake, Bull. Seism. Soc. Am. 64, 555-570.

Bouchon, M. (1980a). The motion of the ground during an earthquake, 1. The case of a strike-slip fault, J. Geophys. Res. 85, 356-366.

Bouchon, M. (1980b). The motion of the ground during an earthquake, 2. The case of a dip-slip fault, J. Geophys. Res. 85, 367-375.

Bouchon, M. and K. Aki (1977). Discrete wave-number representation of seismic-source wave fields, Bull. Seism. Soc. Am. 67, 259-277.

Brady, A.G., V. Perez, and P.N. Mork (1980). The Imperial Valley Earthquake, October 15, 1979, digitization and processing of accelerograph records, U.S. Geol. Surv. Open-File Rept.

Brown, Jr., R.D., P.L. Ward, and G. Plafker (1974). Geologic and seismologic aspects of the Managua, Nicaragua, earthquakes of December 23, 1972 (abstract), Bull. Seism. Soc. Am. 64, 1031.

Burridge, R. and J. Willis (1969). The self-similar problem of the expanding elliptical crack in an anisotropic solid, Proceedings of the Cambridge Philosophical Society 66, 443-468.

Coffman, J.L. (ed.) (1966). The Parkfield, California earthquake of June 27, 1966, preliminary seismological and engineering seismological report, U.S. Coast. Geodetic Surv.

Das, S. and K. Aki (1977a). A numerical study of two-dimensional spontaneous rupture propagation, Geophys. J. Roy. Astr. Soc. 50, 643-668.

Das, S. and K. Aki (1977b). Fault plane with barriers: a versatile earthquake model, J. Geophys. Res. 82, 5658-5670.

Dewey, J.W., S.T. Algermissen, C. Langer, W. Dillinger, and M. Hopper (1973). The Managua earthquake of 23 December 1972: location, focal mechanism, aftershocks, and relationship to recent seismicity of Nicaragua, in Managua, Nicaragua Earthquake of December 23, 1972, Earthquake Engineering Research Institute Conference on Managua, Nicaragua, Earthquake of December 23, 1972, San Francisco, 66-88.

Dewey, J.W. and S.T. Algermissen (1974). Seismicity of the middle America arc-trench system near Managua, Nicaragua, Bull. Seism. Soc. Am. 64, 1033-1048.

Donovan, N.C., B.A. Bolt, and R.V. Whitman (1976). Development of expectancy maps and risk analysis, ASCE Annual Convention, Preprint 2805, 1-19.

Drake, L.A. (1972a). Love and Rayleigh waves in nonhorizontally layered media, Bull. Seism. Soc. Am. 62, 1241-1258.

Drake, L.A. (1972b). Rayleigh waves at a continental boundary by the finite element method, Bull. Seism. Soc. Am. 62, 1259-1268.

Eaton, J.P., M.E. O'Neill, and J.N. Murdock (1970). Aftershocks of the 1966 Parkfield-Cholame, California, earthquake: a detailed study, Bull. Seism. Soc. Am. 60, 1151-1197.

Good, I.J. and R.A. Gaskins (1972). Global nonparametric estimation of probability densities, Virginia J. Science 23, 171-193.

Gutenberg, B. (1955a). The first motion in longitudinal and transverse waves of the main shock and direction of slip, in Earthquakes in Kern County, California, during 1952, Calif. Dept. Nat. Resources, Div. Mines Bull. 171, 165-170.

Hanks, T.C. (1975). Strong ground motion of the San Fernando, California, earthquake: ground displacements, Bull. Seism. Soc. Am. 65, 193-225.

Hanks, T.C. (1978). Measures of high-frequency strong ground motion, in Strong Ground Motion, N.S.F. Seminar Workship Proceeding, San Diego, California, 46-51.

Hartzell, S. (1979). Analysis of the Bucharest strong ground motion record for the March 4, 1977, Romanian earthquake, Bull. Seism. Soc. Am. 69, 513-530.

Hartzell, S. (1980) Faulting process of the May 17, 1976 Gazli, USSR earthquake, Bull. Seism. Soc. Am. 70, 1715-1736.

Haskell, N.A. (1964). Total energy and energy spectral density of elastic wave radiation from propagating faults, Bull. Seism. Soc. Am. 54, 1811-1841.

Haskell, N.A. (1966). Total energy and energy spectral density of elastic wave radiation from propagating faults. Part II. A statistical source model, Bull. Seism. Soc. Am. 56, 125-140.

Heaton, T.H. and D.V. Helmberger (1977). A study of the strong ground motion of Borrego Mountain, California, earthquake, Bull. Seism. Soc. Am. 67, 315-330.

Heaton, T.H. and D.V. Helmberger (1979). Generalized ray models of the San Fernando earthquake, Bull. Seism. Soc. Am. 69, 1311-1341.

Helmberger, D.V. and D.M. Hadley (1981). Seismic source functions and attenuation from local and teleseismic observations of the NTS events, Jorum and Handley, Bull. Seism. Soc. Am. 71, 51-67.

Housner, G.W. and P.C. Jennings (1964). Generation of artificial earthquakes, J. Eng. Mech. Div., ASCE, 90, 113-150.

Housner, G.W. and M.D. Trifunac (1967). Analysis of accelerograms -- Parkfield earthquake, Bull. Seism. Soc. Am. 57, 1193-1220.

Hudson, D.E. (1970). Ground motion measurements, in Earthquake Engineering, R.L. Wiegel (ed.), Prentice-Hall, Inc., Englewood Cliffs, New Jersey, 107-126.

Hudson, D.E. (1979). Reading and interpreting strong-motion accelerograms, EERI, Engineering Monographs on Earthquake Criteria, Structural Design and Strong Motion Records.

Iosif, T. and S. Iosif (1977). The Vrancea earthquake of March 4, 1977 -- a multiple event and its seismotectonic implications, EP-1-1977, Institutal Central de Fizica.

Israel, M. and R.L. Kovach (1977). Near-field motions from a propagating strike-slip fault in an elastic half-space, Bull. Seism. Soc. Am. 67, 977-994.

Johnson, L.R. (1979). Seismic source theory, Reviews of Geophys. and Space Phys. 17, 328-336.

Kamb, B., L.T. Silver, M.J. Abrams, B.A. Carter, T.H. Jordan, and J.B. Minster (1971). Pattern of faulting and nature of fault movement in the San Fernando earthquake, U.S. Geol. Surv. Prof. Paper 733, 41-54.

Kanamori, H. and P.C. Jennings (1978). Determination of local magnitude, M_L from strong-motion accelerograms, Bull. Seism. Soc. Am. 68, 471-485.

Keilis-Borok, V.I. (1960). Investigation of the mechanism of earthquakes, Sov. Res. Geophys. (English Transl.) 4, 29.

Knudson, C.F., V. Perez, and R.B. Matthiesen (1974). Strong-motion instrumental records of the Managua earthquake of December 23, 1972. Bull. Seism. Soc. Am. 64, 1049-1067.

Kostrov, B.V. (1966). Unsteady propagation of longitudinal shear cracks, J. Appl. Math. and Mechanics 30, 1241-1248.

Langer, C.J., M.G. Hopper, S.T. Algermissen, and J.W. Dewey (1974). Aftershocks of the Managua, Nicaragua, earthquake of December 23, 1972, Bull. Seism. Soc. Am. 64, 1005-1016.

Leivas, E., E.W. Hart, R.D. McJunkin, and C.R. Real (1980). Geological setting, historical seismicity and surface effects of the Imperial Valley earthquake October 15, 1979, Imperial County, California, in Reconnaissance Report: Imperial County, California, Earthquake October 15, 1979, G. Brandow (coord'r) and D.J. Leeds (ed.), E.E.R.I.

Lysmer, J. and G. Waas (1972). Shear waves in plane infinite structures, J. Eng. Mech. Div. ASCE 98, 85-105.

May, T.W. and B.A. Bolt (1981). The effectiveness of trenches in reducing seismic motion, J. Earth. Eng. Struct. Dyn., in press.

McCowan, D.W. P. Glover, and S.S. Alexander (1977). A static and dynamic finite element analysis of the 1971 San Fernando, California, earthquake, Geophys. J. Roy. Astr. Soc. 48, 163-185.

McEvilly, T.V., W.H. Bakun, and K.B. Casaday (1967). The Parkfield, California, earthquakes of 1966, Bull. Seism. Soc. Am. 57, 1221-1244.

Mooney, H.M. and B.A. Bolt (1966). Dispersive characteristics of the first three Rayleigh modes for a single surface layer, Bull. Seism. Soc. Am. 56, 43-67.

Morse, P.M. and K.U. Ingard (1968). Theoretical Acoustics, McGraw-Hill, New York, 927 p.

Müller, G., K.P. Bonjer, H. Stöckl, and D. Enescu (1978). The Romanian

earthquake of March 4, 1977: I. Rupture process inferred from fault-plane solution and multiple-event analysis, J. Geophys. 44, 203-218.

Page, R.A., D.M. Boore, W.B. Joyner, and H.W. Coulter (1972). Ground motion values for use in the seismic design of the Trans-Alaska Pipeline system, Washington, D.C., Geological Survey Circular 672.

Penzien, J. (1970). Application of random vibration theory, in Earthquake Engineering, R.L. Wiegel (ed.), Prentice-Hall and Company, Englewood Cliffs, New Jersey, 335-347.

Penzien, J. and M. Watabe (1975). Characteristics of three-dimensional earthquake ground motion, J. Earth. Eng. Struct. Dyn. 3, 365-373.

Porcella, R.L. and R.B. Matthiesen (1979). Preliminary summary of the U.S. Geological Survey strong-motion records from the October 15, 1979 Imperial Valley earthquake, U.S. Geol. Surv. Open-File Rep. 79-1654.

Porcella, R.L., R.B. Matthiesen, R.D. McJunkin, and J.T. Ragsdale (1979). Compilation of strong-motion records from the August 6, 1979 Coyote Lake earthquake, Calif. Div. Mine. Geol. Preliminary Rep. 25; U.S. Geol. Surv. Open-File Rep. 79-385.

Reid, H.F. (1911). The elastic rebound theory of earthquakes, Bull. Dept. Geol. Univ. Calif. 6, 413-444.

Richter, C.F. (1958). Elementary Seismology, W.H. Freeman & Company, San Francisco.

Rojahn, C. (ed.) (1981). Selected papers on the Imperial Valley, California earthquake of October 15, 1979, U.S. Geol. Surv. Open-File Report 80-1094.

Schnabel, P.B. and H.B. Seed (1973). Accelerations in rock for earthquakes in the Western United States, Bull. Seism. Soc. Am. 63, 501-576.

Shoja-Taheri, J. (1977). Seismological studies of strong motion records, Earthquake Engineering Research Center Report No. UCB/EERI-77/04.

Shoja-Taheri, J. and B.A. Bolt (1977). Generalized strong-motion accelerograms based on spectral maximization from two horizontal components, Bull. Seism. Soc. Am. 67, 863-876.

Singh, J.P. (1981). Source directivity and its role in estimation of strong ground motions, Ph.D. Thesis, University of California, Berkeley, manuscript in preparation.

Smith, W.D. (1975a). A finite element study of the effects of structural irregularities on body wave propagation, Ph.D. Thesis, University of California, Berkeley.

Smith, W.D. (1975b). The application of finite element analysis to body wave

propagation problems, Geophys. J. Roy. Astr. Soc. 42, 747-768.

Stump, B.W. and L.R. Johnson (1977). The determination of source properties by the linear inversion of seismograms, Bull. Seism. Soc. Am. 67, 1489-1502.

Trifunac, M.D. and D.E. Hudson (1971). Analysis of the Pacoima dam accelerogram in San Fernando, California, earthquake of 1971, Bull. Seism. Soc. Am. 61, 1393-1411.

Uhrhammer, R.A. (1980). Observations of the Coyote Lake, California, earthquake sequence of August 6, 1979, Bull. Seism. Soc. Am. 70, 559-570.

Uhrhammer, R. (1981). The Pacifica earthquake of April 28, 1979, Bull. Seism. Soc. Am., in press.

Whitcomb, J.H. (1971). Fault-place solutions of the February 9, 1971, San Fernando earthquake and some aftershocks, in The San Fernando, California Earthquake of February 9, 1971, U.S. Geol. Survey Prof. Paper 733, 30-32.

BIBLIOGRAPHY

Aki, K. and B. Chouet (1975). Origin of coda wave; source, attenuation, and scattering effects, J. Geophys. Res. 80, 3322-3342.

Allen, C.R., T.C. Hanks, and J.H. Whitcomb (1972). San Fernando earthquake: seismological studies and their tectonic implications, Calif. Dept. Conserv. Div. Mines Geol., Special Report.

Ben-Menahem, A. (1961). Radiation of seismic surface waves from finite moving sources, Bull. Seism. Soc. Am. 51, 401-435.

Berberian, M. (1979). Earthquake faulting and bedding thrust associated with the Tabas-e-Golshan (Iran) earthquake of September 16, 1978. Bull. Seism. Soc. Am. 69, 1861-1888.

Blandford, R.R. (1975). A source theory for complex earthquakes, Bull. Seism. Soc. Am. 65, 1385-1405.

Boore, D.M. (1972). Finite difference methods for seismic wave propagation in heterogeneous materials, Methods in Computational Physics. Vol. XI, B.A. Bolt (ed.), Academic Press, 1-36.

Boore, D.M., W.B. Joyner, A.A. Oliver III, and R.A. Page (1978). Estimation of ground motion parameters, U.S. Geol. Surv. Circular 795, Arlington Virginia.

Bouchon, M. (1978). "A dynamic source model for the San Fernando earthquake," Bull. Seism. Soc. Am. 68, 1555-1576.

Brune, J.N. (1976). The physics of earthquake strong motion, in Seismic Risk and Engineering Decisions, C. Lomnitz and E. Rosenblueth (editors), Elsevier, Amsterdam, 140-177.

Burdick, L.J. and G.R. Mellman (1976). Inversion of the body waves from the Borrego Mountain earthquake to the source mechanism, Bull. Seism. Soc. Am. 66, 1485-1499.

Burridge, R. (1977). "A repetitive earthquake source model," J. Geophys. Res. 82, 1663-1666.

Chang, F.K. and E.L. Krinitzsky (1977). Duration, spectral content, and predominant period of strong-motion earthquake records from the western United States, Miscellaneous Paper S-73-1, Report 8, U.S. Army Engineers Waterways Experiment Station, Vicksburg, Mississippi.

Gutenberg, B. (1955b). Magnitude determination for larger Kern County shocks, 1952; effects of station azimuth and calculation methods, in Earthquakes in Kern County, California, during 1952, Calif. Dept. Nat. Resources, Div. Mines, Bull. 171, 171-175.

Haskell, N.A. (1969). Elastic displacements in the near field of a propagating fault, Bull. Seism. Soc. Am. 59, 865-908.

Heaton, T.H. and D.V. Helmberger (1978). Predictability of strong ground motion in the Imperial Valley: modeling the M4.9 November 4, 1976, Brawley earthquake, Bull. Seism. Soc. Am. 68, 31-48.

Helmberger, D.V. and P.C. Jennings (1978). Strong ground motion, N.S.F. Seminar Workshop, San Diego, California.

Iwan, W.D. (ed.) (1978). Strong-motion earthquake instrument arrays, Proc. International Workshop on Strong Motion Earthquake Instrument Arrays, Cal. Inst. Tech., May 2-5, 1978.

Langston, C.A. (1978). The February 9, 1971, San Fernando earthquake: a study of source finiteness in teleseismic body waves, Bull. Seism. Soc. Am. 68, 1-29.

Madariaga, R. (1976). Dynamics of an expanding circular fault, Bull. Seism. Soc. Am. 66, 639-666.

McNally, K. (1980). 1979 Calexico earthquake: seismological data, in Reconnaissance Report: Imperial County, California, Earthquake, October 15, 1979, D.J. Leeds (ed.), EERI, 21-31.

Niazy, A. (1975). An exact solution for a finite, two-dimensional moving dislocation in an elastic half-space with application to the San Fernando earthquake of 1971, Bull. Seism. Soc. Am. 65, 1797-1826.

Rautian, T.G. and V.I. Khalturin (1976). Spectral properties of coda of local earthquakes for investigation of source mechanism, Dokladi, Acad. Nauk, USSR, 226, 566-569.

Shoja-Taheri J. (1980). A new assessment of errors from digitalization and base-line corrections of strong-motion accelerograms, Bull. Seism. Soc. Am. 70, 293-303.

Sozen, M.A. and R.B. Matthiesen (1975). Engineering report on the Managua earthquake of 23 December, 1972, National Academy of Sciences, Washington, D.C.

Tchalenko, J.S. and M. Berberian (1975). Dasht-e Bayaz fault, Iran: earthquake and earlier related structures in bedrock, Geol. Soc. Am. Bull. 86, 703-709.

Trifunac, M.D. (1974). A three-dimensional dislocation model for the San Fernando earthquake of February 9, 1971, Bull. Seism. Soc. Am. 64, 149-172.

Trifunac, M.D. and F.E. Udwadia (1974). Parkfield, California, earthquake of June 27, 1966: a three-dimensional moving dislocation, Bull. Seism. Soc. Am. 64, 511-533.

Tsujiura, M. (1978). Spectral analysis of the coda waves from local earthquakes, Bull. Earthquake Res. Inst., Tokyo Univ. 53, 1-48.

APPENDIX A

COMPUTATION OF RICHTER LOCAL MAGNITUDE FROM STRONG-MOTION RECORDS

In order to determine a local magnitude from a strong-motion accelerogram, it is necessary to transform the record to an equivalent ground motion record as would be obtained from a standard Wood-Anderson torsion seismograph, located at the accelerograph site and assuming that the instrument could not be saturated. From the simulated Wood-Anderson record, the local magnitude can be determined in the usual way (Kanamori and Jennings, 1978).

Method

Let $a(t)$ be the time function of ground acceleration. Applying the Fourier transform to $a(t)$ gives the frequency-domain representation of the acceleration time function $\hat{a}(\omega)$:

$$\hat{a}(\omega) = F\{ a(t) \}. \qquad (1)$$

In (1) it is assumed that $a(t)$ is the actual ground acceleration, that is, corrected to eliminate the accelerometer instrument response. If the accelerograph record from a non-linear instrument is used for $a(t)$ instead, then the Fourier transform of $a(t)$ must be divided by the transfer function of the accelerograph, $\hat{R}(\omega)$:

$$\hat{a}(\omega) = F\{ a(t) \} / \hat{R}(\omega) . \qquad (1')$$

If the transfer function of the accelerograph has a flat, unit response in the frequency range that may affect the Wood-Anderson record, then (1) may be used.

The Fourier transform of the ground velocity is

$$\hat{v}(\omega) = \hat{a}(\omega) / i\omega , \qquad (2)$$

where i is $\sqrt{-1}$. Similarly, the ground displacement in the frequency domain is

$$\hat{d}(\omega) = \hat{v}(\omega) / i\omega \quad . \tag{3}$$

The record $w(t)$ of the standard Wood-Anderson, corresponding to ground displacement $d(t)$, is governed by the instrument "response" $W(t)$:

input ground displacement	W-A	output W-A record
$d(t)$ →	$W(t)$	→ $w(t)$

That is, the convolution of $d(t)$ with the impulse response of the Wood-Anderson instrument, $W(t)$ gives the Wood-Anderson record,

$$w(t) = d(t) * W(t) , \tag{4}$$

or, equivalently in the frequency-domain, multiplication of the Fourier transforms gives

$$\hat{w}(\omega) = \hat{d}(\omega) \cdot \hat{W}(\omega) \quad . \tag{5}$$

The "response" function of the Wood-Anderson instrument in frequency given

by $$\hat{W}(\omega) = \frac{\omega^2}{\omega^2 n + 2i\xi\omega_n\omega - \omega^2} \quad , \tag{6}$$

where ω = ground angular frequency;

ω_n = $2\pi/T$, T is the free period of the instrument;

and ξ = damping coefficient of the instrument.

Once the function $\hat{w}(\omega)$ is obtained by (5), the desired equivalent of the Wood-Anderson record is calculated by taking the inverse Fourier transform of $\hat{w}(\omega)$,

$$w(t) = F^{-1} \{ \hat{w}(\omega) \} . \qquad (7)$$

For examples, refer to Figure A1, as well as Figures 3.19, 3.20, and 4.1.

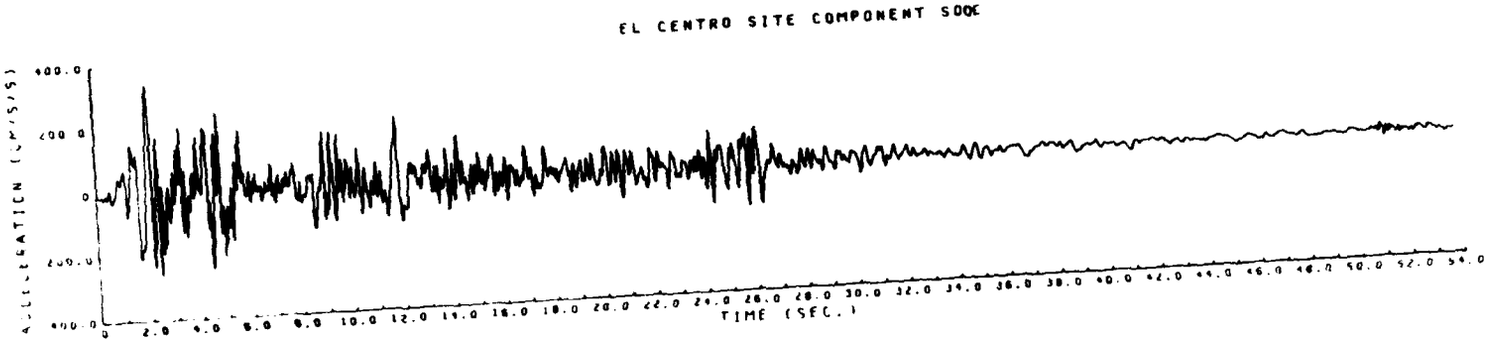

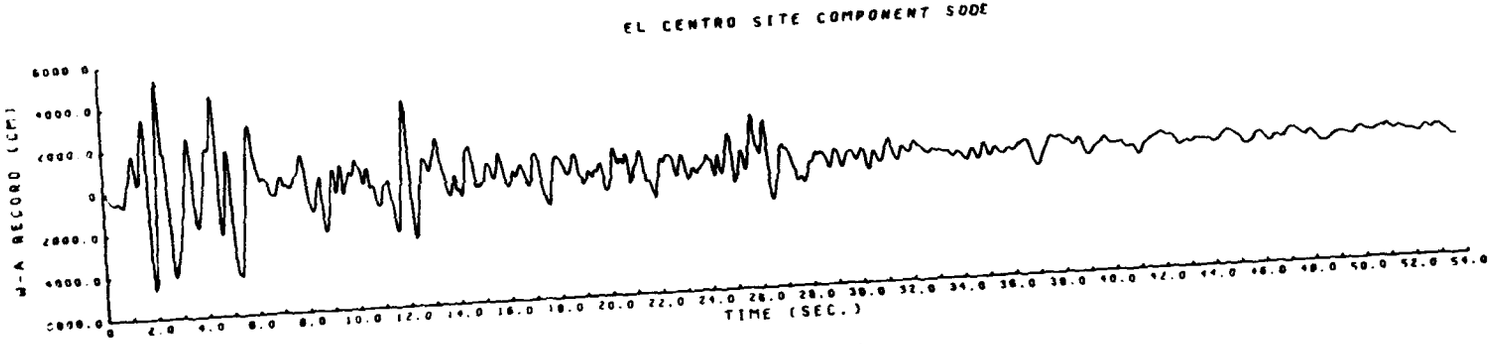

a. N-S component

Figure A1. Corresponding accelerogram and Wood-Anderson seismogram for the N-S and E-W horizontal components of ground motion at El Centro station in the 1940 Imperial Valley, California, earthquake (Continued).

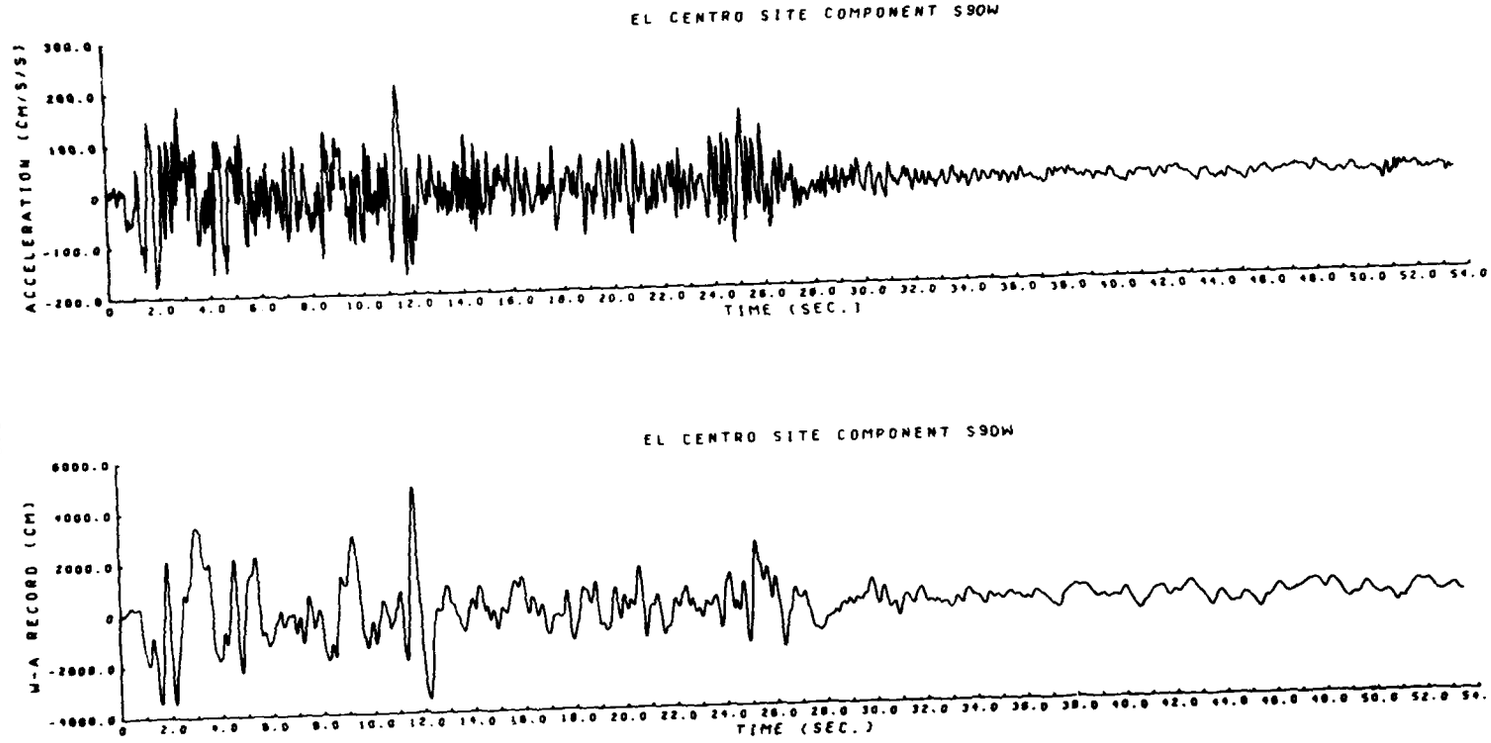

b. E-W component

Figure A1. (Concluded).

APPENDIX B

COMPUTATION OF SEISMIC MOMENT FROM BROAD-BAND RECORDS

A measure of the size of an earthquake is given by the seismic moment M_o. A force couple which is shearing a fault plane produces a moment (M_o). Consider the stress-strain relationship

$$\text{stress} = \mu \times \text{strain} = \mu \frac{D}{L} = \mu \times \frac{\text{average displacement}}{\text{length}}$$

or $$\frac{F}{A} = \frac{\text{force}}{\text{fault area}} = \mu \frac{D}{L} \; ;$$

therefore $$FL = \mu A D \quad \sim \text{moment},$$

or $$M_o = \mu A D \; . \quad \text{(See equation 1.2)} \qquad (1)$$

Thus, one can estimate M_o if A and D can be measured. If the earthquake produces rupture along a fault, D can be estimated directly. The area of the fault rupture is commonly inferred from the spatial distribution of aftershocks which occur during the period following the mainshock. The rigidity μ is generally taken to be 3×10^{11} dynes/cm^2.

The seismic moment M_o can also be estimated from instrumental records of the ground motion. As an example, M_o is estimated from the shear wave (SH) record using the far-field formula (Keilis-Borok, 1960),

$$M_o = \frac{4\pi\rho\beta^3 r}{2R_{\theta\phi}} \; \Omega_o \; . \qquad (2)$$

$R_{\theta\phi}$ accounts for the effects of the radiation pattern of the source, which for the far-field SH component is given by

$$R_{\theta\phi} = \cos 2\theta \cos \phi \qquad (3)$$

where θ = angle between the normal to the rupture plane and the line joining the station and the focus

ϕ = angle between slip axis and the projection onto rupture plane of the line joining the station and the focus

The factor of '2' in the denominator accounts for the effect of the free surface of the Earth which causes the measured surface displacements to be twice the particle motion of the wave front. Ω_o is the zero frequency level of the Fourier spectrum of the horizontal shear wave displacement $U_\theta(r,\tau)$ given by

$$\Omega_o = \int_{\frac{r}{\beta}}^{\frac{r}{\beta}+T} U_\theta(r,\tau)d\tau \quad , \tag{4}$$

where T is the time width of the SH pulse. Therefore,

$$\Omega_o = \frac{1}{2} A T \quad , \tag{5}$$

where A is the maximum amplitude of the SH pulse ground motion and T is taken as the width of the base of the triangle.

Consider the ultra-long-period displacement seismograms (see Figure B1) of the Coyote Lake mainshock (August 6, 1979; M_L = 5.9) recorded at Berkeley (BKS). The seismic moment of the mainshock was estimated from integration of the far-field SH pulse (Ω_o) using (2) to be (6 ± 1.4) x 10^{24} dyne cm, where $4\pi\rho^3 = 1.2 \times 10^{18}$ gm-sec^{-3}. The SH pulse [Ω_o = (0.55 ± 0.08) cm-sec] was measured from BKS displacement seismograms. It should be noted that the direction from the focus to BKS is near a maximum of the radiation pattern for SH (unlike the P phase). Thus, the SH pulse should provide a reliable measure of the overall energy. The calibration of the instruments was checked after the earthquake. The other parameters in (2) are r = 120 km and $R_{\theta\phi}$ = 0.62. The main sources of uncertainty in this calculation are the assessment of source-station distance (since the rupture center rather than the focus is more appropriate) and the assumed value for $4\rho\beta^3$. M_o is probably correct

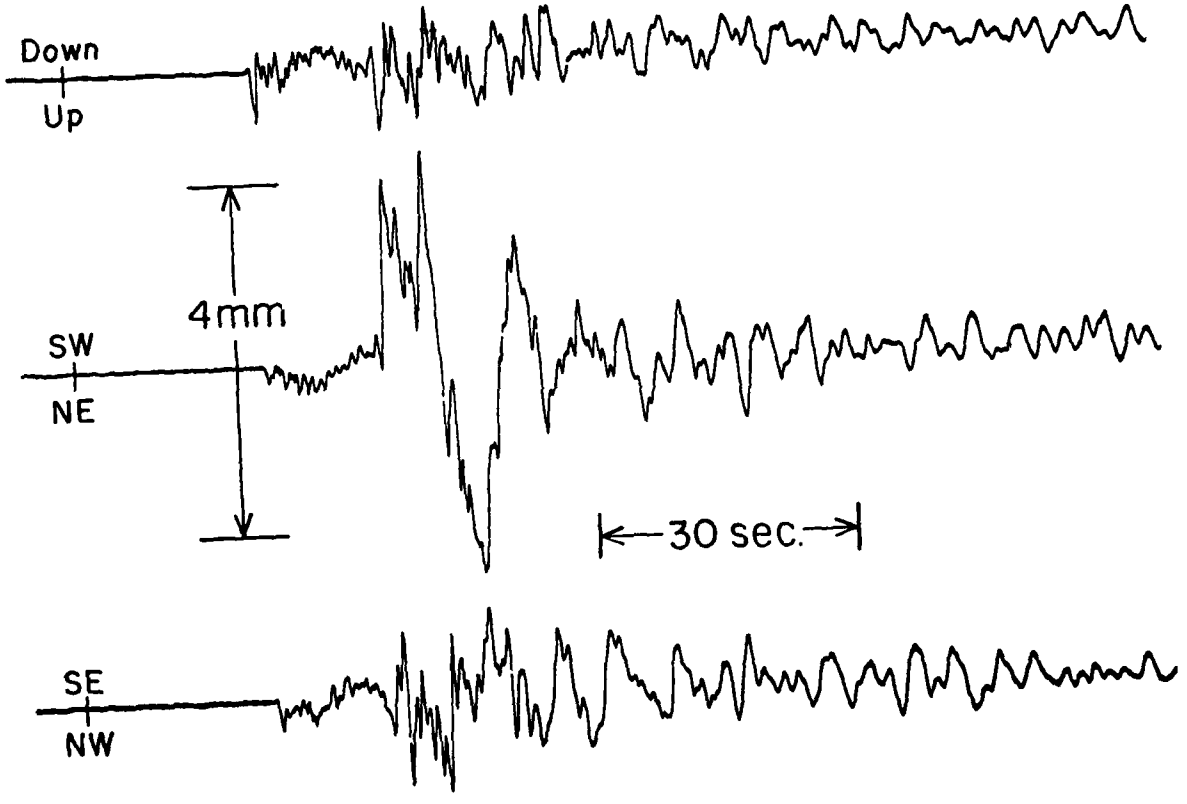

Figure B1. Berkeley (BKS) broadband displacement recorded for the 1979 Coyote Lake earthquake.

within 20 percent. It should be noted, however, that (2) assumes that the SH pulse was measured in the far field (the distance to BKS is about an order of magnitude larger than the rupture length) and the SH pulse does not contain reflections due to crustal structure. The presence of near-field terms or crustal reflections will generally increase the size of the SH pulse and thus lead to an overestimate of M_o.

In accordance with letter from DAEN-RDC, DAEN-ASI dated 22 July 1977, Subject: Facsimile Catalog Cards for Laboratory Technical Publications, a facsimile catalog card in Library of Congress MARC format is reproduced below.

Bolt, Bruce A.
State-of-the-art for assessing earthquake hazards in the United States : Report 17 : Interpretation of strong ground motion records / by Bruce A. Bolt (Department of Geology and Geophysics, University of California, Berkeley). -- Vicksburg, Miss. : U.S. Army Engineer Waterways Experiment Station ; Springfield, Va. ; available from NTIS, 1981.
215 p. : ill. ; 27 cm. -- (Miscellaneous paper / U.S. Army Engineer Waterways Experiment Station ; S-73-1, Report 17)
Cover title.
"October 1981."
"Prepared for Office, Chief of Engineers, U.S. Army under Contract No. DACW39-78-C-0061."
"Monitored by Geotechnical Laboratory, U.S. Army Engineer Waterways Experiment Station."
Bibliography: p. 197-206.

1. Earthquake prediction. 2. Earthquakes. 3. Seismology. I. University of California at Berkeley.

Bolt, Bruce A.
State-of-the-art for assessing earthquake hazards : ... 1981.
(Card 2)

II. United States. Army. Corps of Engineers. Office of the Chief of Engineers. III. U.S. Army Engineer Waterways Experiment Station. Geotechnical Laboratory.
IV. Title V. Series: Miscellaneous paper (U.S. Army Engineer Waterways Experiment Station) ; S-73-1, Report 17.
TA7.W34m no.S-73-1 Report 17

REPORTS IN THIS SERIES
(MP S-73-1)

Report 1	O. W. Nuttli	Design Earthquakes for the Central United States	January 1973
Report 2	E. L. Krinitzsky	Fault Assessment in Earthquake Engineering	May 1974
Report 3	R. B. Hofmann	Factors in the Specification of Ground Motions for Design Earthquakes in California	June 1974
Report 4	Ellis L. Krinitzsky Frank K. Chang	Earthquake Intensity and the Selection of Ground Motion for Seismic Design	September 1975
Report 5	Jack L. Walper	Plate Tectonics and Earthquake Assessment	March 1976
Report 6	David B. Slemmons	Faults and Earthquake Magnitude	May 1977
Report 7	Ellis L. Krinitzsky Frank K. Chang	Specifying Peak Motions for Design Earthquakes	December 1977
Report 8	Frank K. Chang Ellis L. Krinitzsky	Duration, Spectral Content, and Predominant Period of Strong Motion Earthquake Records from Western United States	December 1977
Report 9	Frank K. Chang	Catalogue of Strong Motion Earthquake Records, Volume 1, Western United States, 1933-1971	April 1978
Report 10	Otto W. Nuttli John J. Dwyer	Attenuation of High-Frequency Seismic Waves in the Central Mississippi Valley	July 1978
Report 11	Charles E. Glass David B. Slemmons	Imagery in Earthquake Analysis	December 1978
Report 12	Otto W. Nuttli Robert B. Herrmann	Credible Earthquakes for the Central United States	December 1978
Report 13	M. K. Yegian	Probabilistic Seismic Hazard Analysis	July 1979
Report 14	Erik H. Vanmarcke	Representation of Earthquake Ground Motion: Scaled Accelerograms and Equivalent Response Spectra	August 1979
Report 15	James R. Houston	Tsunamis, Seiches, and Landslide-Induced Water Waves	November 1979
Report 16	Otto W. Nuttli	The Relation of Sustained Maximum Ground Acceleration and Velocity to Earthquake Intensity and Magnitude	November 1979
Report 17	Bruce A. Bolt	Interpretation of Strong Ground Motion Records	October 1981

REPORTS IN PREPARATION

Report 18	Daniele Veneziano	Errors in Probabilistic Seismic Hazard Analysis
Report 19	Ronald B. Meade	The Evidence for Reservoir-Induced Macroearthquakes
Report 20	Ellis L. Krinitzsky	Essentials for Specifying Earthquake Motions in Engineering Design

END

DATE
FILMED

1-82

DTIC